

FOR FURTHER TRAN

USARTL-TR-78-2A

AD A055104

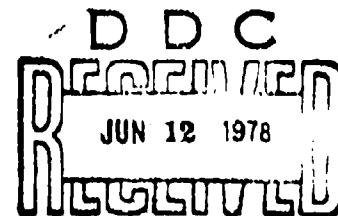
HELICOPTER TRANSMISSION VIBRATION AND NOISE
REDUCTION PROGRAM
Volume I - Technical Report

John J. Sciarra, Robert W. Howells, Joseph W. Lenski, Jr.,
Raymond J. Drago, Edward G. Schaffer
Boeing Vertol Company
P.O. Box 16858
Philadelphia, Pa. 19142

March 1978

Final Report for Period June 1974 - October 1977

Approved for public release;
distribution unlimited.



Prepared for

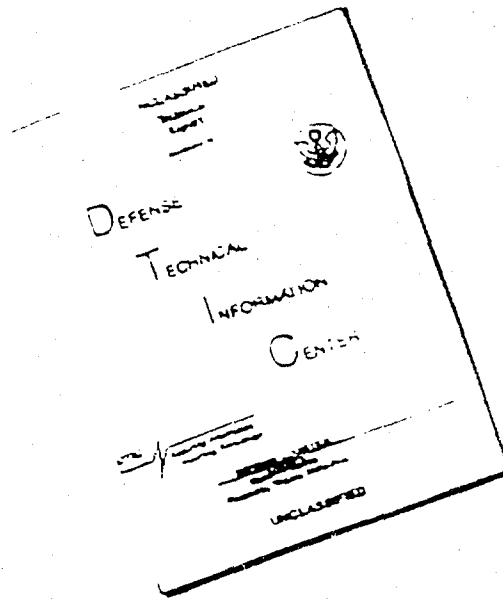
APPLIED TECHNOLOGY LABORATORY
U. S. ARMY RESEARCH AND TECHNOLOGY LABORATORIES (AVRADCOM)
Fort Eustis, Va. 23604

U. S. ARMY MATERIALS AND MECHANICS RESEARCH CENTER
WATERTOWN, MASS. 02172

DDC No.

DDC FILE COPY

DISCLAIMER NOTICE



THIS DOCUMENT IS BEST QUALITY AVAILABLE. THE COPY FURNISHED TO DTIC CONTAINED A SIGNIFICANT NUMBER OF PAGES WHICH DO NOT REPRODUCE LEGIBLY.

APPLIED TECHNOLOGY LABORATORY POSITION STATEMENT

This report provides the details of a program that is the culmination of at least 16 years of Army funded efforts aimed at analyzing and controlling the vibration and noise characteristics of helicopter gearboxes which currently exhibit varying degrees of adverse effects on crews, passengers, and component life. The result of this effort is an analytical tool that, at first application to a CH-47C forward transmission, has resulted in a test stand demonstrated 7-dB reduction in internal noise level at a location corresponding to the cockpit. The ultimate benefit is the application of this analysis as a design tool with anticipated payoffs in reduced development costs for new helicopter gearboxes having improved reliability and reduced noise/vibration levels.

Mr. Allen C. Royal of the Propulsion Technical Area, Technology Applications Division, served as project engineer for this effort.

DISCLAIMERS

The findings in this report are not to be construed as an official Department of the Army position unless so designated by other authorized documents.

When Government drawings, specifications, or other data are used for any purpose other than in connection with a definitely related Government procurement operation, the United States Government thereby incurs no responsibility nor any obligation whatsoever; and the fact that the Government may have formulated, furnished, or in any way supplied the said drawings, specifications, or other data is not to be regarded by implication or otherwise as in any manner licensing the holder or any other person or corporation, or conveying any rights or permission, to manufacture, use, or sell any patented invention that may in any way be related thereto.

Trade names cited in this report do not constitute an official endorsement or approval of the use of such commercial hardware or software.

DISPOSITION INSTRUCTIONS

Destroy this report when no longer needed. Do not return it to the originator.

UNCLASSIFIED

SECURITY CLASSIFICATION OF THIS PAGE (When Data Entered)

REPORT DOCUMENTATION PAGE		READ INSTRUCTIONS BEFORE COMPLETING FORM	
1. REPORT NUMBER USARTL PR-78-2A		2. GOVT ACCESSION NO.	
3. TITLE (and Subtitle) HELICOPTER TRANSMISSION VIBRATION AND NOISE REDUCTION PROGRAM Volume I, Technical Report		4. REPORT NUMBER Final report June 1974-October 1977 PERFORMING ORG. REPORT NUMBER D218-11236-1	
5. AUTHOR(s) John J. Sciarra, Raymond J. Drago Robert W. Howells, Edward G. Schaeffer Joseph W. Lenski, Jr.		6. PERFORMING ORG. REPORT NUMBER DAAG 62-74-C-0049	
7. PERFORMING ORGANIZATION NAME AND ADDRESS Boeing Vertol Company P.O. Box 16858 Philadelphia, Pennsylvania 19142		8. PROGRAM ELEMENT PROJECT, TASK AREA AND SUBPROJECT 62207A RG2622/7AH89/2 004 BK	
9. CONTROLLING OFFICE NAME AND ADDRESS Applied Technology Laboratory, U.S. Army Research and Technology Laboratories (AVRADCOM), Fort Eustis, Virginia 23604		10. SECURITY CLASSIFICATION OF THIS REPORT Unclassified	
11. MONITORING AGENCY NAME AND ADDRESS (if different from Controlling Office) U.S. Army Materials and Mechanics Research Center Watertown, Massachusetts 02172		12. SECURITY CLASSIFICATION OF THIS REPORT Unclassified	
13. DISTRIBUTION STATEMENT (of this Report) Approved for public release; distribution unlimited.		14. DISTRIBUTION STATEMENT (of the abstract entered in Block 20, if different from Report) v. 2. A154 847	
15. SUPPLEMENTARY NOTES Volume I of a 2-volume report			
16. KEY WORDS (Continue on reverse side if necessary and identify by block number) Helicopter transmission Compare theory with test Reduction of vibration and noise Design and fabricate modified components Trade studies Conduct test Design stage Analytical approach			
17. ABSTRACT (Continue on reverse side if necessary and identify by block number) The objective of the Helicopter Transmission Vibration/Noise Reduction Program was to generate analytical tools for the prediction and reduction of helicopter transmission vibration/noise that provide the capability to perform trade studies during the design stage of a program. Application of this optimization capability yields drive train components that are dynamically quiet with reduced vibration/noise levels and inherently longer life.			

DD FORM 1 JAN 73 1473

EDITION OF 1 NOV 68 IS OBSOLETE

UNCLASSIFIED

SECURITY CLASSIFICATION OF THIS PAGE (When Data Entered)

403 682

UNCLASSIFIED

SECURITY CLASSIFICATION OF THIS PAGE (When Data Entered)

Block 20. Continued.

The work described herein represents a major step toward the long-range objective of a minimum vibration and noise, minimum weight, highly reliable, advanced technology transmission system. The major goals of the program were to:

1. Define an analytical approach to vibration/noise reduction.
2. Correlate existing experimental test data with data predicted by the analytical tools.
3. Design and fabricate modified transmission components utilizing the verified version of the prediction technique.
4. Conduct verification testing of the entire transmission with the modified components installed.
5. Compare test results of the baseline and modified versions of the transmission.
6. Disseminate information to government and industry personnel through final report and user's conference.

An analytical approach using finite element and strain energy computer techniques was selected for this work. A finite element model of the complete forward rotor transmission for the Boeing Vertol CH-47 helicopter was developed and applied to reduce transmission vibration/noise. The internal components were analyzed using computer programs GGEAR, TORRP, and D-82. The housing was modeled using NASTRAN. In addition to a description of the model, the technique for vibration/noise prediction and reduction is outlined. Also included are the predicted dynamic response, correlation with test data, the use of strain energy methods to optimize the transmission for minimum vibration/noise, and determination of the design modifications which were manufactured and tested.

UNCLASSIFIED

SECURITY CLASSIFICATION OF THIS PAGE (When Data Entered)

PREFACE

This report summarizes the results of the "Helicopter Transmission Vibration and Noise Reduction Program". The report covers the work accomplished during the 40-month period from June 1974 through October 1977 and is composed of two volumes. Volume I is the Technical Report, and Volume II is the User's Manual.

The work outlined herein has been performed under U.S. Army contract DAAJ02-74-C-0040 and under the technical cognizance of Mr. Allen Royal, U.S. Army Research and Technology Laboratories (AVRADCOM), Fort Eustis, Virginia.

The fabrication of graphite/aluminum doubler plates (Appendix B) was sponsored by the U.S. Army Materials and Mechanics Research Center, Watertown, Mass, under the technical cognizance of Mr. Albert P. Levitt.

This program was conducted at the Boeing Vertol Company under the technical direction of Mr. A. J. Lemanski (Program Manager), Chief of the Advanced Power Train Technology Department. Principal Investigators for the program were Mr. John J. Sciarra (Project Engineer), Mr. Robert W. Howells, Mr. Joseph W. Lenski, Jr., Mr. Raymond J. Drago, and Mr. Edward G. Schaeffer.

ADDITIONAL	
NTIS	Write Section <input checked="" type="checkbox"/>
REF	Date Section <input checked="" type="checkbox"/>
UNANNOUNCED	<input checked="" type="checkbox"/>
JUSTIFIED - JUN	
BY	
DIS. DIS. AVAILABILITY CODES	
ONE	AVAIL. AND SPECIAL
A	

TABLE OF CONTENTS

	<u>Page</u>
PREFACE	3
LIST OF ILLUSTRATIONS	6
LIST OF TABLES	23
INTRODUCTION	25
THE NOISE PROBLEM	32
ANALYTICAL APPROACH	37
INTERNAL COMPONENTS - MODEL AND ANALYSIS	42
TRANSMISSION HOUSING - MODEL AND ANALYSIS	55
DETUNING OF THE TRANSMISSION	75
AUXILIARY DEVICES FOR VIBRATION/NOISE REDUCTION	93
NOISE PREDICTION AND REDUCTION	107
BASELINE DATA AND CORRELATION	114
DESIGN MODIFICATIONS	129
VERIFICATION TESTING	140
CONCLUSIONS	189
RECOMMENDATIONS	192
REFERENCES	193
BIBLIOGRAPHY	195
APPENDIX A - VIBRATION AND NOISE TEST DATA	197
APPENDIX B - COMPOSITE DOUBLER PLATE ANALYSIS AND TEST	285
APPENDIX C - KAMAN H-2 TRANSMISSION NASTRAN MODEL	299
LIST OF SYMBOLS	306

LIST OF ILLUSTRATIONS

<u>Figure</u>	<u>Page</u>
1 Sources of Helicopter Noise	26
2 Boeing Vertol CH-47 Helicopter	26
3 Loss of Noise Isolation as Result of an Opening in Acoustical Enclosure (Reference 5)	28
4 Speed Versus Noise (Reference 6)	28
5 Load Versus Noise (Reference 6)	30
6 Influence of Tooth Alignment Error on Gear Noise (Reference 6)	30
7 Internal Noise Trend for Untreated Aircraft . .	31
8 Typical Noise Levels in Variety of Areas and from Several Noise Generating Media. (Chart is merely for comparison, since all noise levels vary with background noise, distance, acoustics, etc.)	33
9 A-Weighting of Sound Pressure Levels	34
10 Contours for Determining Equivalent A-Weighted Sound Level	34
11 Addition of Equal Sounds	36
12 Addition of Unequal Sounds	36
13 Sources of Transmission Noise	38
14 Flow Chart of Technical Approach to Transmission Vibration/Noise Analysis	40
15 CH-47 Forward Rotor Transmission Internal Components	43
16 Finite Element Model of CH-47 Forward Rotor Transmission Internal Components	43
17 Spectrum for CH-47C Forward Transmission Bevel/Sun Gear and Pinion Plus Lower Planetary Gear System at 80% Torque and 7160 RPM - Sync Shaft (244 RPM - Shaft)	44

<u>Figure</u>		<u>Page</u>
18	Computer-Generated Plots of D-82 Model; CH-47C Forward Rotor Transmission Internal Components	45
19	Typical Damped Force Response	50
20	CH-47C Forward Transmission Input Pinion Support Bearings	50
21	CH-47C Forward Transmission Sun Gear Support Bearings	50
22	Bearing Spring Rate (k) Along X; CH-47C Forward Transmission Input Pinion (7460 RPM - Pinion)	52
23	Bearing Spring Rate (k) Along Y; CH-47C Forward Transmission Input Pinion (7460 RPM - Pinion)	52
24	Bearing Spring Rate (k) Along Z; CH-47C Forward Transmission Input Pinion (7460 RPM - Pinion)	52
25	Bearing Spring Rate (k); CH-47C Forward Transmission Input Pinion (7460 RPM - Pinion)	52
26	Bearing Spring Rate (k) Along X; CH-47C Forward Transmission Sun Gear (7460 RPM - Pinion)	53
27	Bearing Spring Rate (k) Along Y; CH-47C Forward Transmission Sun Gear (7460 RPM - Pinion)	53
28	Bearing Spring Rate (k) Along Z; CH-47C Forward Transmission Sun Gear (7460 RPM - Pinion)	53
29	Bearing Spring Rate (k); CH-47C Forward Transmission Sun Gear (7460 RPM - Pinion)	53
30	Boeing Vertol CH-47 Helicopter Forward Rotor Transmission Housing and NASTRAN Model	56
31	CH-47 Forward Transmission Case and Measuring Instruments	58

<u>Figure</u>		<u>Page</u>
32	Computer-Generated Plots of NASTRAN Model; CH-47C Forward Rotor Transmission Case With Sump	60
33	CH-47 Forward Transmission NASTRAN Model	61
34	Transmission Noise Generated by Out-Of- Plane Displacements of Housing	63
35	Computer-Generated Plot of NASTRAN Model; CH-47C Forward Rotor Transmission Upper Cover (Undeformed Shape)	66
36	Spectrum of Forcing Frequencies Versus NASTRAN Predicted Natural Frequencies for CH-47C Forward Transmission Upper Cover	67
37	Spectrum of Forcing Frequencies Versus NASTRAN Predicted Natural Frequencies for CH-47C Forward Transmission Upper Cover (Legs Simply Supported)	68
38	CH-47 Forward Rotor Transmission Ring Gear; Existing Configuration and Resulting Spectrum (at 80% Torque, 7460 RPM Sync Shaft Speed)	69
39	Spectrum of Forcing Frequencies Versus NASTRAN Predicted Natural Frequencies for CH-47C Forward Transmission Case (Free-Free)	70
40	NASTRAN Plot of Deformed Housing, Mode #46, Frequency 3141 Hz	71
41	Spectrum of Forcing Frequencies Versus NASTRAN Predicted Natural Frequencies of CH-47C Forward Transmission Case (With Sump; Simply Supported)	72
42	CH-47 Forward Transmission Case (With Sump) Modal Deformation	73
43	Amplification Factor	76
44	Flat Disk in Resonance	76
45	D-87 Plot of CH-47C Sun Bevel Pinion and Gear and Lower Planetary Gear System	79

<u>Figure</u>		<u>Page</u>
46	Use of Gap to Change Bearing Stiffness Through Preload	80
47	Maximum Measured Noise Levels (7460 RPM at 80% Torque)	83
48	CH-47 Forward Rotor Transmission Ring Gear; Modified Configuration and Resulting Spectrum (at 80% Torque, 7460 RPM Sync Shaft Speed) . . .	85
49	CH-47C Forward Rotor Transmission Case (With Sump) NASTRAN Model: Areas of High Strain Density	87
50	CH-47C Forward Transmission Case With Modifications (Crosshatched Areas) to Wall Thickness	89
51	Spectrum of Forcing Frequencies Versus NASTRAN Predicted Natural Frequencies for CH-47C Forward Transmission Case (With Sump; Simply Supported) - Modified "A"	90
52	Comparison of Significant Frequencies for Baseline and Modified "A" CH-47C Forward Transmission Case	91
53	Concept of the Dynamic Vibration Absorber . . .	94
54	Absorber Locations	94
55	Geometry and Sample Calculation for Bending Type Dynamic Vibration Absorbers as Applied to Ring Gear	96
56	Possible Damped Sun and Spiral Bevel Gear Configuration	98
57	Possible Ring Gear Damping Strap	98
58	Summary of Absorber Test Results	99
59	Comparison of Predicted and Measured Spiral Bevel Torsional Absorber Response	100
60	Vibration Data Showing Sidebands	101
61	Proposed Points of Attachment for Radial Absorbers	103

<u>Figure</u>		<u>Page</u>
62	Effect of Skin Damping on Cabin Noise Levels (Reference 16)	104
63	Cabin Noise Reduction From Isolating Element Between Transmission Housing and Airframe (Reference 16)	104
64	Airborne and Structure-Borne Noise	106
65	Selection of Correlation RPM for Spiral Bevel Mesh Frequency	115
66	Example of Test Data for Correlation Study . . .	117
67	Typical Baseline Noise Spectrum-Third- Octave Band Analysis	119
68	Measured Noise Levels for CH-47 Forward Transmission (Baseline) at 7460 Sync Shaft RPM and 80% Torque	120
69	CH-47 Forward Transmission Case Vibration Spectra (Baseline) at 7460 Sync Shaft RPM and 80% Torque	121
70	Prediction of Sun Gear Shaft Response to Bevel Frequency Excitation	123
71	Lissajous Figures of Sun Gear Shaft Responding to Bevel Frequency	123
72	Mode Shape Correlation of Bevel Gear Shaft Responding to Bevel Mesh Frequency	123
73	Shaft Displacements - Correlation of D-82 Predictions with Test Data	124
74	Finite Element Model of Lower Housing Showing Grid Point Locations for Noise Prediction . . .	128
75	CH-47 Forward Transmission Bevel Pinion (Baseline) with Finite Element Idealization Superimposed	130
76	CH-47 Forward Transmission Bevel/Sun Gear (Baseline) with Finite Element Idealization Superimposed	131
77	CH-47 Forward Transmission Bevel/Sun Gear (Modified) with Finite Element Idealization Superimposed	131

<u>Figure</u>		<u>Page</u>
78	Modifications to Bevel/Sun Gear Shaft Hardware	132
79	Modified Bevel/Sun Gear Shaft With Two Sleeves Installed	133
80	CH-47 Forward Transmission Ring Gear; Modified Version Manufactured for Testing	134
81	Modified Ring Gear With Split Ring Installed . .	136
82	Magnesium Contoured Doubler Plates	137
83	SK27064-1 (L) - Magnesium Contoured Doubler Plate Installed	138
84	Transmission Cover Leg Attachment to Main Frame	139
85	Schematic Diagram of Closed-Loop Test Stand . .	141
86	CH-47 Forward Transmission Test Facility Control Console	142
87	Schematic of Transmission in Acoustic Enclosure	143
88	CH-47 Forward Transmission Installed in Dynamic Test Rig With Acoustic Enclosure	144
89	Accelerometer Locations	145
90	Typical Accelerometer Installation	146
91	Microphone Locations Within Enclosure	148
92	Typical Microphone Installation	149
93	Data Acquisition System	150
94	Microphone System Calibration Chart	152
95	Typical Accelerometer Calibration Chart	153
96	CH-47C Forward Transmission - Test Configuration for Vibration/Noise Reduction Testing	155
97	Installation of Ring Gear Detuning Band	156

<u>Figure</u>		<u>Page</u>
98	Installation of Detuning Sleeve and Plates on Sun/Bevel Gear and Transmission Lower Case .	156
99	Typical Sump Accelerometer Response	158
100	Typical Ring Gear Accelerometer Response	158
101	Typical Transmission Noise Spectrum	161
102	Vibration Data at Lower Planetary Mesh Frequency (Baseline, Isolators, and Detuned Sun Gear)	162
103	Vibration Data at Lower Planetary Mesh Frequency (Detuned Sun Gear and Isolators, Detuned Sun Gear and Magnesium Plates, and Magnesium Plates)	163
104	Vibration Data at Lower Planetary Mesh Frequency (Magnesium Plates and Detuned Ring Gear, Detuned Sun Gear and Detuned Ring Gear, and Magnesium Plates)	164
105	Vibration Data at Lower Planetary Mesh Frequency (Detuned Sun Gear and Composite Plates, and Composite Plates)	165
106	Change in Vibration Level at Lower Planetary Frequency (LP1 = 1566 Hz, Accelerometers 1, 2, and 3)	166
107	Change in Vibration Level at Lower Planetary Frequency (LP1 = 1566 Hz, Accelerometers 4, 5, and 6)	167
108	Radiated Noise Data at Lower Planetary Mesh Frequency	169
109	Radiated Noise Data at Lower Planetary Mesh Frequency	170
110	Radiated Noise Data at Lower Planetary Mesh Frequency	171
111	Radiated Noise Data at Lower Planetary Mesh Frequency	172
112	Change in Sound Pressure Level at Lower Planetary Mesh Frequency (Microphones 1, 2, and 3) Compared to Baseline	173

<u>Figure</u>		<u>Page</u>
113	Change in Sound Pressure Level at Lower Planetary Mesh Frequency (Microphones 4, 5, and 6) Compared to Baseline	174
114	Comparison of Averaged Sound Pressure Levels at Lower Planetary Mesh Frequency	175
115	Change in Averaged Sound Pressure Level Compared to Baseline at Lower Planetary Mesh Frequency	176
116	Comparison of Averaged Sound Pressure Levels at Spiral Bevel Mesh Frequency	177
117	Typical Effect of Sound Transmission Enclosures on Source Attenuation	181
118	Relationship of CH-47C Forward Transmission Noise to MIL-A-8806 Requirements at Flight Operation Speed	182
119	Relationship of CH-47C Forward Transmission Noise to MIL-A-8806 Requirements at Ground Operation Speed	183
120	Relative Weight of Acoustical Treatment Required to Reduce CH-47C Forward Transmission Noise Levels to MIL-A-8806 Requirements	184
121	Effect of Sound Transmission Enclosures on Source Attenuation of CH-47C Forward Transmission Noise	186
122	Effect of Sound Transmission Enclosures on Source Attenuation of CH-47C Aft Transmission Noise	187
123	Flow Diagram of NASTRAN Stress Analysis	190
124	Flow Diagram of NASTRAN Thermal Analysis	190
A1	Accelerometer Data From Tape 6L1 With Baseline CH-47C Forward Transmission at 7,460 RPM and 80-Percent Torque	197
A2	Accelerometer Data From Tape 6L1 With Baseline CH-47C Forward Transmission at 7,460 RPM and 60-Percent Torque	198

<u>Figure</u>		<u>Page</u>
A3	Accelerometer Data From Tape 6L1 With Baseline CH-47C Forward Transmission at 6,600 RPM and 80-Percent Torque	199
A4	Accelerometer Data From Tape 6L1 With Baseline CH-47C Forward Transmission at 6,600 RPM and 60-Percent Torque	200
A5	Accelerometer Data From Tape 6L2 With Baseline CH-47C Forward Transmission and Isolators at 7,460 RPM and 80-Percent Torque	201
A6	Accelerometer Data From Tape 6L2 With Baseline CH-47C Forward Transmission and Isolators at 7,460 RPM and 60-Percent Torque	202
A7	Accelerometer Data From Tape 6L2 With Baseline CH-47C Forward Transmission and Isolators at 6,600 RPM and 80-Percent Torque	203
A8	Accelerometer Data From Tape 6L2 With Baseline CH-47C Forward Transmission and Isolators at 6,600 RPM and 60-Percent Torque	204
A9	Accelerometer Data From Tape 6L3 With Detuned Sun Gear and No Isolators at 7,460 RPM and 80-Percent Torque	205
A10	Accelerometer Data From Tape 6L3 With Detuned Sun Gear and No Isolators at 7,460 RPM and 60-Percent Torque	206
A11	Accelerometer Data From Tape 6L3 With Detuned Sun Gear and No Isolators at 6,600 RPM and 80-Percent Torque	207
A12	Accelerometer Data From Tape 6L3 With Detuned Sun Gear and Isolators at 6,600 RPM and 60-Percent Torque	208
A13	Accelerometer Data From Tape 6L4 With Detuned Sun Gear and Isolators at 7,460 RPM and 80-Percent Torque	209
A14	Accelerometer Data From Tape 6L4 With Detuned Sun Gear and Isolators at 7,460 RPM and 60-Percent Torque	210
A15	Accelerometer Data From Tape 6L4 With Detuned Sun Gear and Isolators at 6,600 RPM and 80-Percent Torque	211

<u>Figure</u>		<u>Page</u>
A16	Accelerometer Data From Tape 6L4 With Detuned Sun Gear and Isolators at 6,600 RPM and 60-Percent Torque	212
A17	Accelerometer Data From Tape 6L5 With Detuning Magnesium Contour Plates, Detuned Sun Gear, and No Isolators at 7,460 RPM and 80-Percent Torque	213
A18	Accelerometer Data From Tape 6L5 With Detuning Magnesium Contour Plates, Detuned Sun Gear, and No Isolators at 7,460 RPM and 60-Percent Torque	214
A19	Accelerometer Data From Tape 6L5 With Detuning Magnesium Contour Plates, Detuned Sun Gear, and No Isolators at 6,600 RPM and 80-Percent Torque	215
A20	Accelerometer Data From Tape 6L5 With Detuning Magnesium Contour Plates, Detuned Sun Gear, and No Isolators at 6,600 RPM and 60-Percent Torque	216
A21	Accelerometer Data From Tape 6L6 With Detuning Magnesium Contour Plates, Original Sun Gear, and No Isolators at 7,460 RPM and 80-Percent Torque	217
A22	Accelerometer Data From Tape 6L6 With Detuning Magnesium Contour Plates, Original Sun Gear, and No Isolators at 7,460 RPM and 60-Percent Torque	218
A23	Accelerometer Data From Tape 6L6 With Detuning Magnesium Contour Plates, Original Sun Gear, and No Isolators at 6,600 RPM and 80-Percent Torque	219
A24	Accelerometer Data From Tape 6L6 With Detuning Magnesium Contour Plates, Original Sun Gear, and No Isolators at 6,600 RPM and 60-Percent Torque	220
A25	Accelerometer Data From Tape 6L7 With Detuning Magnesium Contour Plates, Original Sun Gear, Thickened Ring Gear, and No Isolators at 7,460 RPM and 80-Percent Torque	221

<u>Figure</u>		<u>Page</u>
A26	Accelerometer Data From Tape 6L7 With Detuning Magnesium Contour Plates, Original Sun Gear, Thickened Ring Gear, and No Isolators at 7,460 RPM and 60-Percent Torque.	222
A27	Accelerometer Data From Tape 6L7 With Detuning Magnesium Contour Plates, Original Sun Gear, Thickened Ring Gear, and No Isolators at 6,600 RPM and 80-Percent Torque	223
A28	Accelerometer Data From Tape 6L7 With Detuning Magnesium Contour Plates, Original Sun Gear, Thickened Ring Gear, and No Isolators at 6,600 RPM and 60-Percent Torque	224
A29	Accelerometer Data From Tape 6L8 With Detuning Magnesium Contour Plates, Detuned Sun Gear, Thickened Ring Gear, and No Isolators at 7,460 RPM and 80-Percent Torque	225
A30	Accelerometer Data From Tape 6L8 With Detuning Magnesium Contour Plates, Detuned Sun Gear, Thickened Ring Gear, and No Isolators at 7,460 RPM and 60-Percent Torque	226
A31	Accelerometer Data From Tape 6L8 With Detuning Magnesium Contour Plates, Detuned Sun Gear, Thickened Ring Gear, and No Isolators at 6,600 RPM and 80-Percent Torque	227
A32	Accelerometer Data From Tape 6L8 With Detuning Magnesium Contour Plates, Detuned Sun Gear, Thickened Ring Gear, and No Isolators at 6,600 RPM and 60-Percent Torque	228
A33	Accelerometer Data From Tape 6L9 With Detuning Magnesium Contour Plates, Detuned Sun Gear, Thickened Ring Gear, and Isolators at 7,460 RPM and 80-Percent Torque	229
A34	Accelerometer Data From Tape 6L9 With Detuning Magnesium Contour Plates, Detuned Sun Gear, Thickened Ring Gear, and Isolators at 7,460 RPM and 60-Percent Torque.	230
A35	Accelerometer Data From Tape 6L9 With Detuning Magnesium Contour Plates, Detuned Sun Gear, Thickened Ring Gear, and Isolators at 6,600 RPM and 80-Percent Torque	231

<u>Figure</u>		<u>Page</u>
A36	Accelerometer Data From Tape 6L9 With Detuning Magnesium Contour Plates, Detuned Sun Gear, Thickened Ring Gear, and Isolators at 6,600 RPM and 60-Percent Torque	232
A37	Accelerometer Data From Tape 6L10 With Detuning Graphite-Aluminum Composite Contour Plates and Detuned Sun Gear at 7,460 RPM and 80-Percent Torque	233
A38	Accelerometer Data From Tape 6L10 With Detuning Graphite-Aluminum Composite Contour Plates and Detuned Sun Gear at 7,460 RPM and 60-Percent Torque	234
A39	Accelerometer Data From Tape 6L10 With Detuning Graphite-Aluminum Composite Contour Plates and Detuned Sun Gear at 6,600 RPM and 80-Percent Torque	235
A40	Accelerometer Data From Tape 6L10 With Detuning Graphite-Aluminum Composite Contour Plates and Detuned Sun Gear at 6,600 RPM and 60-Percent Torque	236
A41	Accelerometer Data From Tape 6L11 With Detuning Graphite-Aluminum Composite Contour Plates at 7,460 RPM and 80-Percent Torque	237
A42	Accelerometer Data From Tape 6L11 With Detuning Graphite-Aluminum Composite Contour Plates at 7,460 RPM and 60-Percent Torque	238
A43	Accelerometer Data From Tape 6L11 With Detuning Graphite-Aluminum Composite Contour Plates at 6,600 RPM and 80-Percent Torque	239
A44	Accelerometer Data From Tape 6L11 With Detuning Graphite-Aluminum Composite Contour Plates at 6,600 RPM and 60-Percent Torque	240
A45	Microphone Data From Tape 6L1 With Baseline CH-47C Forward Transmission at 7,460 RPM and 80-Percent Torque	241
A46	Microphone Data From Tape 6L1 With Baseline CH-47C Forward Transmission at 7,460 RPM and 60-Percent Torque	242

<u>Figure</u>		<u>Page</u>
A47	Microphone Data From Tape 6L1 With Baseline CH-47C Forward Transmission at 6,600 RPM and 80-Percent Torque	243
A48	Microphone Data From Tape 6L1 With Baseline CH-47C Forward Transmission at 6,600 RPM and 60-Percent Torque	244
A49	Microphone Data From Tape 6L2 With Baseline CH-47C Forward Transmission and Isolators at 7,460 RPM and 80-Percent Torque	245
A50	Microphone Data From Tape 6L2 With Baseline CH-47C Forward Transmission and Isolators at 7,460 RPM and 60-Percent Torque	246
A51	Microphone Data From Tape 6L2 With Baseline CH-47C Forward Transmission and Isolators at 6,600 RPM and 80-Percent Torque	247
A52	Microphone Data From Tape 6L2 With Baseline CH-47C Forward Transmission and Isolators at 6,600 RPM and 60-Percent Torque	248
A53	Microphone Data From Tape 6L3 With Detuned Sun Gear and No Isolators at 7,460 RPM and 80-Percent Torque	249
A54	Microphone Data From Tape 6L3 With Detuned Sun Gear and No Isolators at 7,460 RPM and 60-Percent Torque	250
A55	Microphone Data From Tape 6L3 With Detuned Sun Gear and No Isolators at 6,600 RPM and 80-Percent Torque	251
A56	Microphone Data From Tape 6L3 With Detuned Sun Gear and No Isolators at 6,600 RPM and 60-Percent Torque	252
A57	Microphone Data From Tape 6L4 With Detuned Sun Gear and Isolators at 7,460 RPM and 80-Percent Torque	253
A58	Microphone Data From Tape 6L4 With Detuned Sun Gear and Isolators at 7,460 RPM and 60-Percent Torque	254
A59	Microphone Data From Tape 6L4 With Detuned Sun Gear and Isolators at 6,600 RPM and 80-Percent Torque	255

<u>Figure</u>		<u>Page</u>
A60	Microphone Data From Tape 6L4 With Detuned Sun Gear and Isolators at 6,600 RPM and 60-Percent Torque	256
A61	Microphone Data From Tape 6L5 With Detuning Magnesium Contour Plates, Detuned Sun Gear, and No Isolators at 7,460 RPM and 80-Percent Torque	257
A62	Microphone Data From Tape 6L5 With Detuning Magnesium Contour Plates, Detuned Sun Gear, and No Isolators at 7,460 RPM and 60-Percent Torque	258
A63	Microphone Data From Tape 6L5 With Detuning Magnesium Contour Plates, Detuned Sun Gear, and No Isolators at 6,600 RPM and 80-Percent Torque	259
A64	Microphone Data From Tape 6L5 With Detuning Magnesium Contour Plates, Detuned Sun Gear, and No Isolators at 6,600 RPM and 60-Percent Torque	260
A65	Microphone Data From Tape 6L6 With Detuning Magnesium Contour Plates, Original Sun Gear, and No Isolators at 7,460 RPM and 80-Percent Torque	261
A66	Microphone Data From Tape 6L6 With Detuning Magnesium Contour Plates, Original Sun Gear, and No Isolators at 7,460 RPM and 60-Percent Torque	262
A67	Microphone Data From Tape 6L6 With Detuning Magnesium Contour Plates, Original Sun Gear, and No Isolators at 6,600 RPM and 80-Percent Torque	263
A68	Microphone Data From Tape 6L6 With Detuning Magnesium Contour Plates, Original Sun Gear, and No Isolators at 6,600 RPM and 60-Percent Torque	264
A69	Microphone Data From Tape 6L7 With Detuning Magnesium Contour Plates, Original Sun Gear, Thickened Ring Gear, and No Isolators at 7,460 RPM and 80-Percent Torque	265

<u>Figure</u>		<u>Page</u>
A70	Microphone Data From Tape 6L7 With Detuning Magnesium Contour Plates, Original Sun Gear, Thickened Ring Gear, and No Isolators at 7,460 RPM and 60-Percent Torque	266
A71	Microphone Data From Tape 6L7 With Detuning Magnesium Contour Plates, Original Sun Gear, Thickened Ring Gear, and No Isolators at 6,600 RPM and 80-Percent Torque	267
A72	Microphone Data From Tape 6L7 With Detuning Magnesium Contour Plates, Original Sun Gear, Thickened Ring Gear, and No Isolators at 6,600 RPM and 60-Percent Torque	268
A73	Microphone Data From Tape 6L8 With Detuning Magnesium Contour Plates, Detuned Sun Gear, Thickened Ring Gear, and No Isolators at 7,460 RPM and 80-Percent Torque	269
A74	Microphone Data From Tape 6L8 With Detuning Magnesium Contour Plates, Detuned Sun Gear, Thickened Ring Gear, and No Isolators at 7,460 RPM and 60-Percent Torque	270
A75	Microphone Data From Tape 6L8 With Detuning Magnesium Contour Plates, Detuned Sun Gear, Thickened Ring Gear, and No Isolators at 6,600 RPM and 80-Percent Torque	271
A76	Microphone Data From Tape 6L8 With Detuning Magnesium Contour Plates, Detuned Sun Gear, Thickened Ring Gear, and No Isolators at 6,600 RPM and 60-Percent Torque	272
A77	Microphone Data From Tape 6L9 With Detuning Magnesium Contour Plates, Detuned Sun Gear, Thickened Ring Gear, and Isolators at 7,460 RPM and 80-Percent Torque	273
A78	Microphone Data From Tape 6L9 With Detuning Magnesium Contour Plates, Detuned Sun Gear, Thickened Ring Gear, and Isolators at 7,460 RPM and 60-Percent Torque	274
A79	Microphone Data From Tape 6L9 With Detuning Magnesium Contour Plates, Detuned Sun Gear, Thickened Ring Gear, and Isolators at 6,600 RPM and 80-Percent Torque	275

<u>Figure</u>		<u>Page</u>
A80	Microphone Data From Tape 6L9 With Detuning Magnesium Contour Plates, Detuned Sun Gear, Thickened Ring Gear, and Isolators at 6,600 RPM and 60-Percent Torque	276
A81	Microphone Data From Tape 6L10 With Detuning Graphite-Aluminum Composite Contour Plates and Detuned Sun Gear at 7,460 RPM and 80-Percent Torque	277
A82	Microphone Data From Tape 6L10 With Detuning Graphite-Aluminum Composite Contour Plates and Detuned Sun Gear at 7,460 RPM and 60-Percent Torque	278
A83	Microphone Data From Tape 6L10 With Detuning Graphite-Aluminum Composite Contour Plates and Detuned Sun Gear at 6,600 RPM and 80-Percent Torque	279
A84	Microphone Data From Tape 6L10 With Detuning Graphite-Aluminum Composite Contour Plates and Detuned Sun Gear at 6,600 RPM and 60-Percent Torque	280
A85	Microphone Data From Tape 6L11 With Detuning Graphite-Aluminum Composite Contour Plates at 7,460 RPM and 80-Percent Torque	281
A86	Microphone Data From Tape 6L11 With Detuning Graphite-Aluminum Composite Contour Plates at 7,460 RPM and 60-Percent Torque	282
A87	Microphone Data From Tape 6L11 With Detuning Graphite-Aluminum Composite Contour Plates at 6,600 RPM and 80-Percent Torque	283
A88	Microphone Data From Tape 6L11 With Detuning Graphite-Aluminum Composite Contour Plates at 6,600 RPM and 60-Percent Torque	284
B1	CH-47C Forward Transmission Dynamic Housing Deflection at Operating Temperature	287
B2	Typical Spectrum of Forcing Frequencies Versus Natural Frequencies	289
B3	Computer-Generated Plot of -1 Graphite/Aluminum Doubler Plate	290

<u>Figure</u>		<u>Page</u>
B4	Computer-Generated Plot of -2 Graphite/ Aluminum Doubler Plate	291
B5	Lamina Notation	292
B6	Graphite/Aluminum Doubler Plates	297
B7	Partially Delaminated Corner of SK27064-3 Graphite/Aluminum Contoured Doubler Plate (L) . .	297
C1	Kaman UH-2 Helicopter Main Transmission	300
C2	Noise/Vibration Reduction Program, Kaman UH-2 Main Transmission, Upper Housing (Undeformed Shape)	301
C3	Noise/Vibration Reduction Program, Kaman UH-2 Main Transmission, Intermediate Housing (Undeformed Shape)	302
C4	Noise/Vibration Reduction Program, Kaman UH-2 Main Transmission, Lower Housing (Undeformed Shape)	303
C5	Noise/Vibration Reduction Program, Kaman UH-2 Main Transmission, Computer Generated Model (Incomplete - Input Drive Housing Not Included)	304

LIST OF TABLES

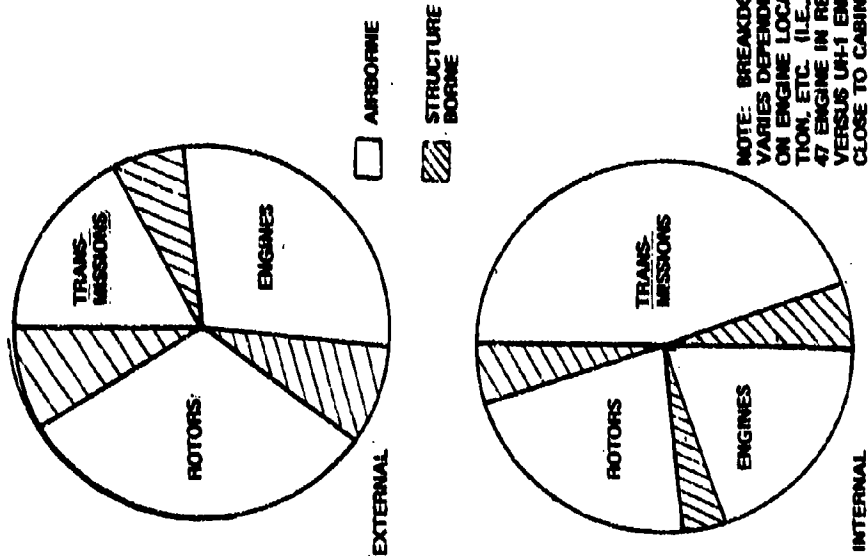
<u>Table</u>		<u>Page</u>
1	CH-47 Forward Transmission Input Pinion; Equivalent Beam Areas (In. ²) Bearings in D-82 Model	54
2	CH-47 Forward Transmission Bevel/Sun Gear; Equivalent Beam Areas (In. ²) Bearings in D-82 Model	54
3	Summary of CH-47 Forward Transmission Housing NASTRAN Model.	64
4	Natural Frequencies	80
5	Tracking Sun Mesh (800 Hz - 1600 Hz)	108
6	Tracking/Bevel Mesh	108
7	Summary of Test Configurations	154
8	CH-47C Forward Transmission Gear Speeds and Mesh Frequencies at Normal Flight Operation Speed	159
9	CH-47C Forward Transmission Gear Speeds and Mesh Frequencies at Normal Ground Operation Speed	159
10	Acoustical Treatment Weight Comparison for Baseline and Modified Transmissions.	188
B1	Material Properties: T50 Graphite Fiber/ 201 Aluminum Matrix	294
B2	Stiffener Comparison	295
C1	Kaman UH-2 Helicopter Main Transmission NASTRAN Model Parameters	305

INTRODUCTION

Considerable attention has been focused in recent years on the reduction of noise levels for both military and civil helicopters as evidenced, for example, by the noise requirements outlined in specification MIL-A-8806, the Occupational Safety and Health Act (OSHA), and the Walsh-Healy Act. Helicopter noise emanates from three major sources - the rotor blade, engines, and transmissions. Exterior noise is dominated by the rotors and engines, although the transmissions also contribute to this noise. Minimization of the exterior noise is important to reduce the annoyance to communities near civil helicopter operations and to reduce the detectable noise signature of military helicopters. The interior cabin noise is predominantly due to the structure-borne and airborne noise generated by the transmissions (Figure 1), with the engines and rotors being secondary sources. The transmissions are generally located near the flight crew and passengers (Figure 2). If preventive measures are not taken, they produce an environment which degrades personnel performance by causing annoyance and undue fatigue of crew and passengers, interferes with reliable communication, causes temporary hearing threshold shifts, and eventually (after repeated extended exposure) causes permanent hearing loss. Furthermore, continuous exposure to high noise levels (in excess of 90 dBA) can cause vertigo, nausea, headache, tenseness, blurred vision, and temporary or permanent loss of hearing. Comfortable interior noise levels are essential for passenger acceptance of civil helicopters. The question of acoustical treatment of helicopter transmissions, therefore, is not whether it shall be done, but how much and in what manner.

In order to ensure compliance with MIL-A-8806 as the best compromise between an optimum acoustical environment and the penalties imposed on an aircraft by the inclusion of a sound-reducing treatment (e.g., weight, cost, maintenance, and incompatibility with other operational requirements), methods of predicting noise levels and tools to perform trade studies (i.e., source noise reduction versus enclosures) must be further developed. Transmission noise is a symptom of the inherent structural vibrations which generate this noise. Until recently, analytical methods have not been available to predict and reduce transmission vibration/noise levels in advance. The conventional means of controlling transmission noise has generally been to add acoustical enclosures after the hardware is built and a noise problem has become evident.

PRECEDING PAGE BLANK



TWIN-ENGINE RATING - 4474 KW AT 246 RPM (6000 HP)
 SINGLE-ENGINE RATING - 2236 KW (3000 HP)
 GROSS WEIGHT - 20000 Lb (9000 Kg)

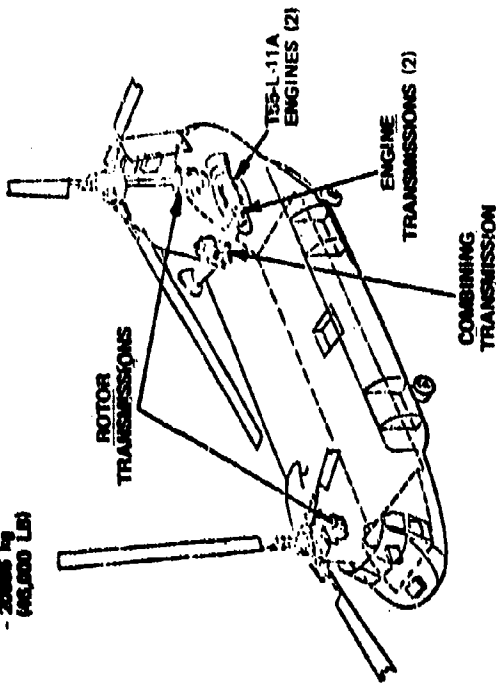


Figure 2. Boeing Vertol CH-47 Helicopter.

Figure 1. Sources of Helicopter Noise.

Significant acoustical treatment is required in order to meet the internal noise levels for military helicopter crew and cabin areas as specified in MIL-A-8806. Operational aircraft employ one or more of several noise control techniques which include skin damping and limp material blanketing to reduce fuselage radiated or structure-borne noise, and high-density rigid sound barriers or source enclosures to reduce the airborne noise. Reduction of the airborne noise by the use of enclosures is considered to be effective, but the actual noise attenuation that can be achieved is dependent upon the completeness of the enclosure. Consequently, the noise reduction limitation in the speech frequency range with typical acoustical enclosures and seals is about 25 dB, with up to 35 dB obtainable through use of improved seal configurations (References 1 and 2).

Further reductions in noise level up to 50 to 60 dB can be achieved with fume-tight enclosures, such as those employed in some commercial helicopters and in some commercial transport aircraft engine installations operating today. To date, fume-type enclosures have not been employed on military helicopters. Since practical enclosures are limited in noise attenuation by unavoidable sound leaks in seams and access doors (Figure 2), adequate attenuation is not provided for advanced helicopter drive systems of increased power (References 3 and 4). As indicated by Figure 3, a 10% opening in the enclosure permits 100% noise escape. Not only do these enclosures impose

1. Sternfeld, H., Spencer, R.H., and Schaeffer, E.G., STUDY TO ESTABLISH REALISTIC ACOUSTIC DESIGN CRITERIA FOR FUTURE ARMY AIRCRAFT, Vertol Division, The Boeing Company, TREC TR 61-72, U.S. Army Transportation Research Command, Fort Eustis, Virginia, June 1961.
2. Sternfeld, H., Schairer, J., and Spencer, R., AN INVESTIGATION OF HELICOPTER TRANSMISSION NOISE REDUCTION BY VIBRATION ABSORBERS AND DAMPING, Vertol Division, The Boeing Company, USAAMRDL TR 72-34, U.S. Army Air Mobility Research and Development Laboratory, Fort Eustis, Virginia, August 1972, AD752579.
3. Hartman, R.M., A DYNAMICS APPROACH TO HELICOPTER TRANSMISSION NOISE REDUCTION AND IMPROVED RELIABILITY, Paper Presented at the 29th Annual National Forum of the American Helicopter Society, Washington, D.C., May 1973, Preprint No. 772.
4. Hartman, R.M., and Badgley, R., MODEL 301 HUH/ATC TRANSMISSION NOISE REDUCTION PROGRAM, Vertol Division, The Boeing Company, USAAMRDL TR 74-58, Eustis Directorate, U.S. Army Air Mobility Research and Development Laboratory, Fort Eustis, Virginia, May 1974, AD784132.

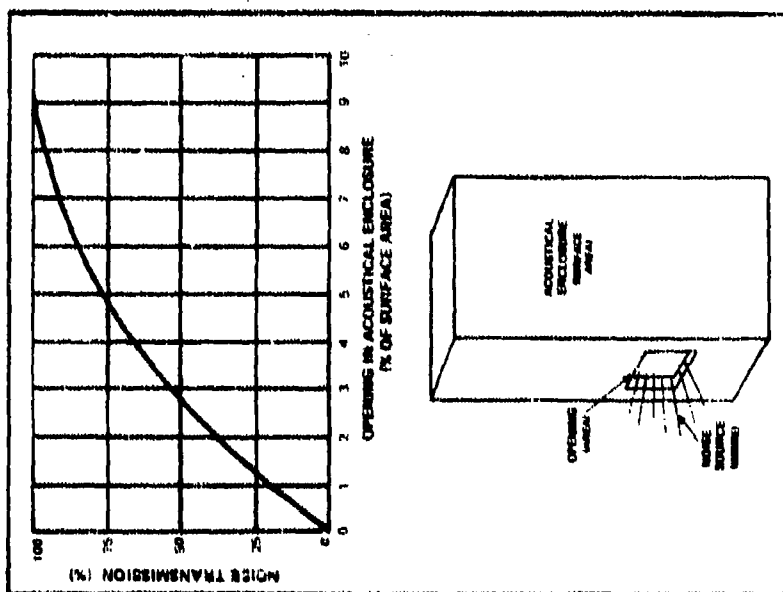


Figure 3. Loss of Noise Isolation as Result of an Opening in Acoustical Enclosure (Reference 5).

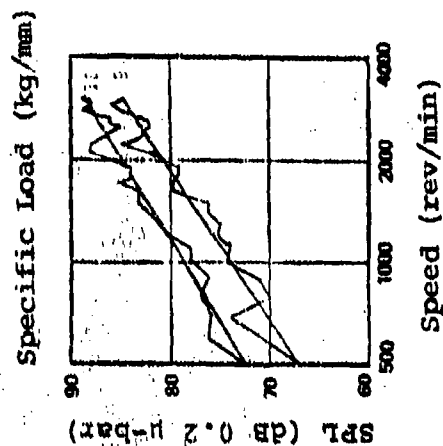


Figure 4. Speed Versus Noise (Reference 6).

5. Lawrence, H.C., NOISE AND OSHA, Design News, March 17, 1975, Pages 61-64.
6. George, C., GEAR NOISE SOURCES AND CONTROLS, Detroit Diesel Allison Division of General Motors Corporation, Presentation Notes.

considerable weight and maintainability penalties, but they do not reduce the deleterious effect of the accompanying vibrations which contribute to material fatigue and fretting at joints.

Transmission vibration/noise levels will continue to increase with increasing speed (Figure 4) and transmitted load (Figure 5). Furthermore, greater loads result in greater housing deflections and misalignment effects which in turn lead to even higher noise levels (Figure 6). Therefore, vibration/noise problems will continue to become more critical as helicopter transmission power and speed requirements increase (Figure 7). These factors have led to a need for the development of techniques for the prediction and reduction of transmission vibration/noise.

A new approach in helicopter transmission noise control aimed at reducing acoustical energy at the source is being investigated herein. The basic premise of this program is to reduce transmission gear shaft deflections at the bearings and avoid resonances by control of dynamic response through stiffness, mass, and inertia distribution, thus reducing transmission noise at its source. Controlling the dynamic response of the transmission is a desirable approach to noise reduction, since reducing deflections at the bearings and avoiding resonances also inherently increases bearing lives and improves transmission reliability.

Previous dynamic testing of a CH-47C forward transmission conducted in the Boeing Vertol closed-loop test stand (Reference 4) provided a substantial volume of vibration/noise data. The transmission was instrumented internally to measure strains, displacements, and accelerations of rotating components, and externally to measure case acceleration and noise levels. This data was obtained and successfully correlated with predicted results. As a result of this test program, the mechanism of noise generation initially postulated has been experimentally verified. Also, application of the partial design tool available in Reference 5 indicated that a significant improvement in noise level could be achieved. This existing data is being used for correlation with the results of the analytical methods.

As a convenience, the lower planetary and spiral bevel meshes will be referred to as "LP" and "SB" throughout the ensuing discussion. In addition, harmonics of frequencies associated with these meshes will be designated by numbers immediately following the abbreviations (e.g., the lower planetary first harmonic would be written as "LP1").

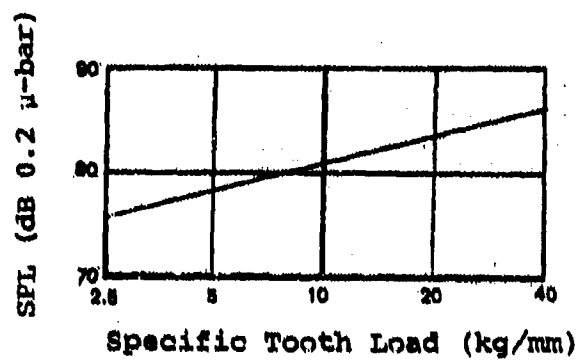


Figure 5. Load Versus Noise
(Reference 6).

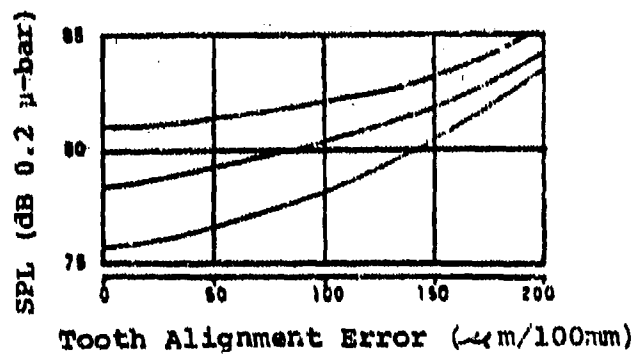
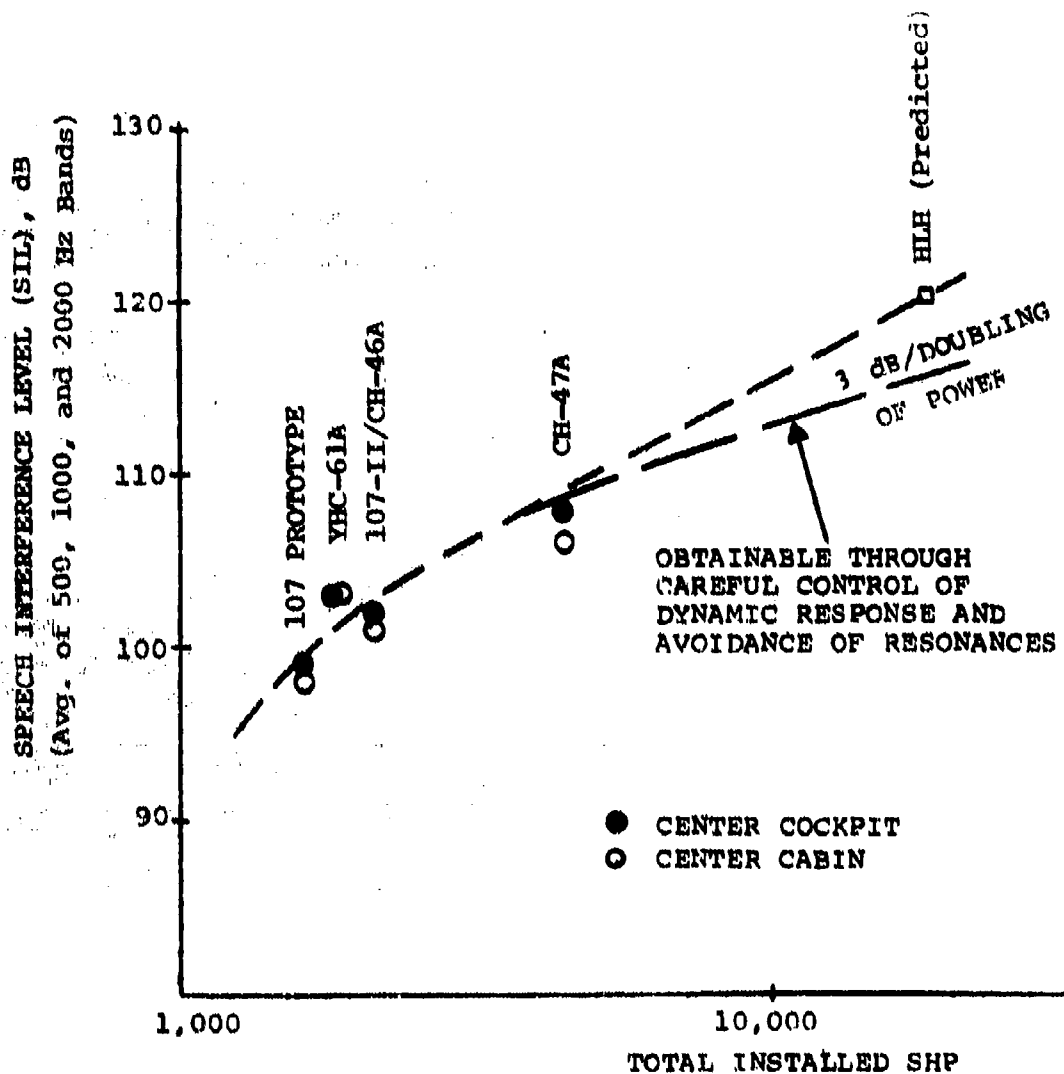


Figure 6. Influence of Tooth Alignment
Error on Gear Noise
(Reference 6).



NOTE:

THE PRIMARY TRANSMISSION
GEAR MESH FREQUENCIES
OF ALL AIRCRAFT INCLUDED
OCCUR IN THE THREE
FREQUENCY BANDS OF THE SIL.

Figure 7. Internal Noise Trend for Untreated Aircraft.

THE NOISE PROBLEM

Because of the general awareness and resentment of the increasing high levels of noise produced by noise sources in the environment and the adverse effects such as ear damage and physical and psychological irritation, greater understanding of sound, its causes, effects and control is necessary. Helicopter transmission noise presents an especially difficult problem due to three factors - high sound pressure levels, frequencies in the range most sensitive to the ear, and pure tonal content.

The sound pressure level (dB) and the frequency (Hz) of sound waves are the properties of sound that are measurable using ordinary engineering techniques. Unfortunately, sound pressure decibels are not the scale that the human ear uses to judge loudness. Loudness of a sound is the magnitude of the auditory sensation produced by the amplitude of the disturbances reaching the ear. Vibrational energy of sound is a physical property, while loudness is a mental interpretation. Loudness of a sound is therefore a subjective quantity and cannot be measured exactly with any instrument. Because hearing is frequency sensitive, rating loudness is a complex task. Since the adverse impact of noise upon human beings is a primary concern, numerous psychoacoustic criteria for assessing the subjective effect of noise have been developed. By any of the numerous standards in existence for scaling annoyance and reactions to noise (Reference 7), transmission noise is particularly objectionable. Sound pressure in excess of 120 dB has been measured for the transmission of a medium transport helicopter (References 3 and 4) which, for comparison, approaches the level of an air raid siren (Figure 8).

A-weighted sound pressure level in dBA units is commonly used to measure the loudness of a sound. This factor provides a single number representing a subjective assessment of the loudness or noisiness of many types of sound and was designed to approximate the response of the human ear. A-level is presently used as a single number rating for industrial noise and its effect on employees by the Department of Labor under the Occupational Safety and Health Act (OSHA), and for traffic and everyday noises by the Environmental Protection Agency (EPA).

The A-weighted sound pressure level is obtained electrically by reducing the effect of low-frequency noise with a series of filters; this frequency weighting is shown in Figure 9. Figure

7. Munch, C., A STUDY OF NOISE GUIDELINES FOR COMMUNITY ACCEPTANCE OF CIVIL HELICOPTER OPERATIONS, Journal of the American Helicopter Society, January 1975, Pages 11-19.

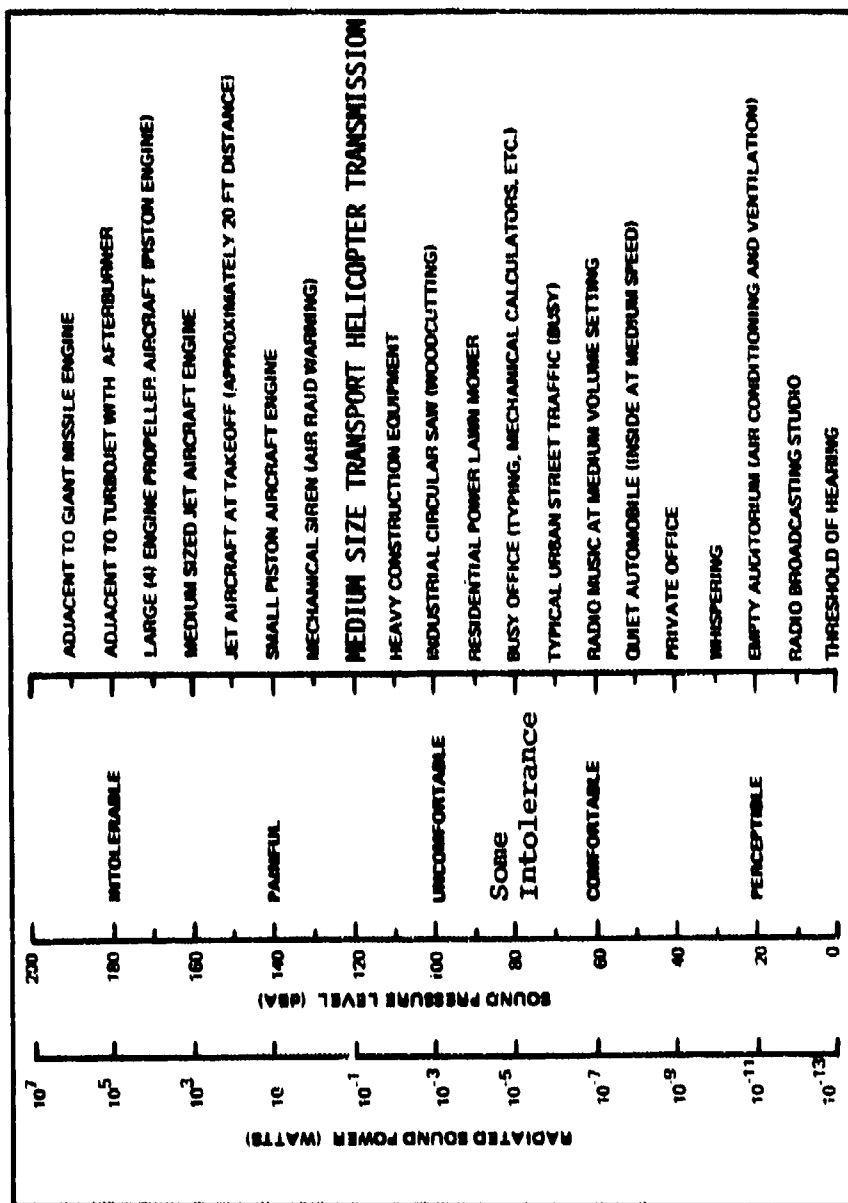


Figure 8. Typical Noise Levels in Variety of Areas and from Several Noise Generating Media. (Chart is merely for comparison, since all noise levels vary with background noise, distance, acoustics, etc.)

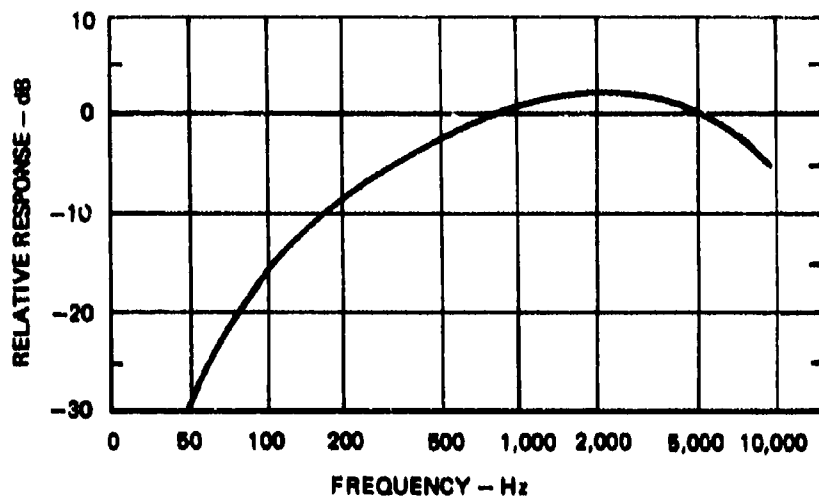


Figure 9. A-Weighting of Sound Pressure Levels.

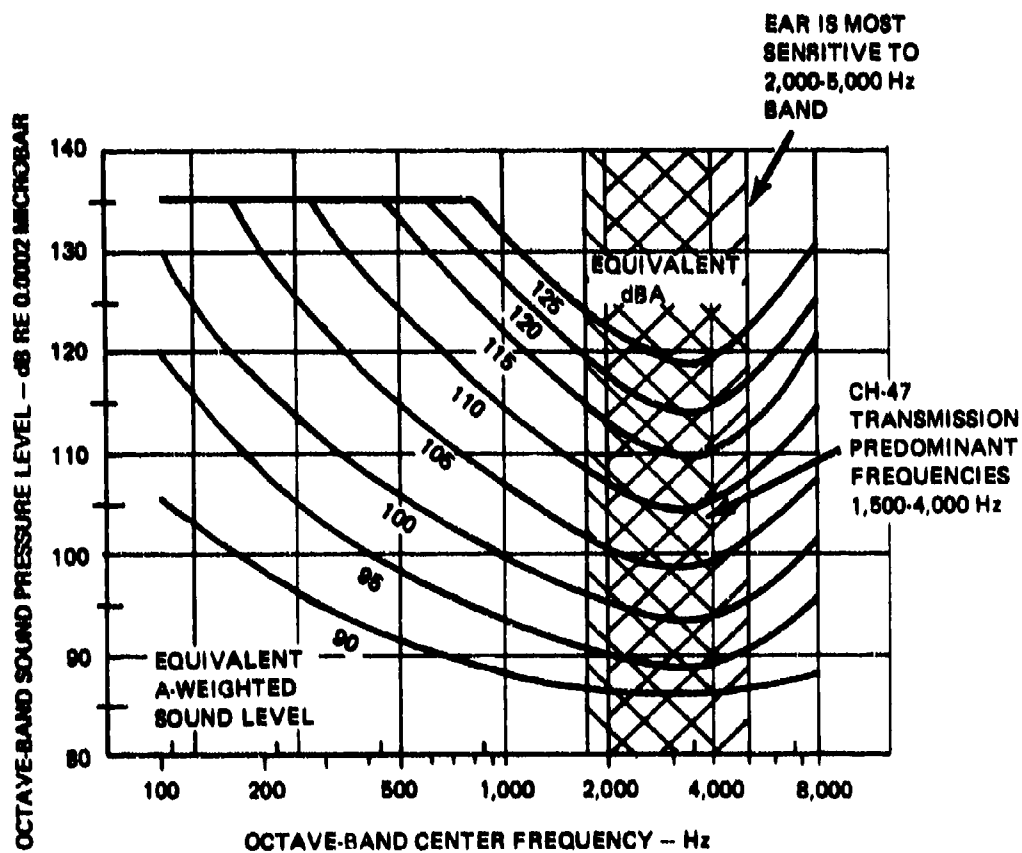


Figure 10. Contours for Determining Equivalent A-Weighted Sound Level.

10 shows contours of equivalent A-weighted sound levels over a range of audible frequencies. Not only is the transmission noise at a high sound pressure level, but also the frequencies at which it occurs are usually within the sensitive and heavily weighted 2,000 to 5,000-Hz range, which is most easily heard and is thus particularly annoying to the human ear.

Pure tonal content, which is characteristic of rotating machinery and results in a high-pitched whine, is subjectively much more annoying and potentially more damaging than broad-band noise. Therefore, for pure tones and narrow-band noise sources (helicopter transmissions), hearing conservation programs such as that recommended by Department of the Army TB MED 251 suggest levels which are 5 dBA below those of broad-band noise.

The task of noise reduction is further complicated by the logarithmic nature of the decibel scale sound levels. This is illustrated by the following simple example. Suppose that an observer is located equidistant among four identical sound sources. When all four sources are operating the observer measures 86 dB. Turning off two of the sources cuts the sound power in half which, from the definition of sound power level

$$PWL \text{ (dB)} = 10 \log_{10} \left[\frac{P}{P_{ref}} \right]$$

reduces the sound level by 3 dB to 83 dB. Turning off one of the two remaining sources again reduces the sound power by one half and reduces the level by 3 dB to 80 dB.

The combined effect of up to ten equal sound sources is shown in Figure 11. The addition of sources with different levels is also easily accomplished using Figure 12. With this figure the difference in the pressure levels of two sounds is used to find the amount by which their combined level exceeds the higher of the two. To add a third level, the same process is applied to combine it with the total of the first two.

The above discussion of noise addition, in which it was shown that a 50% reduction in the sound power radiated by a noise source yields a reduction of only 3 dB, indicates the extreme difficulty in achieving large dB reductions. Assuming a one-to-one relationship between transmission vibration levels and radiated noise, the conclusion which follows is that the transmission vibration level must be reduced by 50% to achieve a 3 dB reduction in noise level.

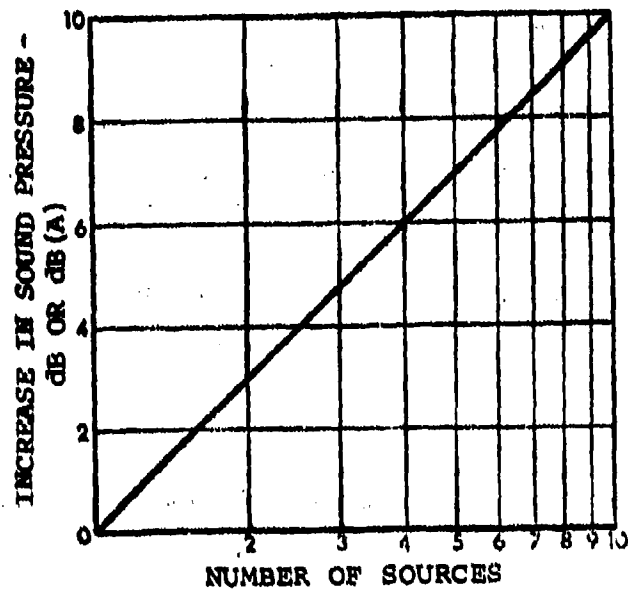


Figure 11. Addition of Equal Sounds.

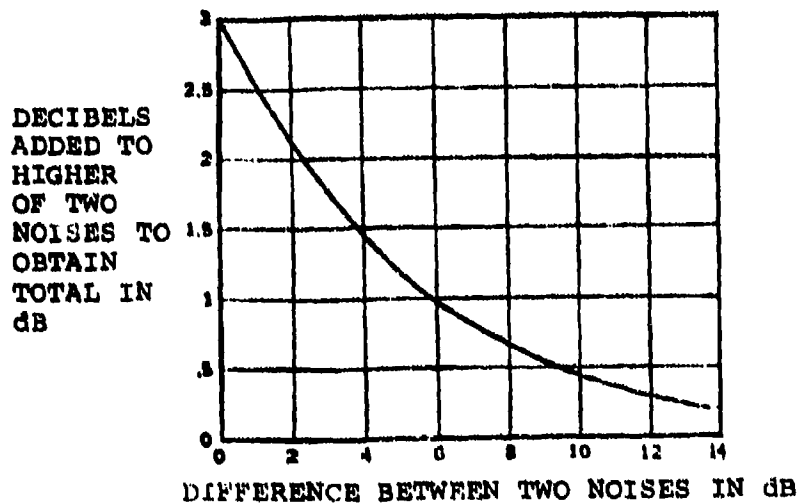


Figure 12. Addition of Unequal Sounds.

ANALYTICAL APPROACH

TRANSMISSION NOISE GENERATION AND REDUCTION

Gear shaft deflections and their effect on case deflections and noise production have been under investigation for several years. The mechanism which has been identified is that noise is generated by the transmission housing as a result of the nonuniform transfer of torque between mating gears (References 3 and 4). The nonuniform transfer of torque is due to tooth profile and spacing tolerance, the elastic deformation (bending and contact) of the gear teeth under load, and the deformation of the tooth backup rim and web. The combined excitation due to all of the above factors is calculated by computer program GGEAR (R-67). This nonuniform transfer of torque produces a dynamic force at the gear mesh frequency (number of teeth x rpm/60) and its multiples for a simple gear set. For the planet/sun gears the mesh frequencies are the difference of the sun cps and the speed of rotation (cps) of the planet center about the center of the sun gear times the number of teeth in the sun gear, plus the harmonic multiples. This dynamic load is calculated by computer program TORRP (R-32). This dynamic force, which excites the coupled torsional/lateral/vertical vibratory modes of the gear shaft, is then applied at the tooth mesh to excite a finite element model of the internal components (shafts, gears, bearings). The vibration, which is calculated by computer program D-82, produces displacements at the bearing locations. These excite the housing and cause it to vibrate at all mesh frequencies, thus radiating noise. The dynamic characteristics of the internal components may magnify this excitation. Furthermore, the dynamic characteristics of the housing, which are calculated using NASTRAN, may magnify its displacements and the resulting noise (Figure 13).

By controlling the dynamic response of the internal components, resonances can be avoided and displacements at the bearing locations can be reduced. This is a desirable approach to vibration/noise reduction, since it also leads to increased bearing life and improved overall transmission performance and reliability. A three-pronged analysis for the reduction of vibration/noise at its source has been developed which includes the reduction of dynamic excitation, the reduction of dynamic response of the shaft and housing, and the use of auxiliary devices for vibration absorption.

An analytical approach using finite element computer techniques has been identified by the contractor for this program. Technical approach for the overall program is depicted in Figure 14.

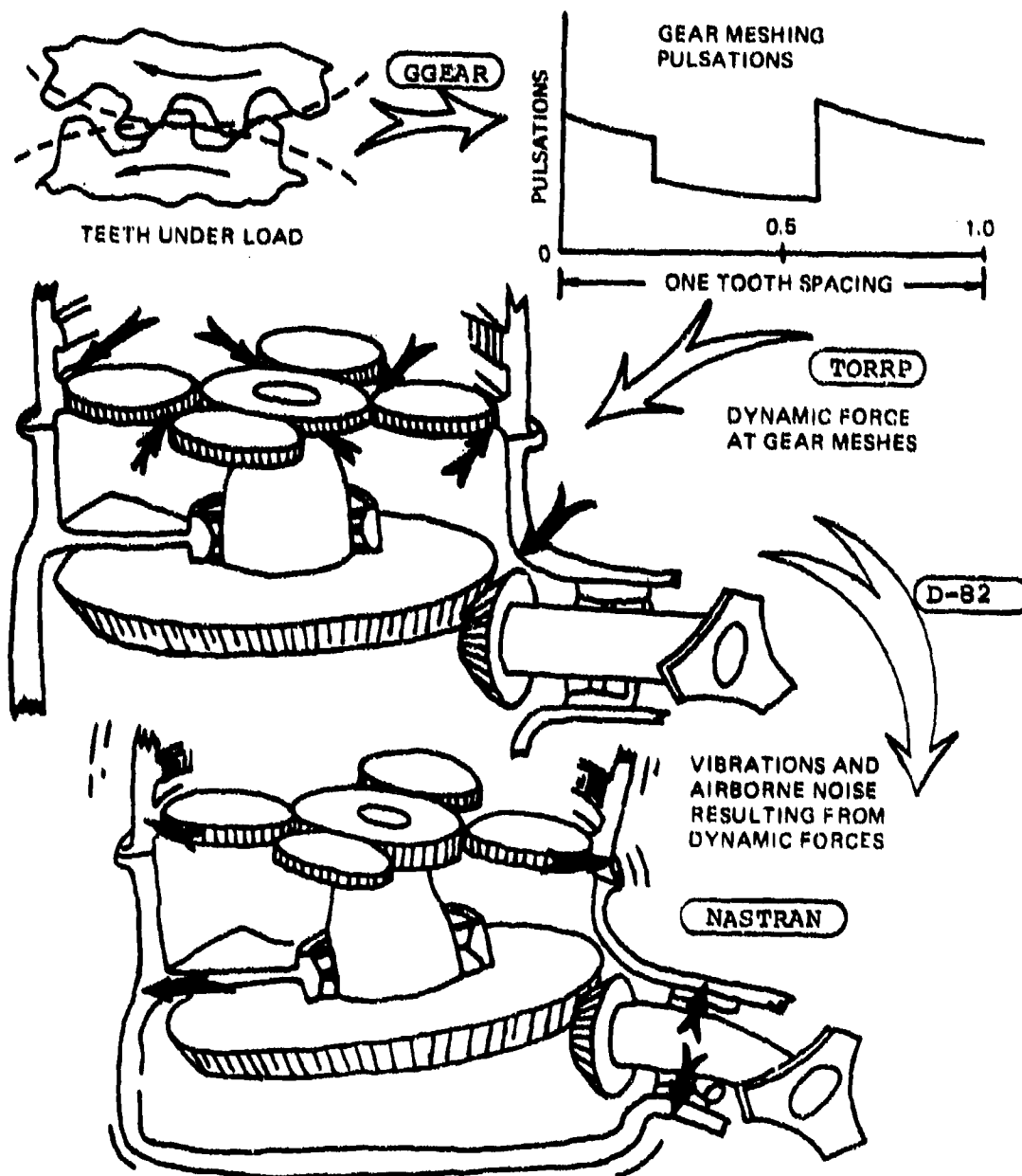


Figure 13. Sources of Transmission Noise.

This figure includes several significant features which are included in the program as follows:

1. The analysis of the internal components includes:
 - Noise calculation based on energy at bearings.
 - Strain energy techniques for vibration reduction.
 - Finite element dynamic stress analysis.
 - Optimization criteria.
 - Extension of GGEAR computer program to include high-contact-ratio spur gears.
 - Computer-generated plotting for model checkout.
2. The analysis of the transmission housing includes:
 - Strain energy techniques for vibration reduction.
 - Finite element dynamic stress analysis.
 - Impedance and mobility methods for vibration absorption.
 - Optimization criteria.

This program is highly computer oriented and makes extensive use of several computer programs as indicated in Figure 14. The accompanying User's Manual describes these computer programs, presents rationale for their use, and discusses their application.

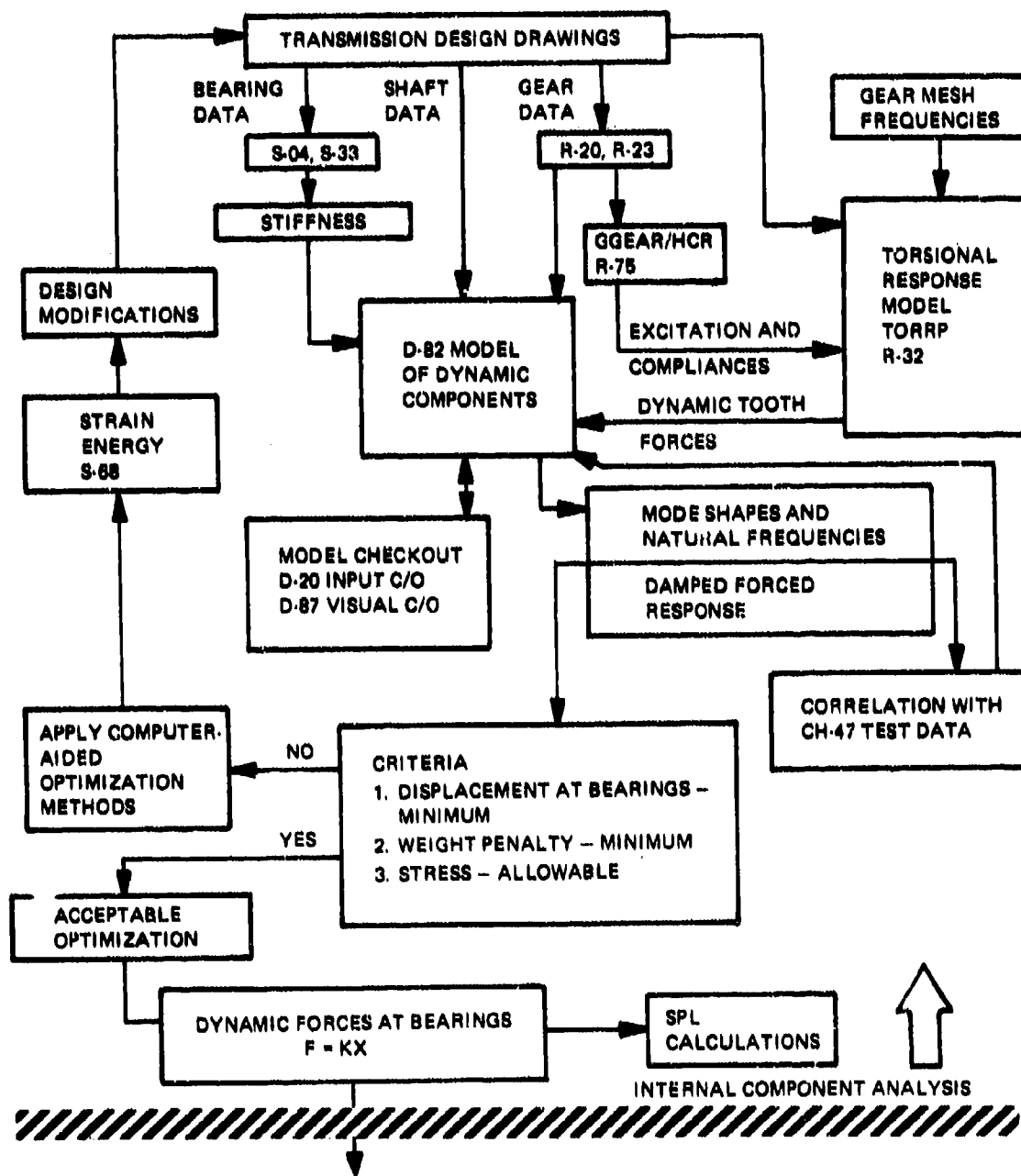


Figure 14. Flow Chart of Technical Approach to Transmission Vibration/Noise Analysis.

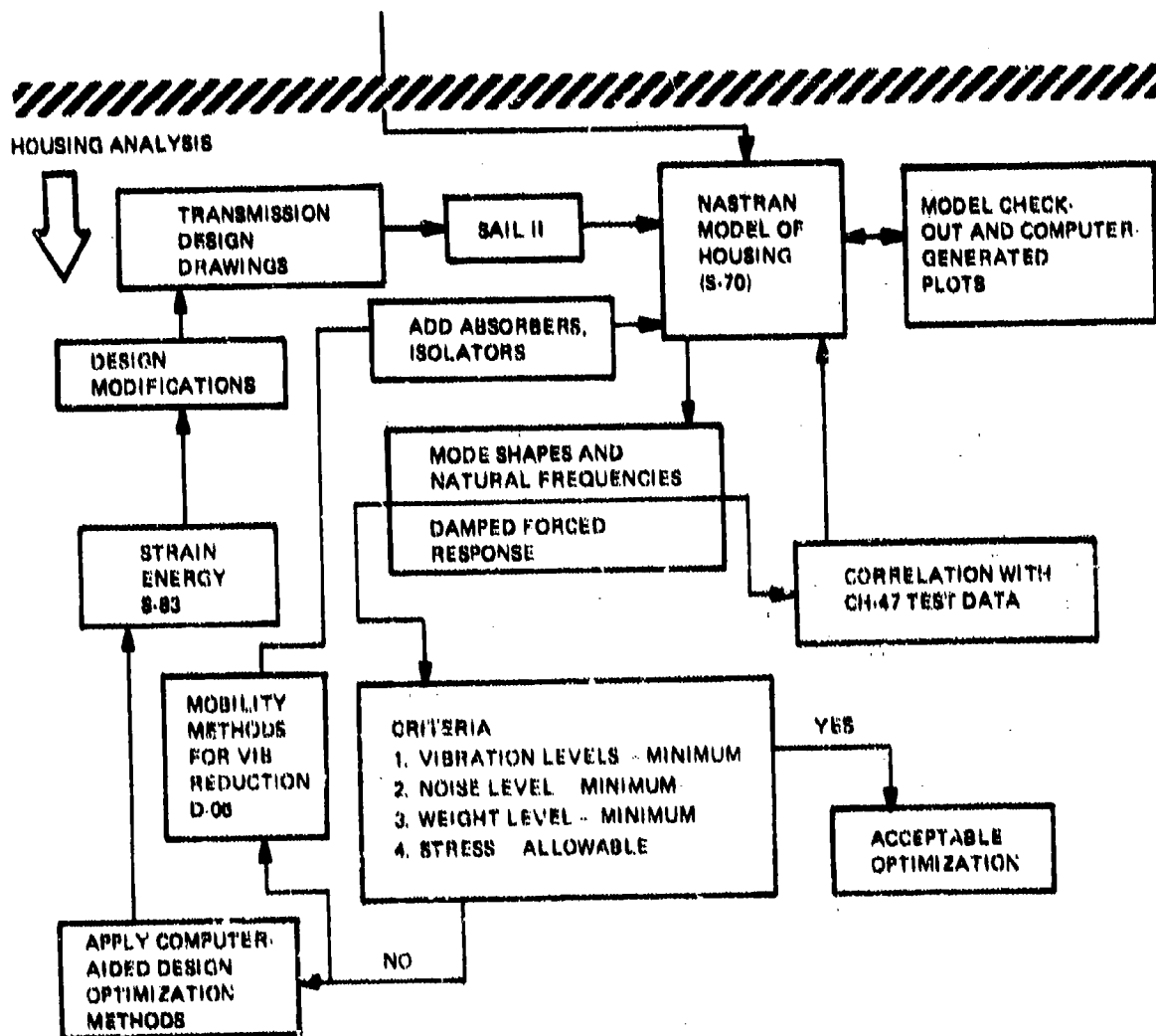


Figure 14. Continued.

INTERNAL COMPONENTS - MODEL AND ANALYSIS

DESCRIPTION OF THE MODEL

The internal components of the CH-47 forward rotor transmission are shown in Figure 15, and the finite element model of these components for use with program D-82 is shown in Figure 16. This model, which was developed previously (Reference 4), was checked and refined. Using the refined model, the dynamic response of the shafts was determined and then a second computer program S-68 (Reference 8) was used to identify the segments of the shafts demonstrating high strain energy densities at the mesh frequencies. By modifying these segments, the dynamic response of the shaft was altered most effectively.

The methodology for the shaft model, the D-82 program, and the normal mode analysis for the damped forced response are given in Reference 4 and will not be repeated here. A listing and further description of D-82 are also given in Reference 8.

DYNAMIC RESPONSE

Figure 17 is a spectrum of the natural frequencies of the baseline internal components, and the first 20 mode shapes have also been automatically plotted (Figure 18). It is to be noted that the results are coupled bending/torsion and that the input pinion and gear/sun/planet systems are also coupled.

The damped forced response of the internal components has also been calculated. Excitation at the lower planetary first harmonic (LP1) is illustrated here. The plotted results (Figure 19) are in absolute value, and the motion is coupled vertical-lateral confined mainly to the pinion components.

The dynamic loads calculated for each bearing at each mesh frequency are phased (sine and cosine components due to structural damping) and subsequently applied to determine the forced response of the transmission case and resulting dB output.

-
8. Sciarra, J.J., USE OF THE FINITE ELEMENT DAMPED FORCED RESPONSE STRAIN ENERGY DISTRIBUTION FOR VIBRATION REDUCTION, U.S. Army Research Office-Durham, Contract DAHC04-71-C-0048, Boeing Vertol Document D210-10819-1, July 1974.

CH-47 TRANSMISSION CROSS SECTION

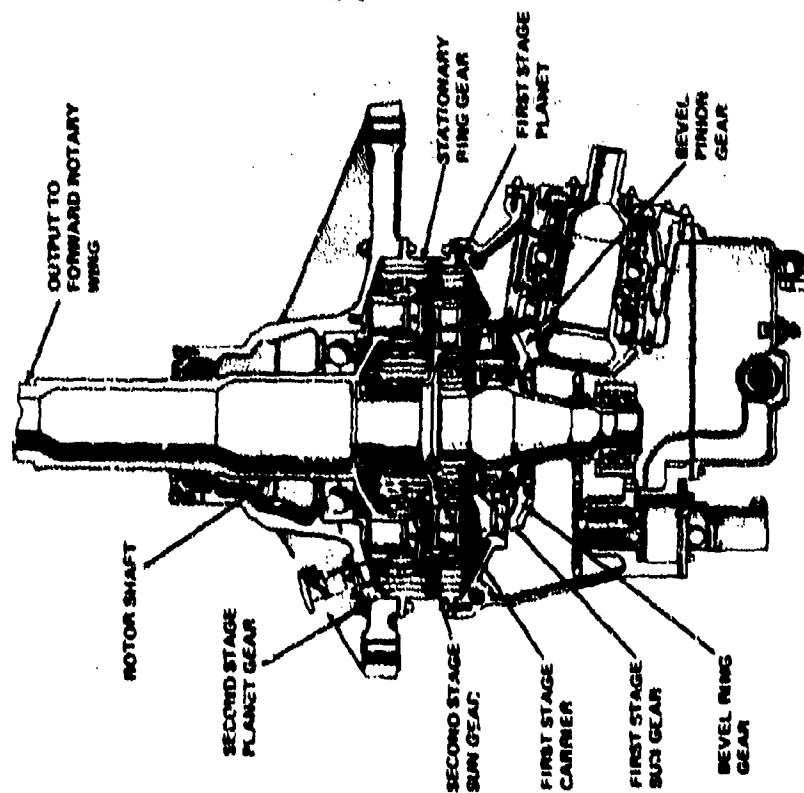


Figure 15. CH-47 Forward Rotor Transmission Internal Components.

MATHEMATICAL MODEL

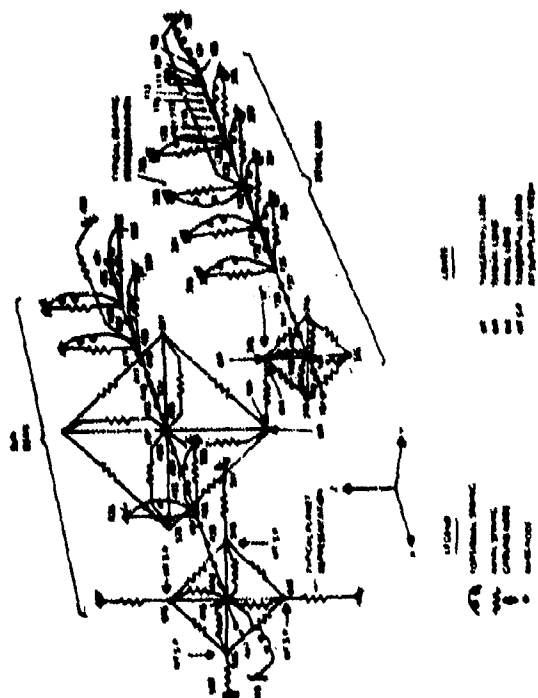


Figure 16. Finite Element Model of CH-47 Forward Rotor Transmission Internal Components.

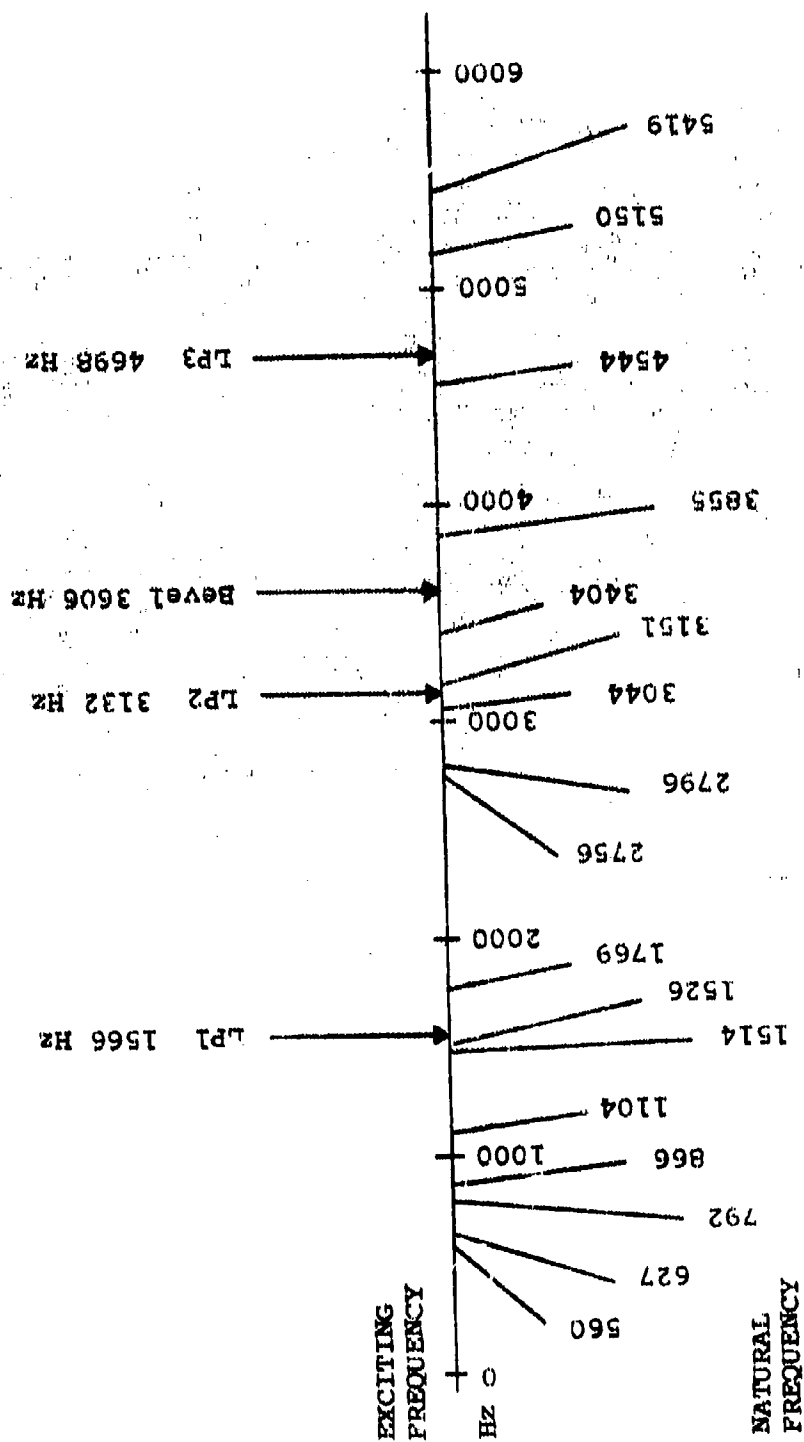
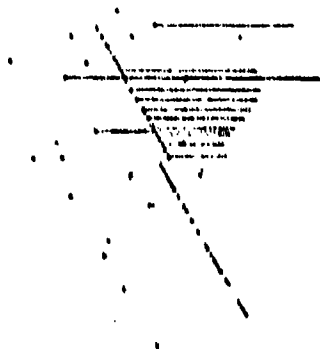
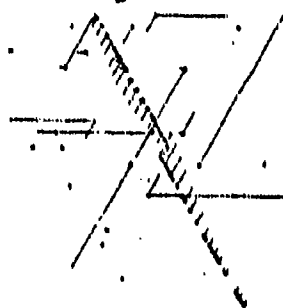


Figure 17. Spectrum for CH-47C Forward Transmission Bevel/Sun Gear and Pinion Plus Lower Planetary Gear System at 80% Torque and 7460 RPM - Sync Shaft (244 RPM - Shaft).

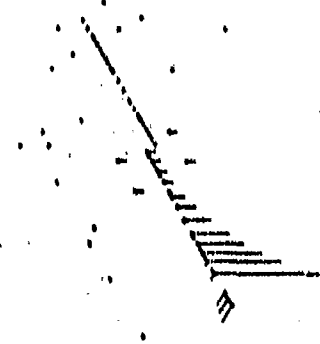
MODE SHAPE 1
240 Hz
SUB VERTICAL



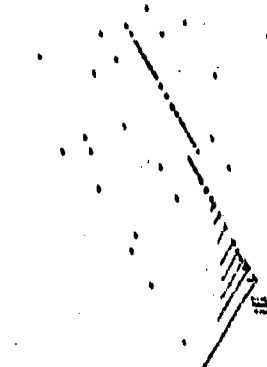
MODE SHAPE 2
417 Hz
LATERAL-SUBSTIS



MODE SHAPE 3
792 Hz
RYEL VERTICAL



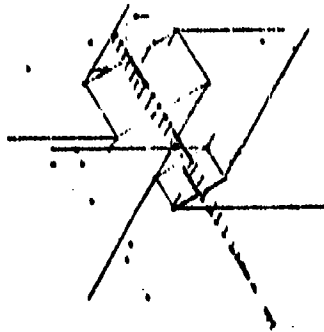
MODE SHAPE 4
846 Hz
RYEL LATERAL



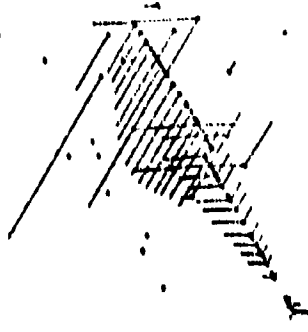
NOTE: POINTS REPRESENT MODEL
NODE POINTS. LINES REPRESENT
DISPLACEMENT VECTORS OF MODEL
NODE POINTS.

Figure 18. Computer-Generated Plots of D-82 Model; CH-47C
Forward Rotor Transmission Internal Components.

MODE SHAPE 5
1534 Hz
LATERAL-TORSIONAL



MODE SHAPE 6
1534 Hz
FOR L-T-TOR-TOR-TOR
VERTICAL-TORSIONAL
A (Hz) = 16.6 (Hz) = 156 Hz



MODE SHAPE 7
1534 Hz
VERTICAL-TORSIONAL
LATERAL-TORSIONAL
A (Hz) = 16.6 (Hz) = 156 Hz



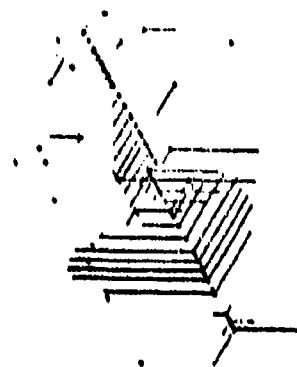
MODE SHAPE 8
1534 Hz
LATERAL-TORSIONAL



NOTE: POINTS REPRESENT MODEL
MODE POINTS. LINES REPRESENT
DISPLACEMENT VECTORS OF MODEL
MODE POINTS.

Figure 18. Continued.

MODE SHAPE 9
2746 Hz
MODE VERTICAL-LATERAL
AND LATERAL TORSION



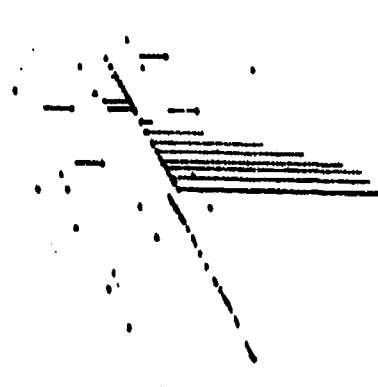
MODE SHAPE 11
3044 Hz
2ND FLOOR LATERAL
 $\Delta(11F2) = 11.6$ (122 = 3132 Hz)



MODE SHAPE 10
2746 Hz
MODE VERTICAL-LATERAL
AND LATERAL TORSION



MODE SHAPE 12
3132 Hz
2ND FLOOR
 $\Delta(12F2) = 16.4$ (122 = 3132 Hz)



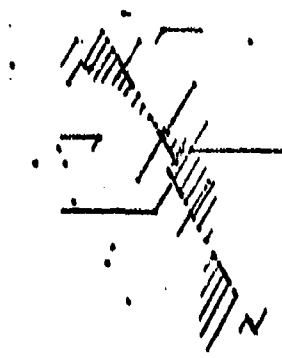
NOTE: POINTS REPRESENT MODEL
MODE POINTS. LINES REPRESENT
DISPLACEMENT VECTORS OF MODEL
MODE POINTS.

Figure 18. Continued.

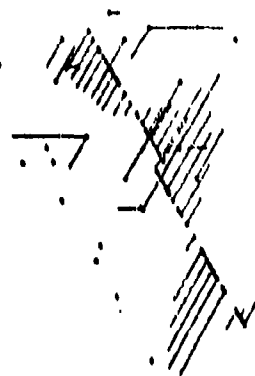
MODE SHAPE 13
3406 Hz
2ND MODE LATERAL-ROTATIONAL
A (Drwell) = 7.3 (Drwell = 3406 Hz)



MODE SHAPE 15
4544 Hz
2ND MODE LATERAL-ROTATIONAL
A (Drwell) = 10.6 (Drwell = 4544 Hz)



MODE SHAPE 14
3406 Hz
2ND MODE LATERAL-ROTATIONAL
A (Drwell) = 7.3 (Drwell = 3406 Hz)



MODE SHAPE 16
5120 Hz
2ND MODE LATERAL-ROTATIONAL
A (Drwell) = 5.7 (Drwell = 5120 Hz)



NOTE: POINTS REPRESENT MODEL
MODE POINTS. LINES REPRESENT
DISPLACEMENT VECTORS OF MODEL
MODE POINTS.

Figure 18. Continued.

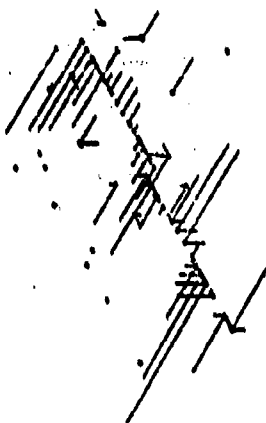
MODE SHAPE 17
5415 Hz



MODE SHAPE 18
5545 Hz



MODE SHAPE 19
5650 Hz



MODE SHAPE 20
7177 Hz



NOTE: POINTS REPRESENT MODEL
MODE POINTS. LINES REPRESENT
DISPLACEMENT VECTORS OF MODEL
MODE POINTS.

Figure 18. Continued.

MODE 7 EXCITED



80% TORQUE
7460 RPM SYEC SHAFT
1P1 1565.8 HZ

NOTE: POINTS REPRESENT MODEL
MODE POINTS. LINES REPRESENT
DISPLACEMENT VECTORS OF MODEL
MODE POINTS.

Figure 19. Typical Damped Force Response.

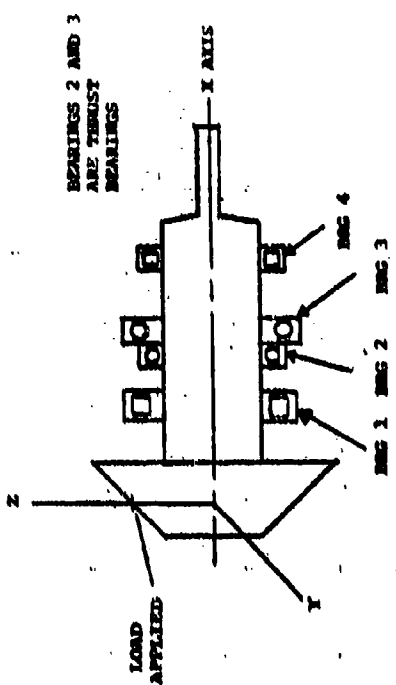


Figure 20. CH-47C Forward Transmission Input Pinion Support Bearings.

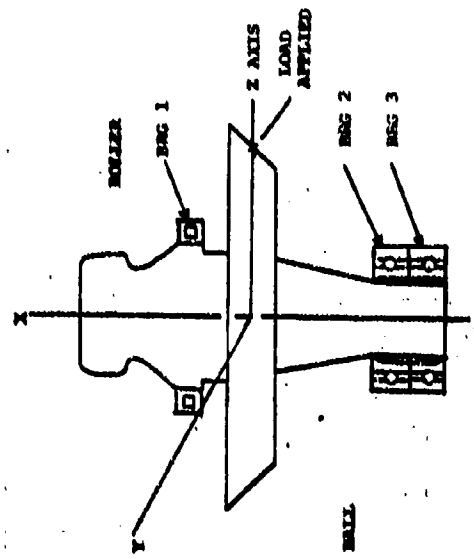


Figure 21. CH-47C Forward Transmission Sun Gear Support Bearings.

SORTIE STUDY

The internal components have been analyzed over the flight profile for a typical sortie. Since a helicopter transmission operates at essentially a constant speed throughout the flight profile, the significant variable is the transmitted torque. Therefore, from an analysis viewpoint a sortie study is actually a study of the nonlinear variation of bearing spring rates with varying torque levels.

The arrangements of the support bearings for the spiral bevel pinion and gear are shown in Figures 20 and 21. The changes in the spring rates with varying torque were calculated using bearing analysis program S-04, and the results are plotted in Figures 22 through 29. Since in the finite element model the bearing stiffness is represented by beams and springs, the effect of the varying operating condition is introduced into the model by adjusting the cross-sectional area (stiffness) and torsional rigidity of these beams. The beam spring stiffnesses and corresponding torsional rigidities are summarized in Tables 1 and 2.

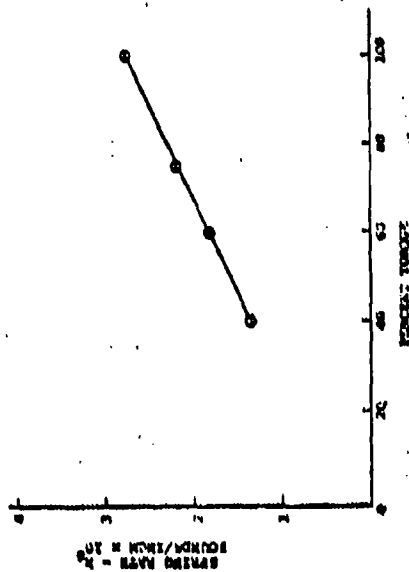


Figure 22. Bearing Spring Rate (k) Along X; CH-47C Forward Transmission Input Pinion (7460 RPM - Pinion).

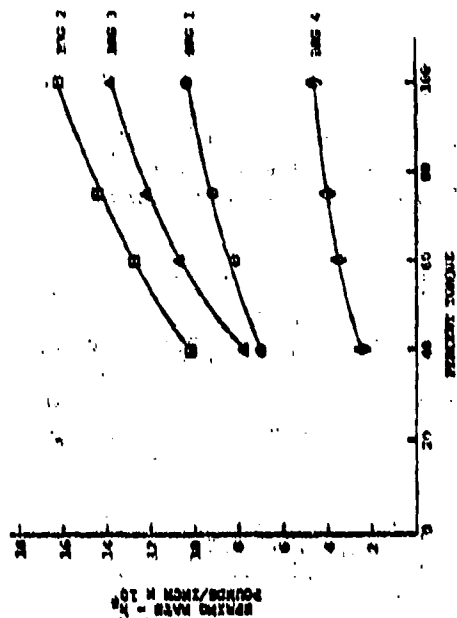


Figure 23. Bearing Spring Rate (k) Along Y; CH-47C Forward Transmission Input Pinion (7460 RPM - Pinion).

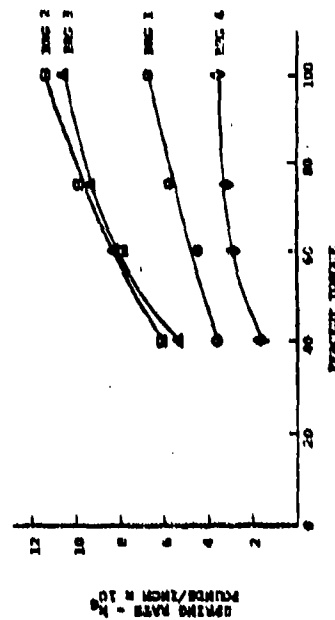


Figure 24. Bearing Spring Rate (k) Along Z; CH-47C Forward Transmission Input Pinion (7460 RPM - Pinion).

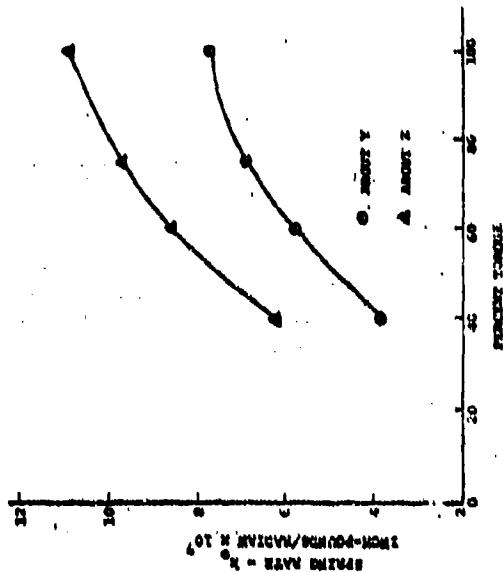


Figure 25. Bearing Spring Rate (k_0); CH-47C Forward Transmission Input Pinion (7460 RPM - Pinion).

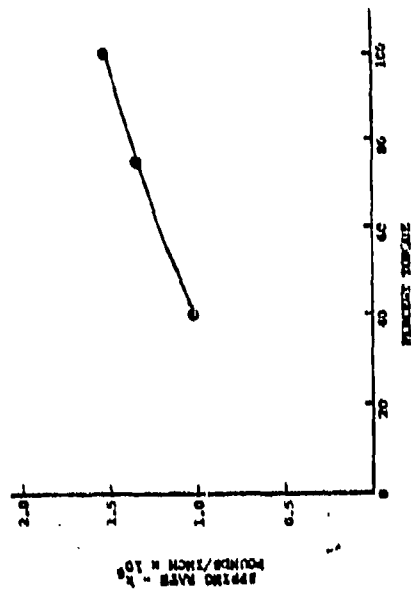


Figure 26. Bearing Spring Rate (k) Along X; CH-47C Forward Transmission Sun Gear (7460 RPM - Pinion).

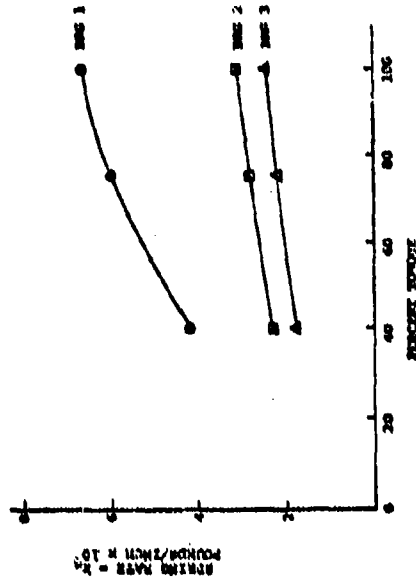


Figure 27. Bearing Spring Rate (k) Along Y; CH-47C Forward Transmission Sun Gear (7460 RPM - Pinion).

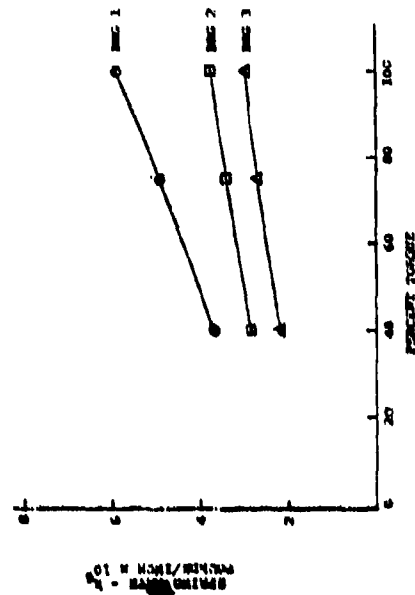


Figure 28. Bearing Spring Rate (k) Along Z; CH-47C Forward Transmission Sun Gear (7460 RPM - Pinion).

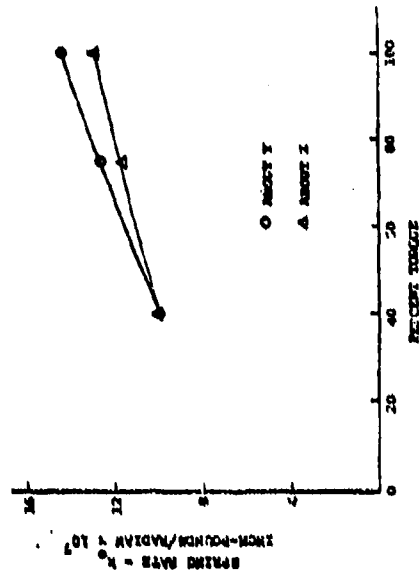


Figure 29. Bearing Spring Rate (k) Along Y; CH-47C Forward Transmission Sun Gear (7460 RPM - Pinion).

TABLE 1. CH-47 FORWARD TRANSMISSION INPUT
PINION; EQUIVALENT BEAM AREAS
(IN.2) BEARINGS IN D-82 MODEL

ACTUALLY $A = \frac{M}{E}$ k is from bearing stiffness
Assume beam length of 10 in.

ELEMENT NUMBER	TORSIONALLY $J = \frac{M}{E}$		
	40%	60%	100%
A1YP	0.80	1.18	1.40
A1ZP	0.57	0.98	1.13
A2YP	2.57	3.58	4.13
A2ZP	1.79	2.71	3.20
A3YP	3.40	4.25	4.87
A3ZP	2.03	2.65	3.33
A4YP	2.33	2.74	3.17
A4ZP	1.21	1.50	1.93

TORSIONALLY $J = \frac{M}{E}$

ELEMENT NUMBER	TORSIONALLY $J = \frac{M}{E}$		
	40%	60%	100%
JTP	33.72	51.40	61.74
JZP	53.88	74.60	86.09

$E = 3.0 \times 10^7$ PSI
 $G = 1.15 \times 10^7$
 $L = 10$ IN.

TABLE 2. CH-47 FORWARD TRANSMISSION
BEVEL/SUN GEAR; EQUIVALENT
BEAM AREAS (IN.2) BEARINGS
IN D-82 MODEL

ACTUALLY $A = \frac{M}{E}$ k is from bearing stiffness
Assume beam length of 10 in.

ELEMENT NUMBER	TORSIONALLY $J = \frac{M}{E}$		
	40%	60%	100%
A1YG	1.41	1.77	2.07
A1ZG	1.22	1.46	1.70
A2YG	0.76	0.87	0.93
A2ZG	0.90	1.03	1.13
A3YG	0.60	0.67	0.73
A3ZG	0.74	0.80	0.90

TORSIONALLY $J = \frac{M}{E}$

ELEMENT NUMBER	TORSIONALLY $J = \frac{M}{E}$		
	40%	60%	100%
JYG	86.68	99.13	112.17
JZG	79.00	95.65	101.74

$E = 3.0 \times 10^7$ PSI
 $G = 1.15 \times 10^7$
 $L = 10$ IN.

TRANSMISSION HOUSING - MODEL AND ANALYSIS

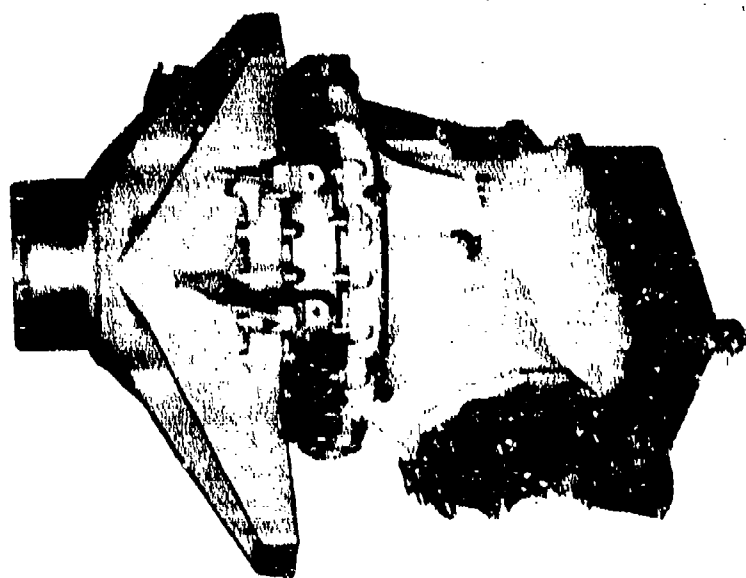
DESCRIPTION OF THE FINITE ELEMENT MODEL

The Boeing Vertol CH-47 forward rotor transmission housing is composed of three major sections: upper cover, ring gear, and bevel gear case (including oil sump). The upper cover provides lugs for mounting the transmission to the airframe and transmits the rotor system loads through its structure and into the airframe. Hence, the entire upper cover structure is a primary load carrying member. The case contains and supports the main spiral bevel gears as well as a lube pump and the oil sump. The upper regions of the case react the bevel gear mesh loads and transmit torque into the ring gear. The lower regions of the case, including the sump, are primarily for containment of the lubricating oil. The ring gear, which connects the upper cover and case, contains the planetary gear system. In addition to reacting the planetary gear mesh loads, the ring gear transmits case loads into the upper cover. This natural division of the housing was adhered to for ease of modeling (Figure 30).

The achievement of good results is dependent upon the development of a model which accurately reproduces the behavior of the actual hardware. Although the solution of a finite element problem is rigorous, the construction of a finite element model is somewhat of an art as opposed to a precise science and is heavily dependant upon the experience and insight of the modeler. The modeler is the interface between the item of hardware being modeled and the analysis being applied to build the model. The critical features of the structure must be accurately represented, but compromises must be made for compatibility with the capabilities of the analytical method. A simple example of model limitations is the restriction imposed upon NASTRAN plate elements that all connecting grid points be nearly co-planar. The degree of detail necessary for a model depends upon several factors, including the type of solution desired (e.g., static or dynamic), the accuracy desired, and the external constraints or applied loads. Model complexity must be traded off against computer time. Ingenuity by the modeler is necessary for minimizing the number of grid points and connecting elements in the model. Therefore, before the actual modeling of the housing structure was started, ground rules for the modeling had to be established.

The first aspect to be addressed was the required grid mesh fineness. Ideally it is desirable to build the model with a fine grid mesh to achieve greater accuracy. However, in practice a trade-off is necessary to establish a grid mesh fine enough to yield sufficient accuracy but not so fine that

CH-47 FORWARD TRANSMISSION



TRANSMISSION HOUSING MODEL

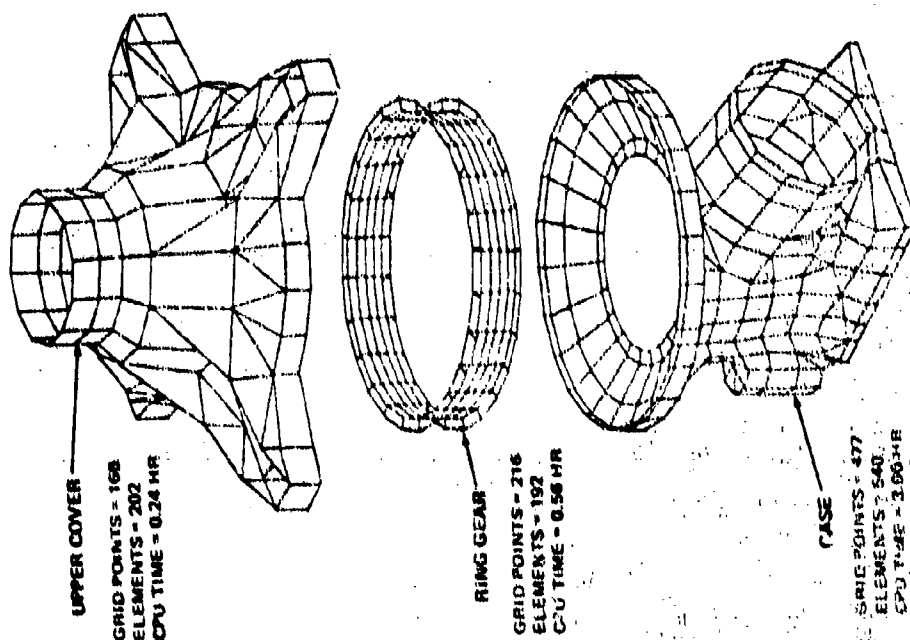


Figure 30. Boeing Vertol CH-47 Helicopter Forward Rotor Transmission Housing and WASTRAY Model.

computer execution time becomes prohibitive. With the study of the circular cylinder and turbine disc models described in the User's Manual as background, an azimuthal spacing of about 15° was required to provide acceptable accuracy. This azimuthal spacing was thus established for both the ring gear and case model, since it was necessary to analyze the behavior of these components in detail. The vertical spacing was generally dictated by the natural changes in hardware shape and wall thickness. For the case a vertical spacing of about 2 inches was used, resulting in elements with linear dimensions ranging from about 1.75 to 3.25 inches. For the ring gear a vertical spacing of from 0.5 to 1.5 inches was used, resulting in elements with linear dimensions ranging from about 0.5 to 2.9 inches. The upper cover was modeled using a coarser grid mesh, since the intent of this aspect of the work is not a detailed model and analysis of the upper cover but rather a more general analysis of its gross effect on the other parts of the housing. The azimuthal spacing for the upper cover is predominantly 30° , although a spacing of 15° was used at the lower boundary for compatibility with the ring gear. A vertical spacing of from 1.4 to 6.7 inches was used. For each portion of the housing, the grid mesh fineness established provides an acceptable accuracy/computer time trade-off for the dynamic analysis conducted herein.

Another aspect of the general modeling procedure which had to be established was the grid point fixity, particularly at the boundaries between the upper cover, ring gear, and case. It would be most desirable to treat the entire housing as a single model, but due to the large computer execution time it was necessary to analyze each of the three sections (upper cover, ring gear, and case) as separate models. Running the three sections independently introduced the requirement to establish constraints on the grid points which form the boundaries between the mating sections. Fixity representative of a simply supported structure was imposed by applying single point constraints (SPC) to constrain the three translational degrees of freedom to zero motion for each boundary grid point along the upper cover/ring gear and ring gear/case interfaces. This fixity simulates the restraint imposed upon the boundary of one member by the structure of its mating member.

Based on the grid mesh guidelines outlined previously and locally modified to be compatible with the hardware structure, the locations of the geometric grid points for the model were defined from design drawings and by cross-checking on an actual housing. Figure 31 shows the case hardware and the measuring instruments used. CQUAD2 (quadrilateral) and CTRIA2 (triangular) homogeneous plate (membrane and bending) elements were used to connect the grid points and build the NASTRAN structural model. The physical properties (thickness and

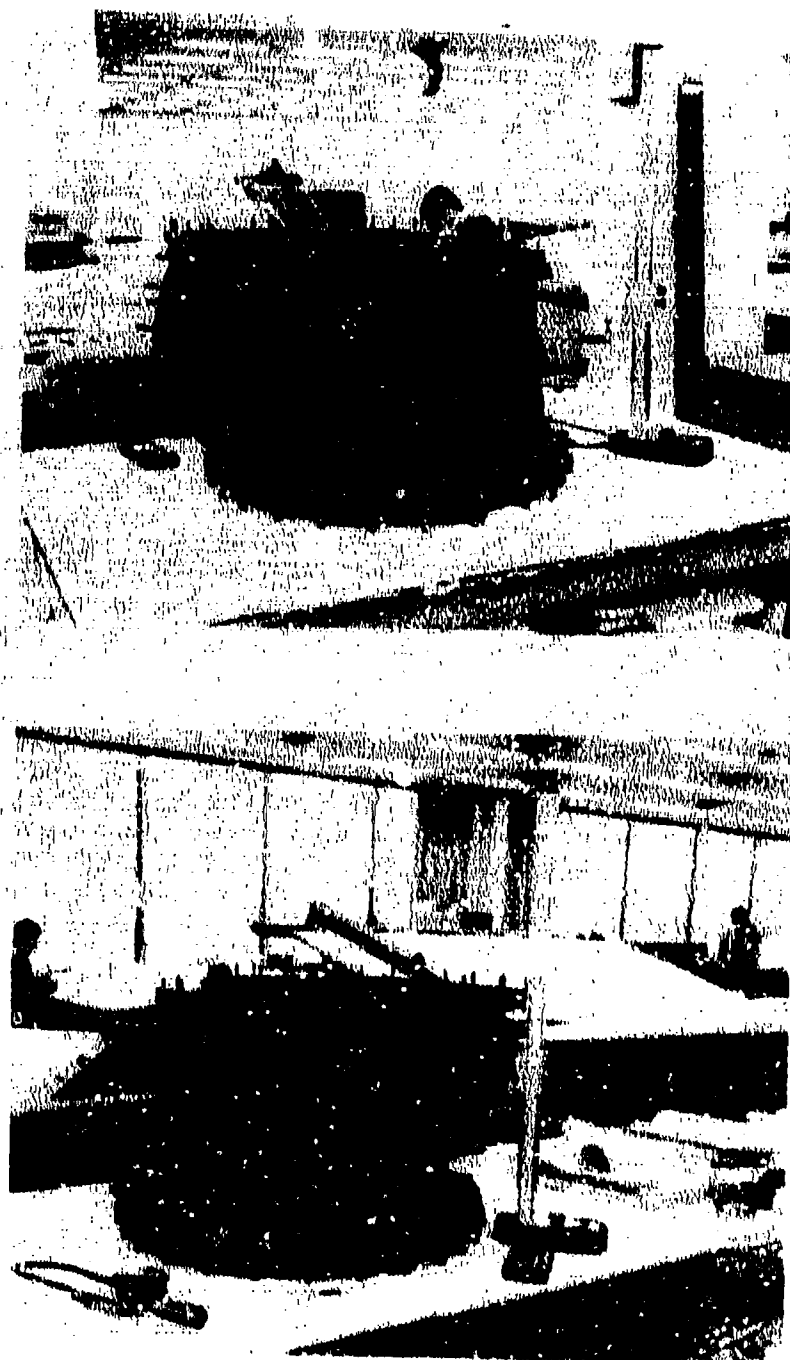


Figure 31. CH-47 Forward Transmission Case and Measuring Instruments.

material) were defined for each element. The mass of each element is considered to be distributed at the grid points connected by the respective element.

A Boeing preprocessor program (SAIL II - Structural Analysis Input Language) for the automatic generation of grid point coordinates and structural element connections was used. This preprocessor allows the user to take advantage of any pattern which occurs in the data by providing straightforward techniques for describing algorithms to generate blocks of data. SAIL II was used to generate the ring gear and the upper cover, including the mounting legs. One leg was modeled and then the other three were generated by a data block transformation. SAIL was also used extensively to generate the symmetrical portions of the case: upper mounting flange, input pinion barrel, pump support, and pump drive support regions. The modeling of the irregular portions of the case as well as the connecting of the SAIL generated regions was done manually. The extensive computer-generated plotting capability of NASTRAN was used both to plot the undeformed structure to debug the structural model and to plot the deformed structure to define the mode shapes. Figures 32 and 33, which show plots of various orientations of the case model, demonstrate the versatility of the NASTRAN plotting capability.

For ease of identification the case was subdivided into several regions and the grid points in each region were labeled with a specific, but arbitrary, series of numbers. Although these grid point numbers act only as labels, they affect the bandwidth of the stiffness and mass matrices. To minimize the matrix bandwidth for most efficient running of NASTRAN, the BANDIT computer program (Reference 9) was used to automatically renumber and assign internal sequence numbers to the grid points. The output from BANDIT is a set of SEQGP cards which are then included in the NASTRAN bulk data deck and which relate the original external grid numbers to the internal numbers.

The model includes grid points representative of the structure where the shafts are supported by their bearings as well as grid points representative of the planet-ring gear tooth meshes. These grid points are used to apply the dynamic excitations at the mesh frequencies to analytically excite the housing. Although each geometric grid point has six possible degrees of freedom (three translational and three rotational), the displacements normal to the outer surface of the housing

-
9. Everstine, G., BANDIT - A COMPUTER PROGRAM TO RENUMBER NASTRAN GRID POINTS FOR REDUCED BANDWIDTH, Naval Ship Research and Development Center Technical Note AML-6-70, February 1970.

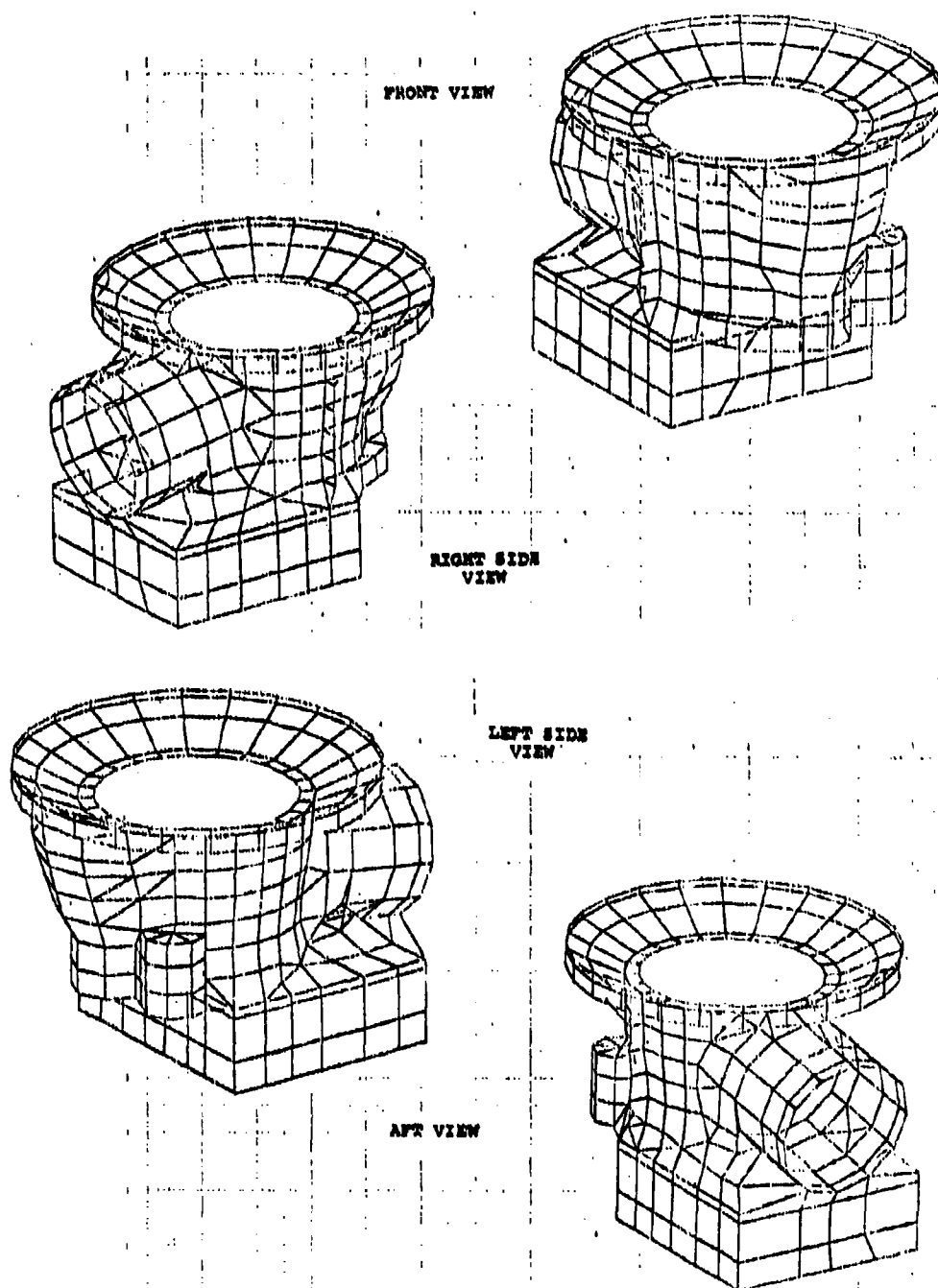


**Figure 32. Computer-Generated Plots of NASTRAN Model;
CH-47C Forward Rotor Transmission Case
With Sump.**

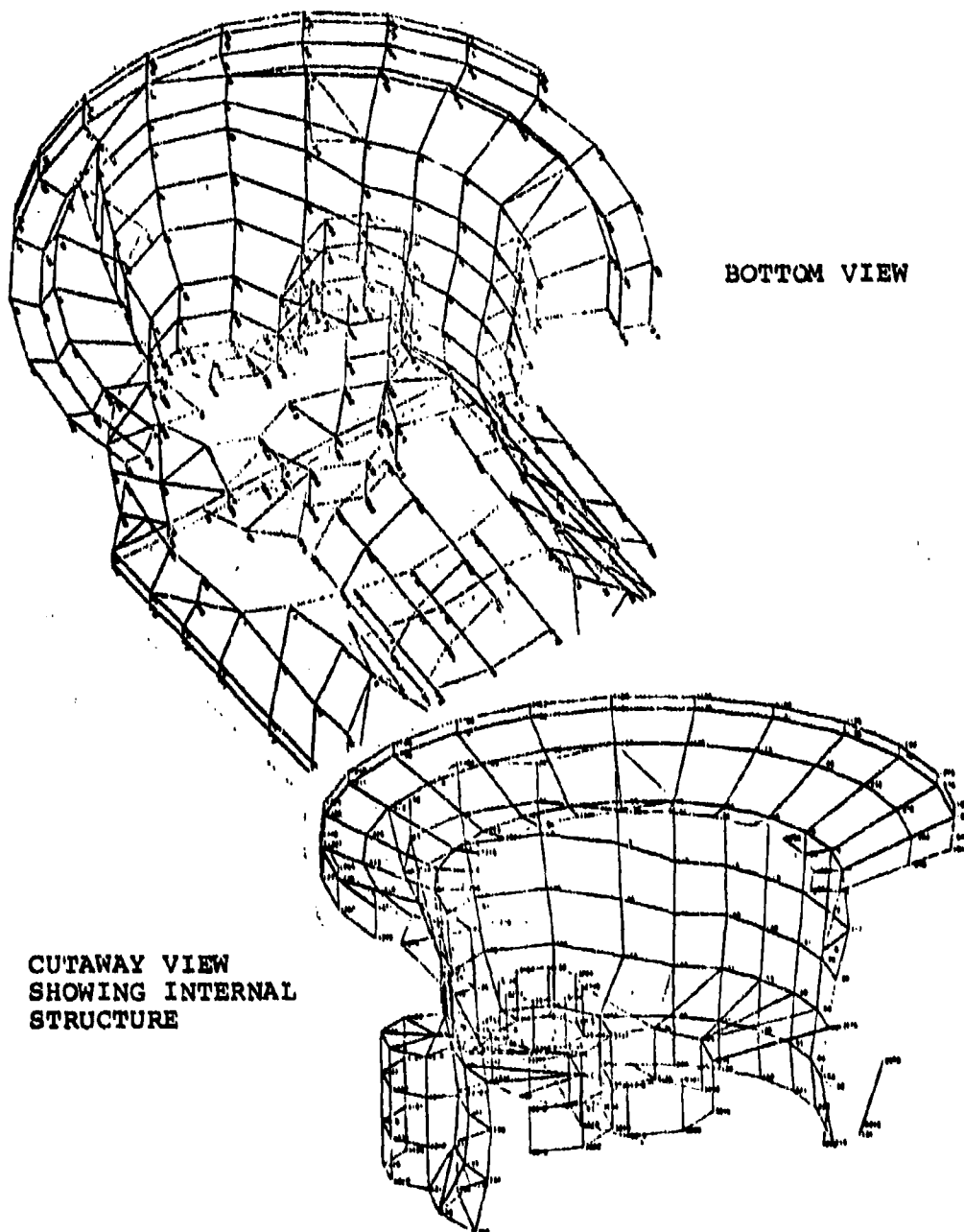


Figure 33. CH-47 Forward Transmission NASTRAN Model.

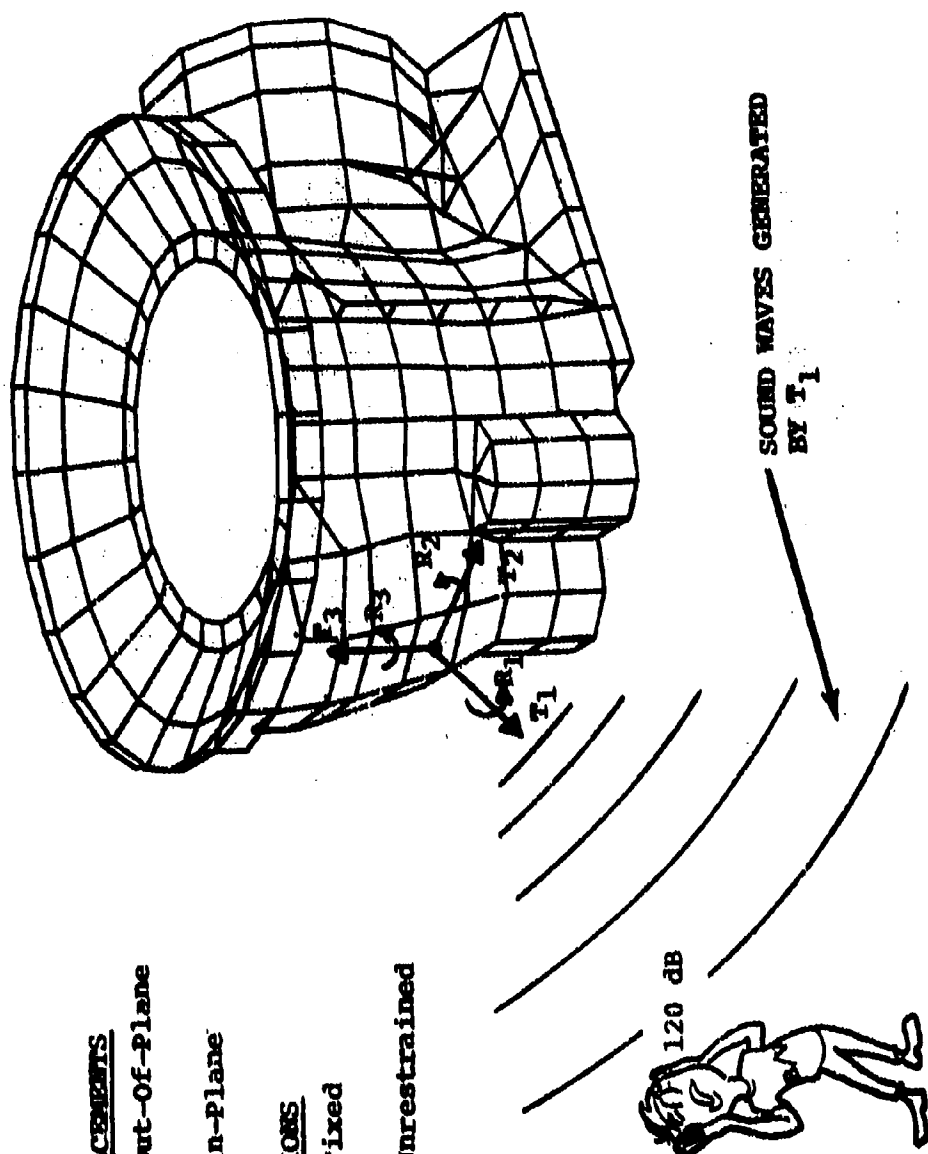
are of most interest for noise evaluation, since this out-of-plane motion generates sound waves. This is illustrated in Figure 34 which shows that as the vibrating body moves forward from its static equilibrium position, it pushes air before it and compresses it. At the same time, a rarefaction occurs immediately behind the body and air rushes in to fill this empty space. In this way the compression of the air is transferred to distant regions and the air is set into motion known as sound waves. The result, sound, is the auditory sensation produced in the human ear by the disturbance of air.

To conveniently evaluate the motion normal to the case surface, numerous local coordinate systems were defined and oriented such that the displacements and accelerations calculated at each grid point could be referred to a coordinate system having an axis normal to the case surface. This was not necessary for the ring gear, since the existing global cylindrical coordinate system provided a normal component. One degree of freedom, rotation about the normal to the surface, was constrained since the stiffness for this component is undefined for NASTRAN plate elements. The other two rotational degrees of freedom were omitted. All translational degrees of freedom were retained to accurately represent the motion of the actual housing. Because of the large model size, the Guyan reduction technique was used to reduce the size of the analysis set. Distributed areas of interest were defined as an ASET (solution set). The Givens method of eigenvalue extraction was used and the model parameters are summarized in Table 3. The NASTRAN weight generator feature was also used by means of a PARAM card in order to calculate the model weight. The weight of the actual hardware items and the weight as predicted by the NASTRAN model are also summarized in Table 3.

The contractor is confident that the model is an accurate representation of the actual transmission housing for the following reasons:

1. Use of a widely accepted and thoroughly validated computer program (NASTRAN).
2. Extensive computer-generated plotting capability used to debug model.
3. Cross-checking of model, design drawings, and hardware.
4. Good correlation of model and hardware weights.

The natural frequencies and mode shapes, as well as the damped forced response for the gear mesh frequencies, have been determined. The dynamic forces at the bearings which excite the system were determined by utilizing the computer model of the CH-47 forward transmission dynamic components discussed in the previous section.



DISPLACEMENTS

T_1 = Out-Of-Plane

T_2 = In-Plane

T_3

ROTATIONS

R_1 = Fixed

R_2 = Unrestrained

R_3

Figure 34. Transmission Noise Generated by Out-Of-Plane Displacements of Housing.

TABLE 3. SUMMARY OF CH-47 FORWARD TRANSMISSION HOUSING NASTRAN MODEL

MODEL PARAMETERS						
NUMBER		NUMBER		NUMBER		CPU TIME (HOURS) *
GRID POINTS ELEMENTS		DEGREES OF FREEDOM		BANDWIDTH		
		TOTAL SPC OMIT RETAINED		FULL REDUCED COLUMNS		ACTIVE
Upper Cover	160	202	960 184 614 162	34	162	0 0.24
Ring Gear	216	192	1296 216 828 252	-	252	0 0.75
Case	477	540	2862 529 2024 309	61	309	0 3.00
TOTAL	853	934				

*RIGID FORMAT 3 ON IBM 370

COMPARISON OF CALCULATED AND ACTUAL WEIGHTS*

	MODEL	HARDWARE	DIFFERENCE
Sump	3.7 kg (8.2 lb)	5.5 kg (12.2 lb)	**
Case	25.1 kg (55.4 lb)	24.6 kg (54.2 lb)	+ 2.2%
Ring Gear	34.9 kg (77.0 lb)	34.9 kg (77.0 lb)	0% (Lumped Masses for Teeth)
Upper Cover	62.8 kg (138.5 lb)	64.1 kg (141.4 lb)	- 2.0%

*(Case weight based on AZ91C cast magnesium alloy, density .065 lb/in³; upper cover weight based on 2014-T6 forged aluminum, density .101 lb/in³, both per MIL-HDBK-5B 1 September 71.)

**Model excludes internal passageways.

Upper Cover Model Results

A computer-generated plot of the finite element model of the upper cover is provided in Figure 35. The dynamic response of the model is summarized by the spectrum (Figures 36 and 37). The model was analyzed with the four legs simply supported to represent attachment to the airframe structure. Also, the grid points along the upper cover/ring gear interface were simply supported to simulate the constraint which would be imposed by the ring gear structure if attached.

Ring Gear Model Results

In order to obtain all the modes, the entire ring was analyzed as a simply supported structure. The effect of the mass of the gear teeth was included by using concentrated masses (CONMASS), but their contribution to radial (hoop) stiffness was excluded. An automatic plot of the ring NASTRAN model is shown in Figure 38. Also in the figure, the natural frequencies of the ring are shown on the lower portion of the spectrum. The main exciting mesh frequencies are shown on the upper portion of the spectrum. It is noted that the natural frequencies are embedded in the exciting mesh frequencies, which could lead to considerable amplification of noise and vibration. A detuning process was conducted using S-83 and is described in a later section.

Case Model Results

The case was initially analyzed without the sump attached and with a free boundary condition at the case/ring gear and case/sump interfaces. The frequency spectrum for this configuration is shown in Figure 39, and a NASTRAN plot of the housing 46th mode, which has a natural frequency closest to the LP2 exciting frequency, is shown in Figure 40. Subsequently, to provide more realistic boundary constraints, the sump was attached to the case and the constraints at the grid points on the case boundary representing the case/ring gear interface were changed from a free to a simply supported condition. The dynamic analysis of the model with the sump attached and with the new boundary condition was rerun on NASTRAN Rigid Format 3. The calculated natural frequencies of the case with sump attached and the main exciting frequencies are plotted on the spectrum shown in Figure 41. The spacing between the natural frequencies of the case has generally been increased and the rigid body modes which previously existed have been eliminated. The mode shapes of the case for the natural modes closest to the exciting frequencies are plotted in Figure 42. The results of the dynamic analysis of the case (with sump attached) were evaluated using the strain energy program (S-83) and the areas for modification of the case structure were defined.

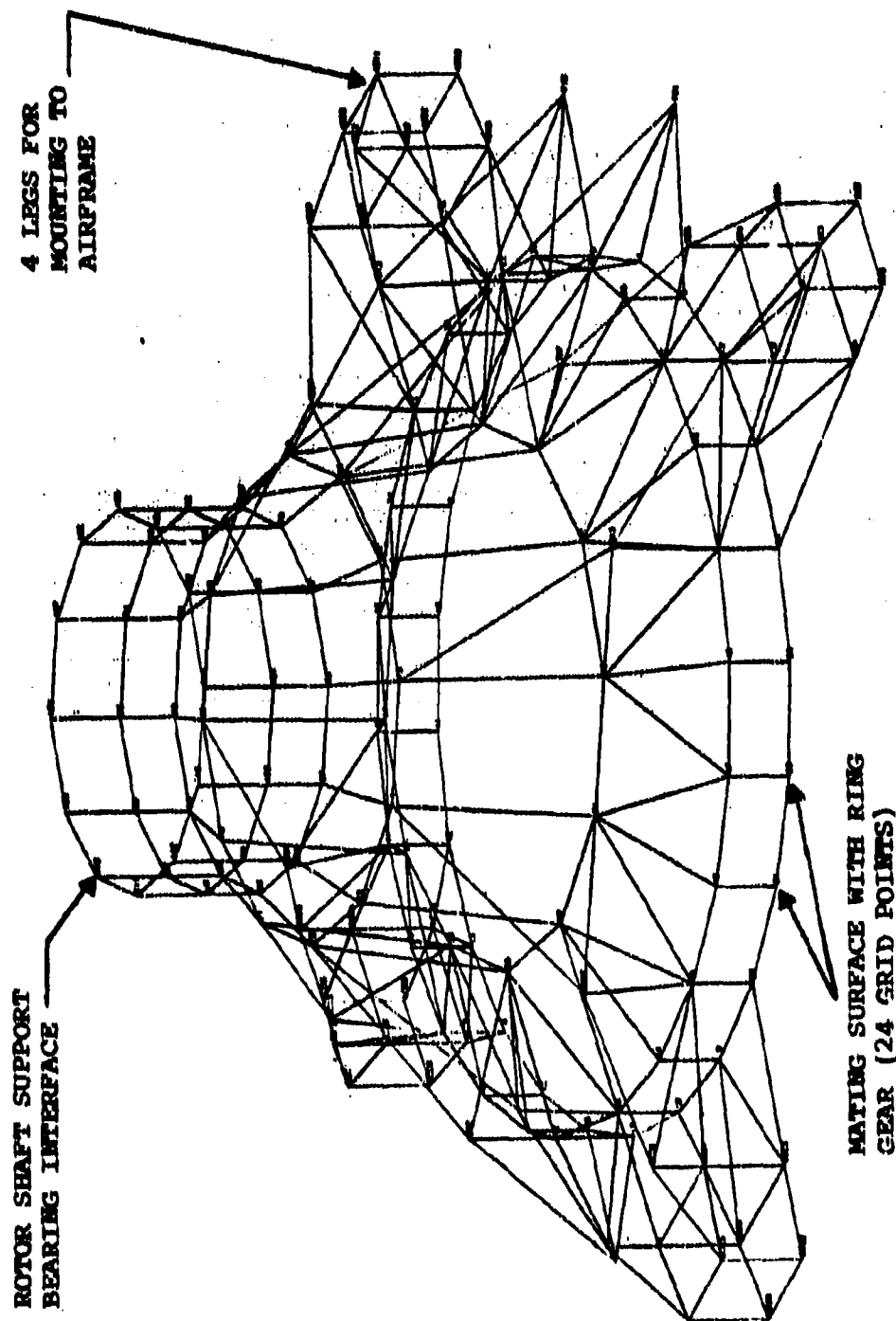


Figure 35. Computer-Generated Plot of NASTRAN Model;
CH-47C Forward Rotor Transmission Upper Cover
(Undeformed Shape).

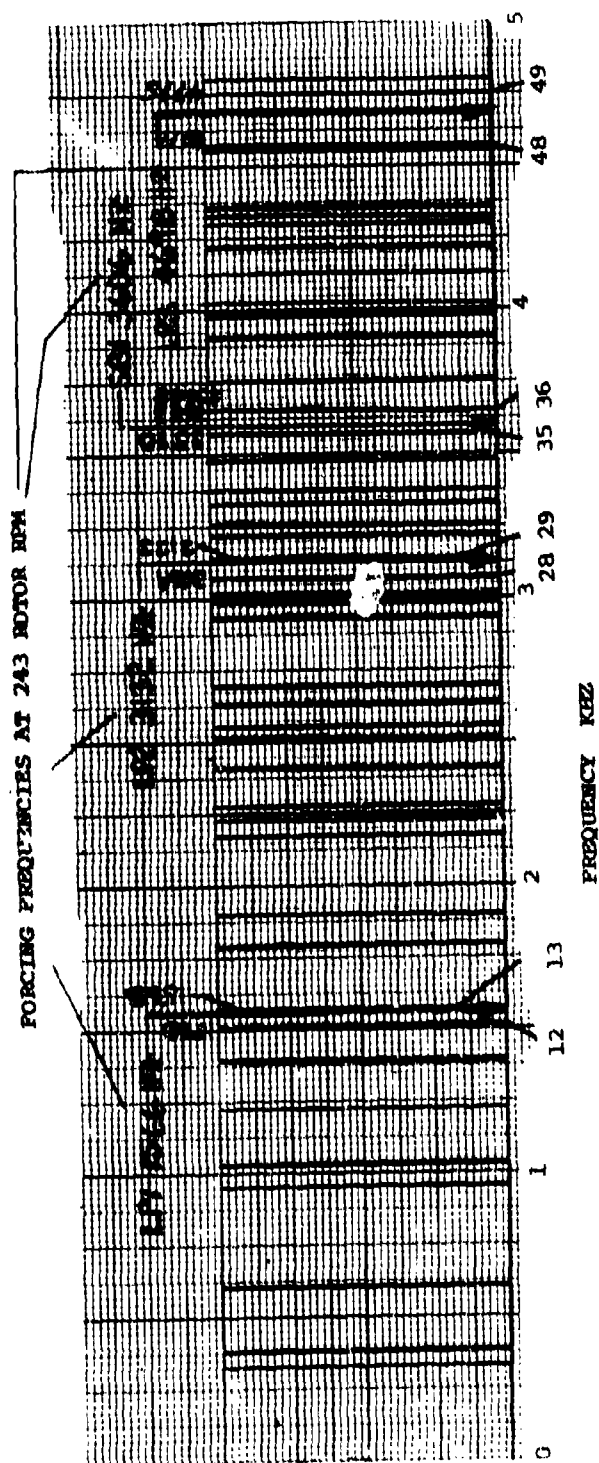


Figure 37. Spectrum of Forcing Frequencies Versus
 NASTRAN Predicted Natural Frequencies for
 CH-47C Forward Transmission Upper Cover
 (Legs Simply Supported).

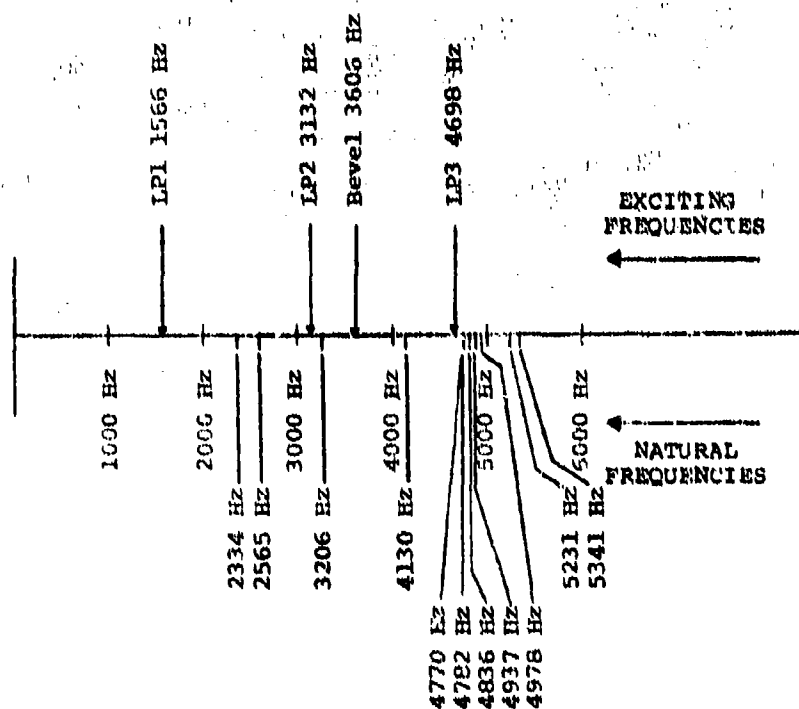
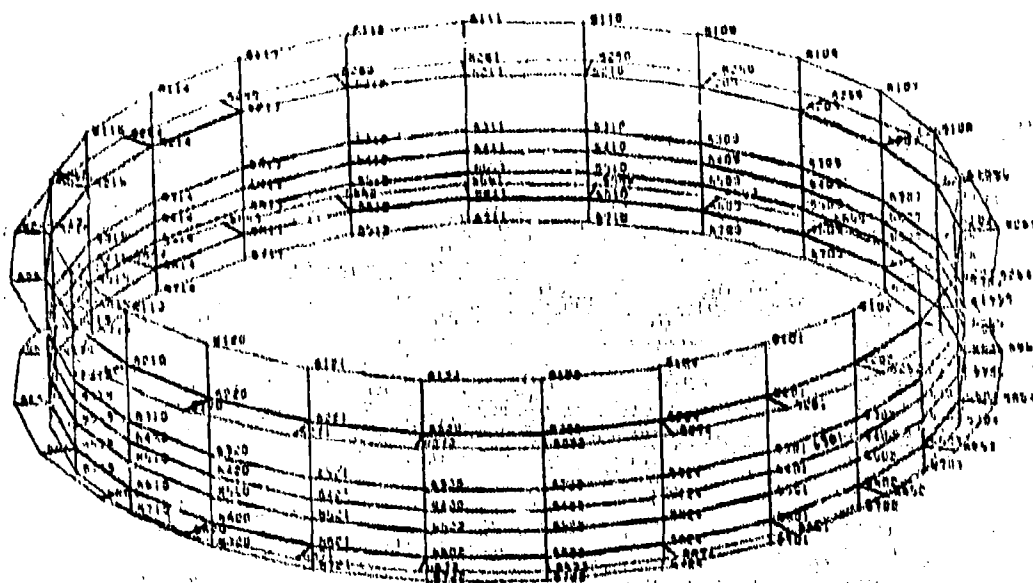


Figure 38. CH-47 Forward Rotor Transmission Ring Gear; Existing Configuration and Resulting Spectrum (at 80% Torque, 7460 RPM Sync Shaft Speed).

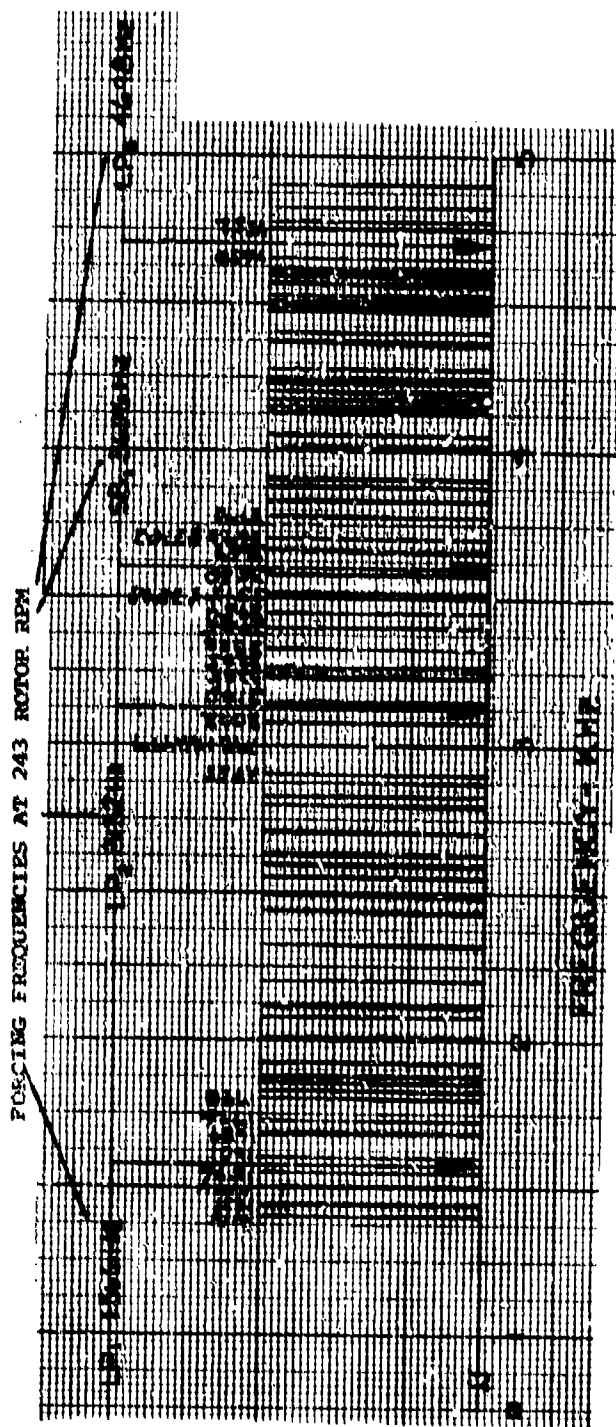


Figure 39. Spectrum of Forcing Frequencies Versus
 NASTRAN Predicted Natural Frequencies for
 CH-47C Forward Transmission Case (Free-Free).

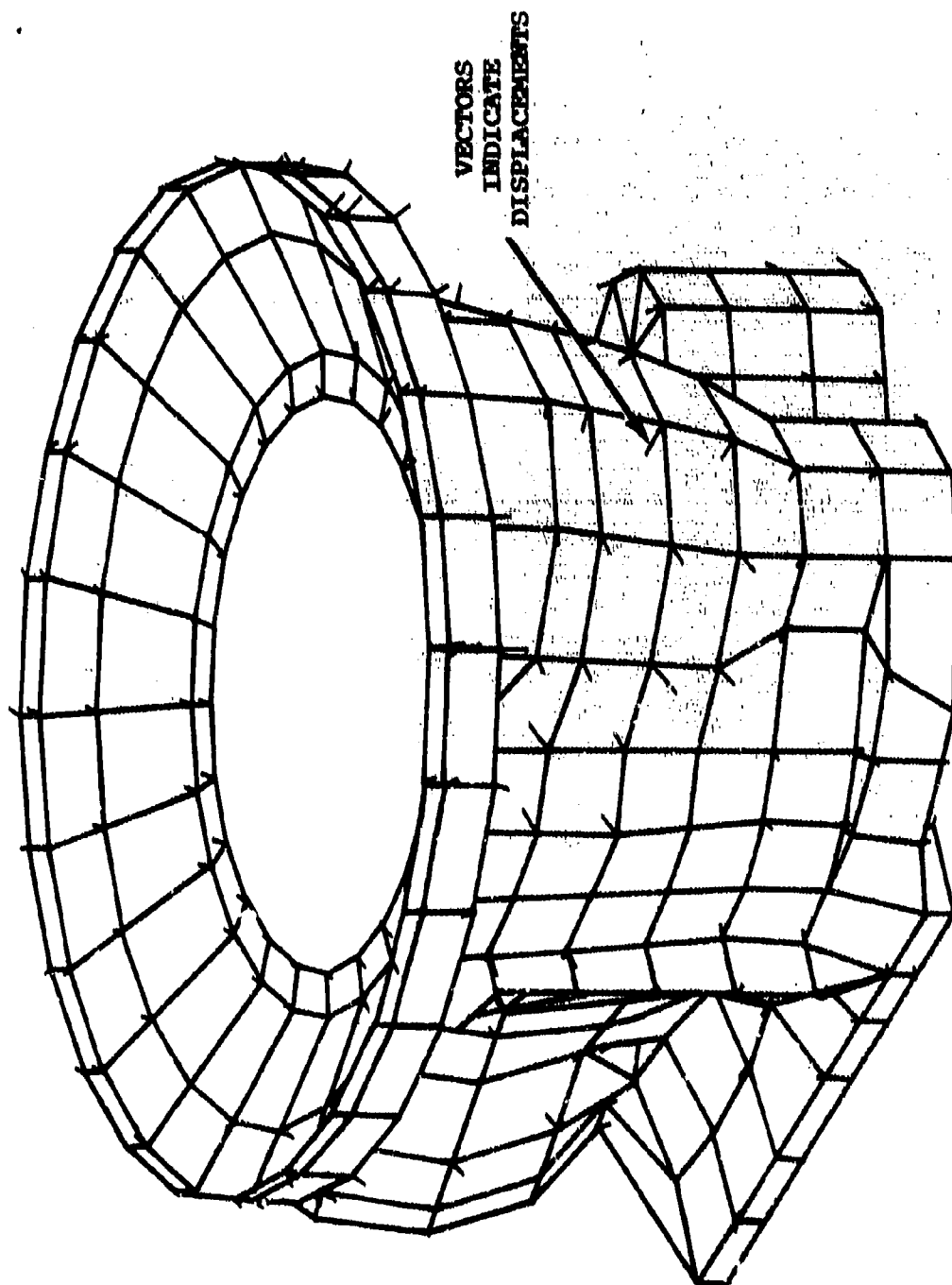


FIGURE 40. NASTRAN Plot of Deformed Housing, Mode #46, Frequency 3141 Hz.

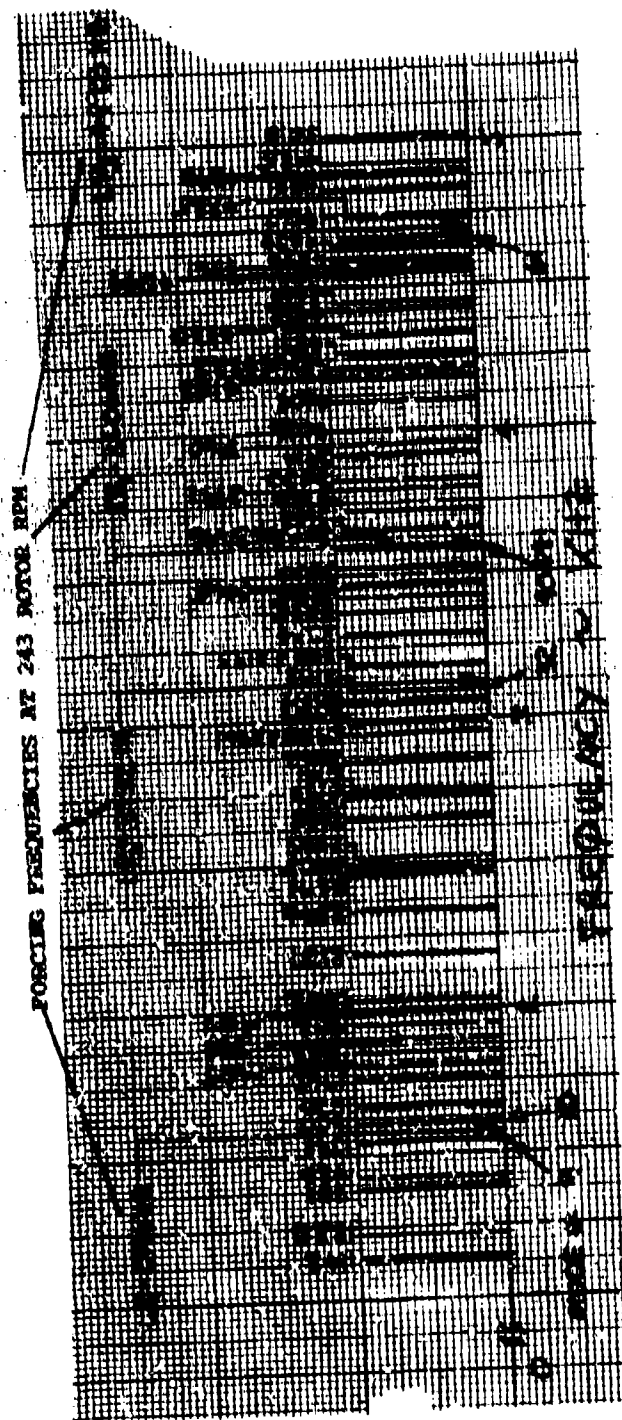
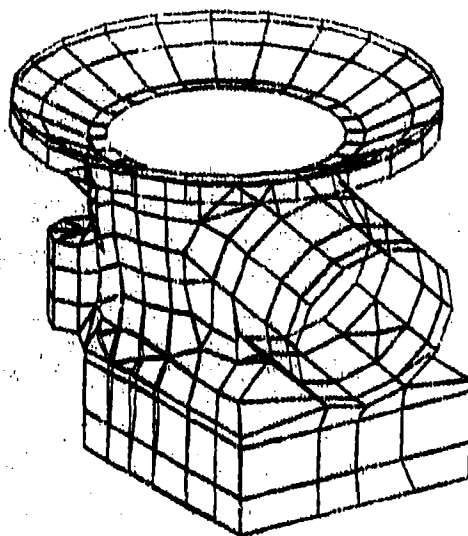
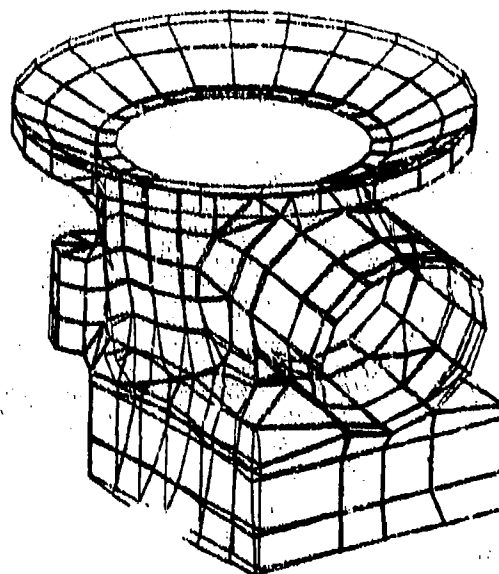


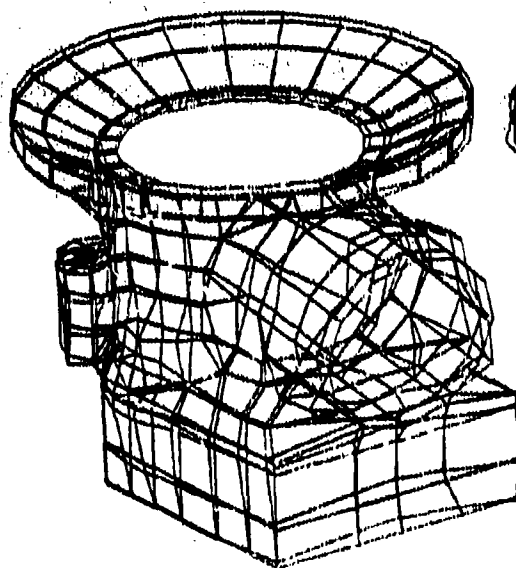
Figure 41. Spectrum of Forcing Frequencies Versus NASTRAN Predicted Natural Frequencies of CH-47C Forward Transmission Case (With Sump; Simply Supported).



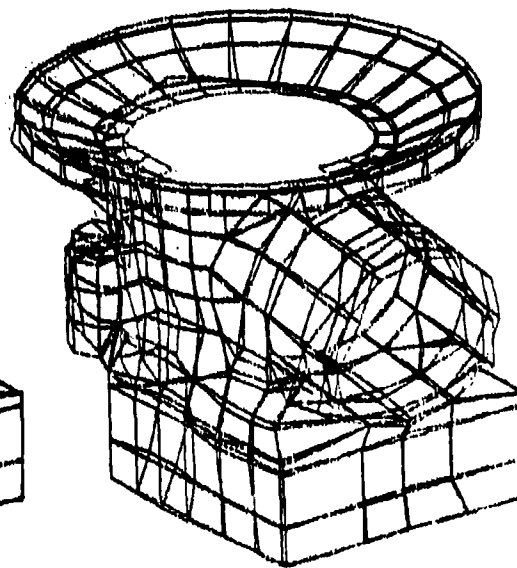
Mode 9 Frequency 1541



Mode 10 Frequency 1603

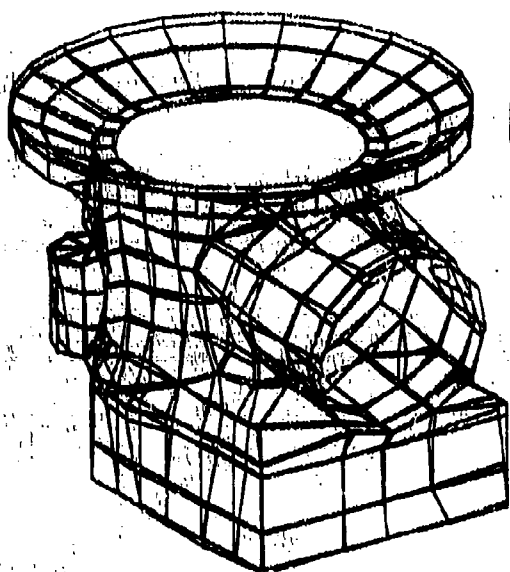


Mode 32 Frequency 3103

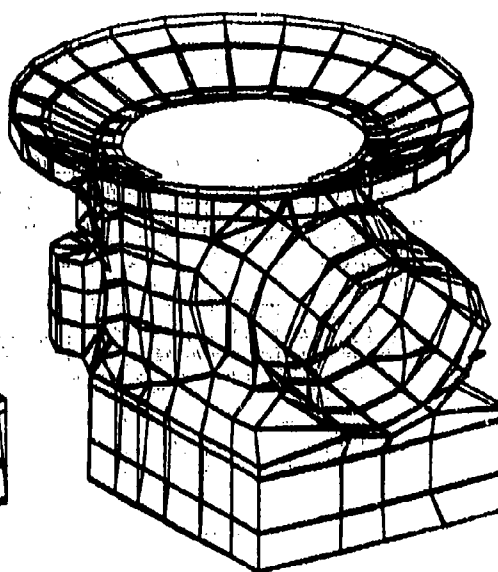


Mode 33 Frequency 3181

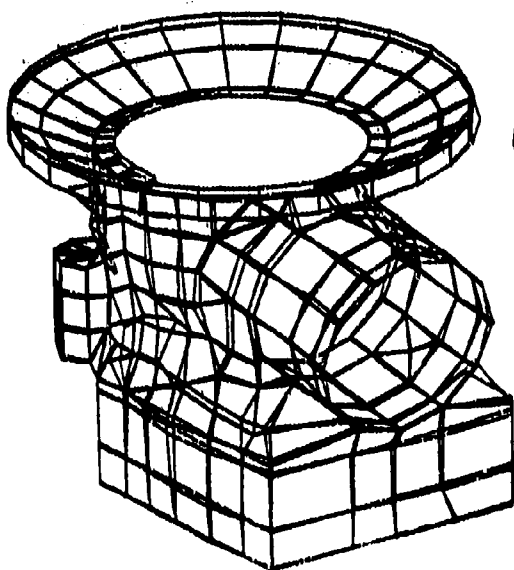
Figure 42. CH-47 Forward Transmission Case (With Sump)
Modal Deformation.



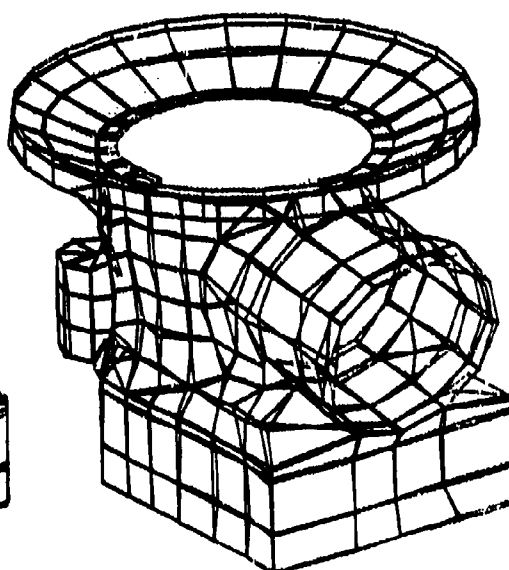
Mode 40 Frequency 3588



Mode 41 Frequency 3606



Mode 61 Frequency 4667



Mode 62 Frequency 4735

Figure 42. Continued.

DETUNING OF THE TRANSMISSION

Every structure possesses characteristic frequencies, called natural frequencies, at which it will vibrate when excited. A hollow metal cylinder which has been excited by striking with a mallet, for example, will develop a wave motion with very small local displacements. Furthermore, sound is emitted and the pitch of this sound is determined by the frequency of the wave motion. Since this natural vibratory wave motion is periodic, it possesses a natural frequency.

If succeeding applications of the exciting force are timed to begin to act just at the instant that the wave motions are about to repeat themselves, a condition known as resonance occurs. Energy will accumulate in the structure to such an extent that the amplitude of the vibration becomes out of proportion to the exciting force producing it. In the case of a transmission housing, the exciting forces are the tooth meshing loads. If this exciting frequency or its harmonics coincides with a housing natural frequency, resonance will exist. At resonance, since the wave motions produce repeating deflections which may become large, a fatigue stress will be imposed. If this stress combined with other stresses exceeds the fatigue strength of the material, failure will occur. In practice, however, due to the damping imposed by the structure and other transmission components, resonant fatigue failure of transmission housings has not been a problem.

A useful index for evaluating the possibility of resonance is the amplification factor (M), which is a function of the ratio of exciting frequency Ω to natural frequency ω and is plotted in Figure 43. Examination of this plot shows that when the exciting frequency equals the natural frequency ($\Omega/\omega = 1$) the amplitude of vibration becomes very large. This is resonance. If damping is present, the amplitude is reduced, but it is still large for damping in the typical range encountered in practice ($Q \approx .1$).

To illustrate the concept of natural modes, consider the simple example of a thin flat disk. When the disk is excited at resonance on the bench, the natural vibration appears as standing waves. That is, segments of the disk are in motion but other areas of no motion (nodes) are also well defined (Figure 44).

From the above discussion of resonance, it is evident that each natural mode of a structure will contribute to vibration in proportion to its amplification factor. Consequently, since each mode whose frequency is in the vicinity of a forcing frequency will be a major contributor to the overall dynamic response, it is desirable to alter the housing natural frequencies so that none falls close to an exciting frequency.

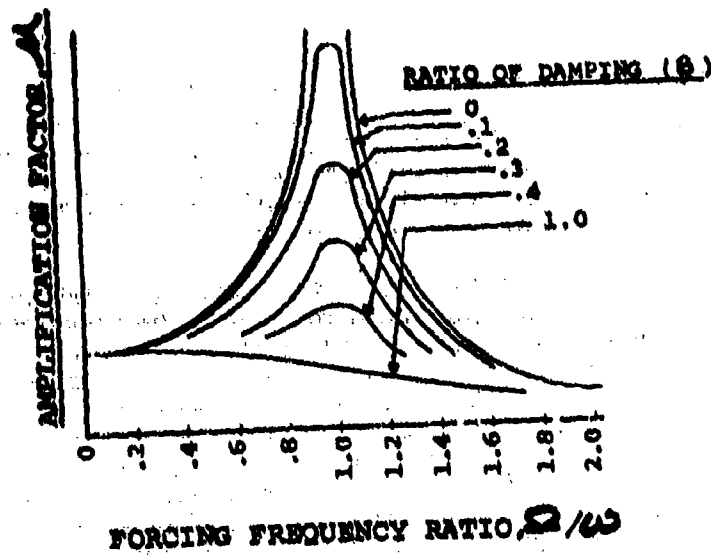


Figure 43. Amplification Factor.

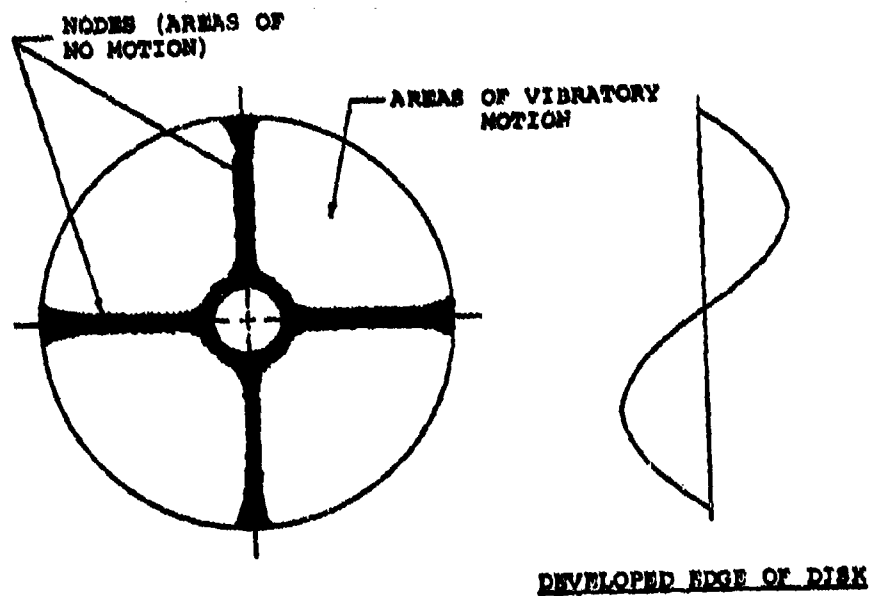


Figure 44. Flat Disk in Resonance.

This may be a difficult task since avoidance of one resonance may create a new resonance elsewhere in the frequency spectrum, unless all natural frequencies can be shifted above the exciting frequencies. In any case, it is usually preferable to stiffen, rather than weaken, a structure to cause the desired frequency shifts, since stiffening results in smaller vibration amplitudes (Reference 10).

Strain energy techniques for structural optimization have evolved in recent years. For applications such as helicopters where weight is critical, it is more appropriate to evaluate the strain density (strain energy/volume) distribution within a structure which provides guidance for vibration reduction by identifying the structural elements participating in the modes.

To optimize the transmission components for minimum vibration/noise, the eigenvectors (mode shapes) and natural frequencies are calculated. The natural frequencies calculated are compared with the gear mesh exciting frequencies to identify each mode shape whose natural frequency is close to an exciting frequency and which it is desirable to shift. For each appropriate mode shape, the strain density distribution throughout the structure is calculated. The structural elements with the highest strain density are the best candidates for effective modification of the natural frequency, since a minimal weight change will yield a maximum shift in natural frequency (Reference 11). By locally altering the housing wall to change the mass and stiffness in these areas of high strain density, the natural frequency may be shifted away from an exciting frequency.

For noise and vibration reduction it is important to minimize the displacement at the bearing locations. This may be done in several ways:

1. Relocate the bearings.
2. Change the shaft stiffness distribution.
3. Change the shaft mass distribution.
4. Change the bearing stiffness.

-
10. Soedel, Werner, SHELL VIBRATIONS WITHOUT MATHEMATICS - PART II, Sound and Vibration, April 1976, p. 12-15.
 11. Sciarra, J.J., VIBRATION REDUCTION BY USING BOTH THE FINITE ELEMENT STRAIN ENERGY DISTRIBUTION AND MOBILITY TECHNIQUES, 45th Shock and Vibration Symposium, Dayton, Ohio, August 1974.

5. Reduce the dynamic tooth forces.

Thus, the possibility of resonance is eliminated and the vibration and radiated noise are reduced.

In summary, therefore, the approach to reducing the noise produced by the transmission was divided into two distinct but complementary areas. First, the internal components were detuned so that their natural frequencies were moved as far as practical from the various mesh excitation frequencies. Second, the housing itself (in this case, the lower case and ring gear portions of the housing) was detuned by identifying the areas of highest strain energy density and then selectively stiffening these areas to reduce the case response to the gear excitation. In addition, the mode shapes of the internal components (specifically, the input spiral bevel pinion and the sun/bevel gear shafts) were evaluated to insure that the excitation at the bearing supports (thus the excitation applied to the housing) was minimum.

DETUNING OF INTERNAL COMPONENT EXCITATION

The dynamic excitation of the housing is reduced by minimizing the dynamic forces at the shaft support bearings. This is a two-fold task. First, the excitation due to the dynamic tooth forces is calculated from the gear geometry and operating conditions. Second, the damped forced response of the shafts responding to the tooth mesh excitation loads is calculated from a finite element model and the shaft is detuned using strain energy methods to minimize the displacement at the bearings. The development of this method, accomplishment of extensive dynamic testing, and correlation of data are described fully in References 3 and 4. Finally, the dynamic forces associated with the optimum configuration of the internal components are then applied to excite the model of the housing. To study the response of the transmission housing to these forces and to minimize the noise produced, a finite element model of the housing was developed and analyzed using NASTRAN.

In Table 4 the natural frequencies of the baseline internal components system, as well as the gear mesh exciting frequencies, are listed. The D-82 model used to predict these frequencies is automatically plotted and shown in Figure 45. In computer program S-68, the model of the internal components was forced to deform in the mode shape of the natural frequency closest to a mesh frequency. The strain energies and

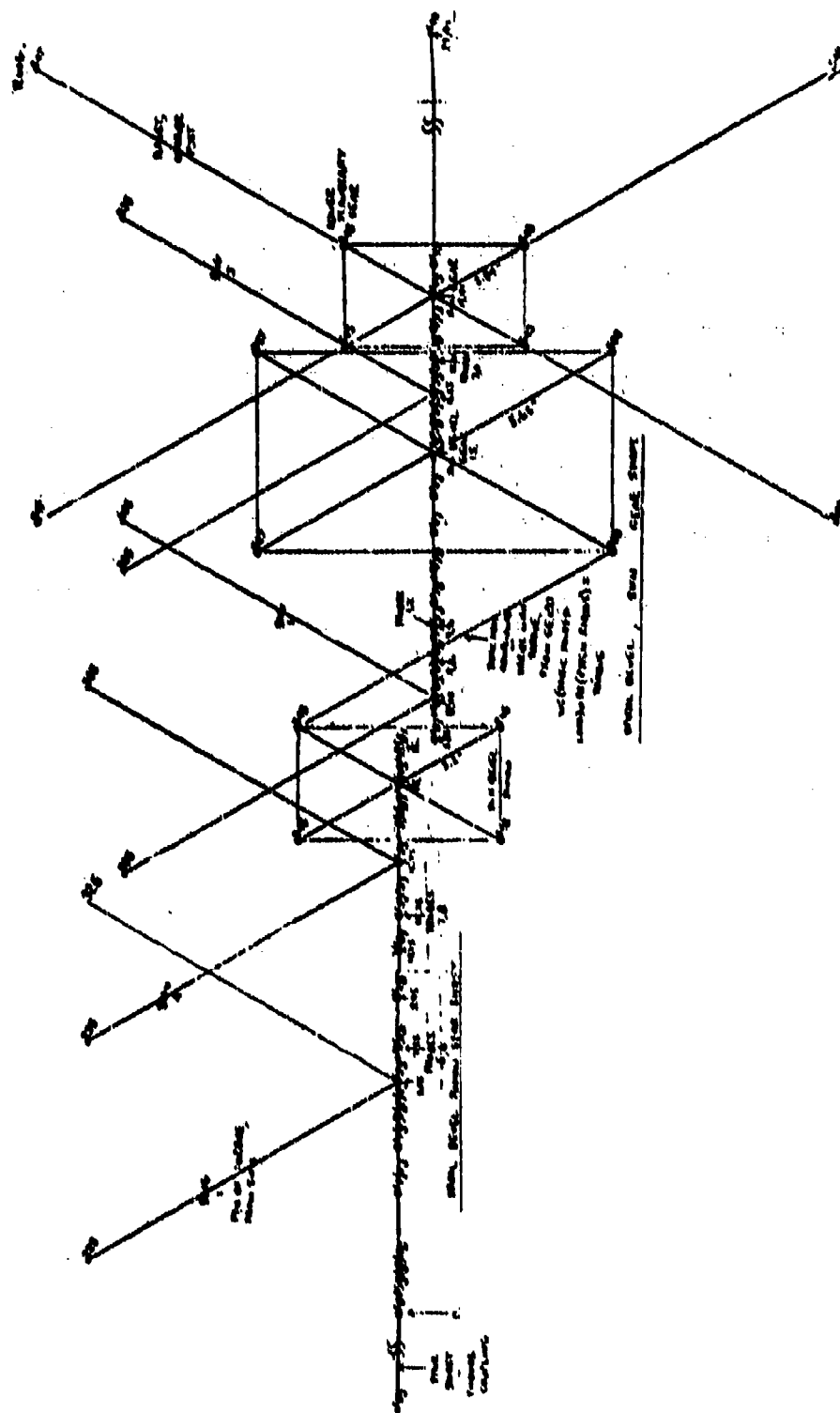


Figure 45. D-87 Plot of CH-47C Sun Bevel Pinion and Gear and Lower Planetary Gear System.

TABLE 4. NATURAL FREQUENCIES

MESHING	FREQUENCIES	BASLINE (Hz)	ITERATION #1	ITERATION #2
		560	583	583
		627	614	619
		792	787	813
		866	864	893
		1104	1089	1122
		1514	1473	1473
LP1	1566 →	1526	1533	1532*
		1769	1740	1738
		2755	2612	2747
		2796	2686	2795
LP2	3132 →	3044	3221	3231
		3151	3375	3375
Bevel	3606 →	3404	3404	3404
		3855	3806	3869
LP3	4698 →	4544	4402	4519
		5150	5240	5452
		5419	5414	5542
		5545	5442	5568
		7172	5579	5797

*Controlled by bearing stiffness.

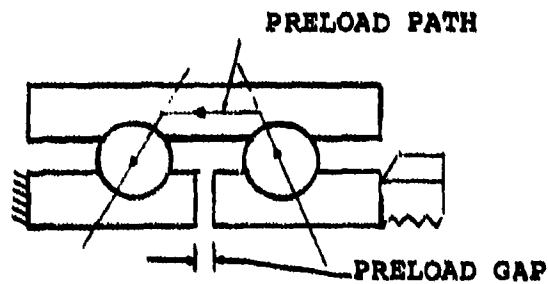


Figure 46. Use of Gap to Change Bearing Stiffness Through Preload.

strain densities of each of the structural elements were determined and tabulated from highest to lowest, the structural elements in the highest strain being the best candidates for modification of the appropriate natural frequencies.

The structural model was modified according to the results of S-68. The new natural frequencies are shown in the third column of Table 4. The natural frequencies just above the lower planetary mesh second and third harmonics were altered upward away from the exciting mesh frequencies, thereby reducing their amplification factors. This reduces the level of vibration and the resulting dynamic bearing loads to the transmission housing. The bevel mesh exciting frequency is relatively centered with respect to the next higher and next lower natural frequencies, so it was not changed. The natural frequency just below the lower planetary first harmonic was unchanged since its value is controlled by a bearing stiffness.

A second iteration was made using S-68, and a new 7th mode shape (lower planetary first harmonic) was obtained. Again, no significant change of this natural frequency occurred. Some bearings may be stiffened by using a preload shim (Figure 46). This was investigated since it controlled the natural frequency closest to the lower planetary first harmonic mesh exciting frequency. The bearing of the pinion gear (shown on Figure 20), however, could not be preloaded. An alternative method, stiffening the internal diameter of the pinion below the bearing, was also attempted. This modification resulted in no change to the natural frequency. The sixth natural frequency (1514 Hz) was found to be controlled by the bevel/sun gear radial bearing.

DETUNING OF HOUSING RESPONSE

A complex gearbox such as a helicopter rotor transmission typically has more than one gear mesh, hence more than one exciting frequency. The Boeing Vertol CH-47C helicopter forward rotor transmission employs a spiral bevel gear mesh plus a two-stage planetary gear system. Hence, each of these fundamental gear mesh frequencies as well as their harmonics must be considered. The primary frequencies for the CH-47 forward rotor transmission at 243 rotor rpm have been identified experimentally as the bevel gear mesh frequency and the lower planetary gear mesh frequency (LP1) and its second (LP2) and third (LP3) harmonics. The occurrence of multiple exciting frequencies, coupled with the fact that the housing possesses many natural frequencies, makes it a complex task

to detune the housing so that none of the exciting frequencies coincides with a natural frequency. Additional sources of exciting frequencies in the form of sidebands are introduced by planetary gear configurations (Reference 12) and manufacturing variations (Reference 13).

The experimental program described in References 3 and 4 included the dynamic testing of a CH-47C forward transmission with internal instrumentation to measure strains, displacements and accelerations of the rotating components and external instrumentation to measure housing acceleration and noise. Correlation of this data with the analysis has indicated that by modifying the gear/shaft/bearing system geometry the internal components may be detuned to minimize excitation of the housing. Application of strain density techniques to these dynamic components has identified modifications which have analytically reduced the loads exciting the housing at the bevel mesh, LP2 and LP3 frequencies. Loads at the LP1 frequency increased slightly. Since the effects of multiple noise sources are added logarithmically, the reduction of three out of four noise sources may not appreciably reduce the overall noise level.

Noise measurements have tended to confirm that housing responses exist and generate noise. This is evidenced, for example, by the LP2 and LP3 frequencies. Although the exciting source for these frequencies is within the ring gear, the maximum noise at these frequencies emanates from the mid-case region (Figure 47).

It is important to note that since the exciting frequencies will vary with changes in operating speed, the housing must be detuned at a specific operating speed. The application of strain density methods has led to identification of the areas of the housing structure (specifically, ring gear and case) which will be modified to detune the housing for reduced vibration/noise. The strain density distribution was determined using the NASTRAN post-processor for the modes with frequencies nearest to the four main exciting frequencies, and the elements with high strain density were identified.

12. Beranek, L.L., NOISE REDUCTION, McGraw Hill Book Co, 1960.
13. Sternfeld, H., Schairer, J., and Spencer, R., AN INVESTIGATION OF HELICOPTER TRANSMISSION NOISE REDUCTION BY VIBRATION ABSORBERS AND DAMPING, Vertol Division, The Boeing Company, USAAMRDL Technical Report 72-34, Eustis Directorate, U.S. Army Air Mobility Research and Development Laboratory, Fort Eustis, Virginia, August 1972, AD752579.

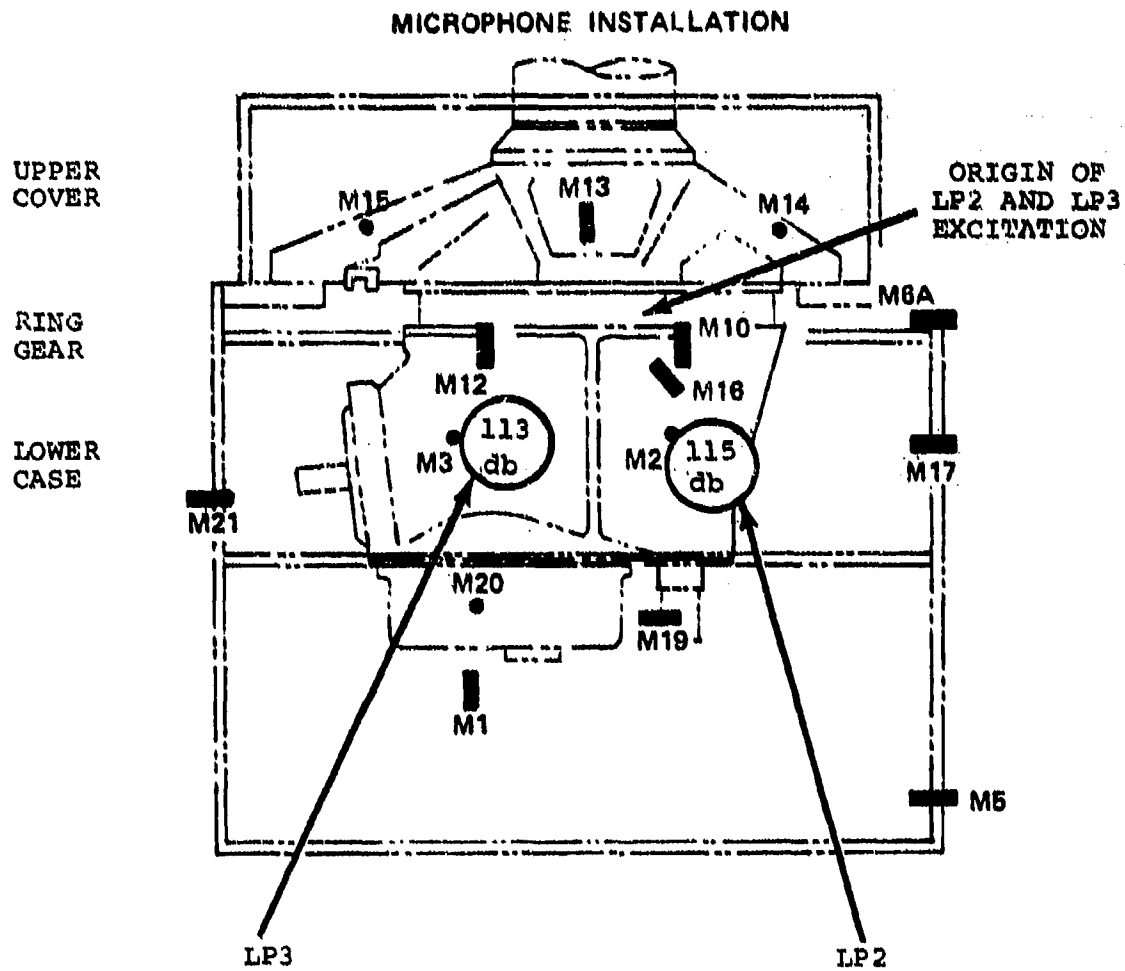


Figure 47. Maximum Measured Noise Levels
(7460 RPM at 80% Torque).

Detuning of the Ring Gear

The principal objective of this analysis was to shift the 4770 Hz natural frequency of the ring gear away from the lower planetary third harmonic frequency. As indicated on the spectrum on Figure 48, this exciting frequency (4698 Hz) had a cluster of natural frequencies close to it. A strain density analysis (S-83) indicated that the upper portion of the wall indentation between the upper and lower planetary gear teeth had the maximum strain density and was the area of the structure which should be modified for optimal change of the third harmonic of the lower planetary mesh frequency. A sample of the S-83 analysis output is shown in Appendix B with the strain density calculated for the outer surface of the ring gear.

As a result of the strain energy analysis, the thickness of the wall sections between the upper and lower flanges was increased by 0.2 inch and the dynamic analysis was rerun with this modified structure. The results of a reanalysis indicated a shifting upward of the whole cluster of natural frequencies. The natural frequency closest to the mesh frequency moved from 4770 Hz to 5179 Hz. This is shown on the spectrum on Figure 48. A natural frequency close to the second harmonic of the lower planetary stage mesh exciting frequency (3132 Hz) was also shifted upward from 3206 Hz (unmodified) to 3352 Hz (modified). Therefore, the mesh exciting frequencies of the ring gear are more centrally located with respect to the natural frequencies with the modification which is goodness for vibration/noise reduction. In fact, the undamped amplification factor

$$M = \frac{1}{1 - \beta^2}$$

$$\beta = \frac{\omega}{\omega_n} = \frac{\text{Mesh Exciting Frequency}}{\text{Natural Frequency}}$$

for the second harmonic lower planetary mesh frequency was reduced from 21.92 to 7.88. For the third harmonic lower planetary mesh exciting frequency, the undamped amplification factor was reduced from 33.38 to 5.645.

Detuning of the Lower Case

When applying a strain energy analysis to a structure, each mode considered will typically result in different elements of the structure being in a state of high strain density and hence will yield a different strain density tabulation sequence. However, some high strain density elements are generally common to two or more of the modes. Strictly speaking,

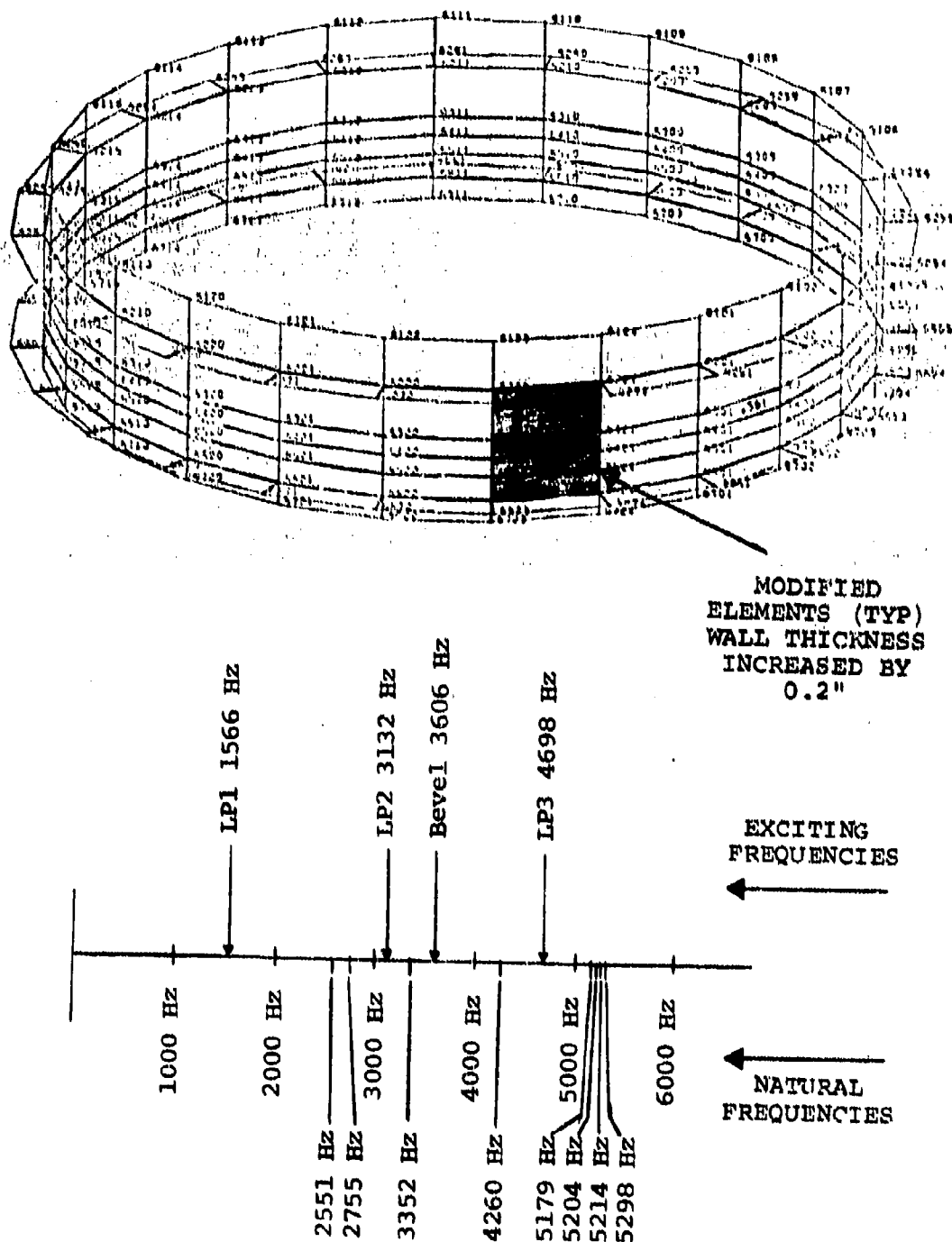


Figure 48. CH-47 Forward Rotor Transmission Ring Gear;
Modified Configuration and Resulting
Spectrum (at 80% Torque, 7460 RPM
Sync Shaft Speed).



the elements with highest strain density for each mode should be modified to achieve the maximum frequency shift for each corresponding mode. This approach would be used during the design of a new structure.

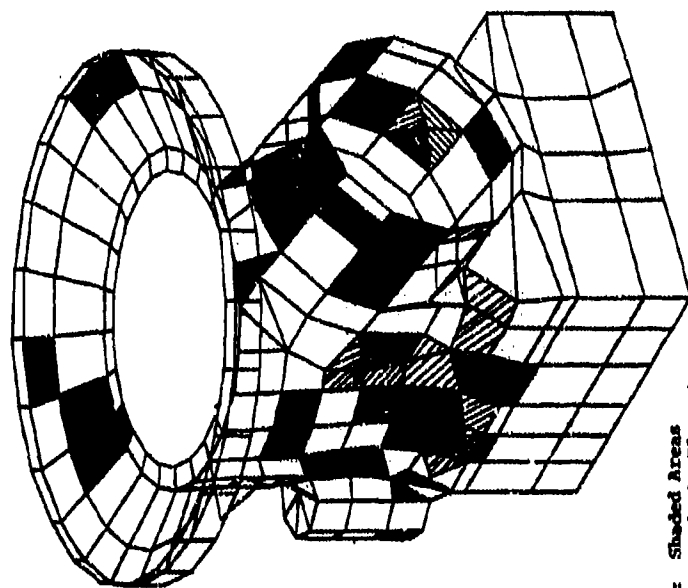
Due to the numerous natural modes of the transmission case and the multiple exciting frequencies, the detuning process here is not quite so straightforward. To modify the existing housing it would be cumbersome if not impossible to incorporate the numerous and varied modifications indicated by a rigorous application of the strain density analysis to each troublesome mode. Therefore, for practical application to the experimental housing herein, those elements with a relatively high strain density and which are common to two or more modes have been identified (shaded areas in Figure 49) and modified to shift the housing frequencies. In this manner a specified structural change alters two or more frequencies, although perhaps no single frequency is shifted maximally. It was more feasible to modify these elements since the actual changes to the existing housing design for testing were limited to a few easily accessible areas on the exterior walls of the housing. This approach, although not the best possible from a rigorous application of the analysis, should provide sufficient detuning to demonstrate the validity of the analysis. The objective of this work is to predict the actual change, whatever it may be, but not necessarily to optimize the housing in the most rigorous way possible.

Considering this strain density distribution and the configuration of the actual hardware (e.g., oil passages, ribs), the areas of the housing wall which were modified are defined in Figure 50. Doubler plates will be bonded to these areas for the test phase in order to simulate an increase in wall thickness. The model was changed to include these modifications by increasing the wall thickness by 0.300 inch in these localized areas, and the dynamic analysis was rerun. Figure 51 shows the frequency spectrum for the modified housing, and Figure 52 is a comparison of the most significant frequencies for the baseline and modified housing configurations. The shifting of frequencies demonstrated by this comparison verifies the effectiveness of the strain energy method. However, some of the modified frequencies are more unfavorable than the original configuration. Because of the multitude of natural frequencies, this was not unexpected.

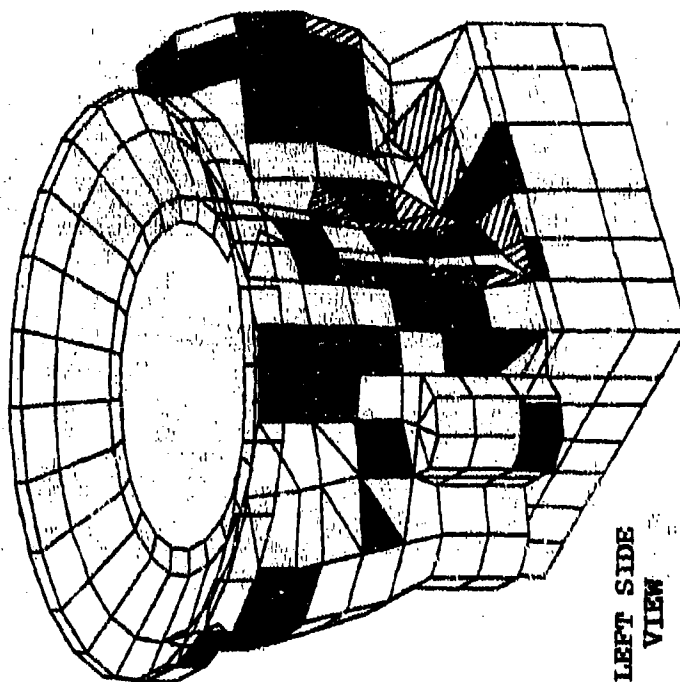
Vibration Absorbers/Isolators

The work herein was modified to include the investigation of isolators in lieu of bending absorbers as originally planned. This change was justified based upon the results of the rather

 Areas of High Strain Density Common to 3 Modes
 Areas of High Strain Density Common to 4 Modes



REAR VIEW



LEFT SIDE VIEW

NOTE: Shaded Areas
 Indicate Elements
 With High Strain
 Density ($\geq .24 \times 10^4$)

Figure 49. CH-47C Forward Rotor Transmission Case (With Sump)
NASTRAN Model: Areas of High Strain Density.

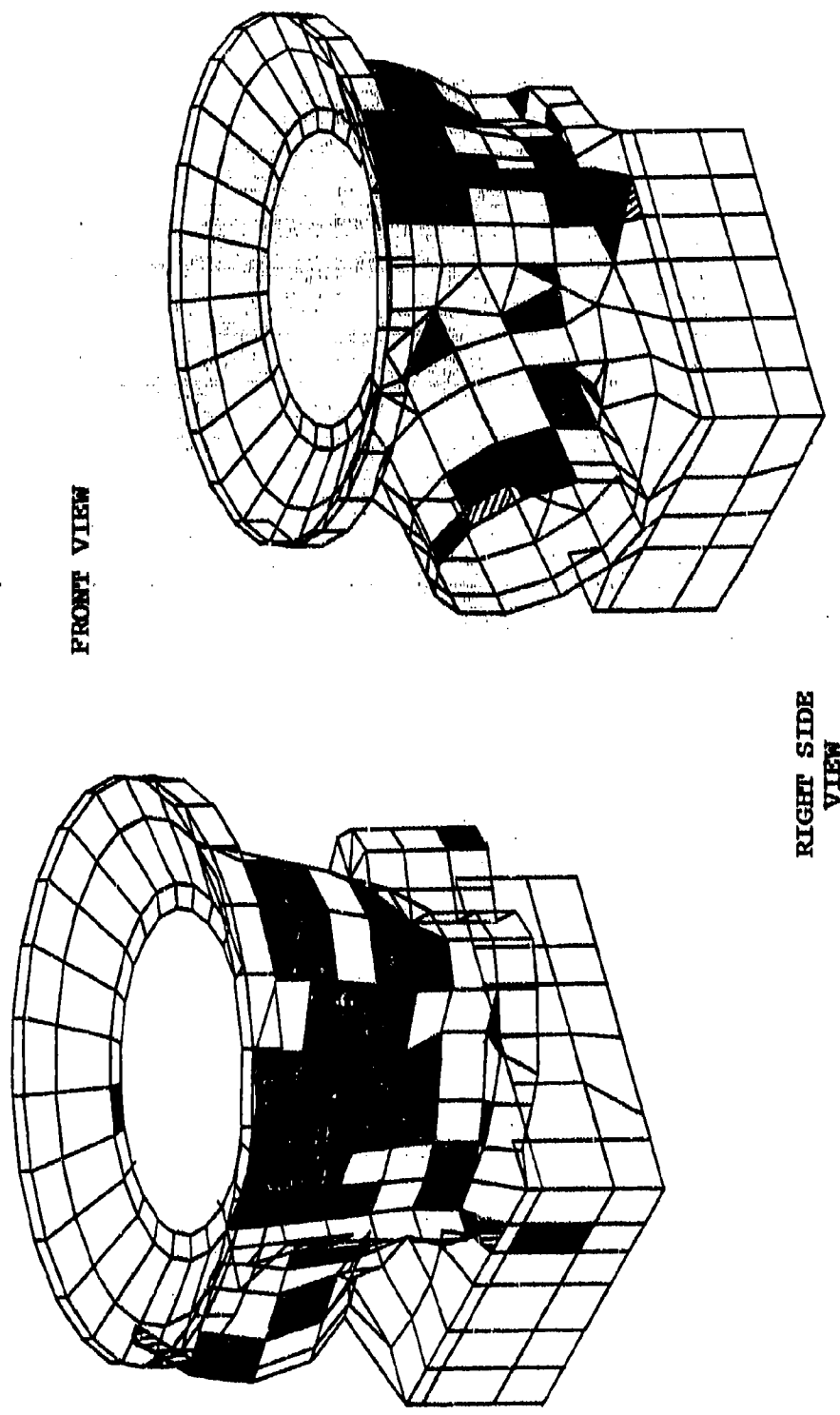


Figure 49. Continued.

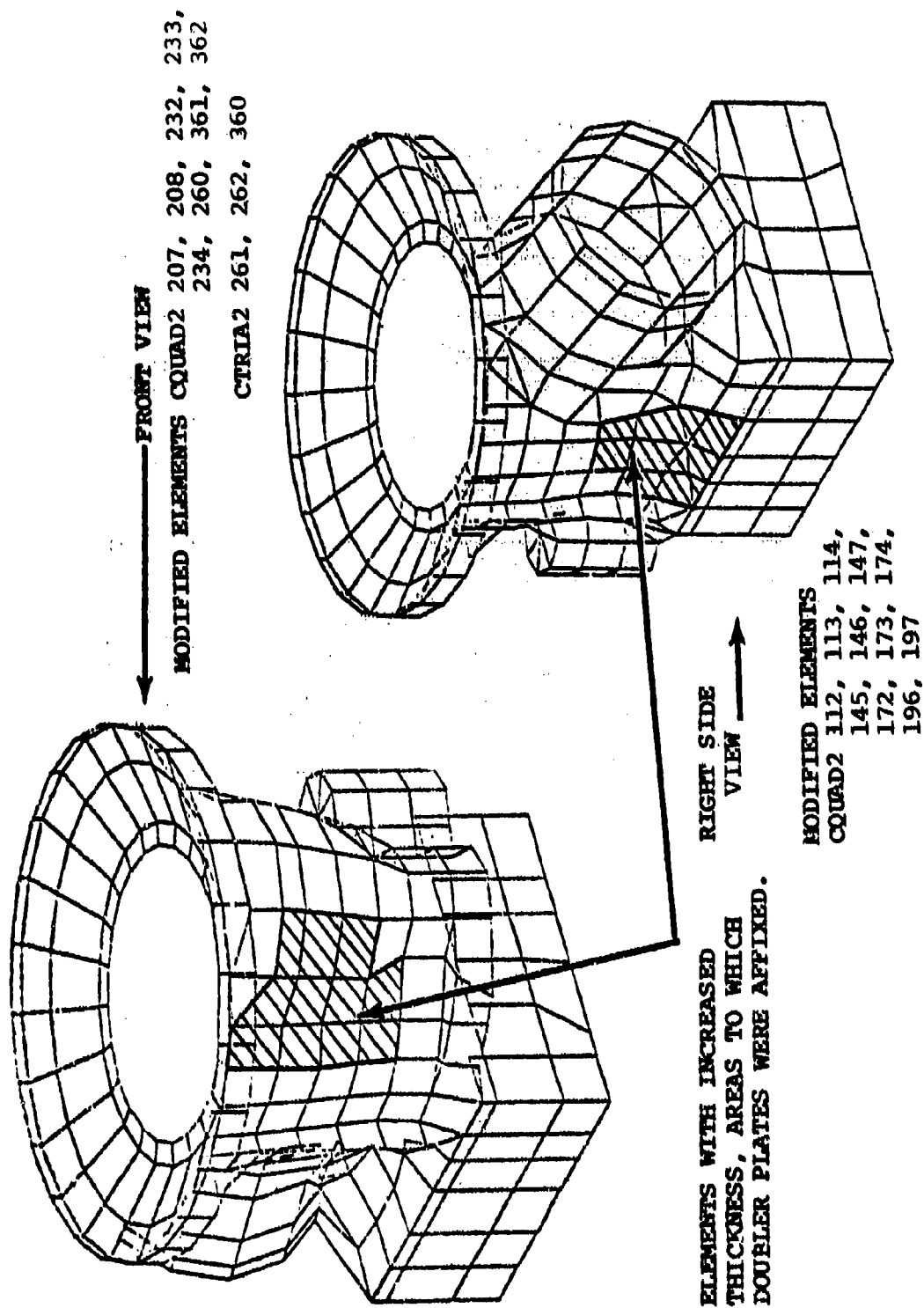


Figure 50. CH-47C Forward Transmission Case With Modifications (Crosshatched Areas) to Wall Thickness.

FORCING FREQUENCIES AT 243 ROTOR RPM

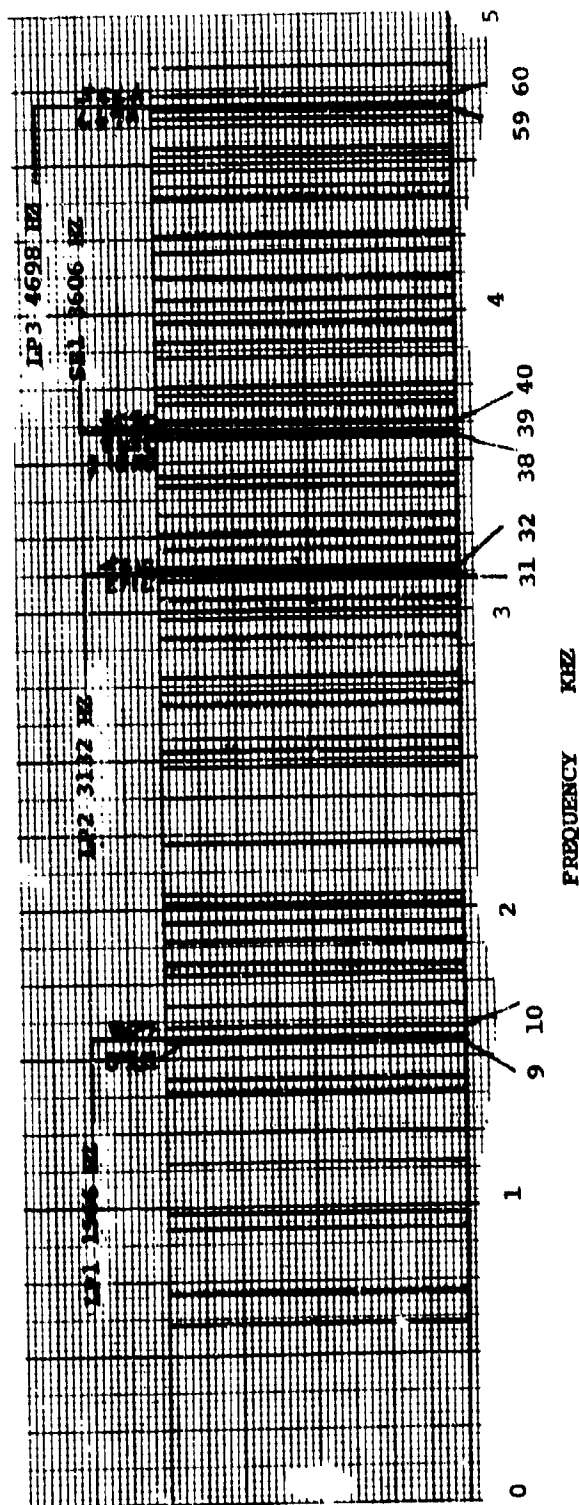


Figure 51. Spectrum of Forcing Frequencies Versus NASTRAN Predicted Natural Frequencies for CH-47C Forward Transmission Case (With Sump; Simply Supported) - Modified "A".

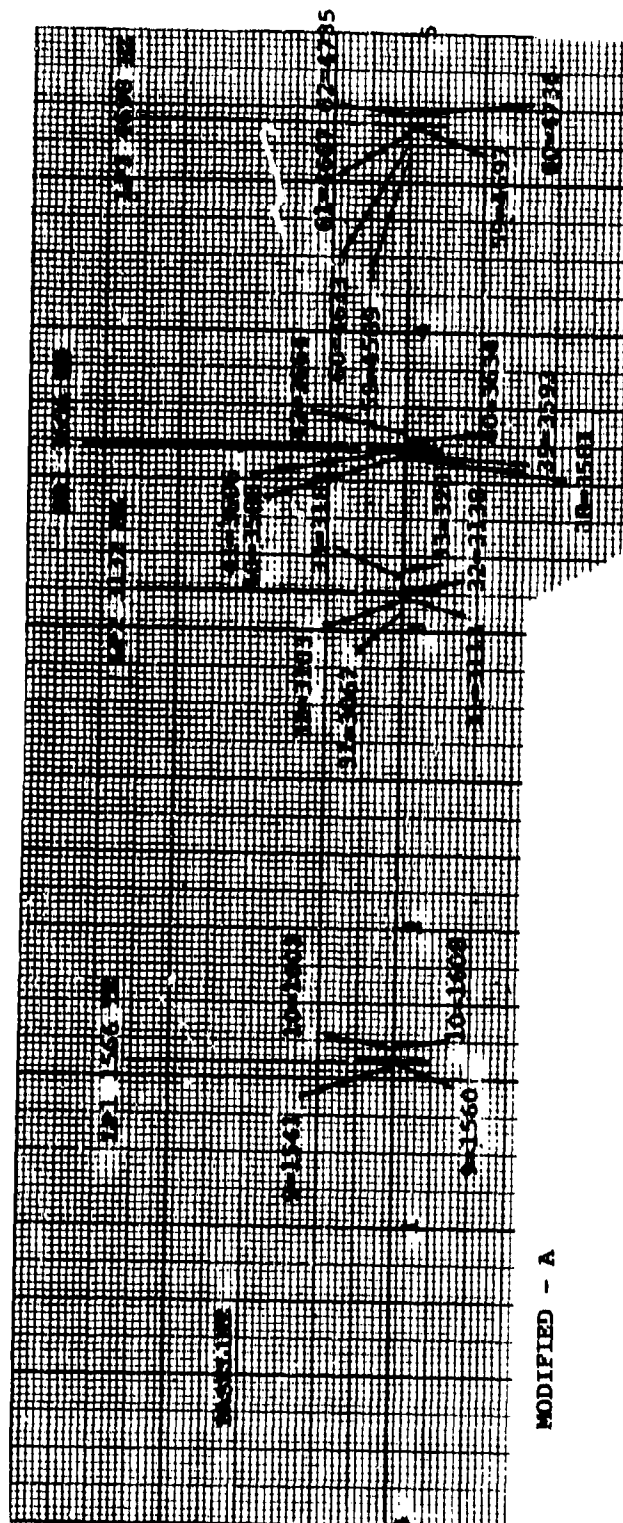


Figure 52. Comparison of Significant Frequencies for Baseline and Modified "A" CH-47C Forward Transmission Case.

extensive previous study of absorbers in Reference 14 and the difficulties with absorbers discussed in the next section. Conversely, work conducted at Boeing Vertol and in Reference 15 indicated that isolators offer promise in reducing the transmittal of high frequency vibration energy across gearbox mounts to the local airframe. Tests indicated that a 10 dB reduction in speech interference level (SIL) noise could be attained by replacing the standard main transmission attachments with rubber mounts having a static spring rate equal to that of the airframe at the attachment point (Reference 15). Follow-on work corroborated the initial results and produced a curve showing SIL noise reduction versus relative airframe-mounting stiffness. Later work using an electromagnetic shaker and impedance head showed the usefulness with regard to noise reduction of both structural damping and also isolation with a static spring rate that is compatible with transmission-airframe relative movement restrictions.

Optimum Configuration

The modifications defined in the previous sections were based on considerations of the separate components which comprise the transmission (i.e., the upper cover, internal components, ring gear, and lower case). Each of these modifications showed potential for reducing the overall noise and vibration level of the transmission; however, their combined effects are difficult to predict analytically. The effect of the isolators, alone or in combination, was not estimated analytically. The predominant noise generator is the lower case (based on the analysis); thus, the changes to the case (adding the doubler plates) and to the internal components which excite it (modified sun/bevel) should provide the maximum benefit. The interraction of the modified ring gear with these two changes was not addressed analytically; however, logically it should provide an additional reduction. Cross coupling of the individual effects may, however, yield contrary data.

-
14. Howells, R.W., and Sciarra, J.J., FINITE ELEMENT ANALYSIS USING NASTRAN APPLIED TO HELICOPTER TRANSMISSION VIBRATION/NOISE REDUCTION, NASA TMX-3278, September 1975.
 15. Badgley, R., and Laskin, I., PROGRAM FOR HELICOPTER GEARBOX NOISE PREDICTION AND REDUCTION, Mechanical Technology Incorporated, USAAMRDL TR70-12, Eustis Directorate, U.S. Army Air Mobility Research and Development Laboratory, Fort Eustis, Virginia, March 1970, AD869822.

AUXILIARY DEVICES FOR VIBRATION/NOISE REDUCTION

The main thrust of the work herein was directed at reduction of vibration/noise at its source by detuning. Nevertheless, the very complex nature of vibration/noise generation in a helicopter transmission may require that some type of auxiliary device be considered. For example, a situation may arise where it is possible to reduce all the troublesome frequencies by detuning except for one.* It may be effective to treat this one remaining frequency by using some type of auxiliary device. It is also conceivable that auxiliary devices may be needed in addition to the detuning approach to meet increasingly stringent noise standards. Therefore, a brief discussion of some types of auxiliary damping devices is included here for completeness.

DISSIPATIVE DAMPING

Application of damping material to the surface of a structure by spraying, gluing, plasma flame coating, etc., may be effective. Since most of the straining action (and thus energy conversion into heat) will be confined to the layers closest to the structure, thin layers of damping material will be more cost and weight effective than thick layers (Reference 10).

Objections to the use of damping materials applied to the exterior surface of helicopter transmission housings include greater cost, added weight, concealment of cracks, and heat retention. Each of these must be traded off against the potential benefits.

DYNAMIC ABSORBERS

The concept of vibration reduction by the use of a dynamic absorber is that at the resonant frequency of the absorber the motion of the structure to which it is attached is attenuated at the point of attachment. The large spring-mass system in Figure 53 represents the structure, and it has a sinusoidal force applied to it. With no absorber attached, the structure vibrates with an amplitude determined by the resonant frequency of the system

$$= \frac{1}{2\pi} \sqrt{\frac{K_m}{M_m}}$$

and the frequency of excitation (Ω). When the absorber is added the system now has two resonant modes; one has a lower

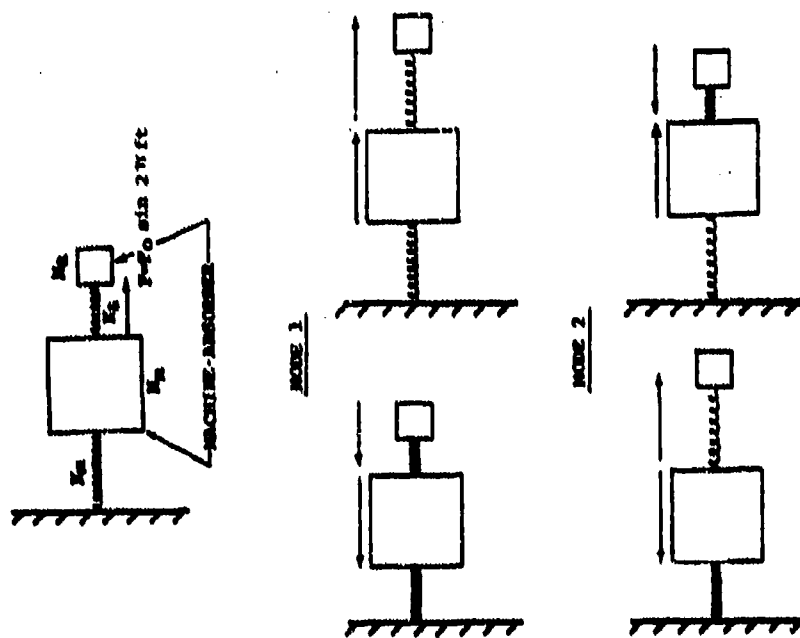


Figure 53. Concept of the Dynamic Vibration Absorber.

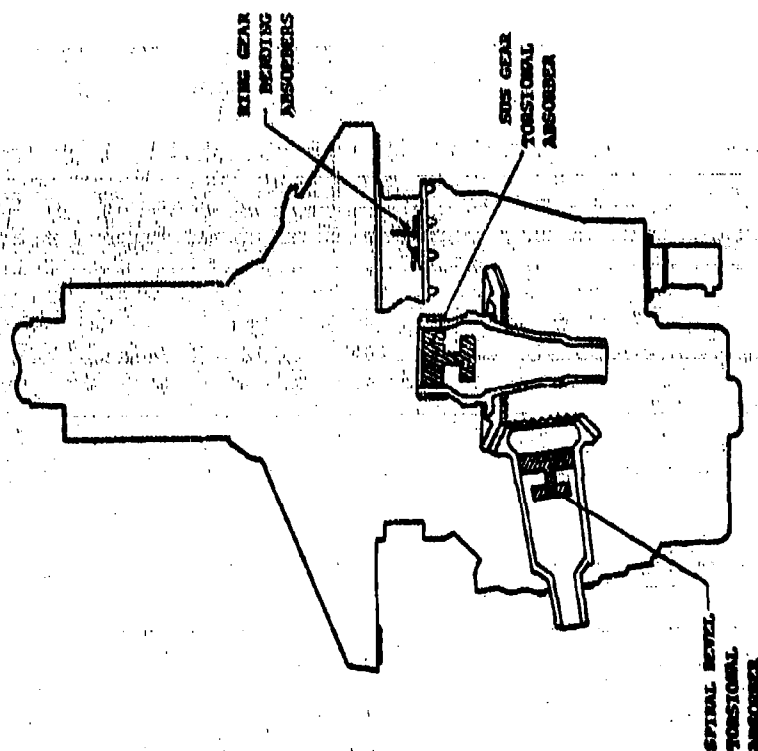


Figure 54. Absorber Locations.

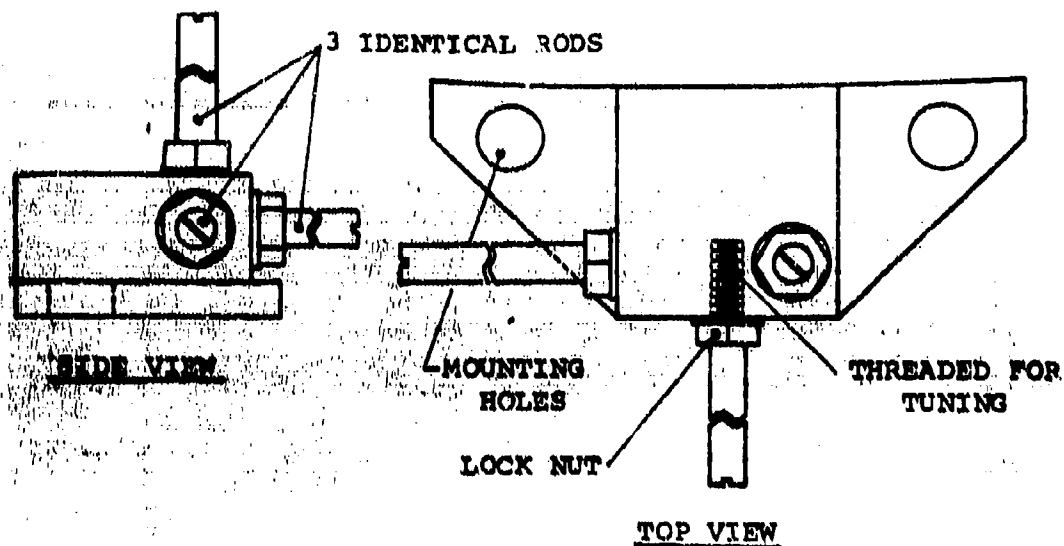
frequency where the two masses (absorber and structure) vibrate together against the larger spring, and the other has a higher frequency where the masses vibrate against each other.

A force applied to the structure can excite either of these modes, but somewhere between them exists a condition where the absorber moves and the machine does not. At this frequency, the force excited by the absorber on the structure exactly cancels the driving force. Since the structure is not moving, the absorber acts as if it were attached to a solid wall. This frequency is thus the resonant frequency of the absorber alone. Therefore, to design a dynamic vibration absorber for an undamped two degree of freedom absorber/transmission system, it is necessary only to establish that the uncoupled natural frequency of the absorber is equal to the frequency of excitation. Reference 16 contains more detail and derivations of the equations.

A previous test program was conducted by Boeing Vertol (Reference 2) to evaluate the effect of auxiliary devices such as vibration absorbers and dampers on the noise generated by a CH-47 forward rotor transmission. Predicted and measured results were compared, and a method for comparing the efficiency of various methods of transmission noise reduction was developed. The two types of absorbers used are illustrated in Figure 54. Dynamic vibration absorbers of a bending type were bolted to the ring gear to stop the motion and thus the sound radiation of that part of the housing. The bending absorbers were tuned at the planet-ring mesh frequency. These were actually simple cantilevered beams - three turnable screw rods for three directions of vibration reduction. A sample calculation for this type absorber is presented in Figure 55. The maximum noise reduction achieved during the test was 2 dB at the microphone closest to the ring gear, and the vibration reduction was 17%.

Torsional absorbers, tuned to the main spiral bevel and sun gear mesh frequencies, were placed inside the bevel/sun gear and spiral bevel pinion, respectively, to reduce the torsional motion of those gears at their tuned frequency. The reduction of the dynamic forces on the gear teeth reduces the forces

-
16. Badgley, R.H., A PLAN TO DEVELOP TECHNOLOGY FOR THE REDUCTION OF INTERNAL NOISE AND HIGH-FREQUENCY VIBRATION IN HELICOPTER AIRCRAFT SYSTEMS, MTI Technical Report MTI-71TR61, Prepared for Eustis Directorate, U.S. Army Air Mobility Research and Development Laboratory, Fort Eustis, Virginia, October 1971.



BENDING TYPE ABSORBER NATURAL FREQUENCY (f)

$$f = \frac{3.56}{2\pi} \left[\frac{4 EI}{\rho \pi d^2 l^4} \right]^{1/2}$$

(From Reference 2)

where

$$I = \frac{\pi}{64} d^4 = \frac{\pi}{64} \times .25^4 = .000192 \text{ in}^4$$

$$f = \frac{3.56}{2\pi} \left[\frac{4 \times 2.9 \times 10^7 \times .000192}{7.32 \times 10^{-4} \times \pi \times .25^2 \times 2.18^4} \right]^{1/2}$$

$$f = 1482 \text{ Hz}$$

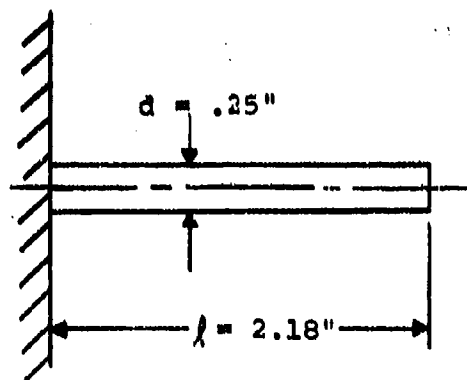


Figure 55. Geometry and Sample Calculation for Bending Type Dynamic Vibration Absorbers as Applied to Ring Gear.

transmitted through the bearings to the casing and the resulting noise. The sun gear absorber provided about an 8 dB reduction. Lack of similar effects in the spiral bevel system was attributed to the fact that the spiral bevel gear is not subjected to purely torsional excitation, but is acted upon by dynamic forces which have axial and radial as well as torsional components. The resulting vibration of the spiral bevel gear thus probably includes axial, radial, and torsional amplitudes. A torsional absorber alone is not suited to the reduction of all these components. The fundamental gear mesh frequencies were accompanied by very strong sidebands due to planetary gear passage. Since the planetary system was not treated, this limited the noise reduction achieved.

Gear damping was achieved by filling the gear shafts with Viton, and by a ring of Viton on the spiral bevel ring gear (Figure 56). Constrained layer damping was also used on the outside of the planetary ring gear (Figure 57). Figure 58 summarizes the measured reduction in transmission case vibration and radiated noise, and compares the weight of each device and the weight required to achieve a similar reduction by conventional airframe acoustical treatment. The results indicated that each of the above methods provided some noise reduction; however, none of them provided a large enough reduction to be immediately applicable to operational aircraft.

The use of dynamic absorbers to reduce vibrations and radiated noise has several inherent problems. For an absorber of any type to be effective, it is desirable to have a sharp resonant frequency; that is, the absorber must be fine tuned to a specific frequency. Figure 59 indicates that a slight deviation of the exciting frequency from the fixed tuned natural frequency results in a large reduction in vibration absorber effectiveness. Typically, rotor speed varies between 2% and 3% during operation. If an absorber tuned to a set frequency is installed, the absorber will become alternately effective and ineffective as the rotor rpm varies. This would result in a beating noise that could be more irritating than the tonal noise. Another troublesome aspect of the noise-vibration spectrum of a transmission is the occurrence of sidebands (Figure 60). These sidebands are created by planet passage, coupled torsional-lateral-axial vibrations, and gear imperfections. An absorber tuned to a mesh frequency would not reduce the levels of the mesh frequency sidebands.

ABSORBER EFFECTIVENESS STUDY (D-06)

External dynamic absorbers were analytically applied to the transmission housing and evaluated using NASTRAN Rigid Format 11. Four absorbers were simulated at grid points 2091, 2093,

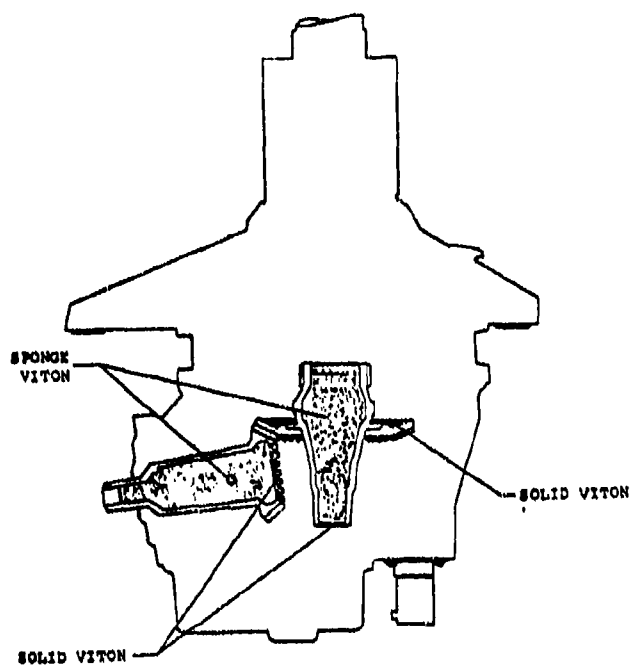


Figure 56. Possible Damped Sun and Spiral Bevel Gear Configuration.

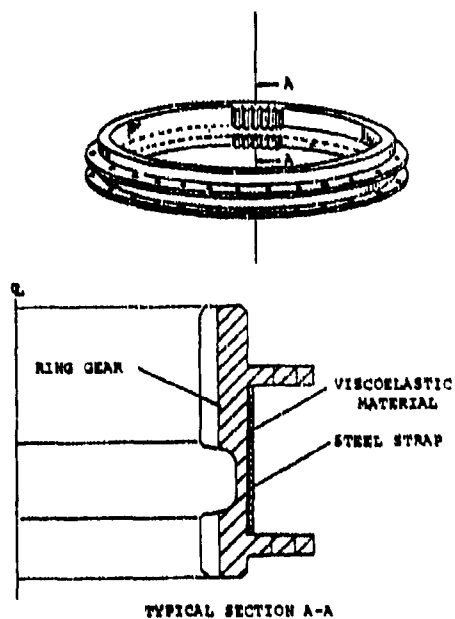


Figure 57. Possible Ring Gear Damping Strap.

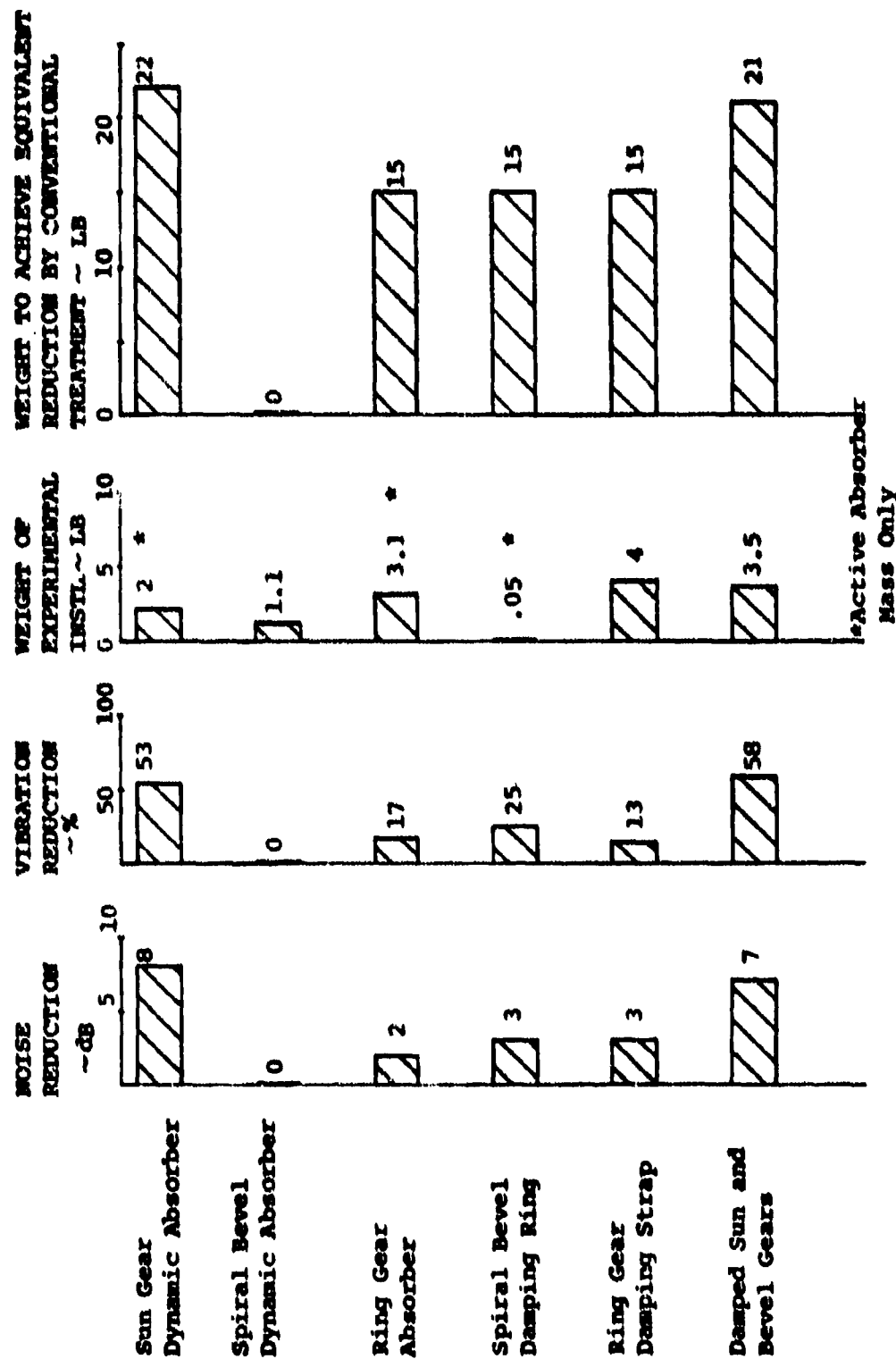


Figure 58. Summary of Absorber Test Results.

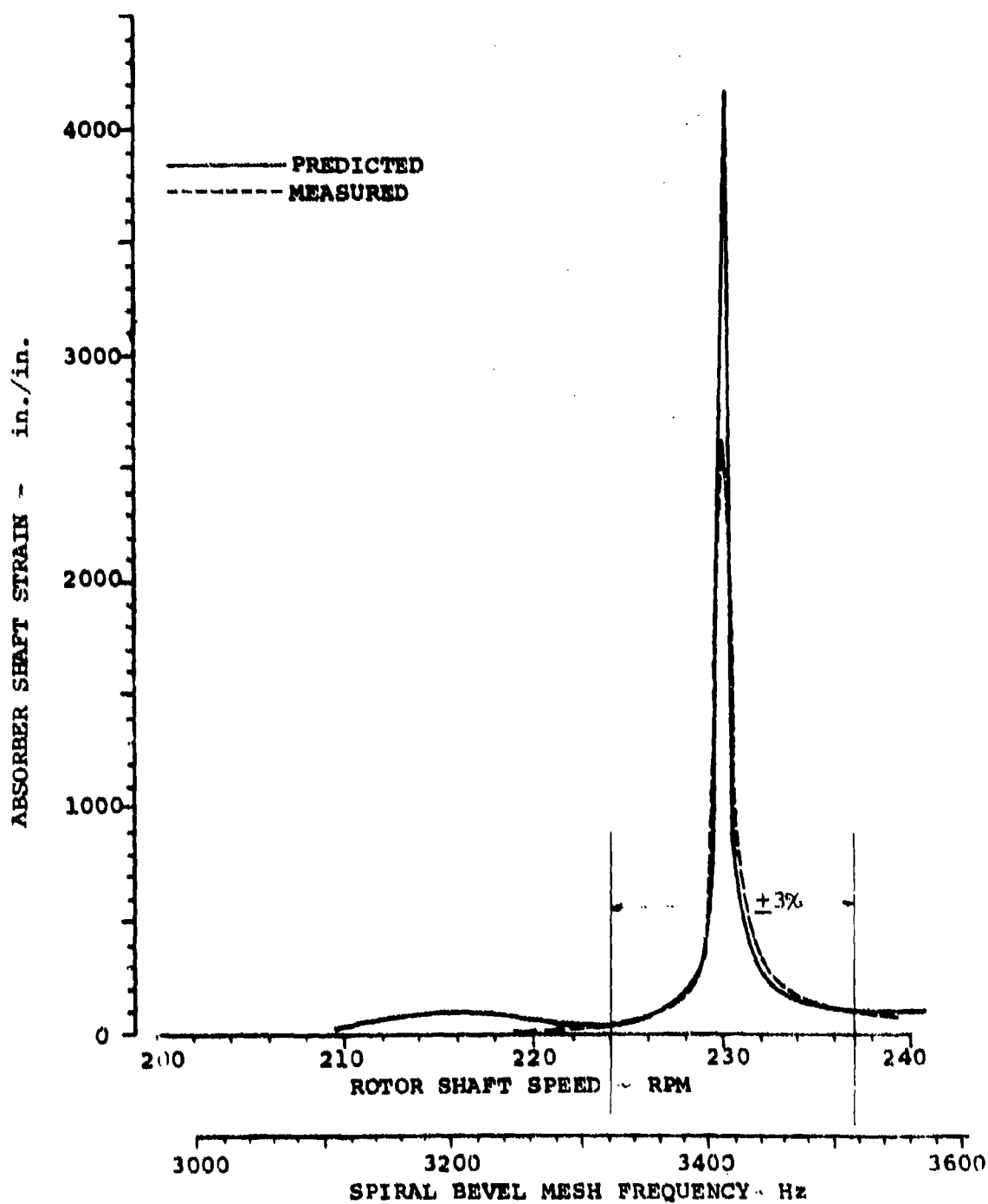


Figure 59. Comparison of Predicted and Measured Spiral Bevel Torsional Absorber Response.

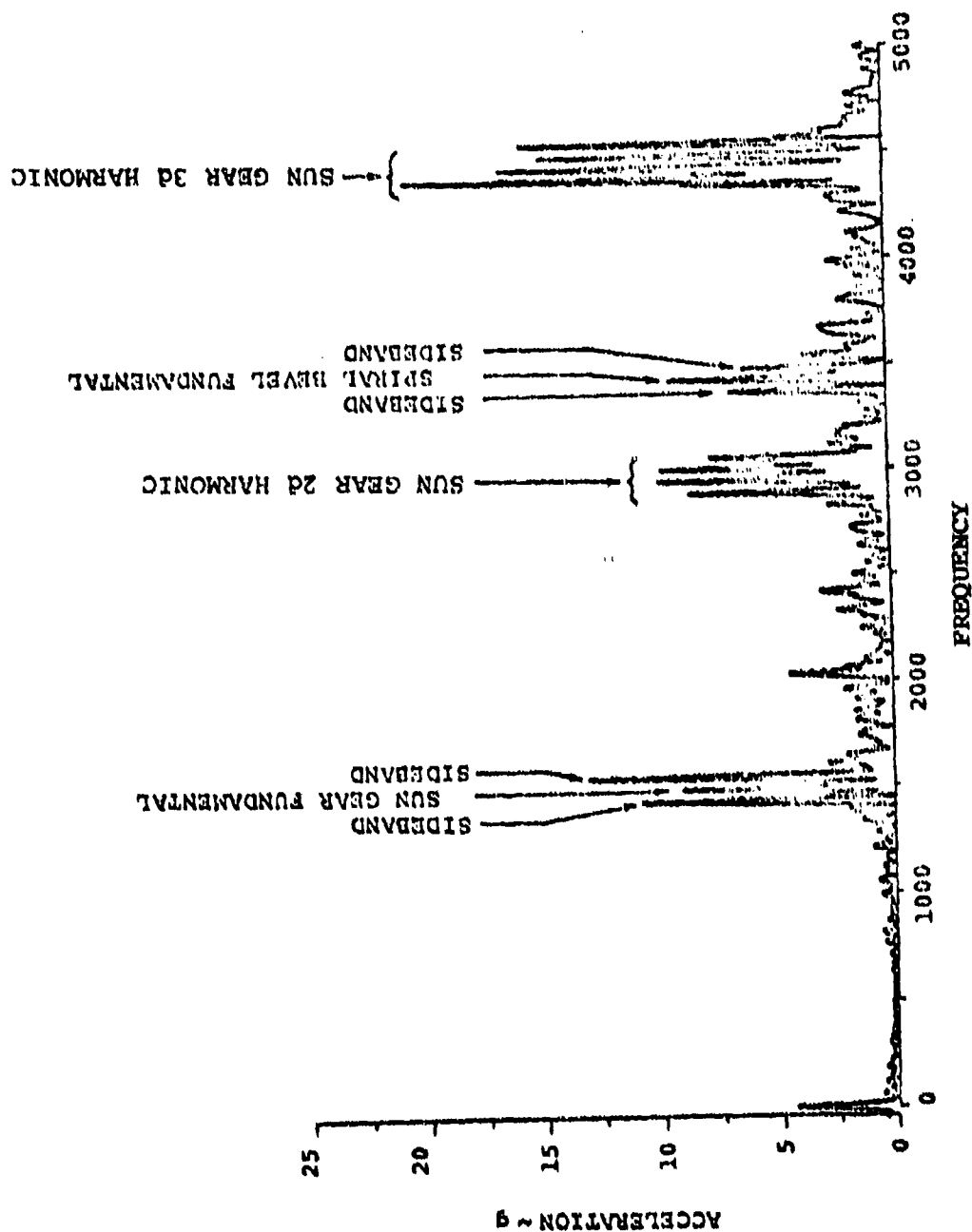


Figure 60. Vibration Data Showing Sidebands.

2001, and 2003 as shown in Figure 61. These points represent the locations at which the pinion support bearings react upon the case. A remote point (2062) was used as an evaluation point. Each of the four absorbers weighed 1.6 lbs and was tuned to the bevel gear mesh frequency of 22654.6 rad/sec.

Evaluation of the model indicated that by applying absorbers analytically on the housing at the points of load application (i.e., bearing supports), the excitation of the housing was reduced. The original deflection of evaluation point 2062 was 260 μ inches. After attachment of the four absorbers, this was reduced to 16 μ inches. However, it is doubtful that this reduction is true throughout the transmission case. There are also several practical considerations that may limit their usefulness. The curvature of the transmission case would make the actual attachment of absorbers difficult.

The high frequency (3605 Hz) could also cause a fatigue failure in the absorber. Further, since a dynamic absorber is effective only for a very narrow range of frequencies to which it is tuned, this approach is effective only if there is a clearly defined excitation frequency at which a low vibration amplitude is desired. By adding a dynamic damper, not only are the natural frequencies of the structure shifted to new values (which may be troublesome), but at least one additional degree of freedom is added which may have a mode with a natural frequency in the range of exciting frequencies.

In view of the above problem areas, the use of dynamic absorbers as a general transmission noise reduction method must be further evaluated. Although they do not provide an overall solution to the vibration/noise problem, dynamic absorbers may be useful to reduce the response at a particularly troublesome frequency which cannot be reduced by other methods. This may be a common situation for helicopter transmissions which possess several exciting frequencies.

ISOLATORS

Direct attachment of the transmission to the primary airframe structure plays a major role in noise amplification by structural response and re-radiation. Figure 62 emphasizes this fact by showing the effect of 13 lbs of skin damping treatment on cabin noise level. Vibration isolators attempt to control the transmission of high frequency vibration energy across gearbox mounts to the local airframe. Tests described in Reference 15 indicate that 10 dB reduction in speech interference level (SIL) was attained by replacing standard main transmission attachments with rubber mounts having a static spring rate equal to that of the airframe at the attachment point. A curve showing SIL noise reduction versus relative

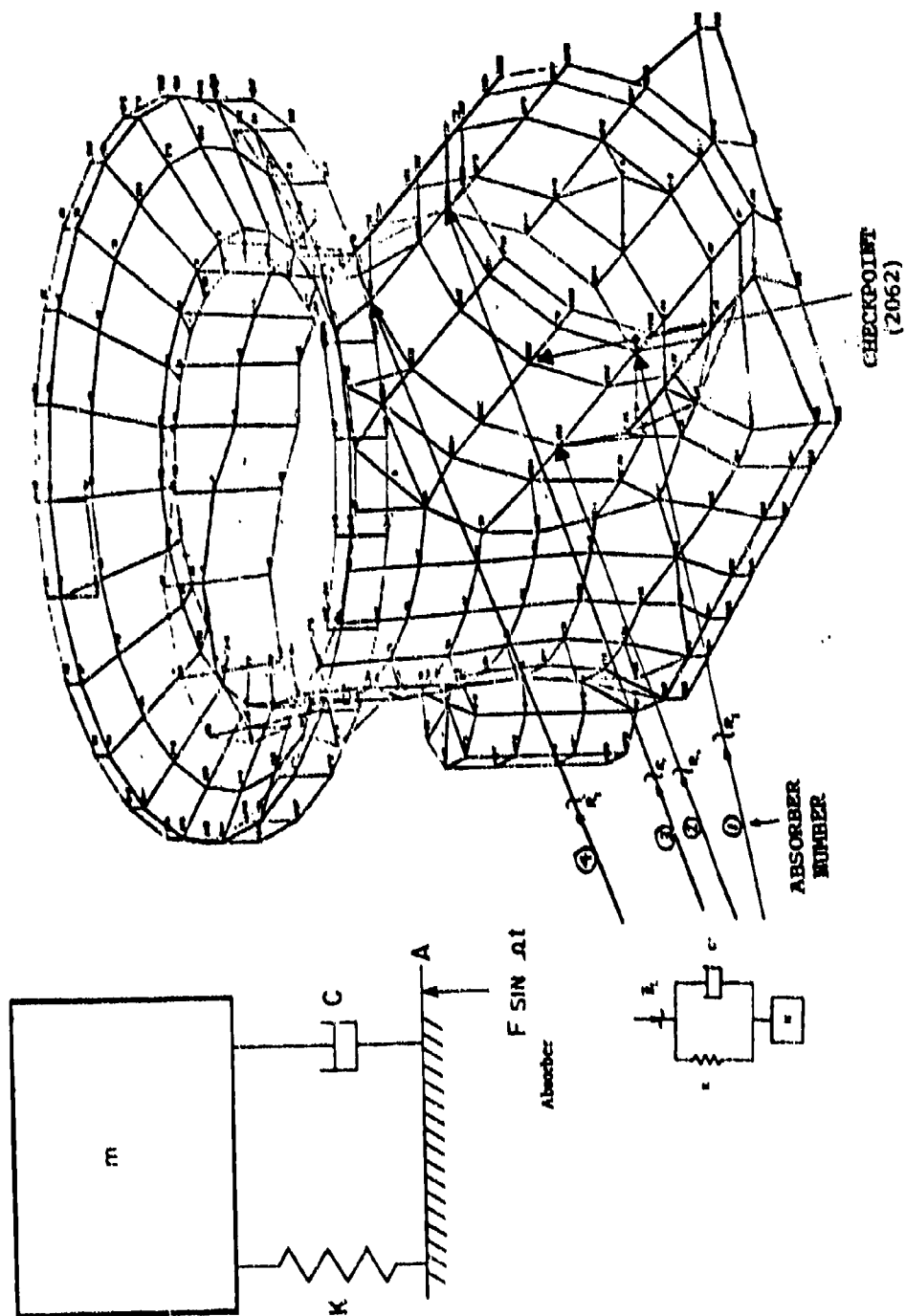


Figure 61. Proposed Points of Attachment for Radial Absorbers.

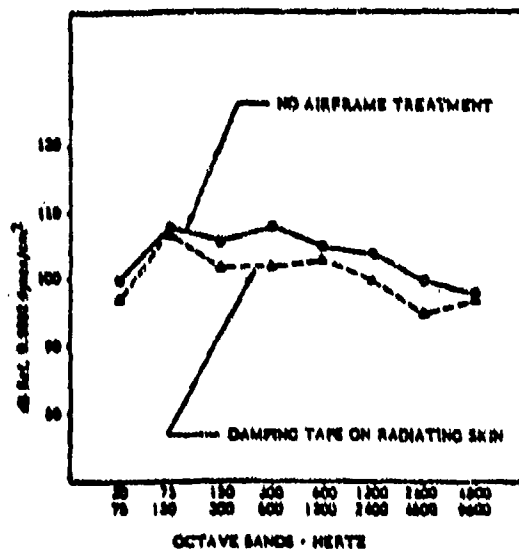


Figure 62. Effect of Skin Damping on Cabin Noise Levels (Reference 16).

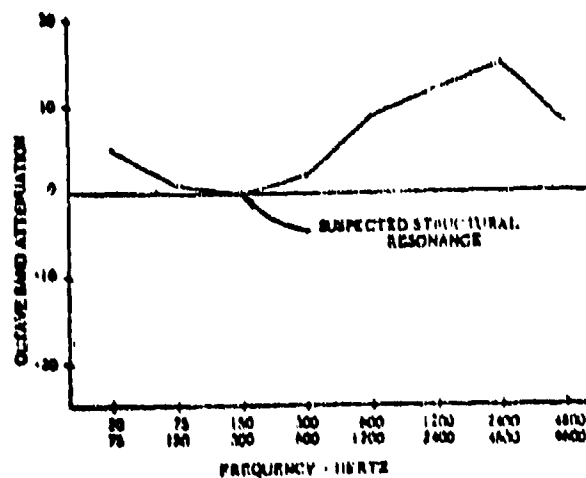


Figure 63. Cabin Noise Reduction From Isolating Element Between Transmission Housing and Airframe (Reference 16).

airframe-mounting stiffness was produced. Later work using an electromagnetic shaker and impedance head showed the noise reduction due to both structural damping and isolation with a static spring rate compatible with transmission-airframe relative movement restrictions (Reference 16). Figure 63 shows the benefits of isolation of the transmission.

To investigate the use of isolators, a 1/4 scale CH-47C forward pylon was tested and indicated that main source of noise was structure-borne with the frames responding mostly at high frequencies. For a full scale application of vibration isolators between the transmission mounting legs and airframe, calculations indicated that the 650 ft-lbs of torque required on the attachment lug of a transmission leg would put 32,400 lbs compressive force (dry) to 62,400 lbs compressive force (wet lubrication) on an isolator. Thus, extrusion could be a problem as well as misalignment. For test purposes, a lightly loaded isolator was used to assess the proportions of structure-borne and airborne noise. Figure 64 indicates the predominance of airborne noise.

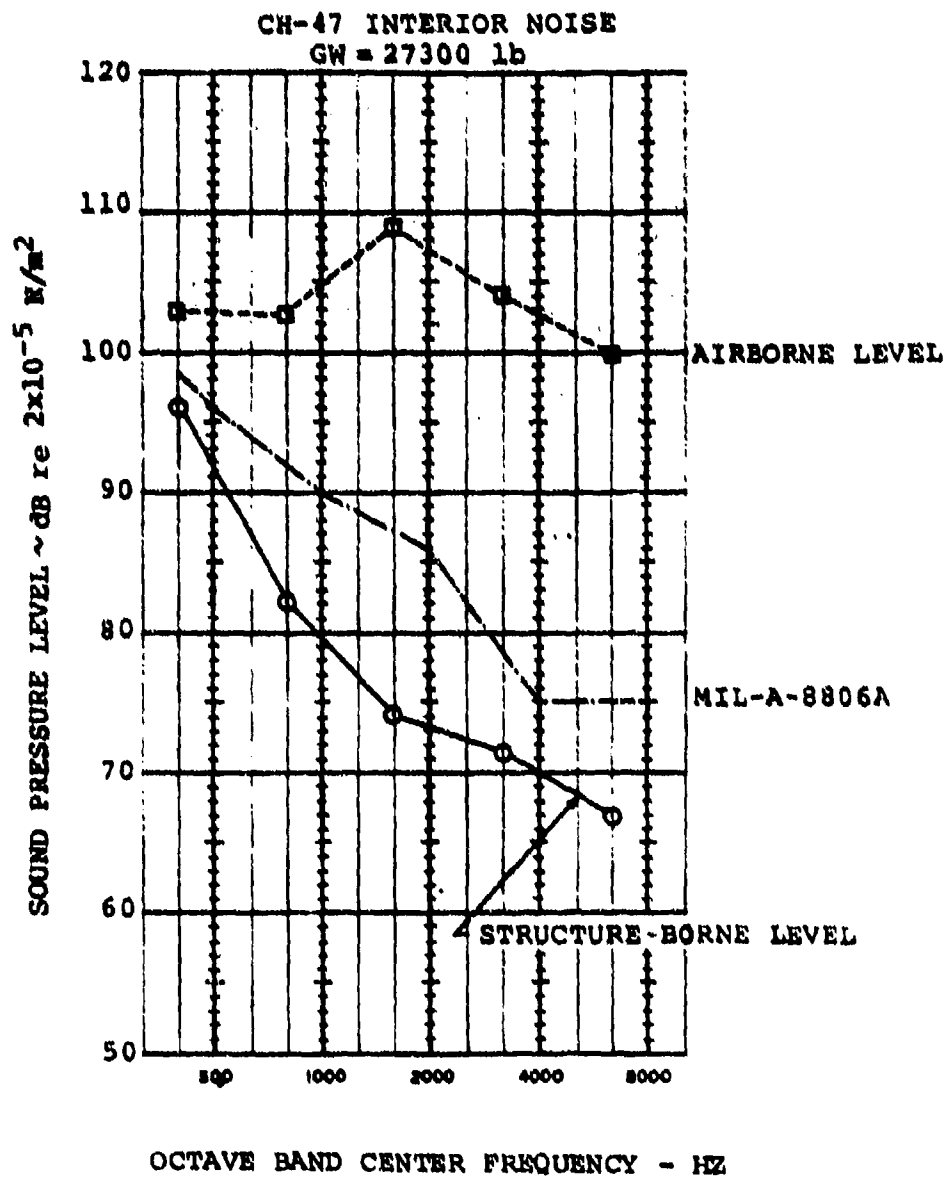


Figure 64. Airborne and Structure-Borne Noise.

NOISE PREDICTION AND REDUCTION

To reduce transmission noise, the shaft displacements at the supporting bearings must be reduced. This is accomplished by predicting the damped forced response (DFR) of the gear shafts using computer program D-82. The shafts are then modified and a new response is determined. This procedure is iterated until minimum displacements are achieved. The change in displacements must then be related to the change in noise level.

The relationship of the resultant noise reduction to the change in shaft displacement is very complex. If a single shaft were supported by a single bearing, the resultant noise reduction would behave approximately as

$$\text{SPL} = 20 \log \frac{(kx)_{\text{New}}}{(kx)_{\text{Baseline}}} \quad (1)$$

where $F = kx$ is the dynamic force at the bearing station. However, in practice transmissions have two primary shafts (excluding the rotor shaft) and several supporting bearings. This presents considerable difficulty in estimating the noise reduction.

There are several ways to consider this problem. One is to consider each bearing as a separate noise source; another is to consider all the bevel shaft bearings as a second source. A third approach is to consider the case as a single large noise source being driven by the resulting sum of the dynamic forces. However, without knowledge of how the case will respond it is not clear which of the above models is suitable (if any).

A method of predicting the change in sound pressure level (SPL) associated with a change in shaft response was developed by Boeing Vertol in the HLH/ATC Noise Reduction Program (Reference 4). This method has been improved upon as a result of a company-sponsored independent research and development program in which a statistical correction factor (B), which is a function of gear mesh frequency, was developed. This factor is incorporated into the analysis as follows:

$$\Delta \text{SPL corrected} = (1 + B) \Delta \text{SPL predicted} \quad (2)$$

where $B = -6.5539 + 6.3943 \times 10^{-3} f - 1.338 \times 10^{-6} f^2$ and
 f = gear mesh frequency.

Using this correction factor, the noise reduction in the lower stage planetary mesh frequency range (800 to 1600 Hz) was

predicted to within ± 3 dB with a 90% confidence level. The results were not as dramatic for the bevel mesh frequency range (1950 to 3600 Hz); however, 42% of the test samples were within 2 dB of measured values as compared to 32% without the correction factor. The results of this program are summarized in Table 5 for the sun frequency range and in Table 6 for the bevel frequency range. It is apparent that this method is still unsatisfactory in the higher (bevel) frequency range, where elastic body modes of the shafts and case may be excited which do not lend themselves to this type of analysis.

TABLE 5. TRACKING SUN MESH (800 Hz - 1600 Hz)

PERCENT OF SAMPLE WITHIN XdB OF PREDICTED						
PREDICTED	2dB	3dB	4dB	6dB	12dB	> 12dB
W/O β	40	50	75	82	98	2
WITH β	90	98	100	-	-	-

NOTE: 8 Microphones, 95 Sample Points

TABLE 6. TRACKING/BEVEL MESH

PERCENT OF SAMPLE WITHIN XdB OF PREDICTED					
PREDICTED	2dB	4dB	6dB	12dB	> 12dB
W/O β	32	53	75	96	4
WITH β	42	55	79	92	8

NOTE: 6 Microphones, 94 Sample Points

Therefore, this approach to predicting changes in SPL should be considered as an interim approach. The approach which will yield the maximum utility will calculate the resultant noise levels as a function of cyclic energy at the shaft supporting bearings. This would also greatly simplify the trade of acoustical treatment weight for shaft weight. The present difficulty arises because the method of calculating overall noise levels is based on torsional resonances of the transmission system, whereas the method of predicting changes in noise reduction is based mainly on lateral resonances.

Due to the very complex relation of noise to vibration, a semiempirical approach to transmission noise prediction, based on cycled energy at the gear mesh, was developed by MTI (Reference 10, page 288). This scheme assumes that some small

fraction (α) of the cycled energy of the power train is lost as acoustic energy. The case is initially assumed to be spherical in geometry, and then a geometry correction factor (β) is employed. These are empirical constants, and the product $\alpha \beta = 2.06 \times 10^{-3}$ was experimentally determined to correlate with the CH-47C transmission test. The SPL is then calculated by the following equation:

$$L_f = 10 \log \left[\frac{4.94 \times 10^4 \alpha \beta f \sum e_o F_o}{r^2} \right] \quad (3)$$

The peak values of the mesh sinusoidal excitation (e_o , inches) are calculated by the computer program GGEAR (R-67), and the dynamic tooth force (F_o , lbs) is calculated using the computer program TORRP (R-32). The sound pressure level L_f is in dB, and f , the mesh frequency, is in CPS. The radial distance, r , to the center of the transmission is in feet. The above formula has generally been used for noise prediction with some degree of success. It is expeditious because it involves only the relatively simple and quick-running computer programs GGEAR and TORRP. It is only necessary as a side calculation to obtain the modified gear contact ratio and the subsequent equivalent gear tooth compliance. Through the use of Tregold's approximation, helical and spiral bevel gears may be included in the noise prediction, since GGEAR applies only to spur gears (Reference 17).

The modified contact ratio is calculated by program R20. For completeness, it is noted that a sample manual calculation for the modified contact ratio for the CH-47 forward rotor transmission spiral bevel gears is shown in Reference 4. A sample calculation for the equivalent gear tooth compliance is as follows:

$$q_{1-2} \text{ (min)} = (QJ1ABC + QJ2ABC) \text{ min} + QJD \quad (4)$$

where

QJ1ABC, QJ2ABC are the compliances of the driving and driven gears.

QJD = 0.04593 in./lb (Hertzian compliance)

(QJ1ABC + QJ2ABC) min = 0.0481 in./lb

-
17. Gu, A.L., and Badgley, R.H., PREDICTION OF GEAR-MESH-INDUCED HIGH-FREQUENCY VIBRATION SPECTRA IN GEARED POWER TRAINS, Mechanical Technology Incorporated, USAAMRDL TR 74-5, U.S. Army Air Mobility Research and Development Laboratory, Fort Eustis, Virginia, January 1974, AD777496.

$$q_{1-2} \text{ (min)} = 0.09403 \text{ in./lb}$$

$$\psi = 25^\circ \text{ mean spiral angle}$$

$$\phi = 22.5^\circ \text{ pressure angle}$$

$$h = m-1 = 1.936 - 1 = 0.936$$

$$q_{R1} = (q_{12}) \text{ min}/(\cos^2 \psi) (\cos^2 \phi) = 0.134117 \text{ in./lb}$$

$$q_{1-2} = q_{R1} (1 - 0.3h) = 0.134117 (1 - 0.3 [0.936]) = 0.09646 \text{ in./lb}$$

$$q_{1-2} = 0.09646 \text{ in./lb (Equivalent Gear Tooth Compliance)}$$

$$K_{1-2} = 1/q_{1-2} = 10.367 \times 10^6 \text{ lb/in. (Equivalent Gear Tooth Stiffness)}$$

Another way to predict noise levels is given on page 3-118 of Reference 18. Here, the SPL is more naturally calculated from the acoustical power generated by a vibrating surface. This would be more appropriate to the analysis of the noise output from the CH-47 transmission case. The development of the analysis is given here.

A surface vibrating in a fluid medium emits sound. The acoustic power that is transferred to a medium by a vibrating surface depends on the physical characteristics of the medium, the oscillatory volume displacement of the fluid caused by the vibrating source, and the size and shape of the generator.

The acoustic power generated by a vibrating surface can be expressed by

$$P = U^2 R_A \times 10^{-7} \text{ watts} \quad (5)$$

where

$$U = \text{rate of volume displacement of fluid (cc/sec)}$$

$$R_A = \text{acoustic radiation resistance seen by source (acoustic ohms)}$$

Let the amplitude of the oscillatory displacement of an area element dA be W , and the frequency be ω throughout the area A at a particular mode. Then,

$$U = 2\pi\omega \int_A W dA = 2\pi\omega \bar{W} A \quad (6)$$

-
18. Gray, D.E., Coordinating Editor, AMERICAN INSTITUTE OF PHYSICS HANDBOOK, Second Edition, McGraw-Hill Book Company, Inc., New York, 1963.

where

$$\bar{W} = \frac{1}{A} \iint_A W \, dA \quad (7)$$

= Average displacement amplitude

The acoustic radiation resistance R_A depends on the size and shape of the generator. Two typical shapes are discussed in Reference 18: pulsating sphere and vibrating piston. In both cases,

$$R_A = K \frac{\rho C}{A} \text{ if } \frac{D}{\lambda} \geq 1 \quad (8)$$

where

ρ = density of medium (gm/cc)

C = velocity of sound in medium (cm/sec)

D = diameter of sphere (or piston) (cm)

$\lambda = \frac{C}{\omega}$ = wavelength (cm)

ω = frequency (Hz)

K = a numerical factor

The numerical factor K is equal to unity when $D/\lambda \geq 1$, i.e., in the high frequency range (see Figure 3i-1 of Reference 18). In the lower frequency range, K is less than 1. To estimate the value of K at low frequency from the gearbox noise standpoint, take the fundamental frequency of the CH-47 upper planetary meshing, 406 Hz for example. The wavelength $\lambda = C/\omega$ is approximately 75 cm or 30 in. Suppose that the diameter of the ring gear is taken as D . Then $D/\lambda = 22/30 = 0.73$. According to Figure 3i-1 of Reference 18, $K = 0.85$ for a spherical source, and $K = 1$ for a vibrating piston. It is therefore concluded that the value of K is not far from unity. For acoustic power computation, set

$$K = 1 \quad (9)$$

Using Equations (6), (8) and (9), Equation (5) can be written as

$$P = \omega^2 \bar{W}^2 A (2\pi)^2 \rho C \times 10^{-7} \quad (10)$$

where

P = acoustic power (watt)

ω = frequency (Hz)

\bar{W} = average displacement amplitude (cm)

A = area (cm²)

ρ = density of medium (gm/cc)

C = velocity of sound in medium (cm/sec)

For helicopter noise, the medium is air, with $\rho = 0.00122$ gm/cc and $C = 33,700$ cm/sec. Thus,

$$P = 1.62 \times 10^{-4} \omega^2 \bar{W}^2 A \text{ (watt)} \quad (11)$$

Choose a reference acoustic power of 10^{-12} watt. Then a power level in dB can be defined as

$$L_{\text{power}} = 10 \log_{10} \frac{P}{10^{-12}} \text{ (dB)} \quad (12)$$

where

L_{power} = power level (dB)

P = acoustic power (watt)

For a point source, the power level is related to the sound pressure level measured at a distance r by

$$L_{\text{power}} = L_{\text{SPL}} + 20 \log_{10} r + 11 \quad (13)$$

where

L_{power} = power level (dB)

L_{SPL} = sound pressure level (dB)

r = distance from the source at which L_{SPL} is measured (meter)

The reference for the power level is 10^{-12} watt, and the reference for the sound pressure level is 0.0002 microbar.

At approximately $r = 1 \text{ ft} = 0.305$ meter, Equation (13) reduces to

$$L_{\text{power}} \approx L_{\text{SPL}} \quad (14)$$

Thus,

$$L_{\text{SPL}} \cong L_{\text{power}} = 10 \log_{10} \frac{P}{10^{-12}} \text{ (dB)} \quad (15)$$

Therefore, the sound pressure level measured at 1 foot from a point source is approximately equal to the power level, both in units of dB. Equations (13), (14), and (15) are valid only for a point source. In applying Equations (13), (14), and (15) to the noise generated by ring-gear casings, a geometrical configuration factor should be introduced to take into account the casing geometry. However, this factor is neglected in the sound pressure level calculation for simplicity.

BASELINE DATA AND CORRELATION

BASELINE DATA

An extensive dynamic test of a CH-47C forward transmission was conducted in the Boeing Vertol closed-loop test stand under a previous USAAMRDL contract (Reference 4). The transmission was instrumented both internally and externally to measure strains, displacements, and accelerations of rotating components, and case acceleration and noise levels, respectively. This test program was unique in that it incorporated instrumentation and rotary transformers operating in the hot-oil environment of the transmission. Two 14-channel tape recorders were used with sequencing schedules to allow for logical groupings of signals recorded simultaneously. Speed sweeps and stabilized speeds were recorded for several transmission torques. Nearly 25,000 data points were successfully recorded during this test program.

The primary objective of the test effort was to obtain experimental data for use in verifying existing computer programs which have been developed for the prediction of the high-frequency vibration characteristics of transmission components. A secondary objective was to demonstrate the feasibility of measuring very small displacements and dynamic loads within the hot-oil environment of an operating transmission. The test setup, hardware, instrumentation, data reduction, and example output data are fully documented in Reference 4.

No additional baseline testing has been conducted for this present program; the data collected in Reference 4 has provided the baseline data. Only a small portion of this raw data, which is stored at the Boeing Vertol Acoustic Laboratory and occupies some 80 reels of 14-channel magnetic tape, had been previously reduced and analyzed. Reduction and analysis of additional test data have continued for this new program.

Shaft displacements, vibrations and accelerations of shafts and case, and noise level data have been reduced. The two primary formats for presenting the data are narrow-band spectrum analysis for stabilized speeds and gear mesh frequency tracking for speed sweeps. Examples of these two formats are shown in Figure 65.

The correlation of the reduced data includes five aspects:

1. Vibration amplitude
2. Vibration mode shape
3. Vibration natural frequencies
4. Noise level spectrum
5. Method improvements

MICROPHONE LOCATION M-17

NOISE SPECTRUM AT 7000 RPM

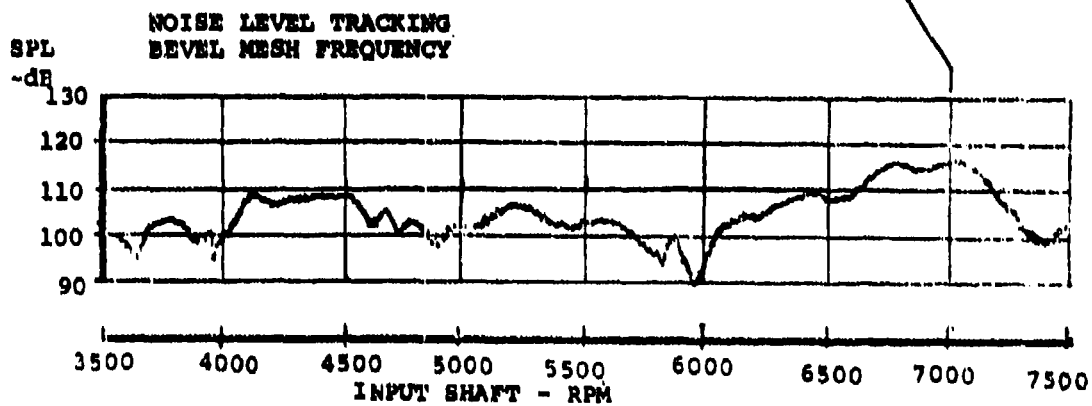
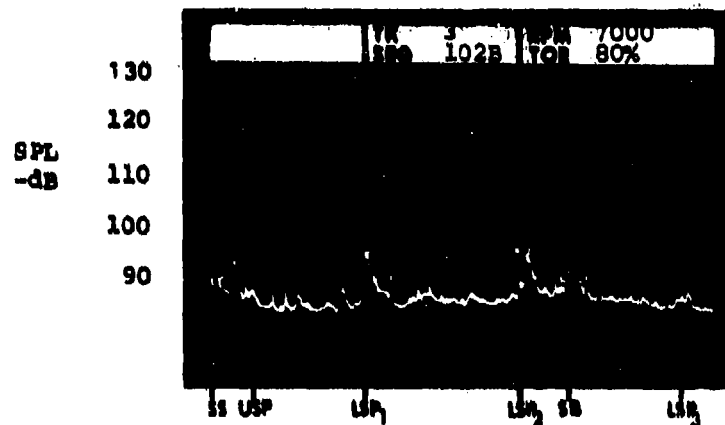


Figure 65. Selection of Correlation RPM for Spiral Bevel Mesh Frequency.

Examples of this correlation process were presented in Reference 3 where mode shapes of the shafts were compared to measured displacements. Another aspect of data correlation is to evaluate the mathematical model and modify it as indicated by test data. For the transmission shafting, two changes to the model were incorporated. First, the data indicated strong coupling of the shafts in the model; so the model was modified. The second change to the original model was to approximate the planet support to the sun gear by linear springs having stiffness equal to 50% of the calculated carrier post stiffness. From a study of the effect of planet support on the DFR of the sun gear, it appears that the two opposite carrier posts are acting as springs in series to maintain the sun gear in position. Therefore, a 50% post stiffness was used in the model, which resulted in excellent agreement.

Another example of correlation and feedback based on earlier results is demonstrated in Figure 66 where the ring gear response is analyzed. In this example, a trace of an accelerometer, mounted on the CH-47 ring gear, is shown tracking the sun mesh frequency. The predicted natural frequencies obtained with the earlier math model are superimposed on this trace. The response of the ring gear to the sun frequency is interesting in that the first natural frequency is predicted at 5400 rpm and no prior response is noted. The nearness of the first five criticals probably accounts for the retained height of the peak. Why the peak does not drop off is not clearly understood. It is speculated that assumptions used in modeling the end fixity of the ring gear were not representative of the actual end fixity. By changing the fixity to provide for a stiffer constraint, the lower predicted frequencies can be shifted to the right (i.e., to higher critical frequencies). Feedback such as this will be incorporated into the case model as part of this program.

A sample of case acceleration spectrum is shown in the lower portion of Figure 66. Note the well defined spikes at the gear mesh frequencies. These accelerations are readily converted to displacements as follows:

$$\begin{aligned} \text{let } x &= A \sin \omega t \\ \text{then } \ddot{x} &= -A\omega^2 \sin \omega t \\ x &= -\ddot{x}/\omega^2 \end{aligned}$$

Using these displacements, the predicted response may be compared to the test data.

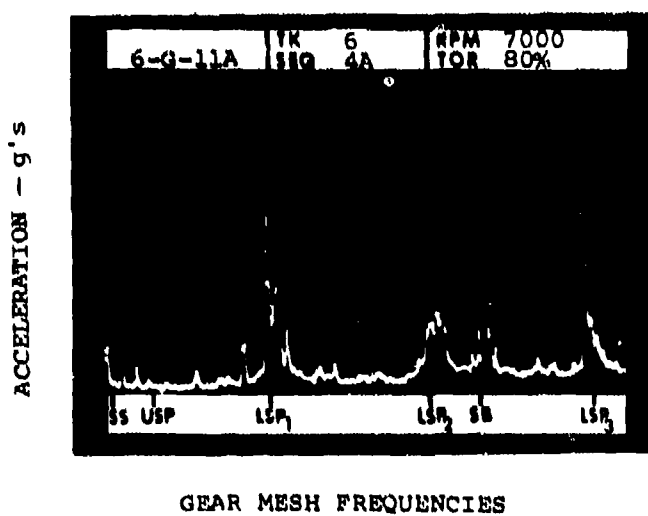
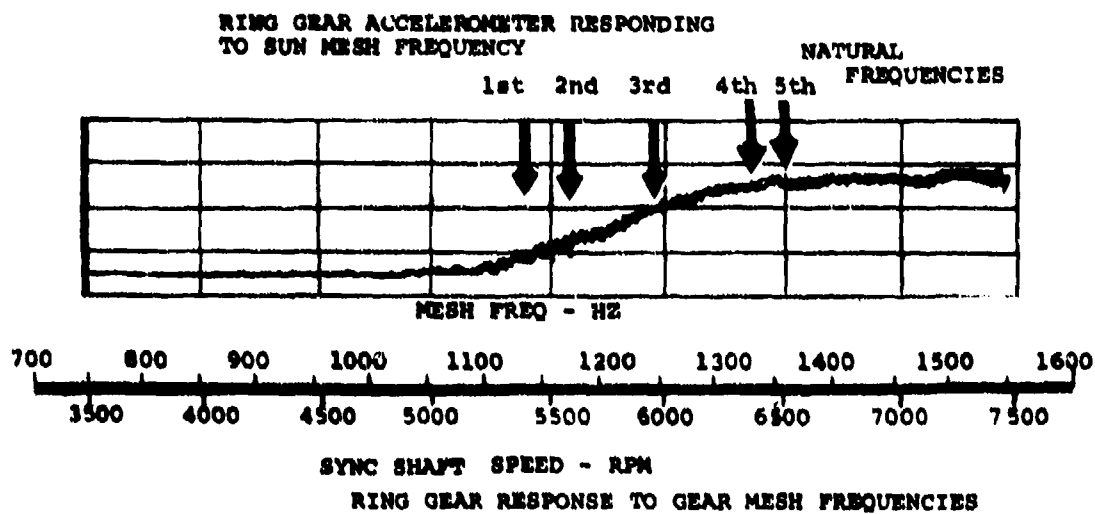


Figure 66. Example of Test Data for Correlation Study.

Figure 67 presents typical baseline noise data in its reduced form. The top of the figure shows a spectrum of the noise output. The lower portion of the figure demonstrates how the data is broken down into a third-octave band analysis. From several such plots the maximum noise levels and corresponding frequencies for various locations on the transmission have been identified. Figure 68 summarizes these maximum baseline noise levels for the LP1, LP2, LP3, and bevel mesh frequencies at an operating condition of 7460 sync shaft rpm and 80% torque.

A further example of the data being reduced for correlation purposes is presented in Figure 69, which summarizes baseline case vibration spectra at several locations.

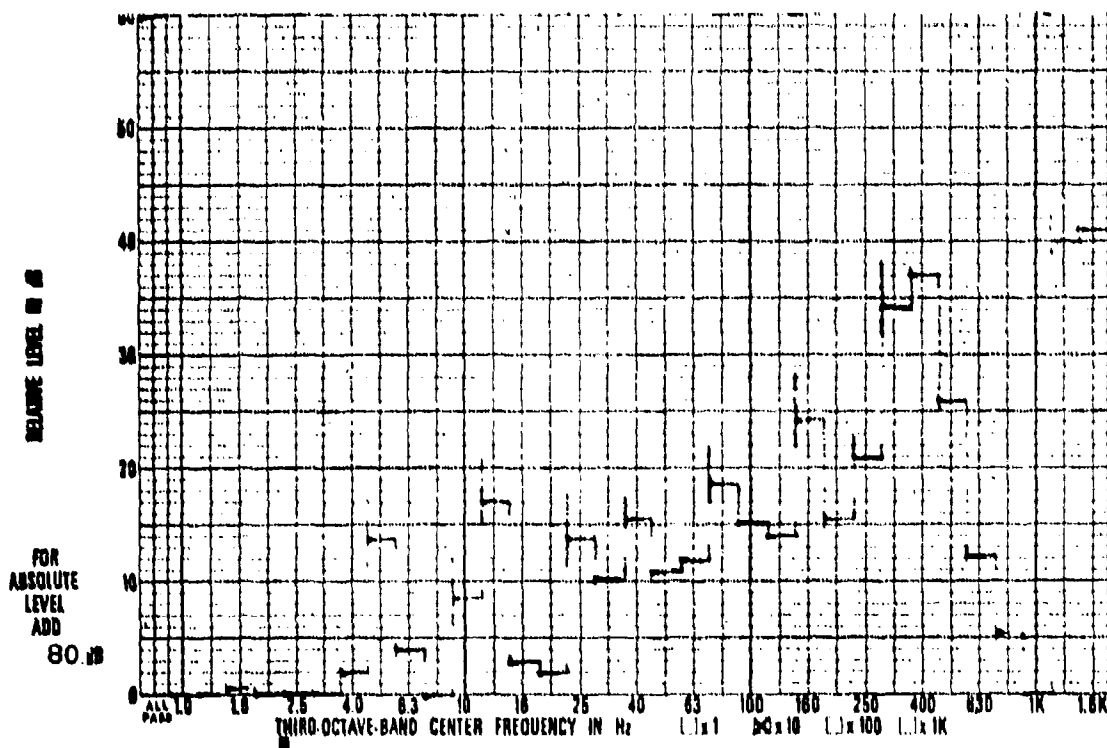
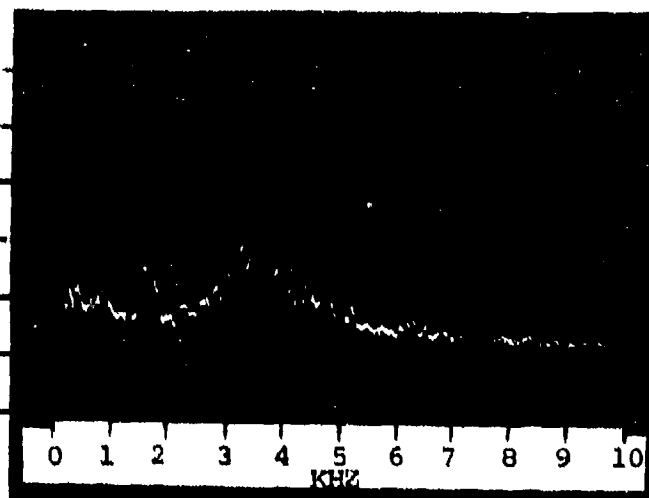
The damped forced response (DFR) is determined by applying the calculated dynamic forces to the D-82 model. The DFR of the sun gear responding to the bevel frequency is shown in Figure 70 with the displacements at right angles to each other identified as Y and Z and the torsional displacements indicated by θ . Since these displacements are not in the direction of the proximity probes, section cuts through the plane of the probes were determined and are shown in Figure 71.

Superimposed on these figures are the test results, as determined by phase-corrected proximity probe data. In terms of amplitude, the agreement of the predicted and measured displacements is excellent for the larger displacement. The correlation of the smaller displacements is not quite as good; however, several things must be considered in evaluating these very small displacements. First, the smaller displacements (i.e., less than 30 microinches) are often associated with nodes, and a small error in predicting its position can result in a larger error in displacement (at least in terms of percentage). Another item to consider is that instrumentation error becomes a factor for very small displacements. Finally, small displacements are a measure of goodness and therefore are not as interesting as the large displacements. What is important is to predict large displacements when they are large and small displacements when they are small.

As important as predicting displacements is predicting mode shapes. The DFR of the bevel shaft responding to the bevel frequency is particularly convenient for determining mode shape, since a node had been predicted between the two proximity probe locations. This confirmed the presence of a node between these two stations. A photograph of the two signals is superimposed on the DFR in Figure 72.

Examples of correlation of the measured and predicted shaft displacements are shown in Figure 73.

110 dB
10 dB/Div.



MICROPHONE #1

7460 RPM

80% TORQUE

Figure 67. Typical Baseline Noise Spectrum-
Third-Octave Band Analysis.

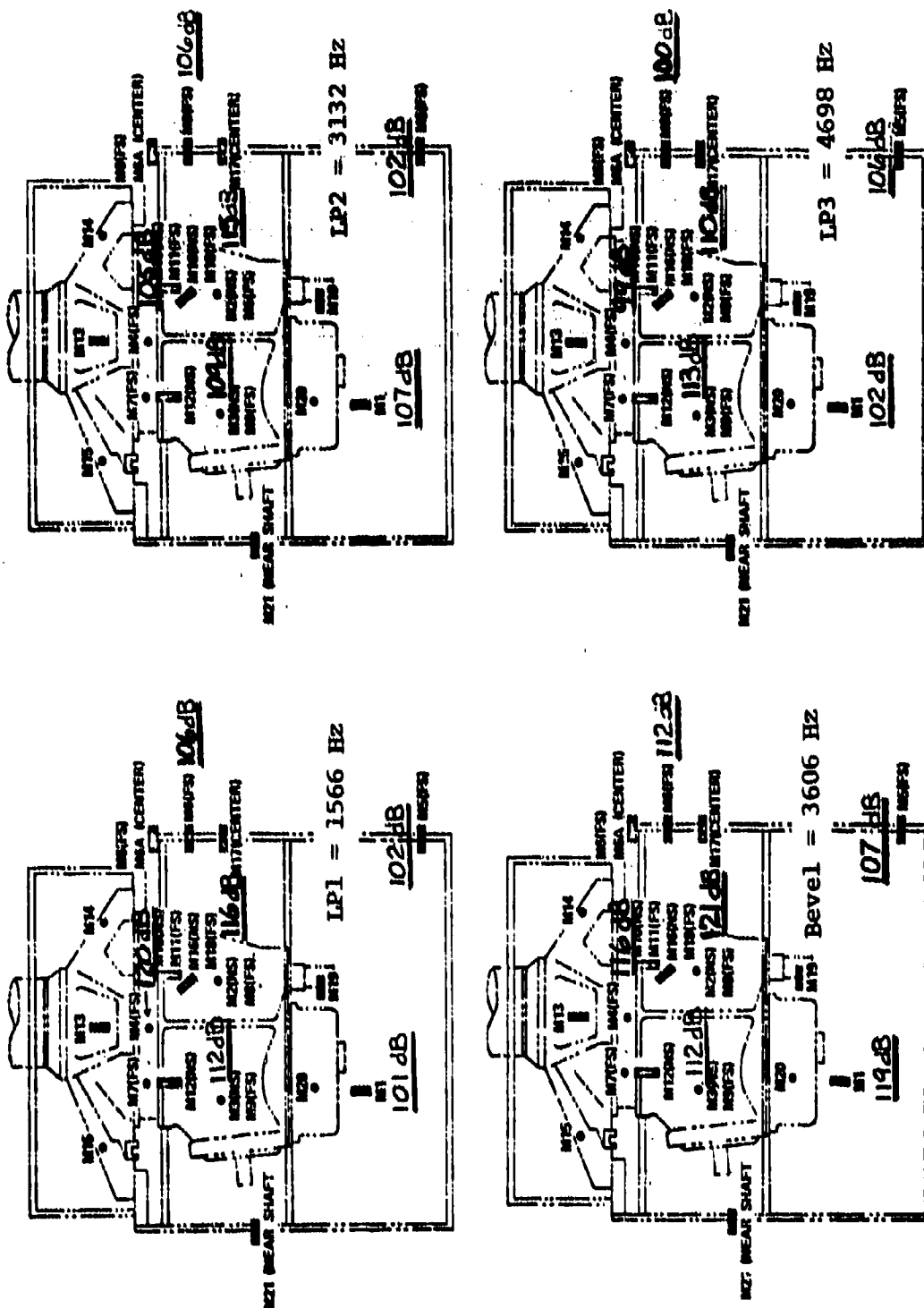


Figure 68. Measured Noise Levels for CH-47 Forward Transmission (Baseline) at 7460 Sync Shaft RPM and 80% Torque.

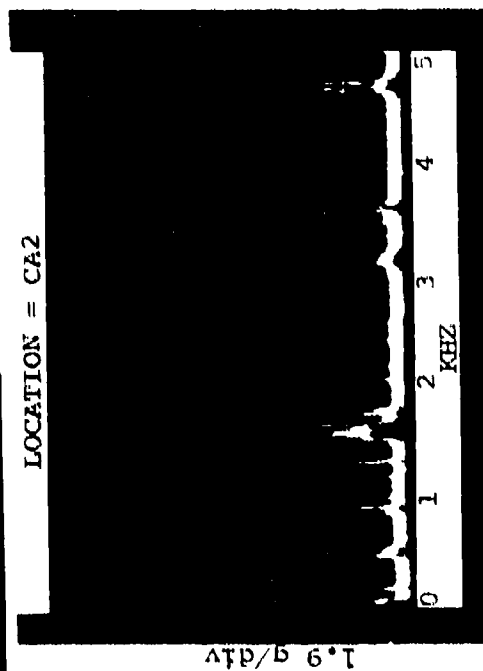
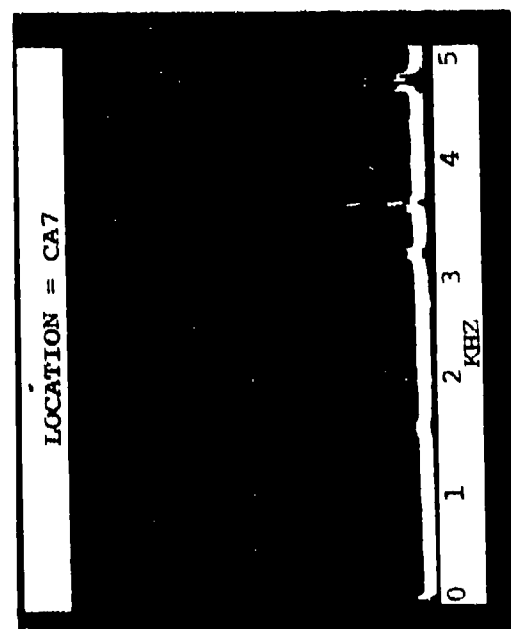
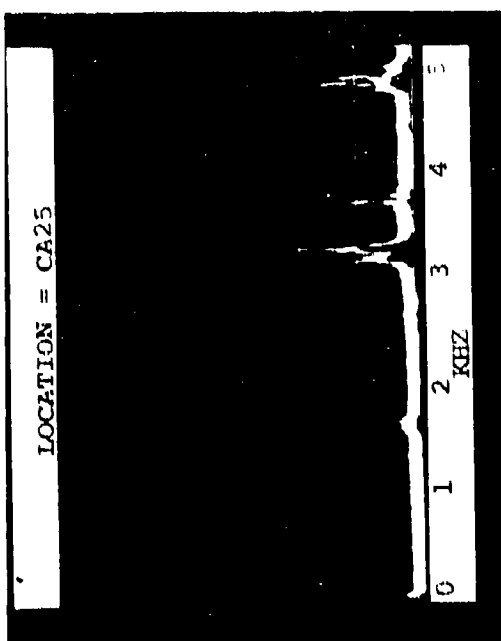
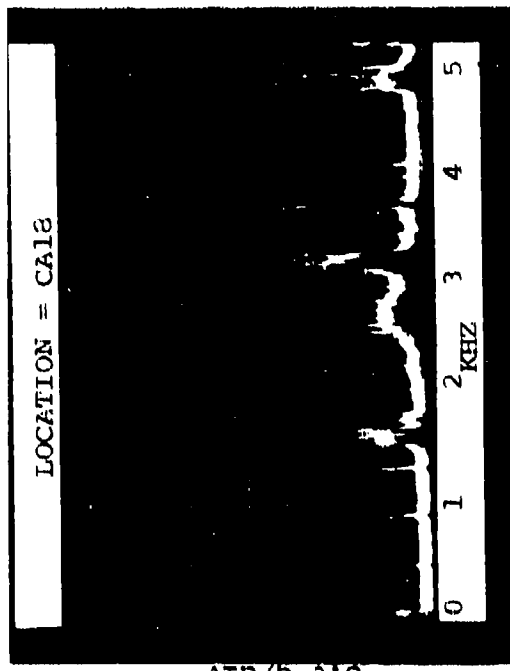
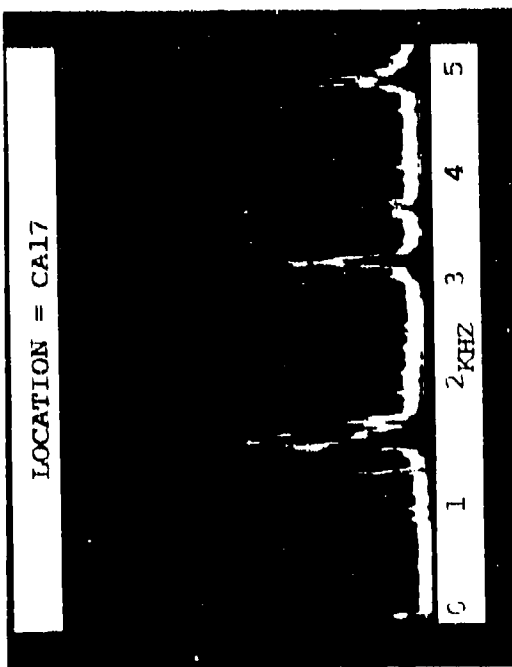


Figure 69. CH-47 Forward Transmission Case Vibration Spectra (Baseline) at 7460 Sync Shaft PPM and 80% Torque.



ACCELEROMETER LOCATIONS

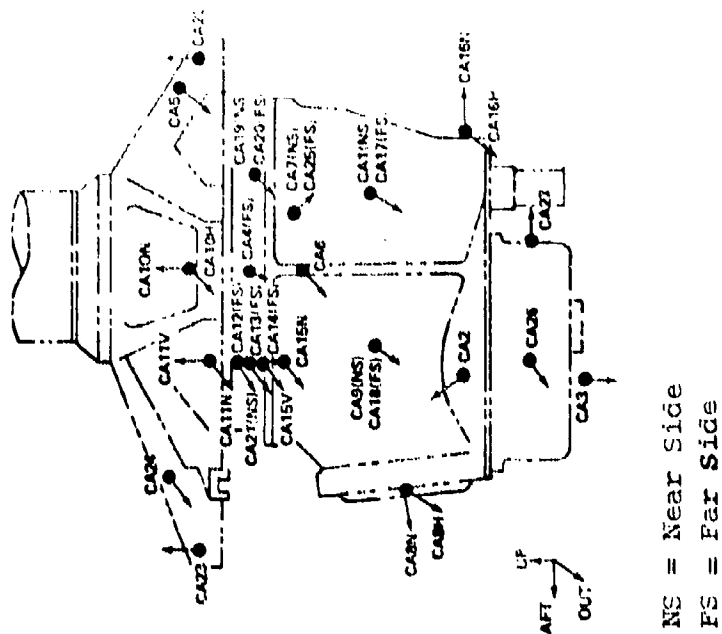


Figure 69. Continued.

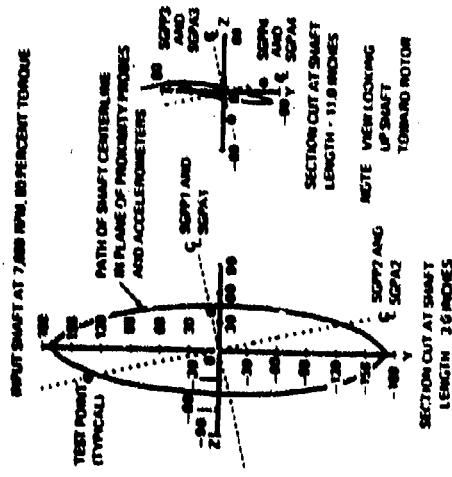


Figure 71. Lissajous Figures of Sun Gear Shaft Responding to Bevel Frequency.

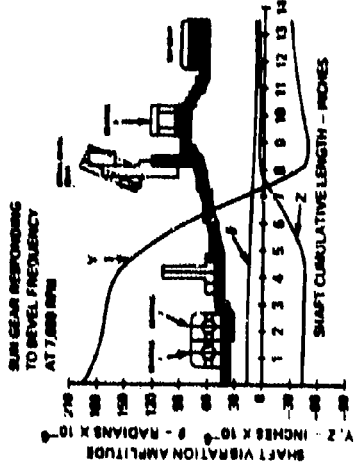


Figure 70. Prediction of Sun Gear Shaft Response to Bevel Frequency Excitation.

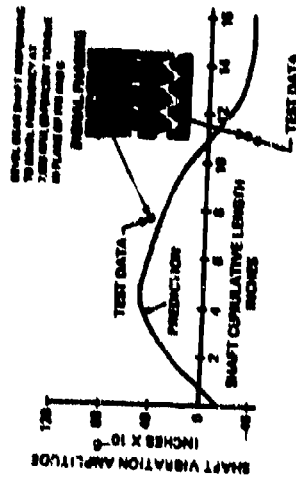


Figure 72. Mode Shape Correlation of Bevel Gear Shaft Responding to Bevel Mesh Frequency.

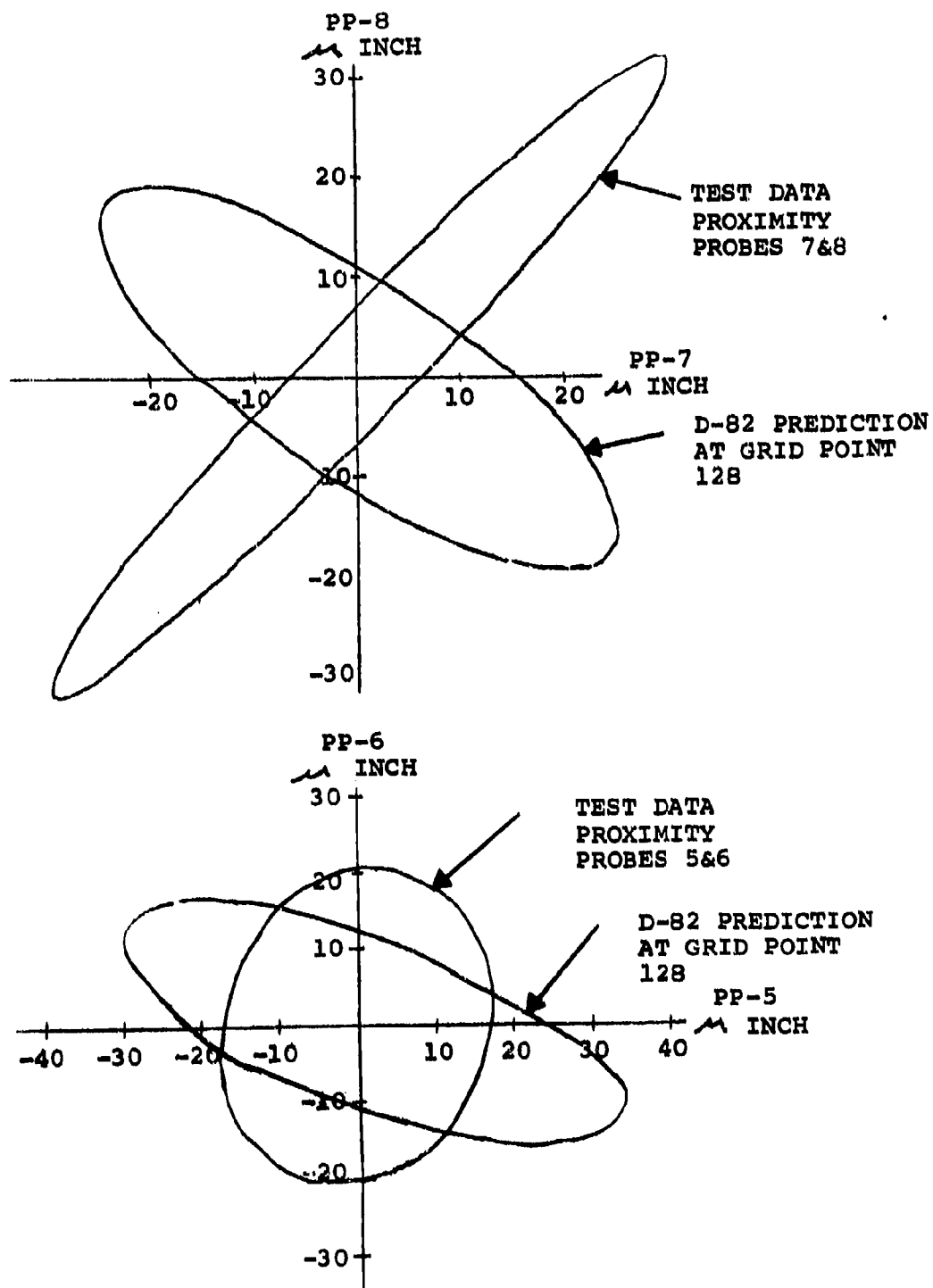


Figure 73. Shaft Displacements - Correlation of D-82 Predictions with Test Data.

CORRELATION OF ANALYSIS WITH BASELINE TEST DATA

Two basic types of data, noise and case acceleration, were obtained for both the baseline and all design modification runs. In an effort to establish the validity of the analytical approach early in the program, the baseline configuration was evaluated using the analytical system herein defined. The results of this analysis were examined in comparison with the baseline experimental data to determine the amount of correlation which exists. Sample correlations for both noise and case vibration data follow.

Noise

Choosing microphone M5, which is located in the general vicinity of the pilot's head (Figure 69), as our sample correlation point, we find that the following baseline noise level data was recorded at 7460 rpm input speed and 80% torque:

102 dB at 1566 Hz (LP1)

102 dB at 3132 Hz (LP2)

107 dB at 3606 Hz (SB)

106 dB at 4698 Hz (LP3)

Combining decibels:

$$\begin{aligned} (\text{dB})_{\text{TOTAL}} &= 10 \log_{10} \left(\text{ANTILOG} \frac{\text{dB}_1}{10} + \text{ANTILOG} \frac{\text{dB}_2}{10} + \dots \right) \\ &= 110.8 \text{ dB.} \end{aligned}$$

Now analytically:

$$(\text{dB})_{\text{TOTAL}} = 10 \log_{10} \frac{P}{10^{-12}} - 11 - 20 \log_{10} r$$

$$\text{where } P = (1.62) (10^{-4}) \omega^2 \bar{W}^2 A$$

r = radius to point of interest, m

ω = exciting frequency, Hz

\bar{W} = housing displacement, cm

A = surface area, cm^2

Grid point 293 on the finite element model (Figure 74) of the lower housing is in the general location of microphone M5 and will be used as our analytical comparison point. Assuming the distance to the noise source is $r = 0.305$ meter (1 foot), the analytically predicted noise results are

110.3 dB at 1566 Hz (LP1)

106.5 dB at 3132 Hz (LP2)

104.9 dB at 3606 Hz (SB)

105 dB at 4698 Hz (LP3)

So correlation of test to analysis is not unreasonable. The log sum of the above is 113.3 dB compared to 110.8 dB from test.

Vibration

If the noise measured is 110 dB for 3606 Hz (spiral bevel), at $r = 1$ ft, for some housing points then

$$SPL = 10 \log_{10} \frac{P}{10^{-12}} \text{ dB} = 110 \text{ dB}$$

$$P = .1 \text{ WATTS}$$

Now using

$$P = (1.62 \times 10^{-4}) \omega^2 \bar{W}^2 A,$$

$$\bar{W} = \sqrt{\frac{(.1)(10^4)}{(3606)^2 (3400) (1.62)}} = .000118 \text{ cm},$$

$$= .000046 \text{ in. and}$$

$$g's = \frac{(2\pi\omega)^2 \bar{W}}{386} = 61 \text{ g's typically}$$

(Higher g's are calculated at other points on the case.)

Working backward, if the displacement at the point is reduced by a factor of 10,

$$\bar{W} = .0000118 \text{ cm},$$

$$P = (1.62 \times 10^{-4}) (3606)^2 (3400) (.0000118)^2$$

$$= .001 \text{ WATTS},$$

$$SPL = 10 \log_{10} \frac{10^{-3}}{10^{-12}} = 90 \text{ dB (which is 20 dB lower).}$$

Badgley (Reference 9) used the formula

$$SPL = 20 \log_{10} \frac{(K_x)_{NEW}}{(K_x)_{BASELINE}}$$

where K_x is the bearing load (lb). If the displacement (x) is reduced by a factor 10,

$$SPL = 20 \log_{10} 10^{-1} = -20 \text{ dB which agrees with the previous result.}$$

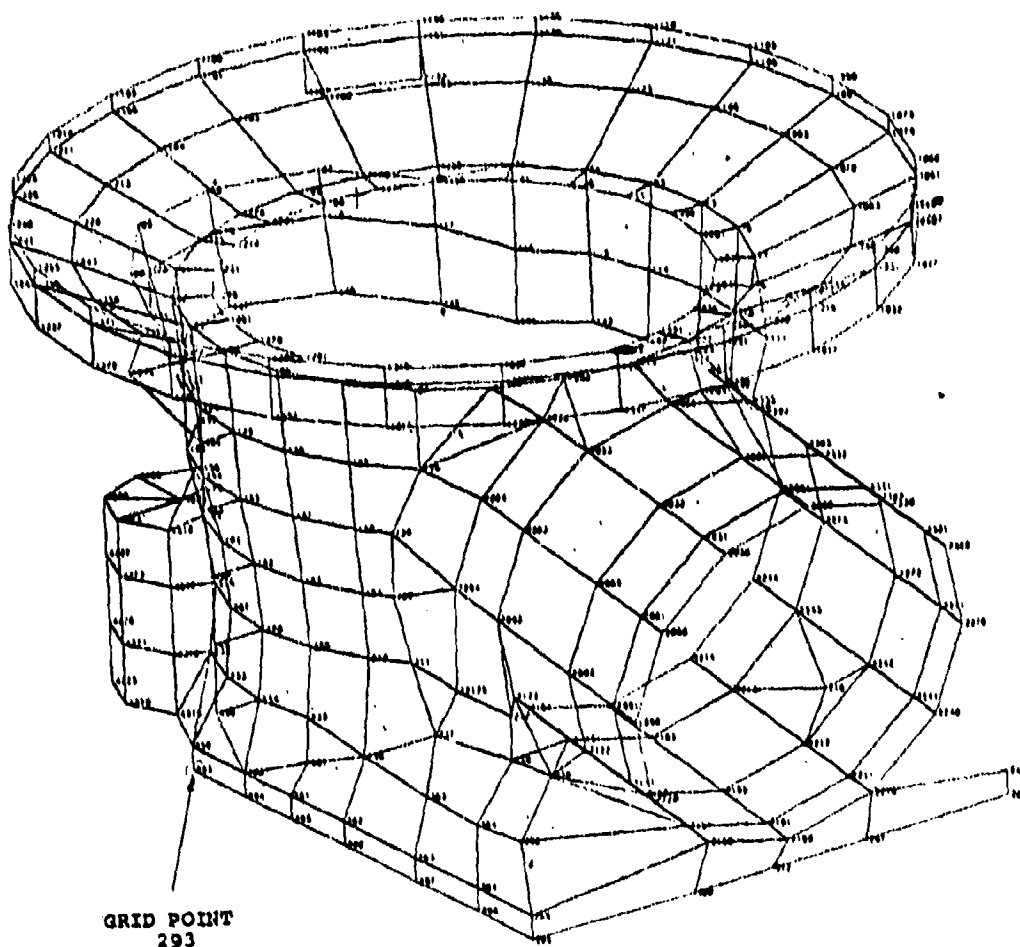


Figure 74. Finite Element Model of Lower Housing Showing Grid Point Locations for Noise Prediction.

DESIGN MODIFICATIONS

Using the finite element analysis, the baseline transmission was analyzed to determine the potential for vibration/noise reduction. Structural modifications for the internal shafting and the housing structure, including the stationary ring gear, were identified, and redesigned components incorporating these modifications were manufactured. Any structural modifications for vibration reduction which are to be applied to flight hardware must consider weight penalty, location, cost, ease of fabrication, and stress levels. For the experimental hardware considered herein, however, the structural changes are based substantially on a consideration of the applicability to an existing hardware item. The design of new hardware for future applications must concentrate on optimizing the structure by rigorously applying the analytical predictions.

The components which were analyzed and redesigned using the finite element methodology and manufactured for use in the test program are described below.

SHAFTING

The baseline bevel pinion and bevel/sun gear shafts are shown in Figures 75 and 76. Superimposed on these drawings are the finite element idealizations which were used for the analysis of these parts. No modification of the pinion was indicated by the analysis. The modifications determined for the model of the bevel/sun gear shaft, limited to changes in the shaft ID for ease of manufacture and economy, are shown in Figure 77. Figure 78 is a cross-sectional drawing of the actual shaft and the sleeve modifications, and Figure 79 is a photograph of the modified bevel/sun shaft.

RING GEAR

The stationary ring gear was modified by applying a 0.2-in.-thick steel band in the form of a split ring around the exterior wall (Figure 80). This band was clamped using integral flanges and bonded in a manner similar to that described below for the case modifications. The modified ring gear is shown in Figure 81.

CASE

Modifications to the case structure were restricted to localized changes of the exterior wall, which were accomplished by bonding preformed doubler plates to the regions of the case exhibiting a high average strain density. The doubler plates were 0.300-in.-thick magnesium and were contoured to fit the exterior surface of the transmission case. The areas to which the plates were applied are identified in Figure 49. The manufacture of the doubler plates was a two-step process.

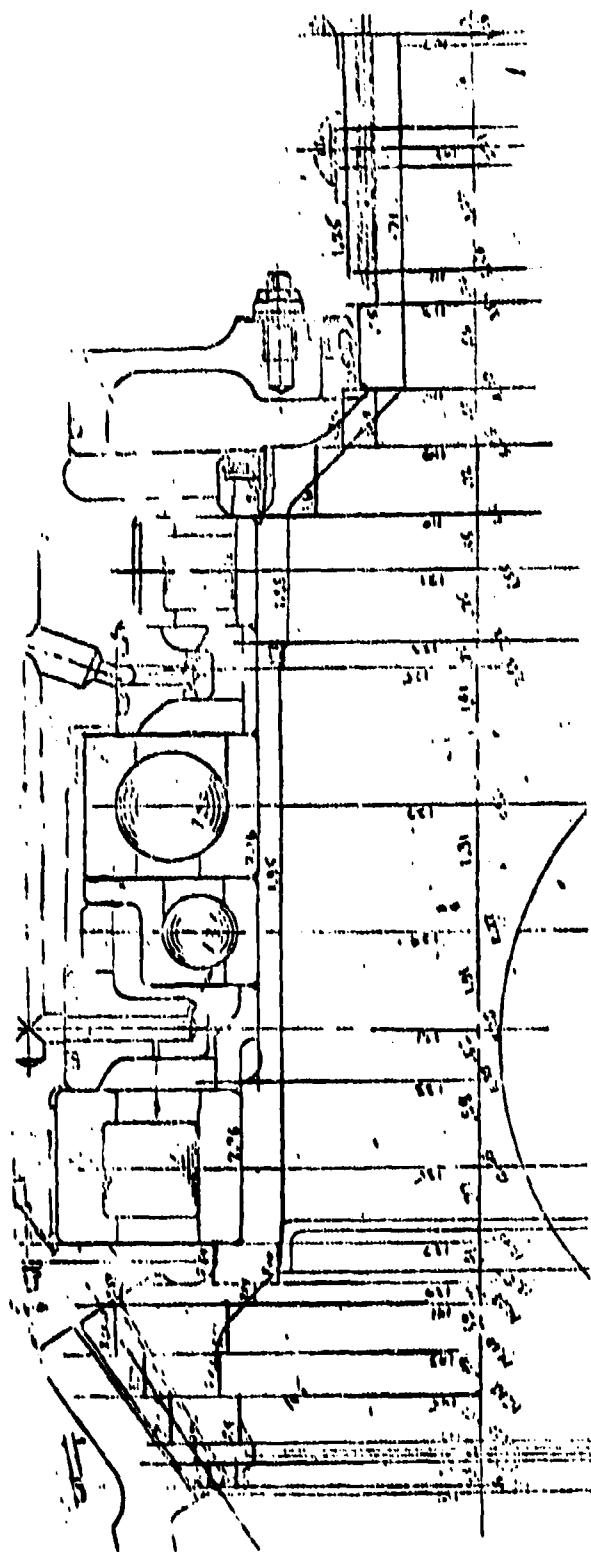


Figure 75. CH-47 Forward Transmission Bevel Pinion (Baseline)
with Finite Element Idealization Superimposed.

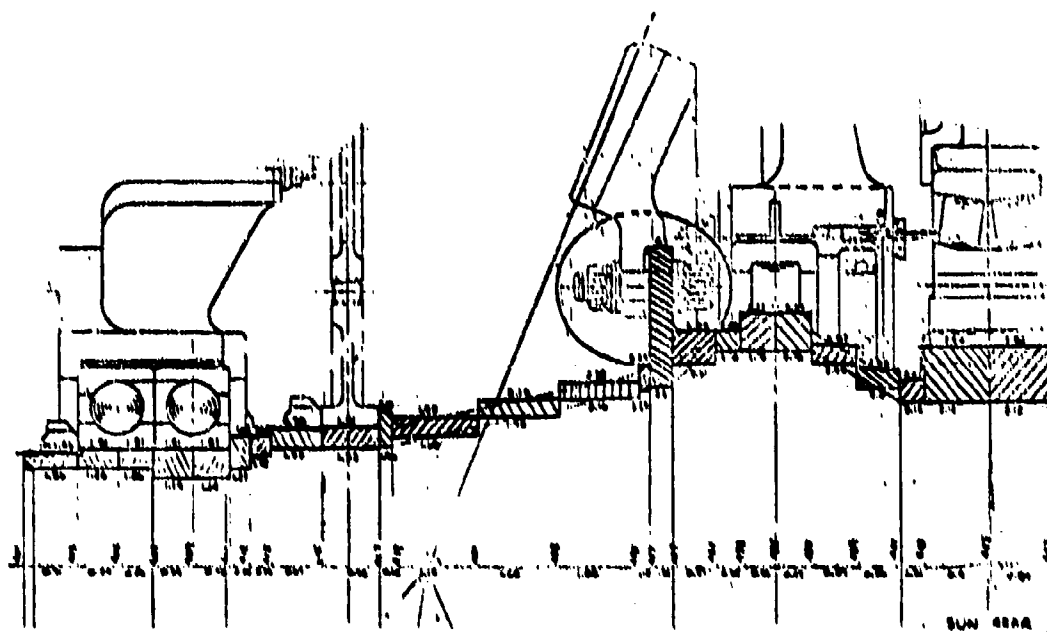


Figure 76. CH-47 Forward Transmission Bevel/Sun Gear (Baseline)
With Finite Element Idealization Superimposed.

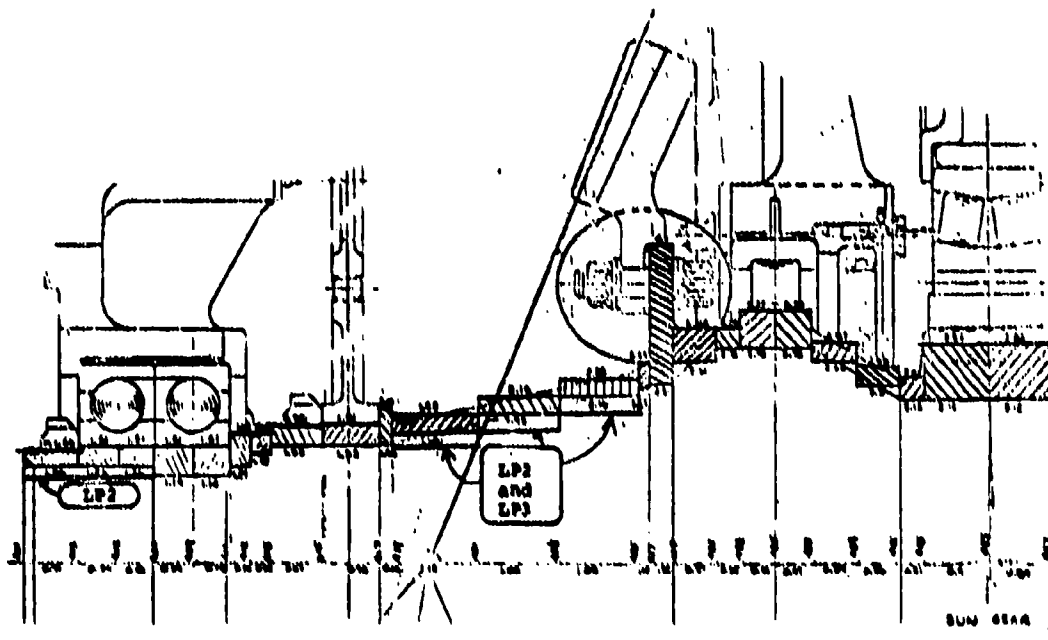


Figure 77. CH-47 Forward Transmission Bevel/Sun Gear (Modified)
With Finite Element Idealization Superimposed.

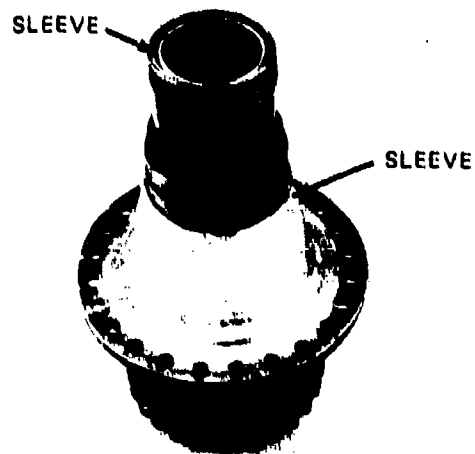
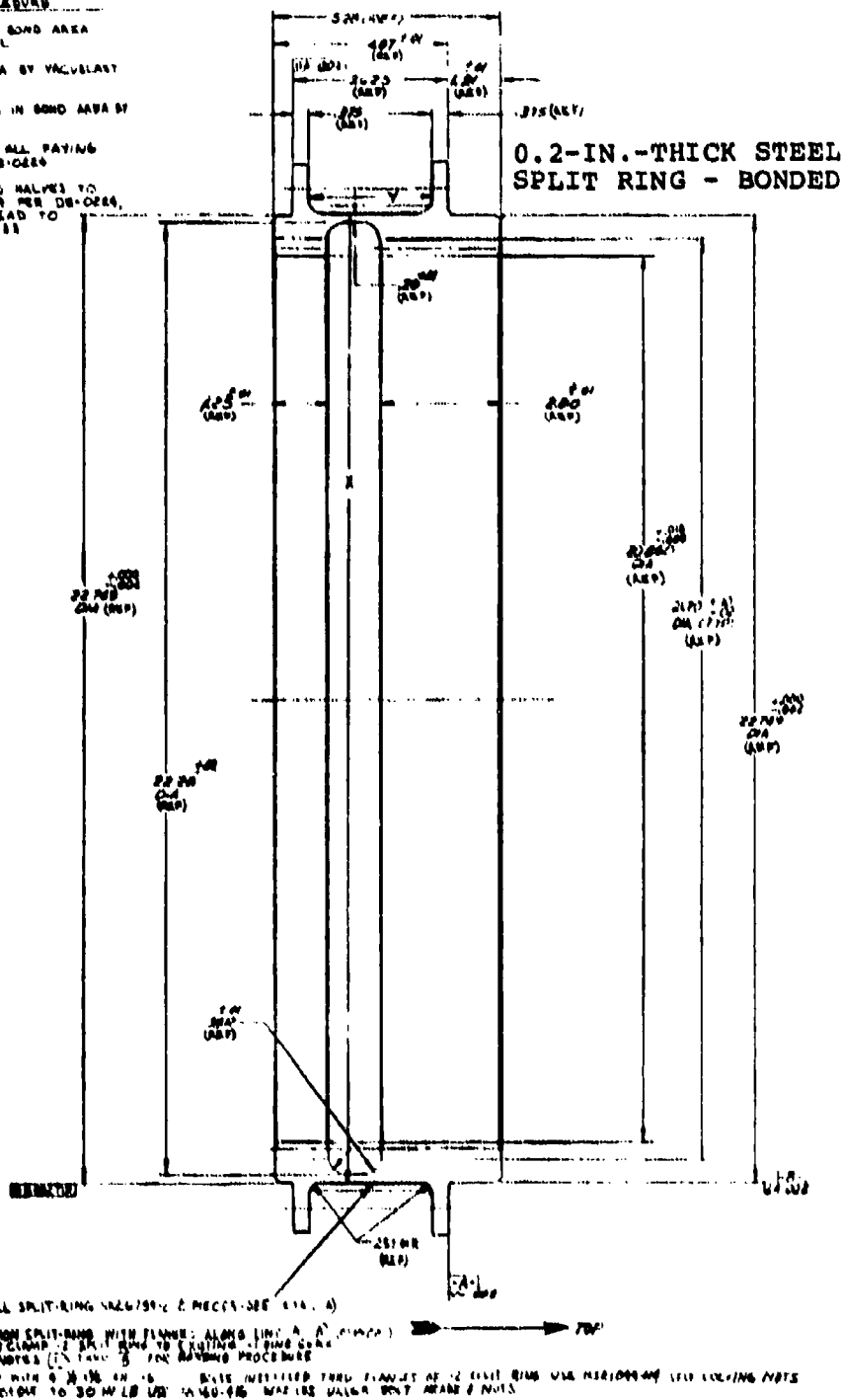
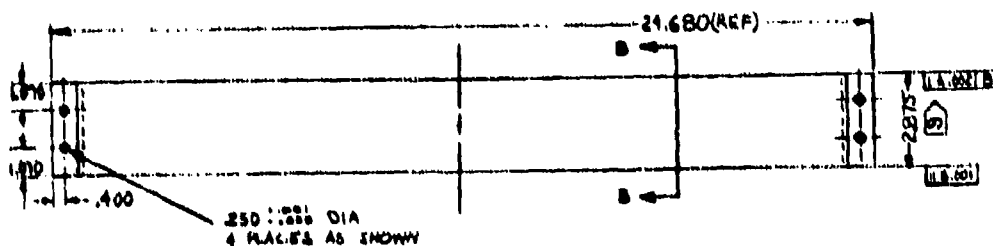
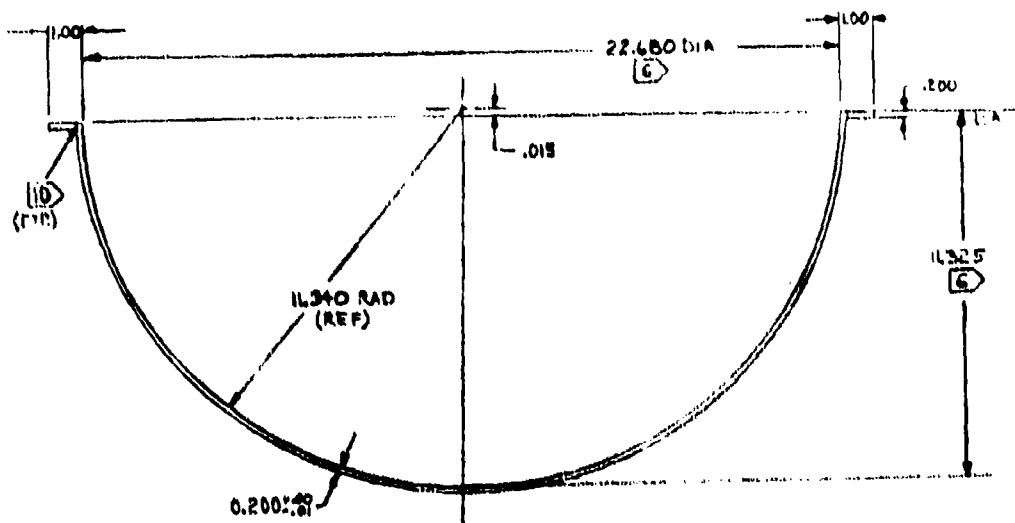


Figure 79. Modified Bevel/Sun Gear Shaft With Two Sleeves Installed.

1. REMOVE CADMIUM PLATE IN BOND AREA WITH REDOX INHIBITED HCL
2. CLEAN - 1 GRAB IN BOND AREA BY VACUUMST FOR DE-OXID
3. CLEAN 1/2 STEEL UNIT W/ING IN BOND AREA BY VACUUMST FOR DE-OXID
4. APPLY EPOXY PRIMER TO ALL PAYING SURFACES AND CURE FOR DE-OXID
5. BOND - 2 STEEL UNIT RING HALVES TO 1 GRAB W/ING W/ING FOR DE-OXID, AND BOND GLASS THROUGH TO MAINTAIN BOND THICKNESS



134



SPLIT RING SK26794-2
(HALF SCALE)

.22 R TYP
SECTION B-B

(G) DIMENSION SHOWN IS APPROXIMATE, MEASURE DIAMETER "X" ON EXISTING -1 GEAR AND FABRICATE TO FIT (.005 ON DIAMETER)

7- BREAK ALL EDGES .010- .015

(H) DIMENSION SHOWN IS APPROXIMATE MEASURE EXISTING -1 GEAR AND FABRICATE TO FIT

(I) DIMENSION SHOWN IS APPROXIMATE, MEASURE DIMENSION "Y" ON EXISTING -1 GEAR AND FABRICATE TO FIT (.005)

(J) ELECTRON BEAM WELD IN ACCORDANCE WITH SAC 5959 CLASS "C" VISUAL & MAGNETIC PARTICLE INSPECTION REQUIREMENTS

Figure 80. Continued.



Figure 81. Modified Ring Gear With Split Ring Installed.

First, matching sets of plaster casts were made from the exterior surface of the housing in the specified areas. Second, these casts were used as holding and tracing patterns for the machining of the doubler plates from magnesium stock. The finished magnesium doubler plates are shown in Figure 82. Figure 83 shows the doubler plates installed on the transmission housing.

COMPOSITE DOUBLER PLATES

A considerable amount of attention has been devoted to the potential improvements which accrue through the use of composite materials with increased strength-to-weight properties. A preliminary effort directed toward defining these potential benefits as applicable to transmission housings was included in this program. Graphite aluminum composite plates, essentially identical in geometry to the magnesium plates defined above, were also installed on the housing (as shown in Figure 83) and tested. The details of this effort are reported in Appendix B.

VIBRATION ISOLATORS

Vibration isolators were fabricated from 0.125-in.-thick MIL-R-6855 CL4-40 (40 Durometer Neoprene) and installed between the transmission upper cover mounting points and the test stand. The retaining bolts were isolated at the top and bottom as shown in Figure 84.



Figure 82. Magnesium Contoured Doubler Plates.

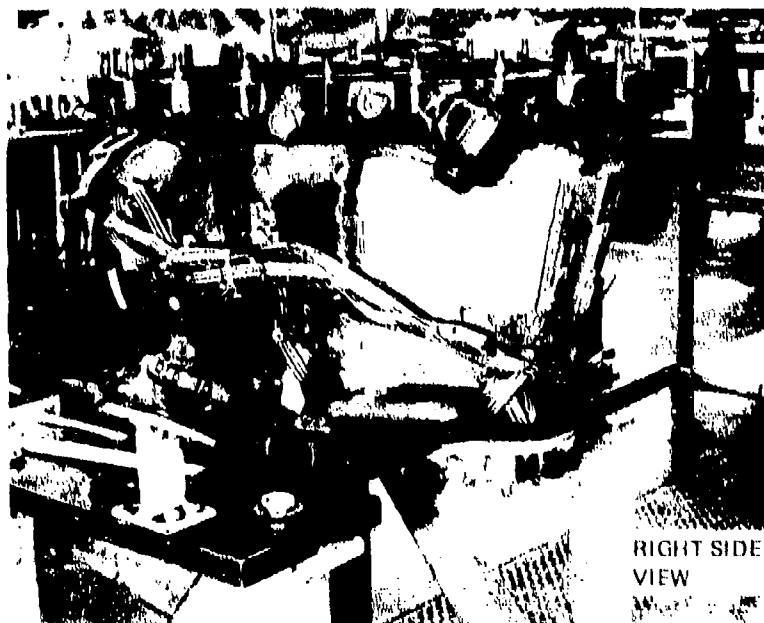
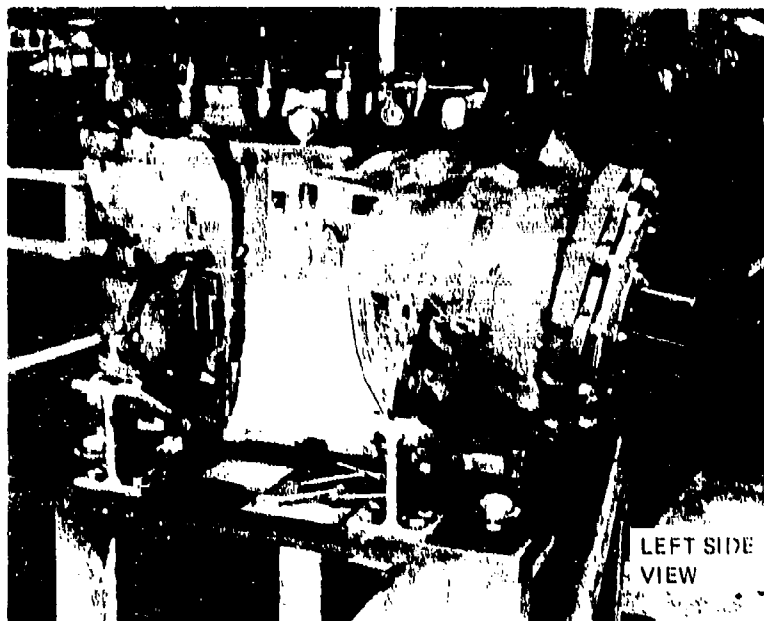


Figure 83. SK27064-1 (L) - Magnesium Contoured Doubler Plate Installed.

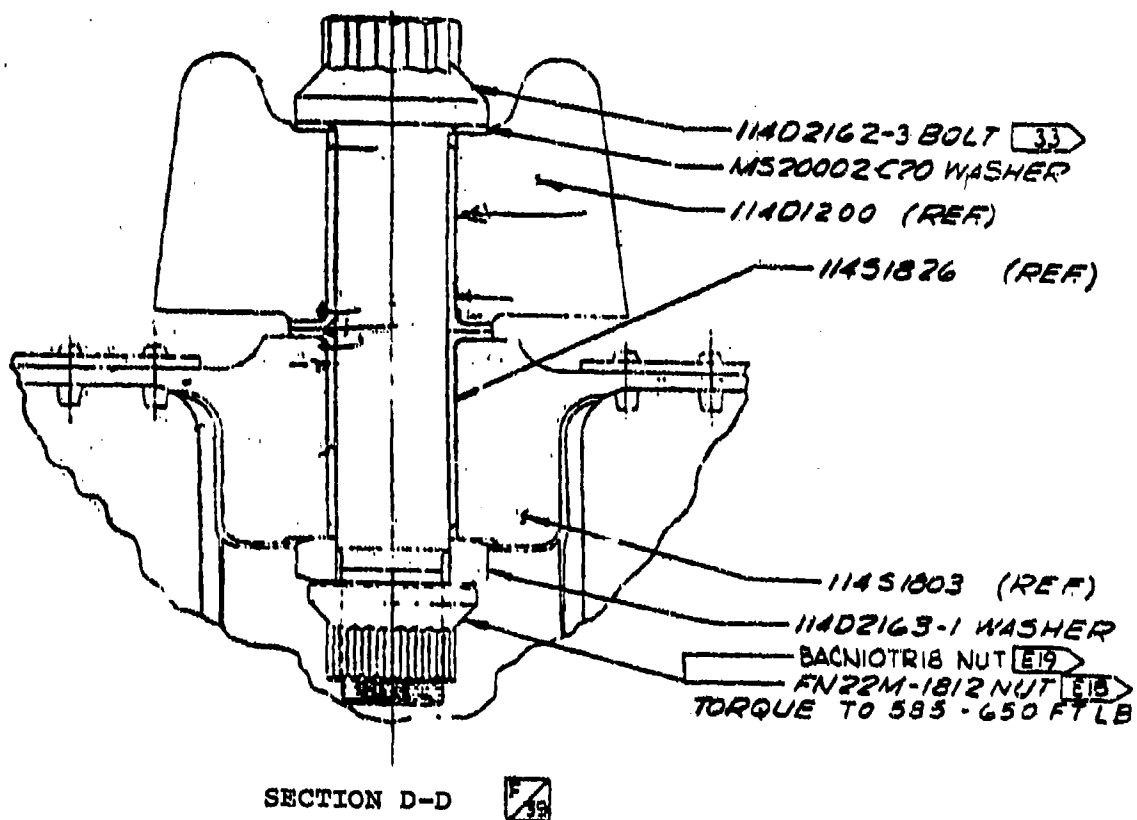


Figure 84. Transmission Cover Leg Attachment to Main Frame.

VERIFICATION TESTING

OBJECTIVE

The objective of this test was to obtain experimental vibration and noise data for the CH-47 forward transmission with the modified components installed for comparison with baseline test data to determine the effectiveness of the analytically predicted structural changes for reducing vibration and noise levels. The degree of correlation obtained, both relatively and absolutely, will also provide an indication of the accuracy of the basic analytical method.

TEST STAND

The dynamic testing was conducted using the Boeing Vertol full-scale, closed-loop CH-47 forward transmission test facility, shown schematically in Figure 85. This rig is of the four-square, locked-in-torque type with variable speed and torque capabilities. Control over temperature is maintained by use of special oil-water heat exchangers with condition monitoring provided by the standard aircraft instrumentation. All operations are controlled from a remote panel (Figure 86) setup outside the cell. The standard aircraft oil system (oil, filter, pumps, etc.) is used on the test boxes; however, the aircraft cooler is not used. Oil-water heat exchangers are substituted for the aircraft cooler to simplify the test system. This test stand provides the capabilities of running a transmission over its full design torque and speed range under controlled conditions, including rotor lift, drag, and pitching moments.

To provide for the acquisition of noise data which was as free as practical from extraneous signals, the test transmission was equipped with an acoustic enclosure, made of 3/4-inch plywood lined with a 3/4-inch-thick acoustic blanket, which minimized noise reflected from the test cell walls. The enclosure is shown schematically in Figure 87, and a photograph of the enclosure installed in the test stand is shown in Figure 88.

DATA ACQUISITION

Six accelerometers were mounted on the transmission case in the locations shown in Figure 89. A block of aluminum was epoxied to the transmission at each of the desired locations, and the accelerometers were attached to these blocks using Endevco studs as shown in Figure 90.

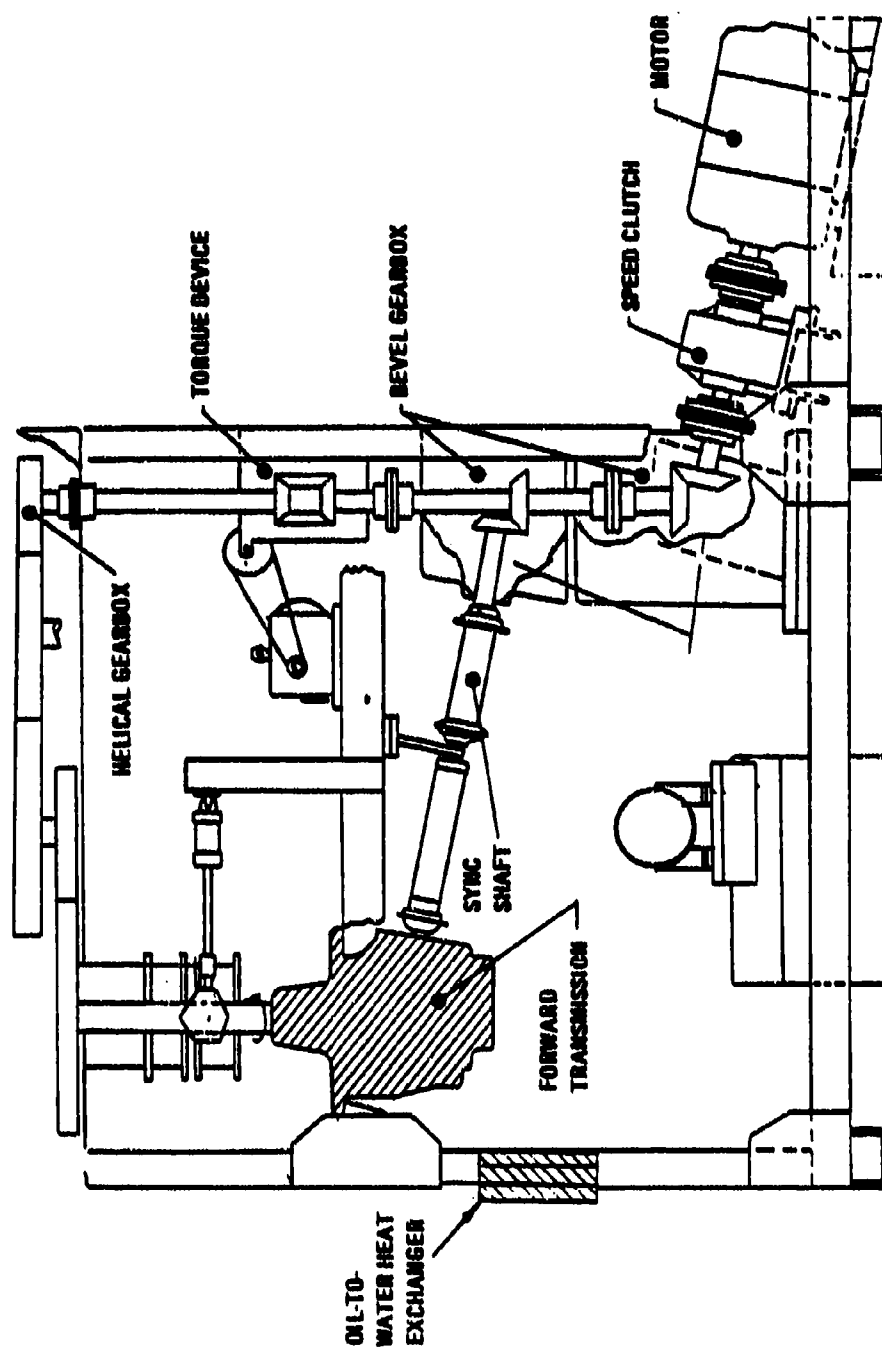


Figure 85. Schematic Diagram of Closed-Loop Test Stand.

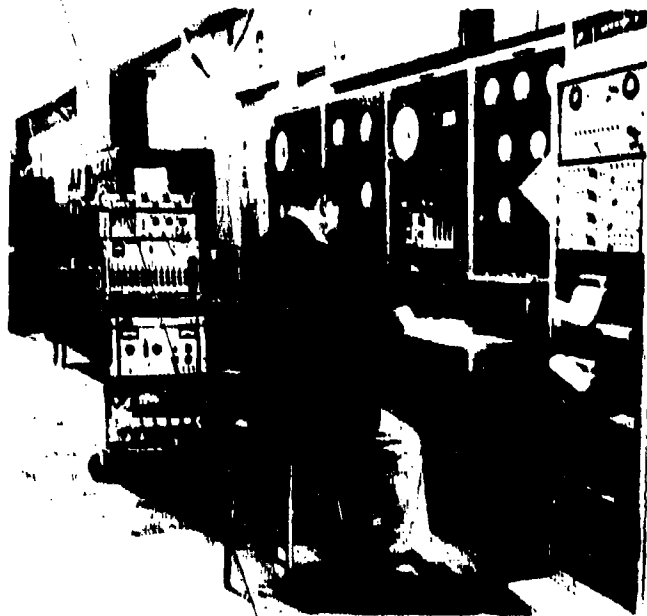


Figure 86. CH-47 Forward Transmission Test
Facility Control Console.

ACOUSTIC ENCLOSURE

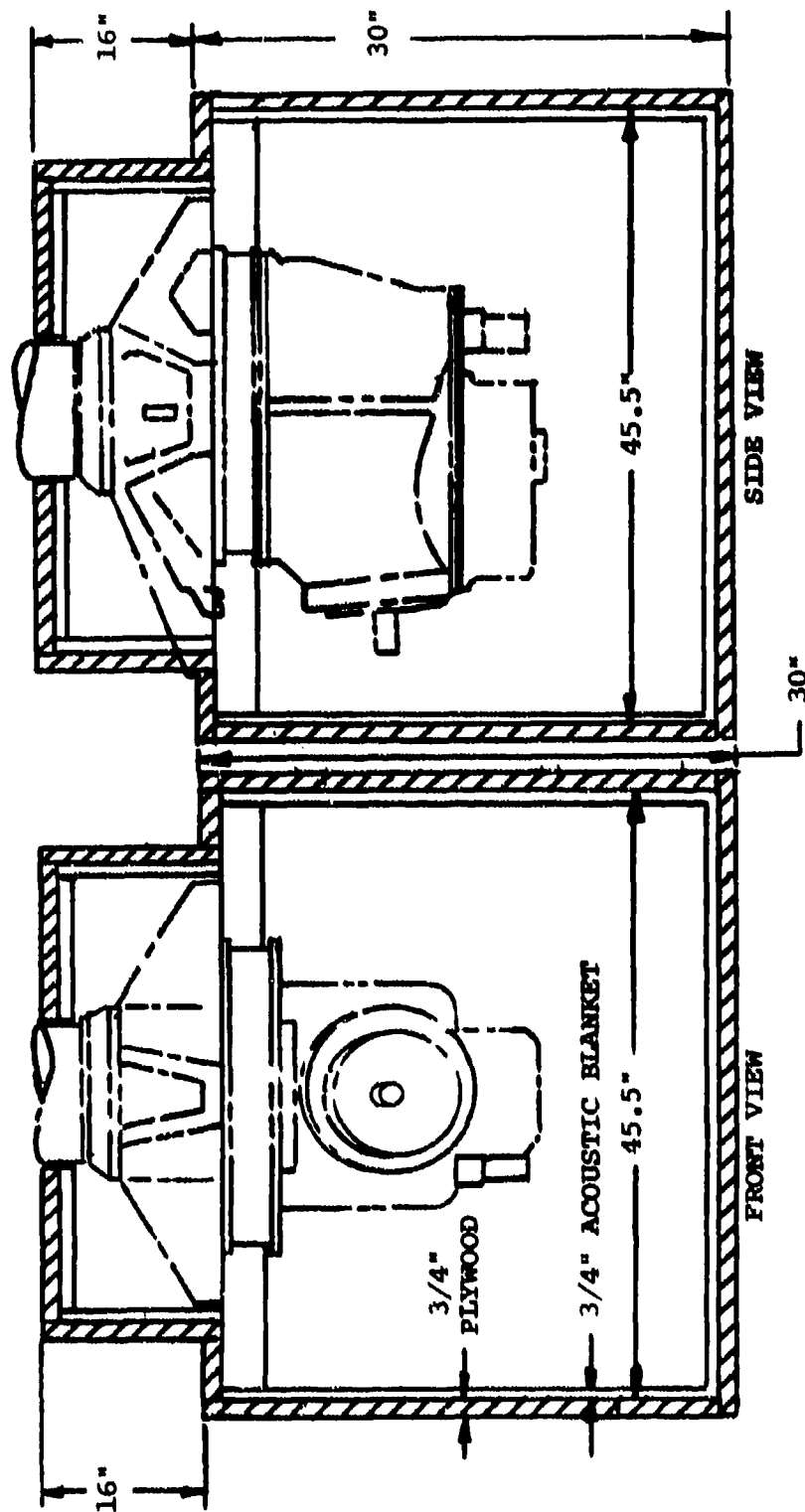


Figure 87. Schematic of Transmission in Acoustic Enclosure.

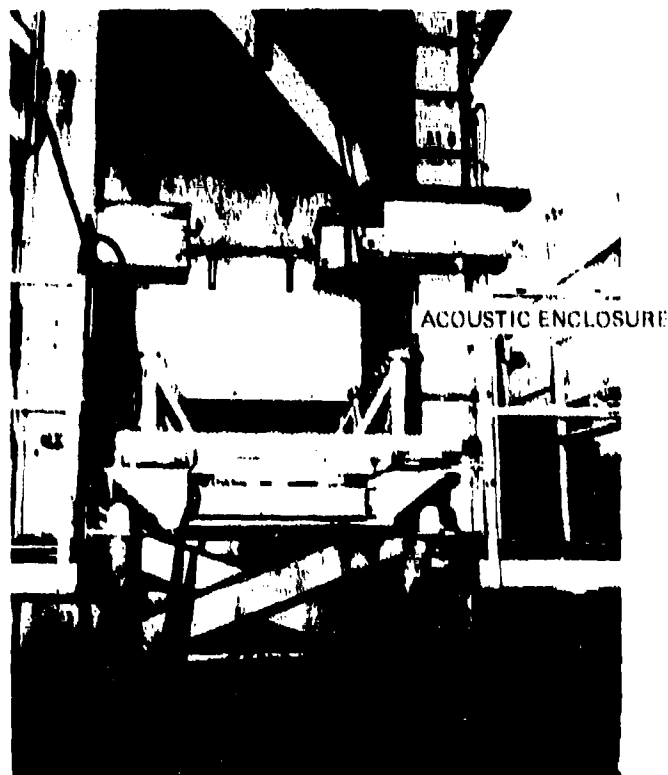


Figure 88. CH-47 Forward Transmission Installed in
Dynamic Test Rig With Acoustic Enclosure.

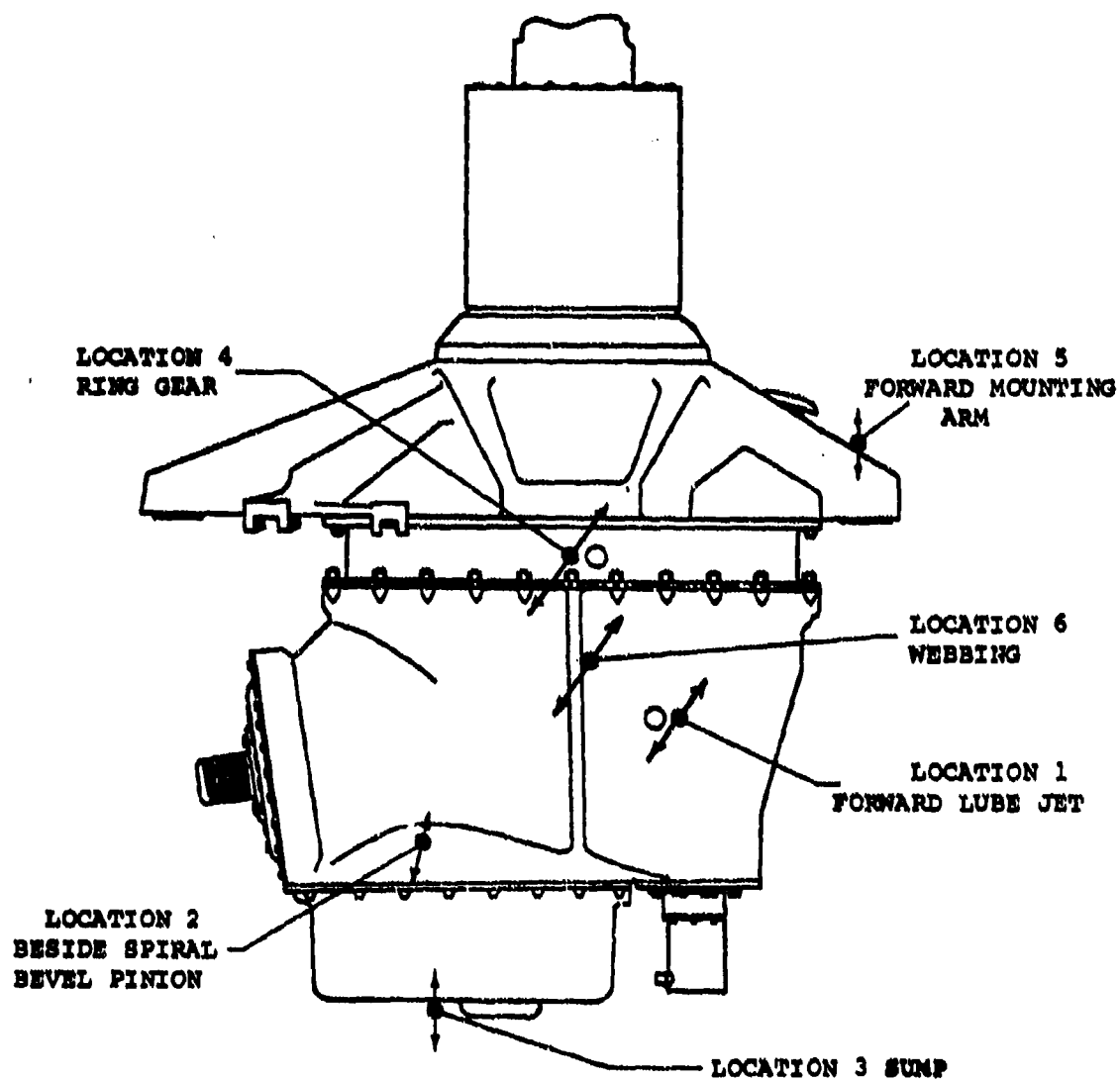


Figure 89. Accelerometer Locations.

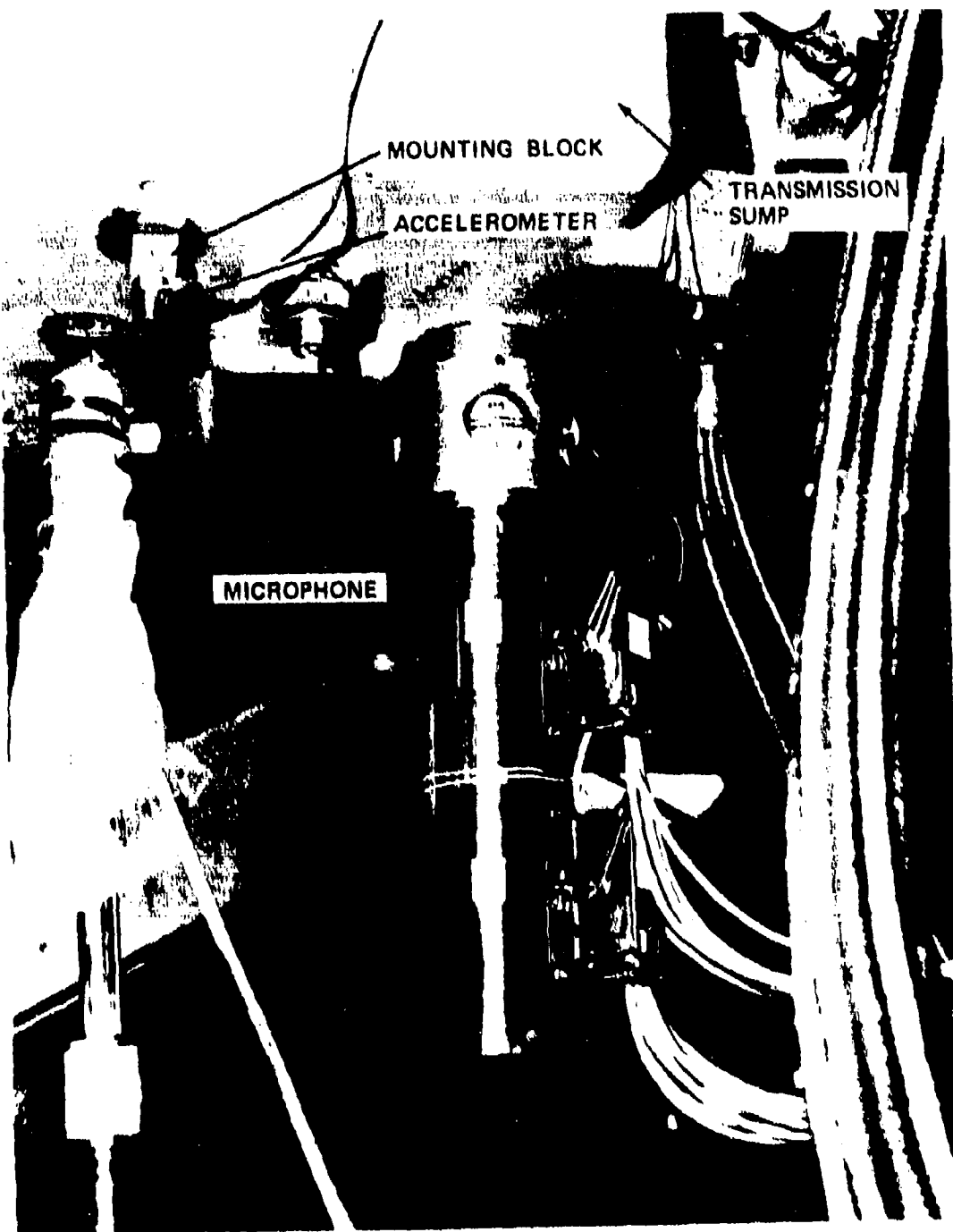


Figure 90. Typical Accelerometer Installation.

The following locations were selected from a previous test program (Reference 4) to provide an overall representation of the case vibrations with each test configuration:

Location No. 1 - Vicinity of forward lube jet (radial direction).

Location No. 2 - Beside spiral bevel pinion (radial direction).

Location No. 3 - Center of oil sump (vertical direction).

Location No. 4 - Center of stationary ring gear (vertical direction, tests 1-A and 2-A), (radial direction, remaining tests).

Location No. 5 - Forward mounting arm (vertical direction).

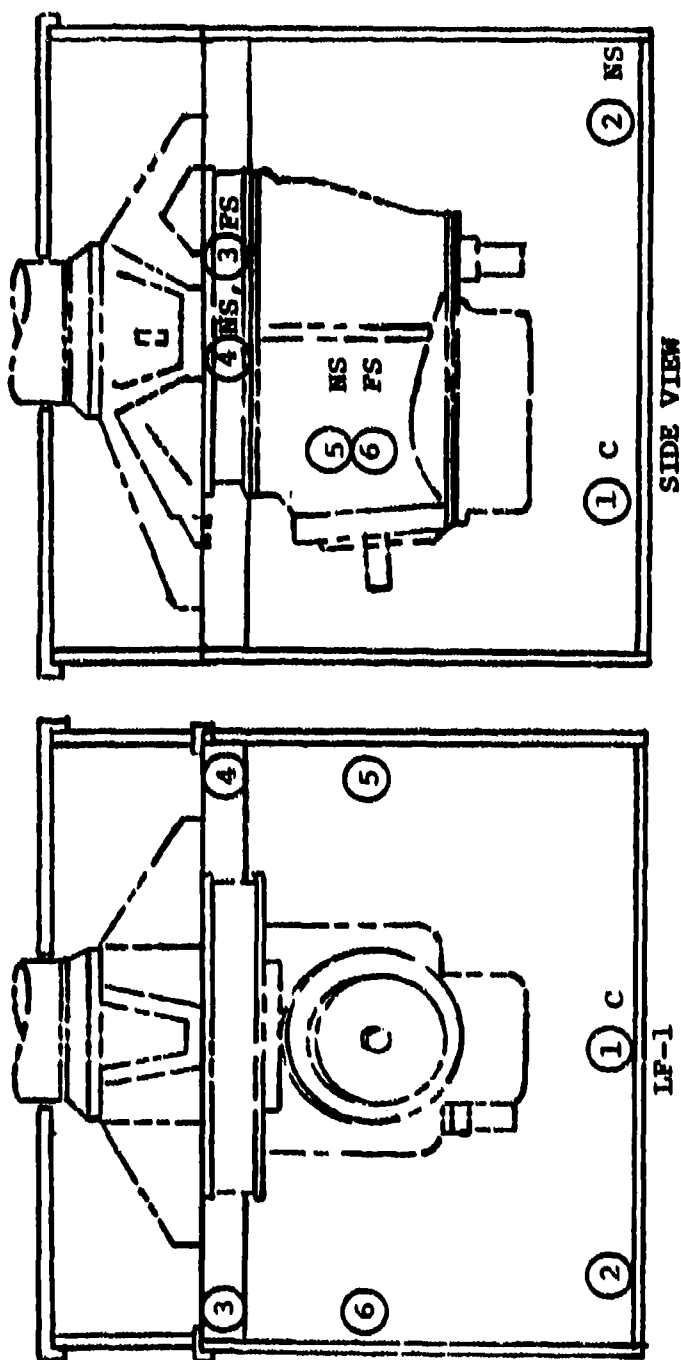
Location No. 6 - Webbing (radial direction).

The accelerometers used were Endevco Model 2213 combined with accelerometer amplifiers for signal conditioning.

Six microphones were placed around the transmission as shown in Figure 91. These were Bruel and Kjaer (B&K) 4145 1-inch microphone cartridges with B&K 2613 cathode followers, and B&K 2807 power supplies. All microphones were contained in an enclosure approximately 41 inches square and 45 inches deep, constructed of 3/4-inch plywood and lined with a soundmat LF 3/4-inch lead-foam sound barrier (Figure 88) to provide both sound attenuation of external test stand noise, and sound absorption on the interior side to minimize the reverberations of transmission noise within the enclosure. Figure 92 shows a typical microphone installation mounted on the transmission.

Because of space limitations within the test stand the enclosure had to be limited to a total depth of 45 inches. All microphones were approximately 6-9 inches from the nearest surface of the transmission case. Their locations were selected from prior test programs (References 2 and 4) as suitable for transmission noise measurement in the test cell.

The accelerometer and microphone data were recorded on an Ampex AR-200 1-inch, 14-channel, wide-band FM magnetic tape recorder at 30 ips. Figure 93 shows a schematic of the data acquisition system. In addition to the 6 microphone and 6 accelerometer recording tracks, a 60/rev signal from the input shaft, used for speed indication, and a voice identification track were used also.



FS FAR SIDE
 NS NEAR SIDE
 C CENTER

① UNDER SUMP, C
 ② DIRECTION OF PILOT'S HEAD
 ③ RING GEAR, FS
 ④ RING GEAR, NS
 ⑤ BEVEL, NS
 ⑥ BEVEL, FS

Figure 91. Microphone Locations Within Enclosure.

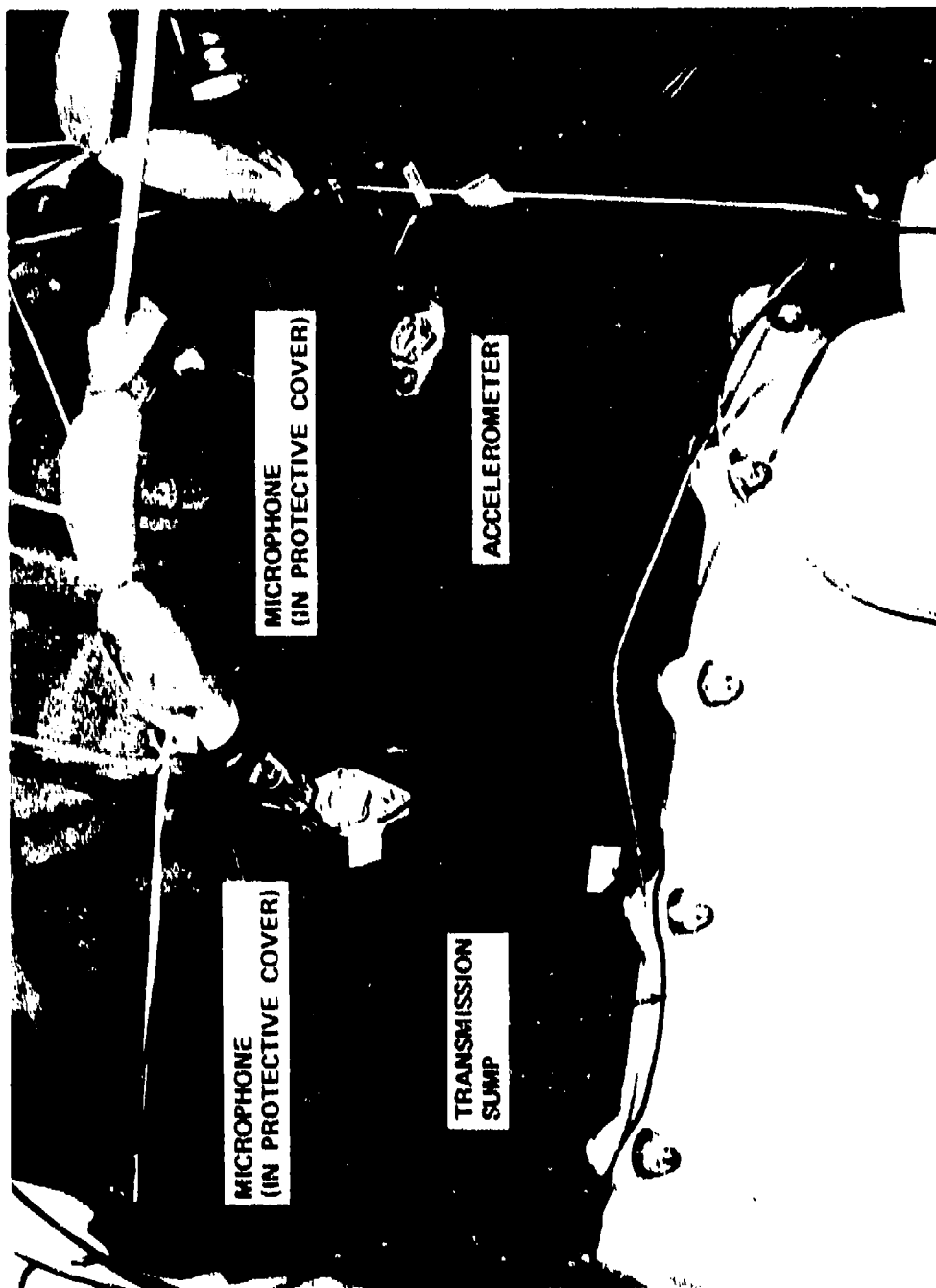


Figure 92. Typical Microphone Installation.

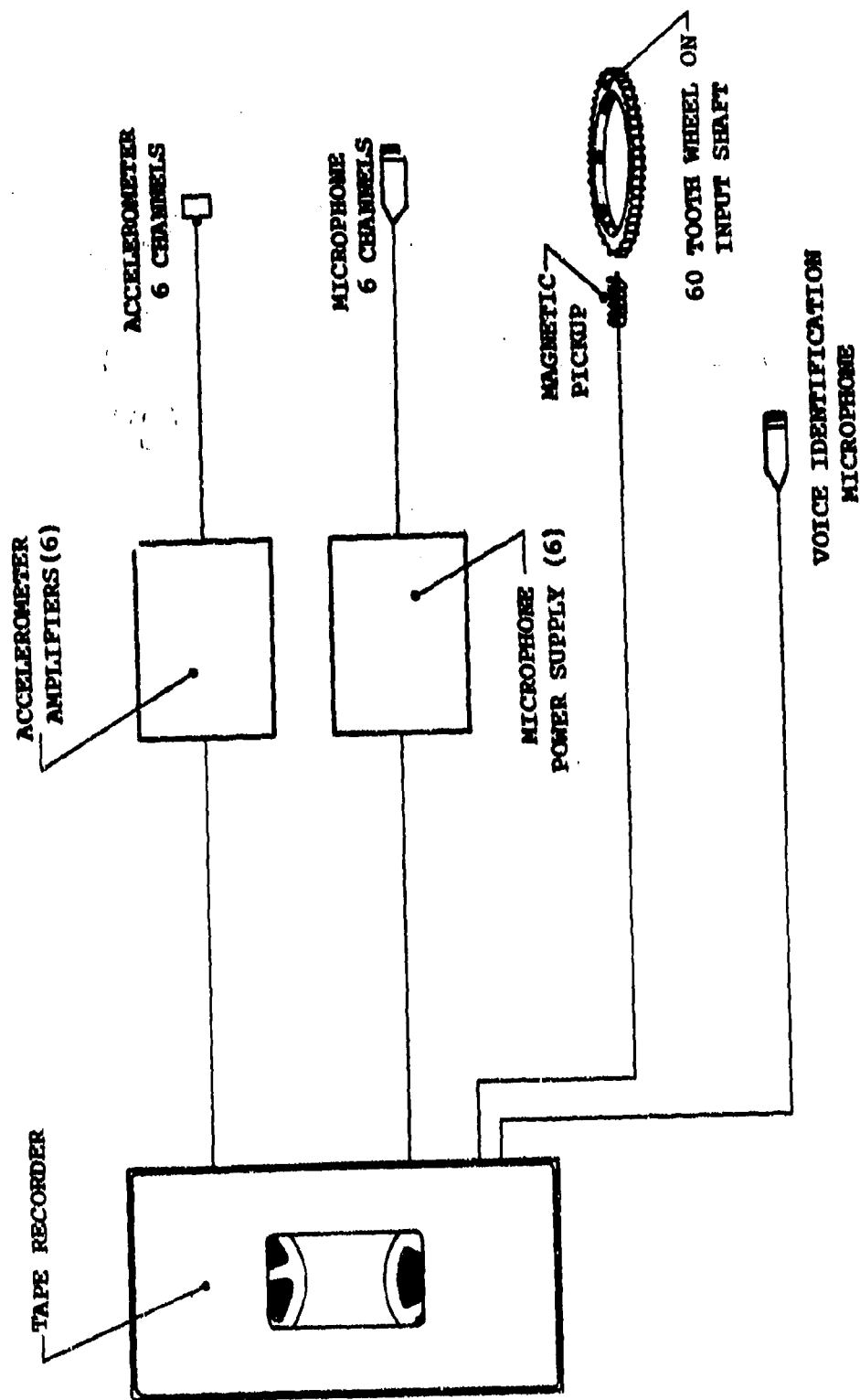


Figure 93. Data Acquisition System.

The frequency responses of both the microphone and accelerometer systems are essentially flat over the frequency range of 50-5000 Hz, well within the range of interest of the program. As shown in Figures 94 and 95, system sensitivity calibrations were recorded prior to each test and at the beginning of each new tape reel.

TEST CONFIGURATION

The transmission used in this program was a standard CH-47C forward rotor transmission, except as modified per the vibration/noise reduction analyses. Test data was obtained for each of the eleven configurations listed in Table 7 in order to assess the effectiveness for vibration/noise reduction of the following analytically determined structural changes, both separately and in combination:

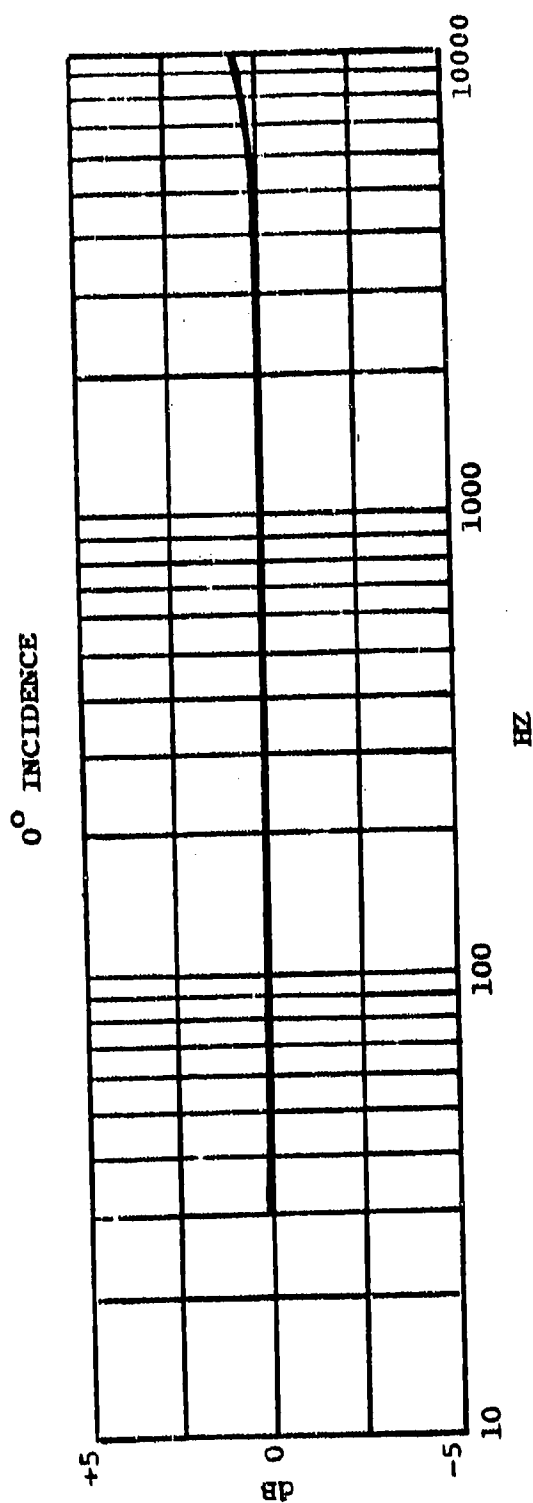
1. Sun/bevel gear detuned by addition of two sleeves.
2. Ring gear detuned by addition of band.
3. Case detuned by addition of two contoured doubler plates.
4. Isolators added.

As noted on Table 7, a reference code has been assigned to each configuration. This code will be used as a shorthand designation in many of the ensuing figures and discussions.

All tests were made directly comparable by maintaining a consistent acoustic enclosure configuration and by using identical microphone and accelerometer locations. The installation of the various items of modified hardware is shown schematically in Figure 96. Figures 97 and 98 show photographs of the actual hardware.

For each of the configurations in Table 7, 1 minute of data was recorded for two input shaft speeds, 7460 rpm (operating baseline - 243 rotor rpm) and 6600 rpm (off-design), and for two torque levels, 80% (design, .844 x 10 inch-lbs output shaft) and 60% (off-design, .64 x 10 inch-lbs). The data from each of the above variations was frequency analyzed as to mesh content, resulting in 264 items of noise information and 264 items of accelerometer information.

No data was obtained until the transmission had completed its warm-up operating period and was stabilized at the scheduled torque and operating speed condition.



FREE FIELD RESPONSE

BRUEL AND KJAER (B&K) TYPE 4145 + 2613 MICROPHONE
 BRUEL AND KJAER (B&K) TYPE 2807 POWER SUPPLY
 BRUEL AND KJAER (B&K) TYPE AO 0029 CABLE

Figure 94. Microphone System Calibration Chart.

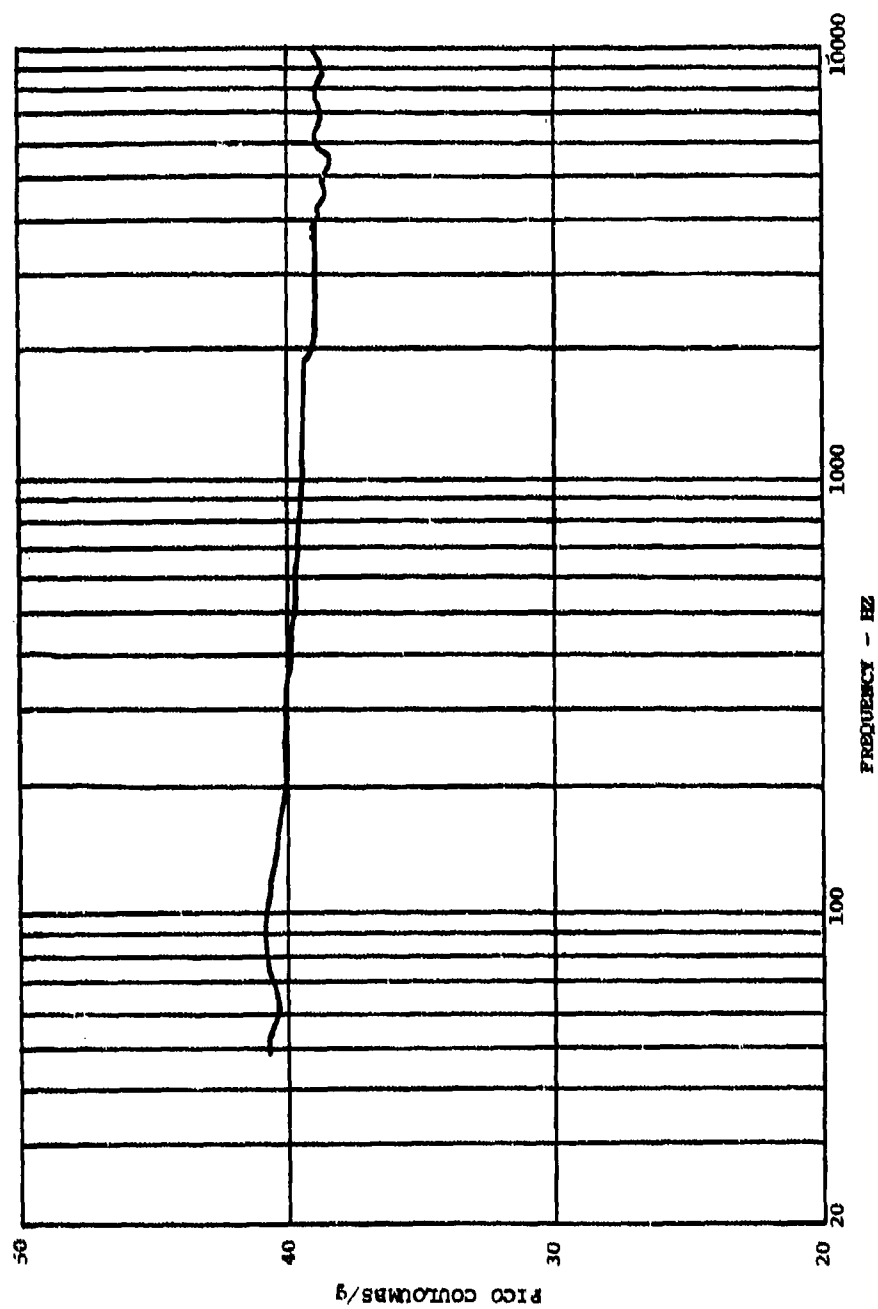


Figure 95. Typical Accelerometer Calibration Chart.

TABLE 7. SUMMARY OF TEST CONFIGURATIONS

DYNAMIC TEST NUMBER	RECORDING TAPE NUMBER	SUN/ BEVEL GEAR	RING GEAR	CASE	VIBRATION ISOLATORS	REFERENCE CODE*
1A	6L1	STD	STD	Standard	None	B
1B	6L3	MOD	STD	Standard	None	G
2A	6L2	STD	STD	Standard	Added	I
2B	6L4	MOD	STD	Standard	Added	IG
3A	6L6	STD	STD	Magnesium Plates Added	None	M
3B	6L5	MOD	STD	Magnesium Plates Added	None	GM
4A	6L7	STD	MOD	Magnesium Plates Added	None	MR
4B	6L8	MOD	MOD	Magnesium Plates Added	None	GMR
5	6L9	MOD	MOD	Magnesium Plates Added	Added	IGMR
6A	6L11	STD	STD	Composite Plates Added	None	C
6B	6L10	MOD	STD	Composite Plates Added	None	GC

*These code letters used in ensuing figures to define configurations.

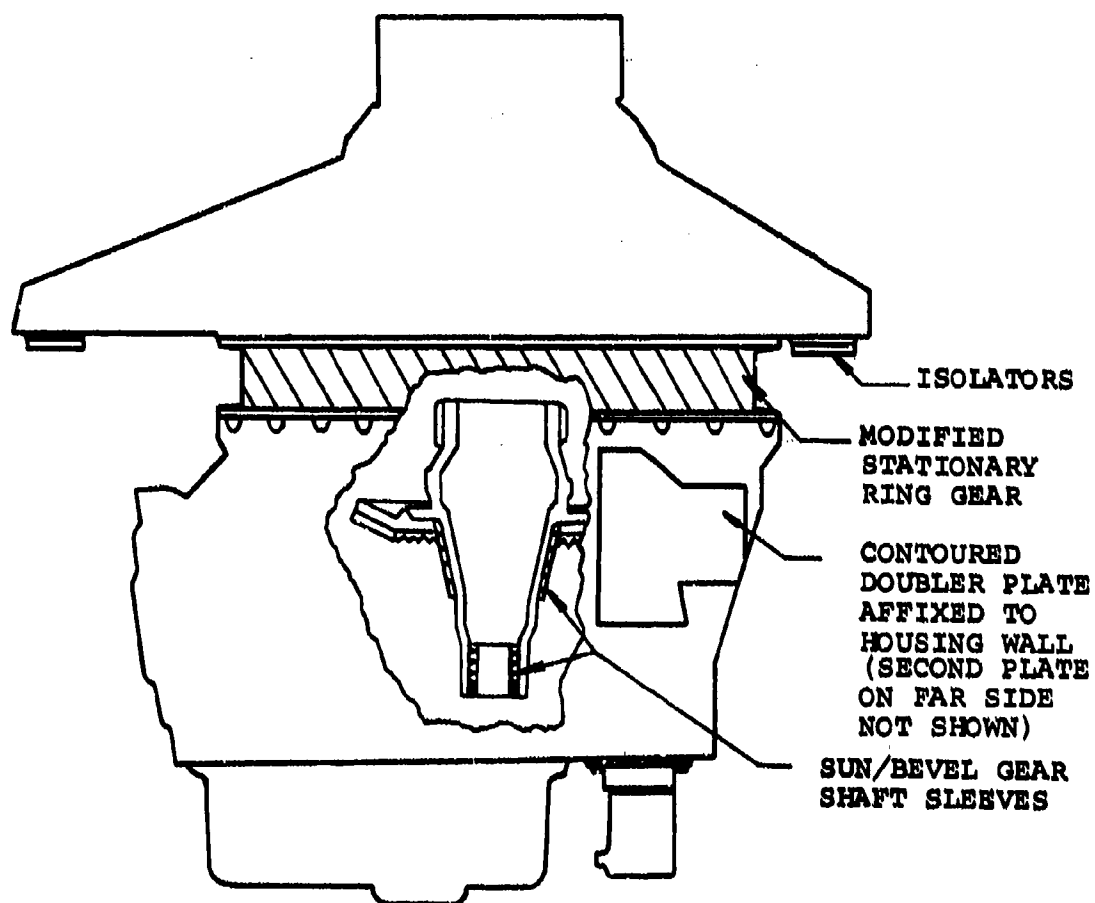


Figure 96. CH-47C Forward Transmission - Test Configuration for Vibration/Noise Reduction Testing.

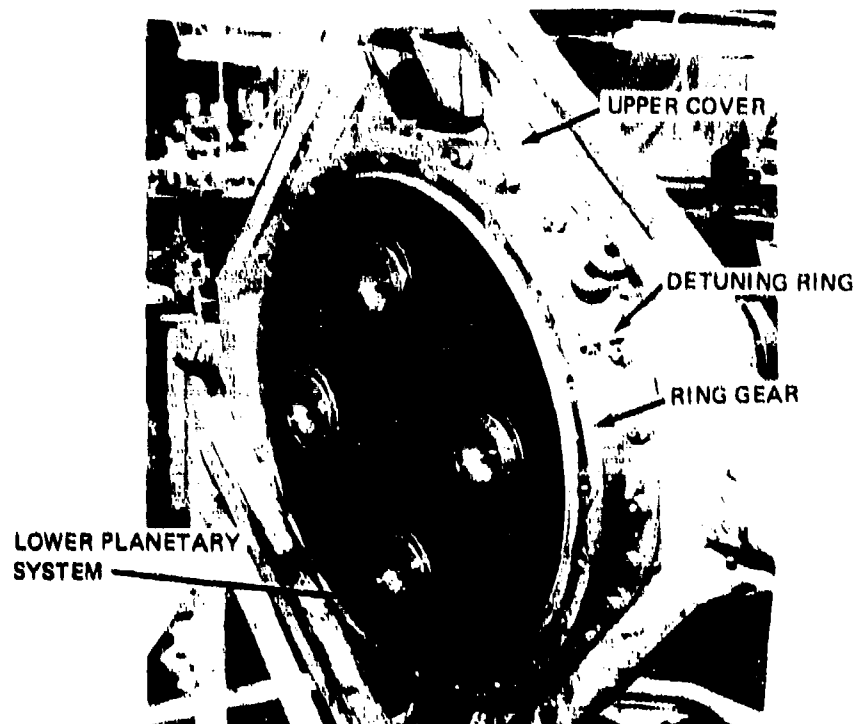


Figure 97. Installation of Ring Gear Detuning Band.

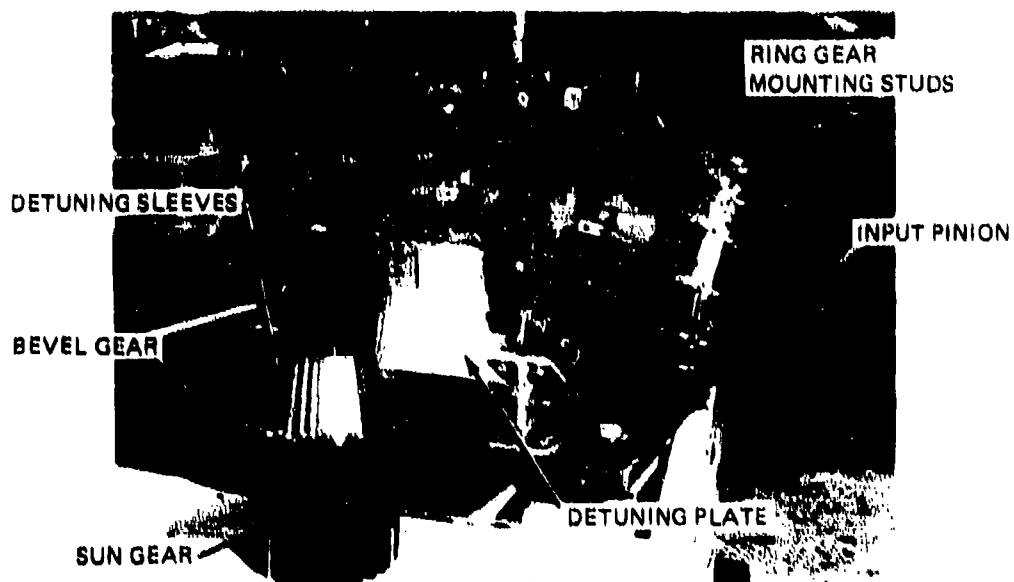


Figure 98. Installation of Detuning Sleeve and Plates on Sun/Bevel Gear and Transmission Lower Case.

DATA ANALYSIS

All recorded data were analyzed using a Nicolet UA-500, real time Ubiquitous Spectrum Analyzer in a mode which gives a constant bandwidth of 10 Hz over the range of 0 to 5000 Hz and allows for the identification of the predominant gear mesh frequencies. The data were averaged 128 times to enhance the effective signal-to-noise ratio and help emphasize those frequencies which contain the higher acoustical/vibration energy. Graphic outputs (sound and acceleration amplitudes by frequency) were then recorded with an oscilloscope and Polaroid scope camera.

Typical spectra of the transmission vibration are shown in Figures 99 and 100. This data is dominated by pure tones at the tooth mesh frequencies of the lower planetary (1st stage) gear system: (LP1) 1566 Hz and its multiples, (LP2) 3132 Hz, (LP3) 4698 Hz, and the spiral bevel input gear set (spiral/bevel) 3606 Hz.

Mesh frequencies of the CH-47C forward rotor transmission are listed in Tables 8 and 9 for input shaft speeds of 7460 and 6600 rpm, respectively.

In many cases not just one frequency is present for each tooth mesh, but many sidebands appear. For instance, the sidebands in Figure 100 around and in place of the sun gear fundamental and the third harmonic are all separated from their center frequencies by $f_n = 59$ Hz, which is the planet passage frequency (speed of planet carrier in Hz times number of planets). Thus,

$$f_n = (886/60) \cdot 4 = 59 \text{ Hz}$$

From this result we can find for the 1st harmonic (LP1)

$$F_{L_1} \text{ (lower sideband)} = f_{LP1} - f_n = 1566 - 59 = 1507 \text{ Hz}$$

$$F_{U_1} \text{ (upper sideband)} = f_{LP1} + f_n = 1566 + 59 = 1625 \text{ Hz}$$

Similarly, for the third harmonic (LP3)

$$f_{L_3} = 4698 - 59 = 4639 \text{ Hz, and } f_3 = 4698 + 59 = 4757 \text{ Hz}$$

In the same manner, the sidebands of the spiral bevel mesh frequency at some accelerometer and microphone locations are separated by 124 Hz or the rotational frequency of the input shaft ($7460/60 = 124$ Hz).

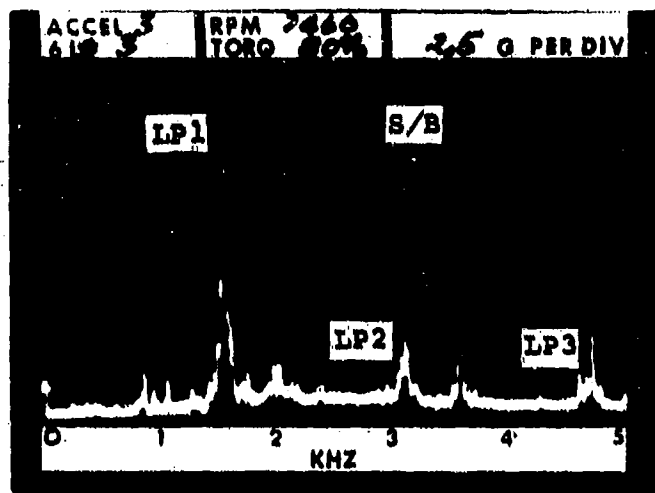


Figure 99. Typical Sump Accelerometer Response.

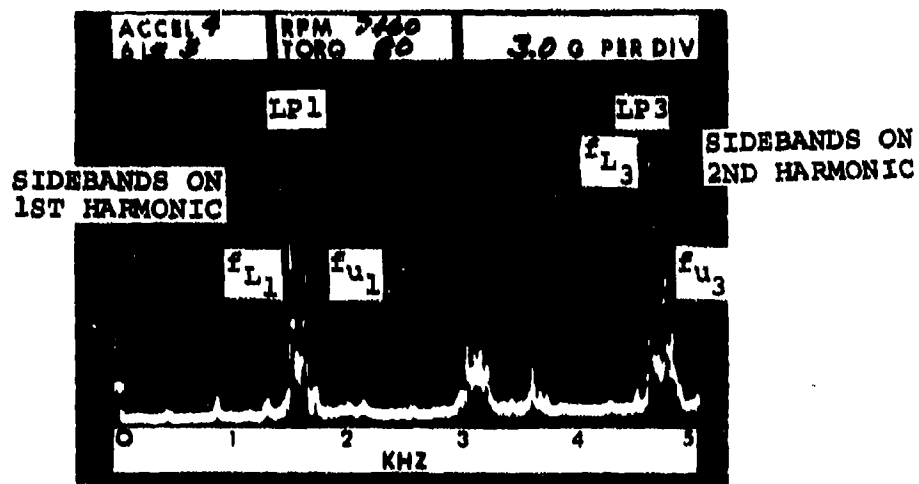


Figure 100. Typical Ring Gear Accelerometer Response.

TABLE 8. CH-47C FORWARD TRANSMISSION GEAR SPEEDS
AND MESH FREQUENCIES AT NORMAL FLIGHT
OPERATION SPEED

GEAR	NUMBER TEETH	SPEED RPM	MESH FREQUENCY HZ
Spiral Bevel Input Pinion	29	7460	3606
Spiral Bevel Gear	51	4242	3606
Lower Stage Sun Gear	28	4242	-
Lower Stage Fixed Ring	106	-	-
Lower Stage Planets (4)	39	-	1566
Lower Stage Planet Carrier	-	886	-
Upper Stage Sun Gear	40	886	-
Upper Stage Fixed Ring	106	-	-
Upper Stage Planets (6)	33	-	429
Upper Stage Planet Carrier	-	243	-
Output - Rotor Shaft	-	243	-

TABLE 9. CH-47C FORWARD TRANSMISSION GEAR SPEEDS
AND MESH FREQUENCIES AT NORMAL GROUND
OPERATION SPEED

GEAR	NUMBER TEETH	SPEED RPM	MESH FREQUENCY HZ
Spiral Bevel Input Pinion	29	6600	3190
Spiral Bevel Gear	51	3753	3190
Lower Stage Sun Gear	28	3753	-
Lower Stage Fixed Ring	106	-	-
Lower Stage Planets (4)	39	-	1386
Lower Stage Planet Carrier	-	784	-
Upper Stage Sun Gear	40	784	-
Upper Stage Fixed Ring	106	-	-
Upper Stage Planets (6)	33	-	379
Upper Stage Planet Carrier	-	215	-
Output - Rotor Shaft	-	215	-

A typical spectrum of the transmission noise, as shown in Figure 101, displays the fundamental gear mesh frequencies and their harmonics of the upper (UP1, UP2, UP3) and lower (LP1, LP2, LP3) planetary systems, the spiral bevel input pinion/gear (spiral/bevel), and in many cases the sidebands of the latter two. In addition, a spike representing the input shaft(s) frequency can be seen at 124 Hz.

The raw data obtained from all test runs were reduced into digital narrow-band frequency domain formats which are included as Figures A1 through A88 in Appendix A. The information contained in these figures was then further reduced to provide the summary data shown in the following sections.

TEST DATA

Case acceleration and acoustical data were recorded during all test runs of the CH-47C transmission to measure the effect on housing vibration and noise radiation reduction for several (see Table 7) combinations of the following structural changes:

1. Sun/bevel gear detuned.
2. Ring gear detuned.
3. Case detuned separately with bonded contoured magnesium plates, and graphite fiber reinforced aluminum composite plates.
4. Isolators added at the mounting arms.

Vibration

The acceleration data for the predominant lower planetary mesh frequency (1566 Hz) is shown in Figures 102 through 105 for each accelerometer location, transmission configuration, and test condition. Figures 106 and 107 show the changes in acceleration for the configurations tested at the design condition of 7460 rpm and 80% torque. As indicated in the figures, most of the configurations resulted in a reduction in vibration level. It is particularly significant that the combination of detuned sun gear and magnesium plates (detuned case) which was the configuration analytically optimized for this condition demonstrated vibration reductions which supported the analytical predictions.

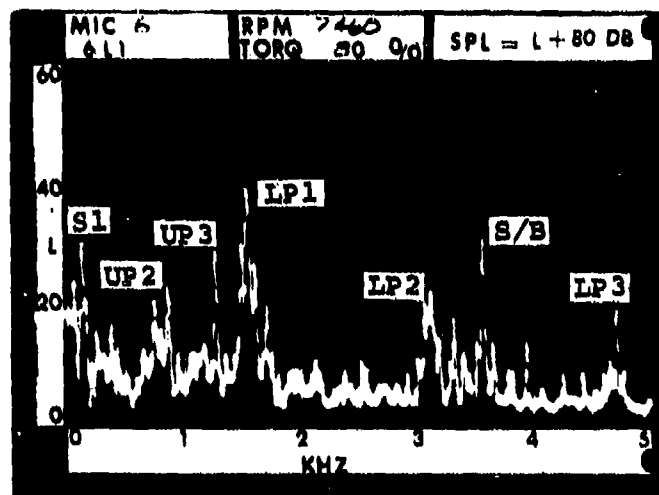


Figure 101. Typical Transmission Noise Spectrum.

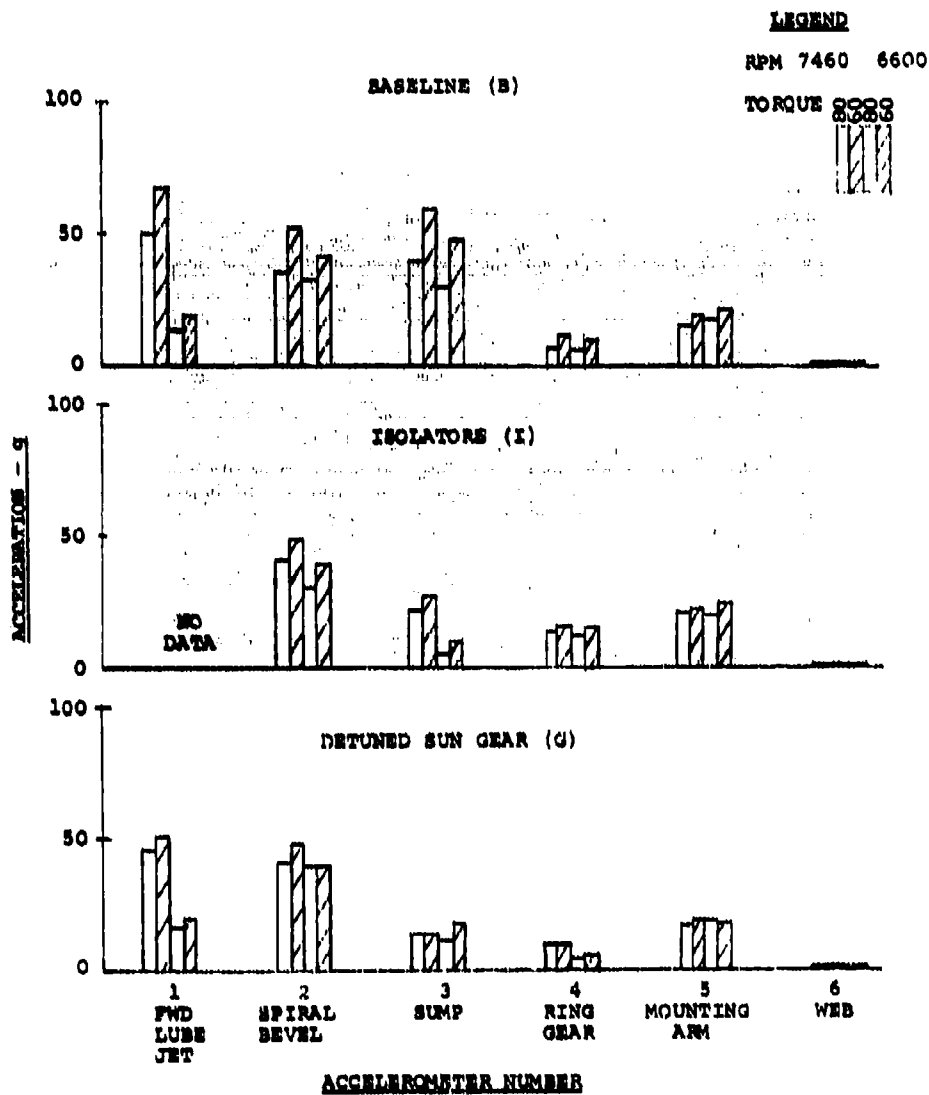


Figure 102. Vibration Data at Lower Planetary Mesh Frequency (Baseline, Isolators, and Detuned Sun Gear).

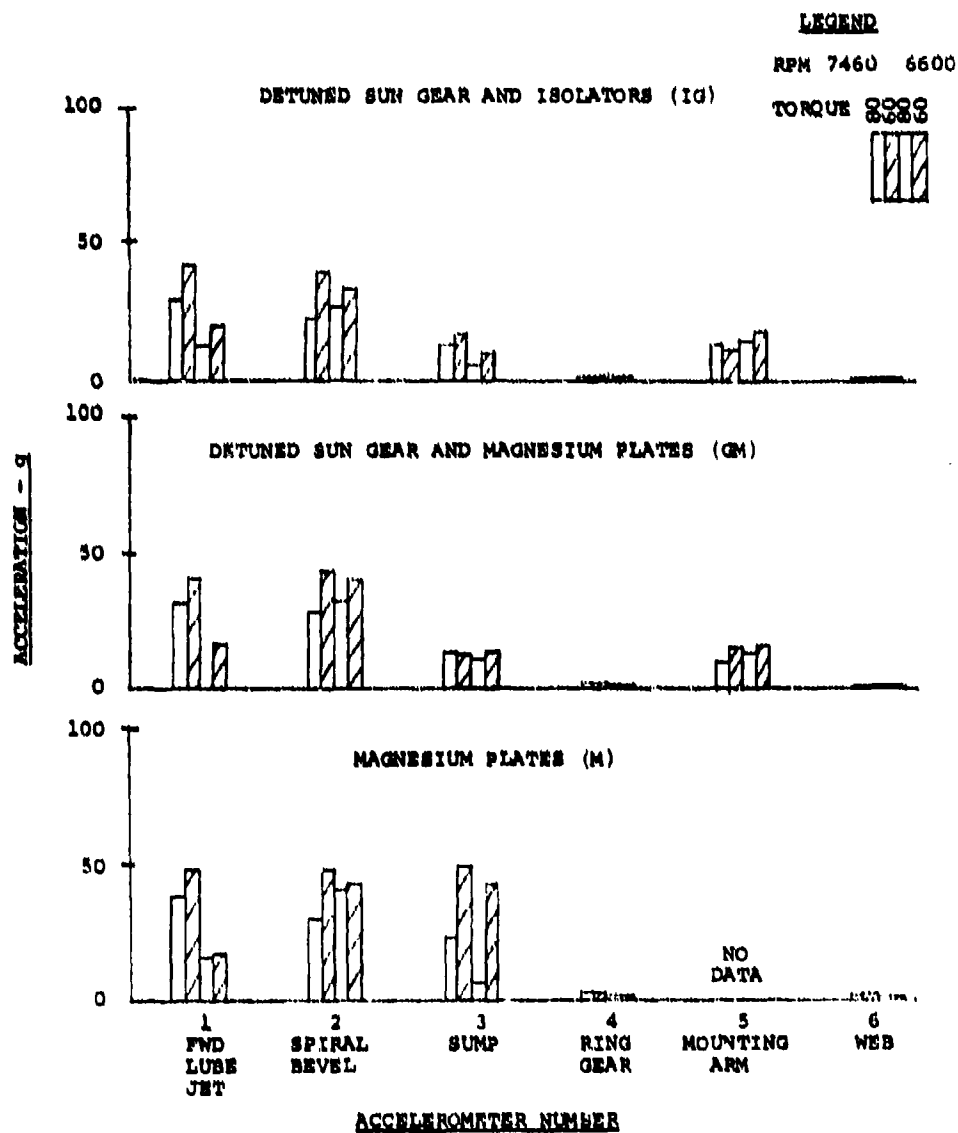


Figure 103. Vibration Data at Lower Planetary Mesh Frequency (Detuned Sun Gear and Isolators, Detuned Sun Gear and Magnesium Plates, and Magnesium Plates).

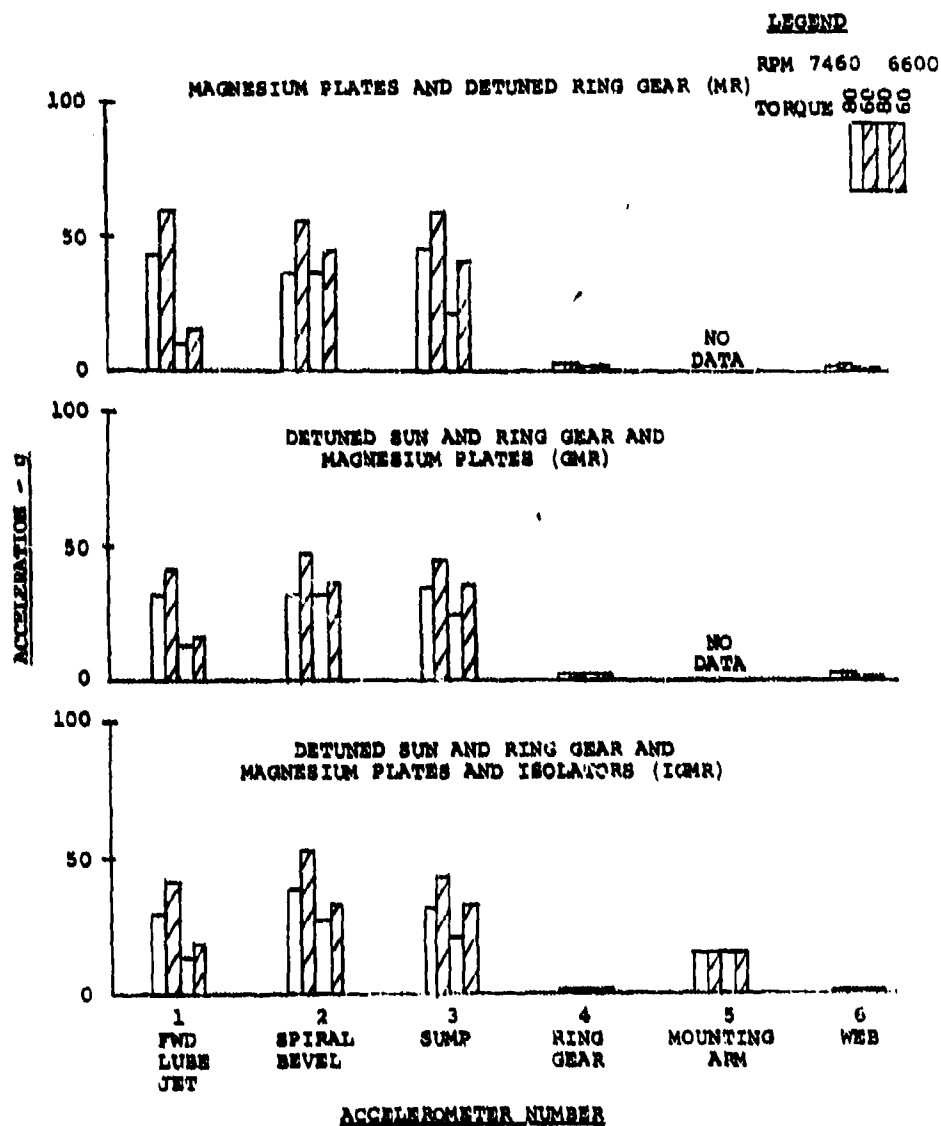


Figure 104. Vibration Data at Lower Planetary Mesh Frequency (Magnesium Plates and Detuned Ring Gear, Detuned Sun Gear and Detuned Ring Gear, and Magnesium Plates).

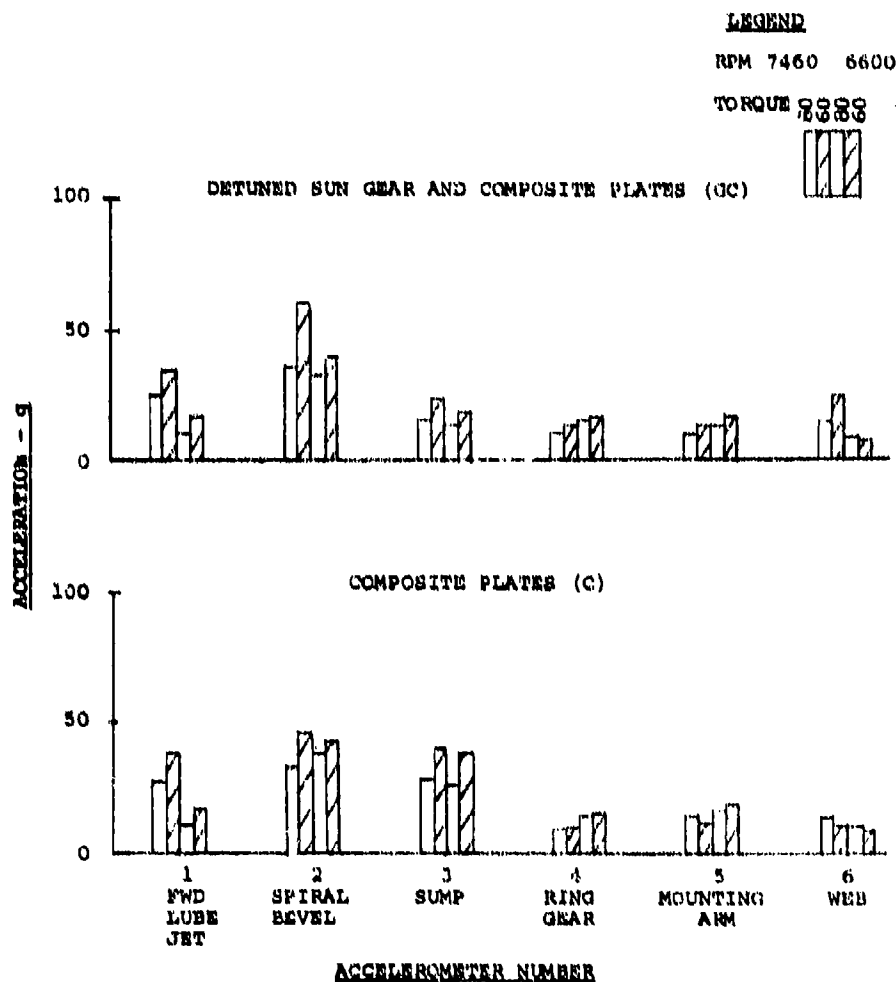
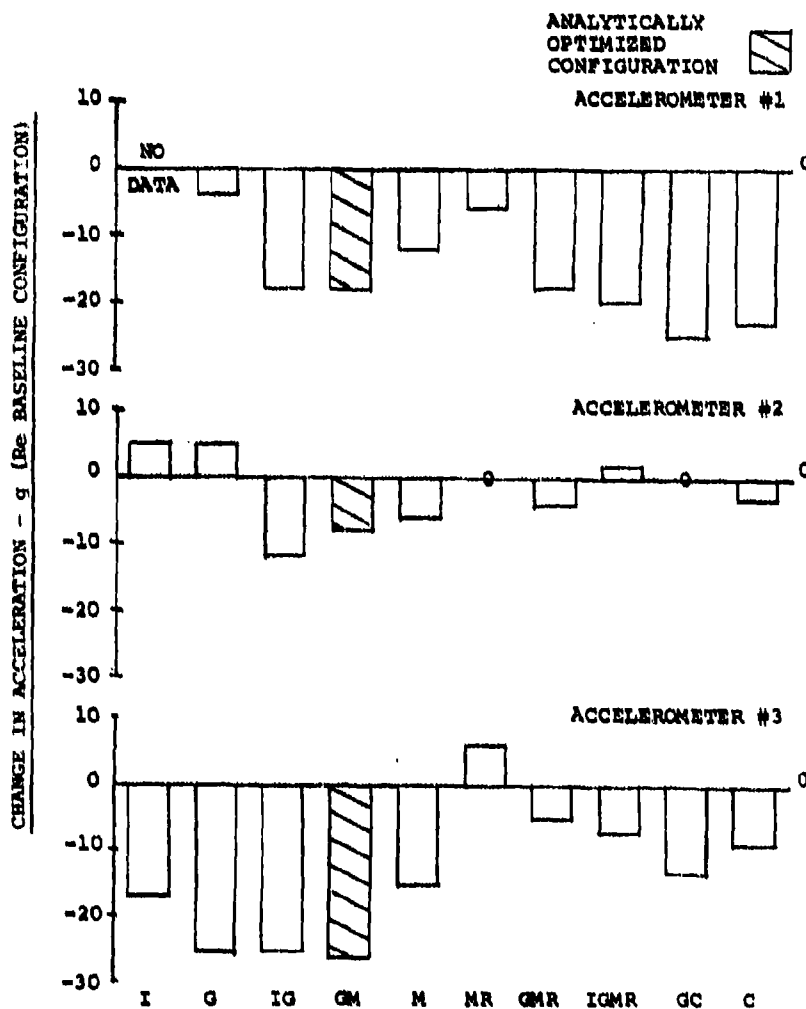


Figure 105. Vibration Data at Lower Planetary Mesh Frequency (Detuned Sun Gear and Composite Plates, and Composite Plates).



ALL DATA AT 7460 RPM AND 80% TORQUE.

Figure 106. Change in Vibration Level at Lower Planetary Frequency (LP1 = 1566 Hz, Accelerometers 1, 2, and 3).

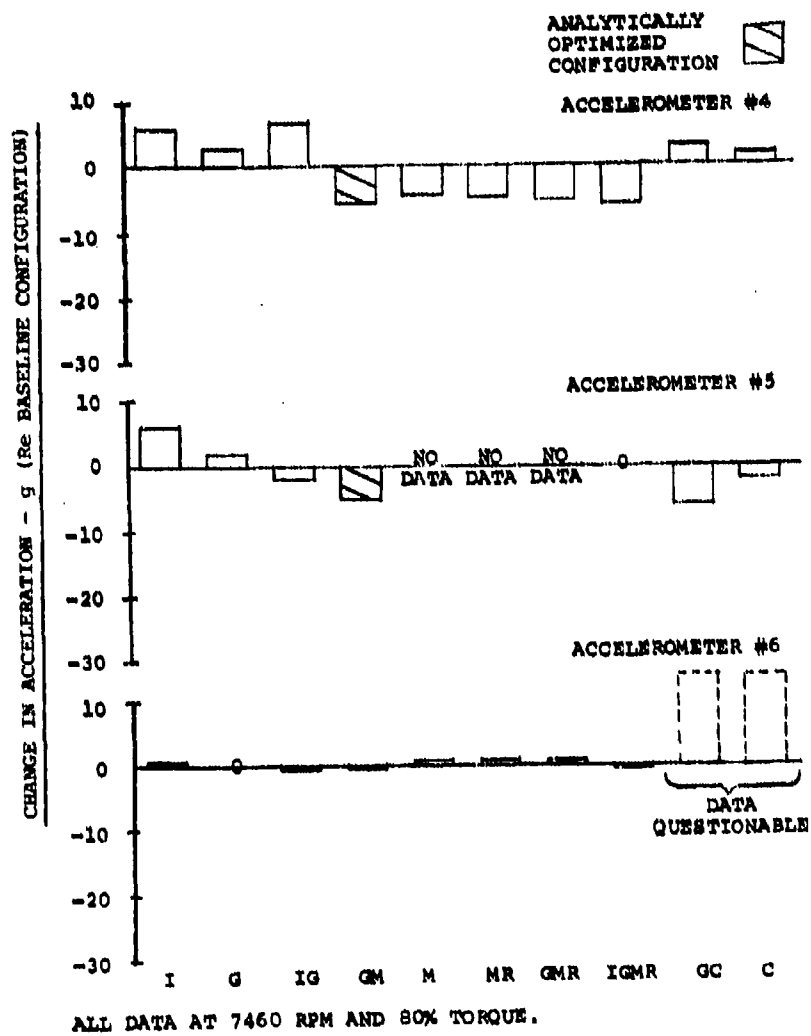


Figure 107. Change in Vibration Level at Lower Planetary Frequency (LPl = 1566 Hz, Accelerometers 4, 5, and 6).

Radiated Noise

The sound pressure level peaks were measured from the oscilloscope pictures at the lower planetary mesh frequency (1566 Hz). These levels are shown in Figures 108 through 111 for each microphone, transmission configuration, and test condition. Figures 112 and 113 indicate the change in level from the unmodified transmission for each of the configurations tested. The condition shown is the normal operating design condition (7460 rpm, 80% torque).

To provide a more comprehensive comparison between configurations tested, a logarithmically averaged sound pressure level was calculated using the data from all six microphones, thus providing a single level representing each configuration. These results are shown in Figure 114 for both rpm's (7460 and 6600) and torques (80% and 60%). These are further summarized in Figure 115 which shows the change in noise level for each configuration as compared with the unmodified transmission.

A significant result of this program is that the combination of the detuned sun gear and case (by the use of magnesium plates), which is the configuration that was analytically optimized by use of the computer program, provided the largest noise reduction (7 dB).

An equally important result is that this combination caused no increase in the spiral bevel mesh frequency noise, and in fact provided a slight decrease when compared to the baseline configuration as shown in Figure 116.

DISCUSSION OF EXPERIMENTAL RESULTS

Simply put, the combined effects of modifying the lower case (adding the magnesium doubler plates) and the sun gear shaft (adding sleeves) resulted in the largest overall net improvement in the basic noise/vibration characteristics of the test transmission when compared to a standard, unmodified transmission. This configuration was defined by analysis, during the early stages of this program, as that which would yield optimum results within the practical restrictions imposed by existing hardware. The other modification suggested by the analysis was that of the ring gear. Based on the results of the testing, some coupling apparently exists between these changes which produced less favorable results than the former modifications acting alone. Unfortunately, these sets of modifications were considered separately in the analysis; thus, this effect was not identified at that time.

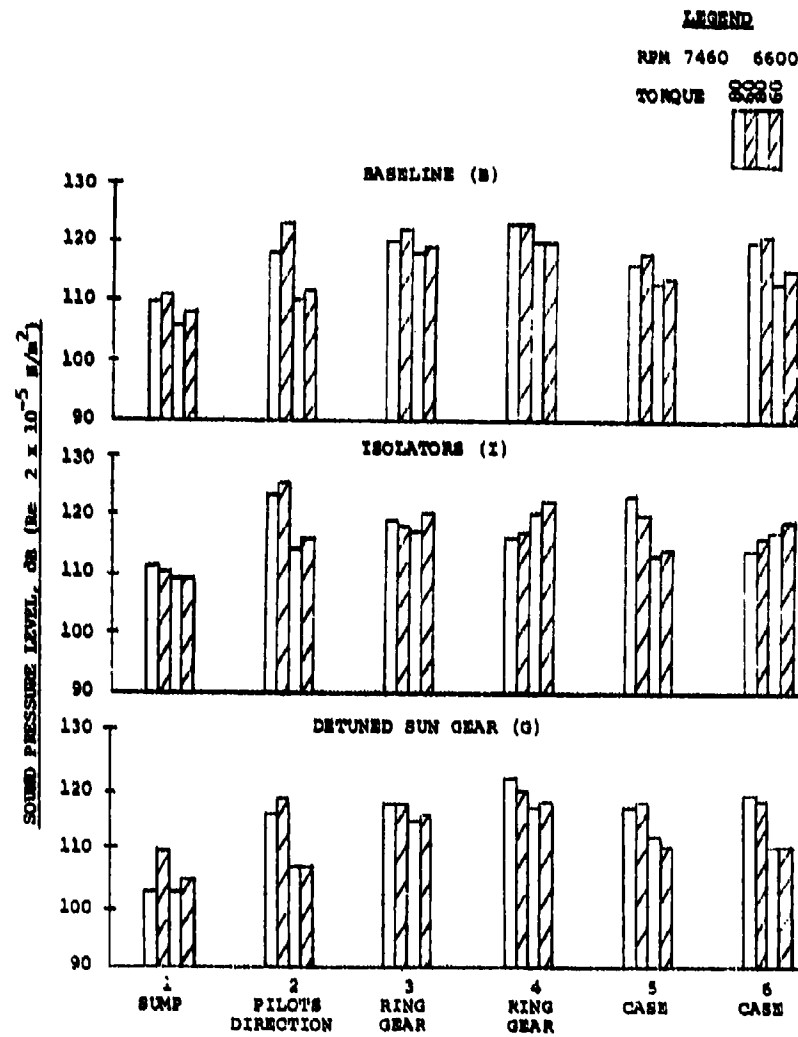


Figure 108. Radiated Noise Data at Lower Planetary Mesh Frequency.

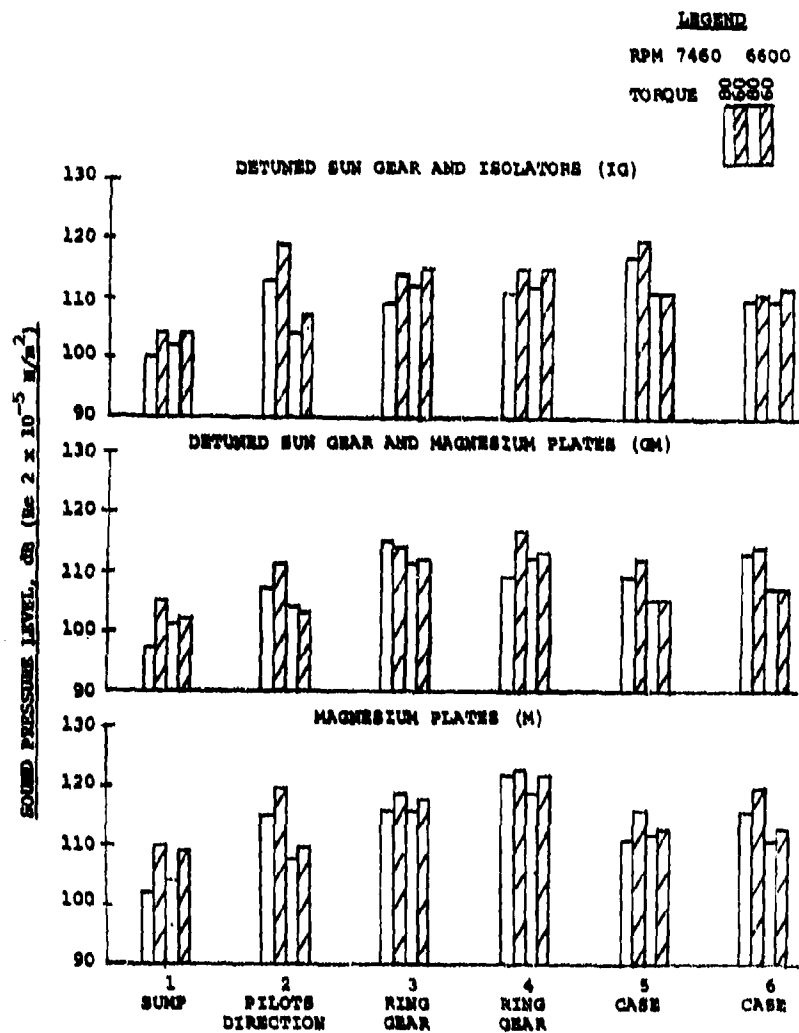


Figure 109. Radiated Noise Data at Lower Planetary Mesh Frequency.

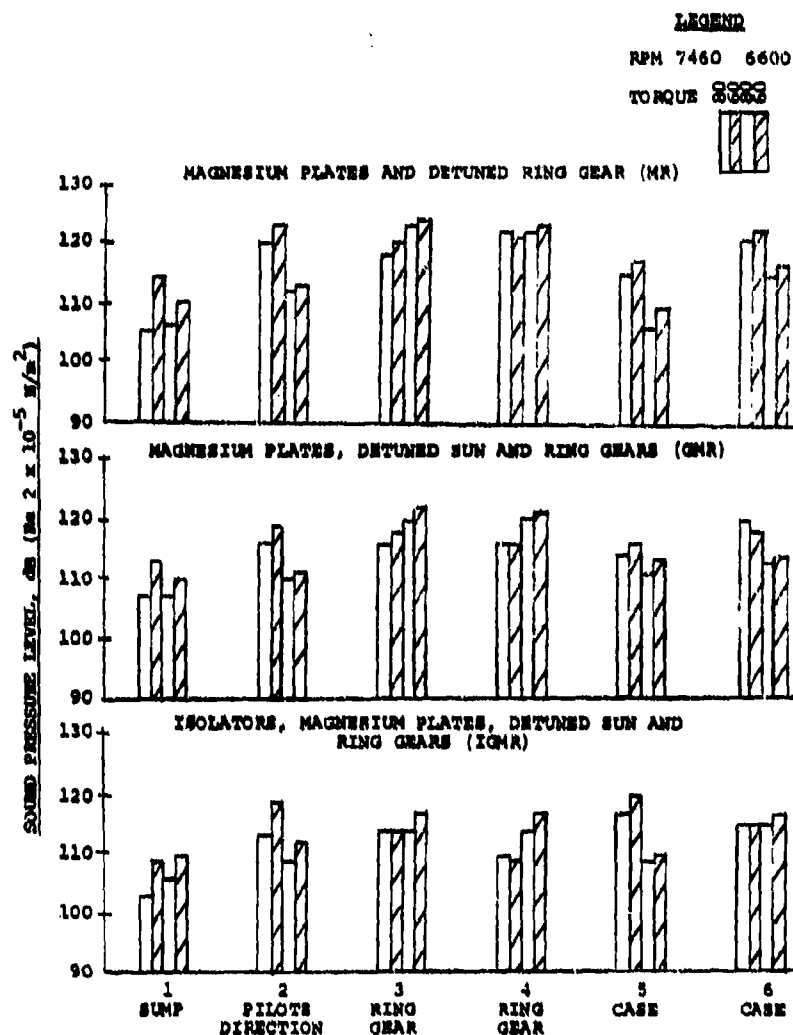


Figure 110. Radiated Noise Data at Lower Planetary Mesh Frequency.

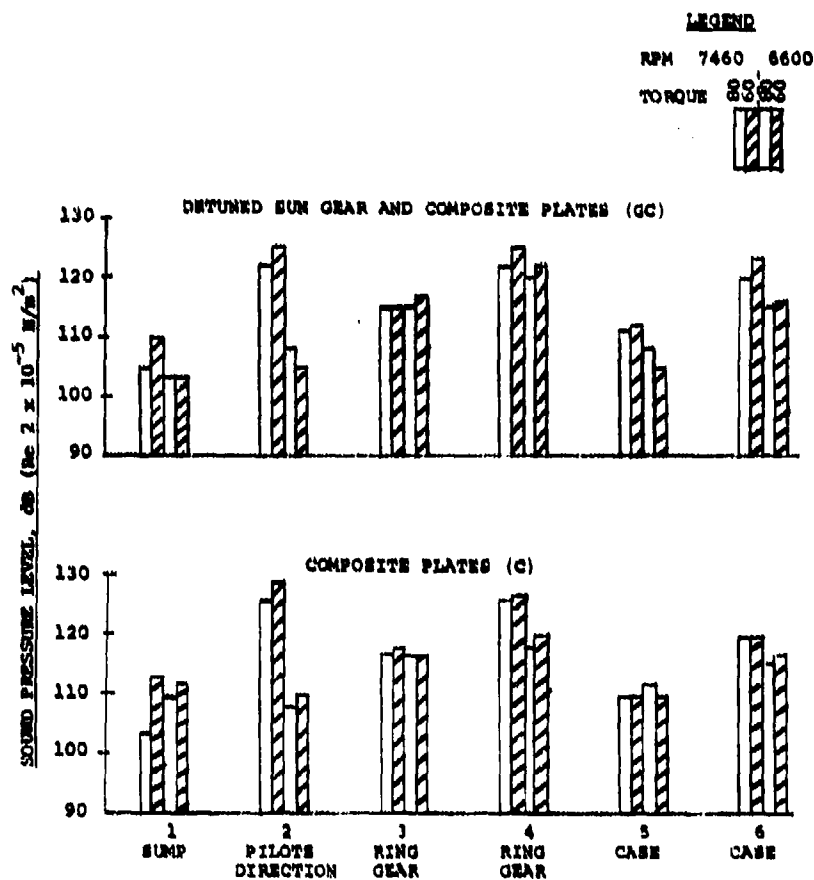


Figure 111. Radiated Noise Data at Lower Planetary Mesh Frequency.

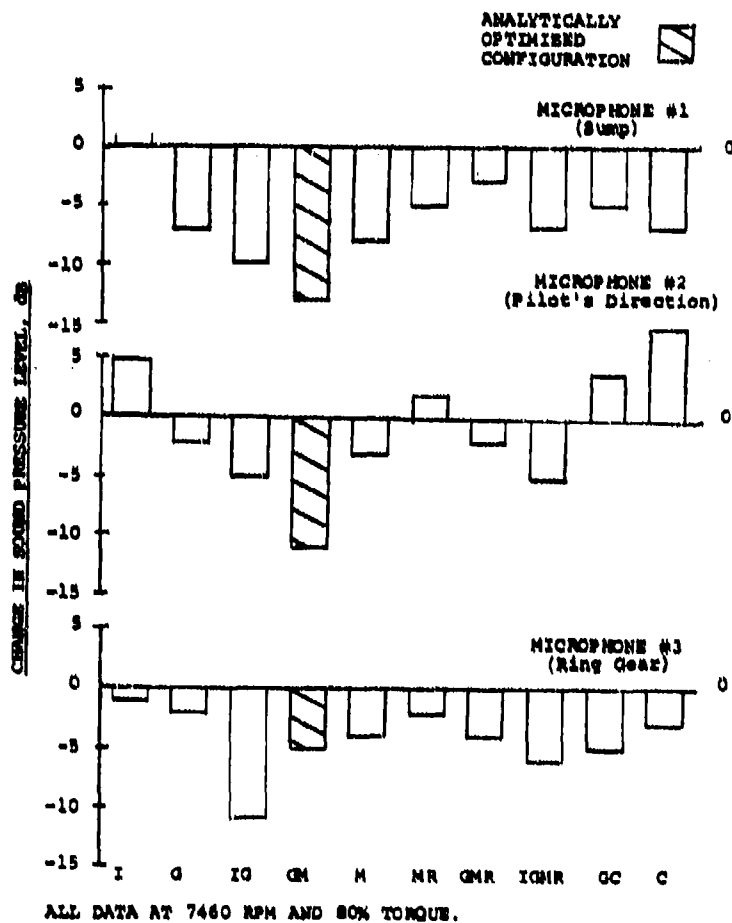


Figure 112. Change in Sound Pressure Level at Lower Planetary Mesh Frequency (Microphones 1, 2, and 3) Compared to Baseline.

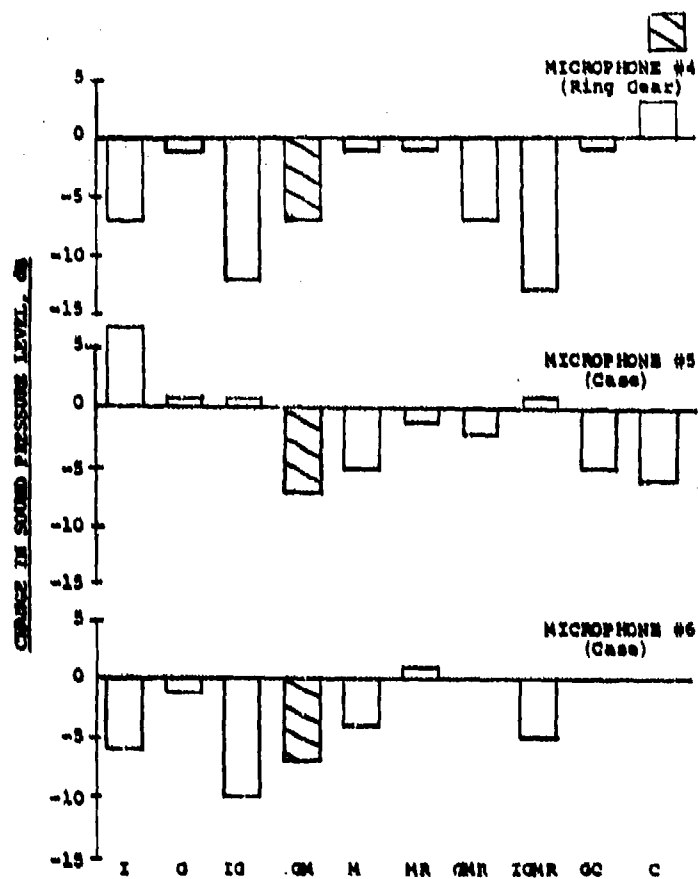


Figure 113. Change in Sound Pressure Level at Lower Planetary Mesh Frequency (Microphones 4, 5, and 6) Compared to Baseline.

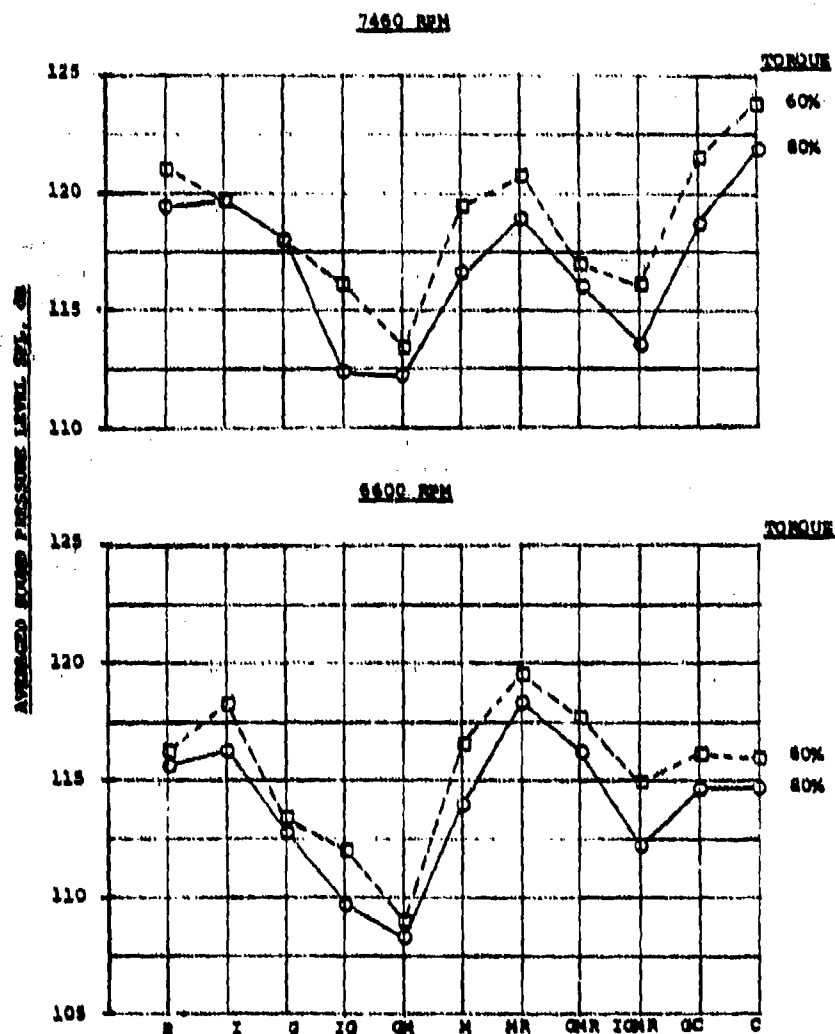


Figure 114. Comparison of Averaged Sound Pressure Levels at Lower Planetary Mesh Frequency.

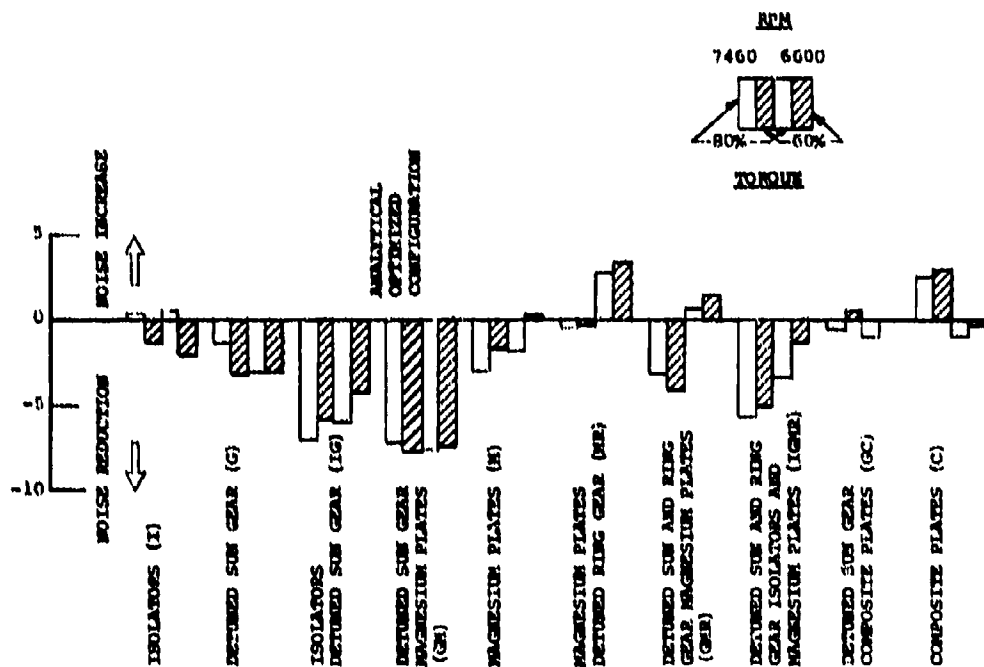


Figure 115. Change in Averaged Sound Pressure Level Compared to Baseline at Lower Planetary Mesh Frequency.

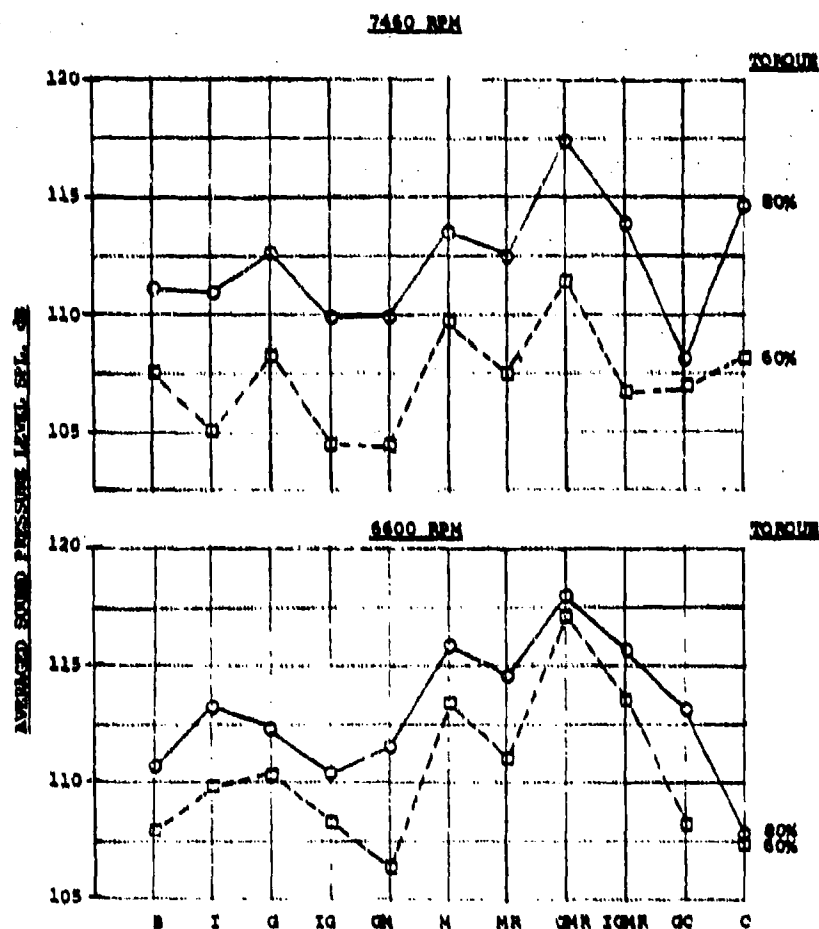


Figure 116. Comparison of Averaged Sound Pressure Levels at Spiral Bevel Mesh Frequency.

The full significance of this improvement in noise/vibration characteristics may most easily be defined by considering the effect of the 7 dB reduction in source noise in terms of the weight and complexity of acoustical treatments (enclosures, etc.) required to achieve similar results.

Acoustical material weight required to reduce transmission noise by enclosures is directly related to the particular frequency being treated. The so-called "normal-incidence, limp-wall mass law" for sound transmission loss (TL) is widely used in noise control work (Reference 12) to determine approximate material surface weights.

TL is defined as the ratio (expressed in decibels) of the acoustic energy transmitted through the enclosure or wall to the acoustic energy incident upon it. Mathematically,

$$TL = 10 \log_{10} \frac{1}{\tau}, \text{ dB}$$

τ = sound transmission coefficient

If the incident sound wave impinges on the wall at normal incidence (that is, perpendicular to the wall surface), the mass law for TL is:

$$TL_{(0^\circ \text{ INCIDENCE})} = 10 \log_{10} \left[1 + \left(\frac{\omega M_s}{2\rho c} \right)^2 \right] \text{ dB}$$

or if the sound waves impinge on the wall surface at random angles of incidence:

$$TL_{(RANDOM)} =$$

$$TL_{(0^\circ \text{ INCIDENCE})} - 10 \log_{10} \left[0.23(TL)_{(0^\circ \text{ INCIDENCE})} \right] \text{ dB}$$

where

$$\omega = 2\pi f$$

f = frequency, Hz

ρc = characteristic resistance of air

ρ = density, slugs/ft³

c = velocity of propagation, ft/sec

M_s = surface density, slugs/ft²

As the product (ωM_s) in the equation implies, higher frequencies require lighter surface densities than do lower frequencies in providing for a constant TL.

In addition, certain materials such as acoustical glass fiber display properties which give attenuation in excess of that expected due to mass alone. Figure 117 shows test results obtained by Boeing Vertol and reported in Reference 13 to determine the attenuation, as a product of surface weight and frequency, of various treatments such as might be used in actual helicopters. Note that the more durable treatments impose some weight penalty.

Figures 118 and 119 indicate the average sound pressure levels of the CH-47C gear meshes recorded during the transmission baseline configuration test, as compared with acoustical noise limits of MIL-A-8806A (Military Specification for Acoustical Noise Level in Aircraft).

Taking into consideration the noise reduction required to comply with the specification, and the associated material weights required to achieve this reduction (Figure 117), relative treatment weights for each mesh frequency and harmonics were computed and are shown in Figure 120. Weights for both materials of maximum durability (with maximum weight) and minimum weight (with minimum durability) are shown.

Reviewing these figures indicates that at 7460 rpm (flight operation) the lower planetary fundamental (LP1) mesh frequency (1566 Hz) dictates the acoustical treatment, while at 6600 rpm (ground operation), both the lower planetary (LP1 - 1386 Hz) and spiral bevel input (spiral/bevel - 3190 Hz) are equally important. Subsequently, the effectiveness of the structural changes tested in the program for reducing transmission case vibrations and generated noise was concentrated on the lower planetary fundamental mesh frequency at the design operating condition (7460 rpm, 80 percent torque).

The helicopter design implication of a 7 dB reduction in radiated rotor transmission noise through source noise reduction is a substantial weight savings in the acoustical treatment required to comply with Table IV of MIL-A-8806A (normal cruise power condition). In the case of the CH-47 helicopter, this amounts to a savings of at least 20 percent of the total material weight required, or about 100 lbs. The CH-47 helicopter has two main rotors which are driven by very similar transmissions (major differences are rotor shaft length and the input shaft angle); thus, the total aircraft weight savings will be based on similar modifications of both transmissions and acoustical treatment of the entire cabin area. Data similar to that shown in Figure 117 has been developed for both forward and aft transmissions and is shown in Figures 121

and 122. Utilizing this data and that shown in Figure 118, the comparison shown in Table 10 was developed. Based on the total weight of acoustical treatment for the entire aircraft, a 20% weight savings is realized; however, over 35% of the acoustical treatment weight for the immediate transmission enclosure areas is saved.

LIMP BLANKETS

- Glass Fiber Batting 1.0" Thick
- + Porous Trim 0.5" Batting
- Porous Trim 1.0" Batting
- ▲ Porous Trim 1.5" Batting
- Scrim Cloth 1.0" Batting/
Scrim Cloth
- ◆ Impervious Trim 1.5" Batting/
Scrim Cloth

DURABLE TRIM

- .040 Stratoglas/1.5" Batting/
.020 Stratoglas
- ⊕ .040 Stratoglas/1.0" Foam/
.020 Stratoglas
- △ .040 Stratoglas
- .040 Aluminum Alloy Panel
- ◇ .040 Aluminum Alloy Panel/
Aluminum Alloy Damping Tape
- .040 Stratoglas/2.0" Foam/
.020 Stratoglas

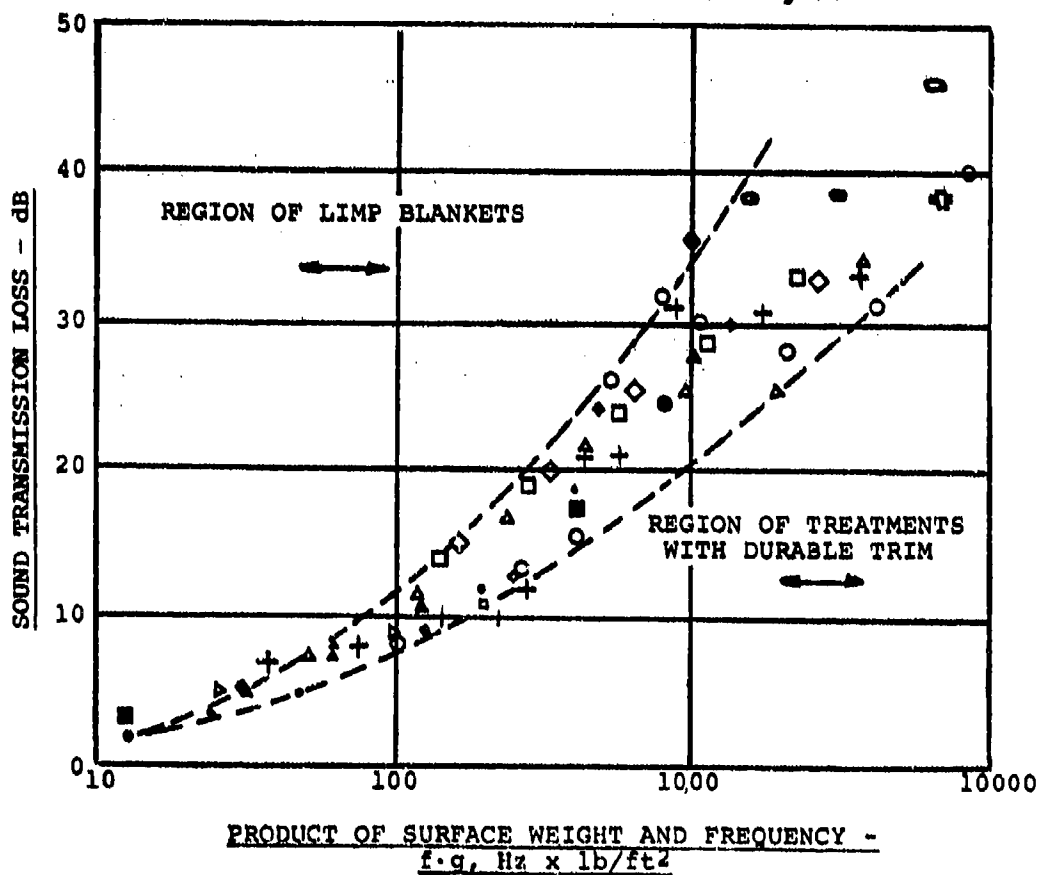


Figure 117. Typical Effect of Sound Transmission Enclosures on Source Attenuation.

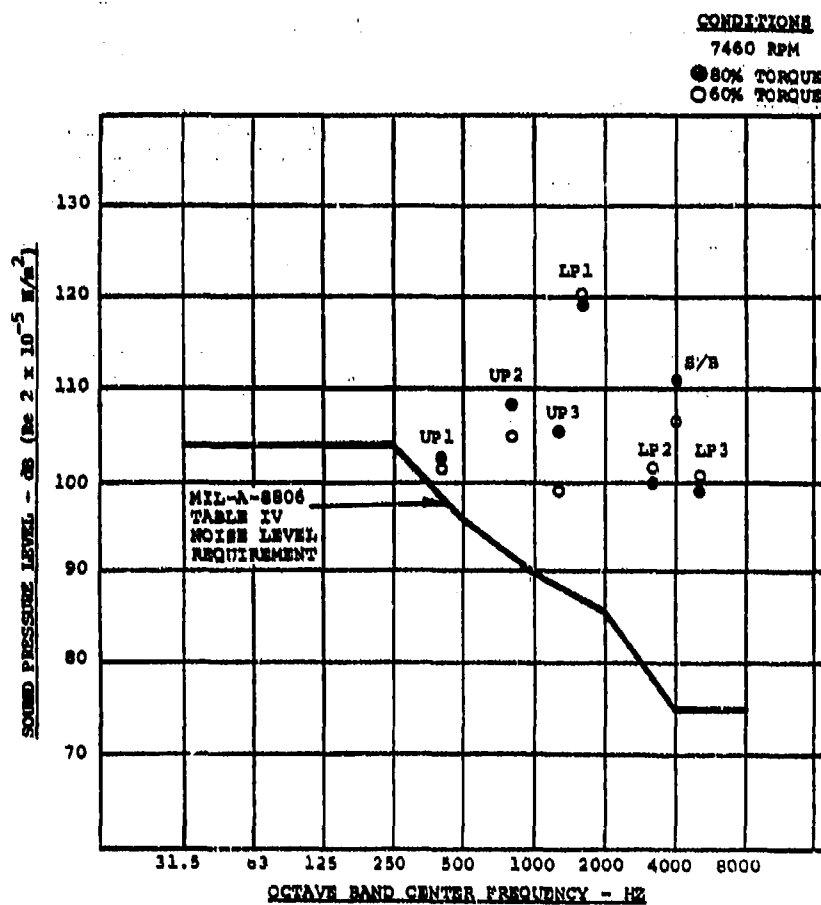


Figure 118. Relationship of CH-47C Forward Transmission Noise to MIL-A-8806 Requirements at Flight Operation Speed.

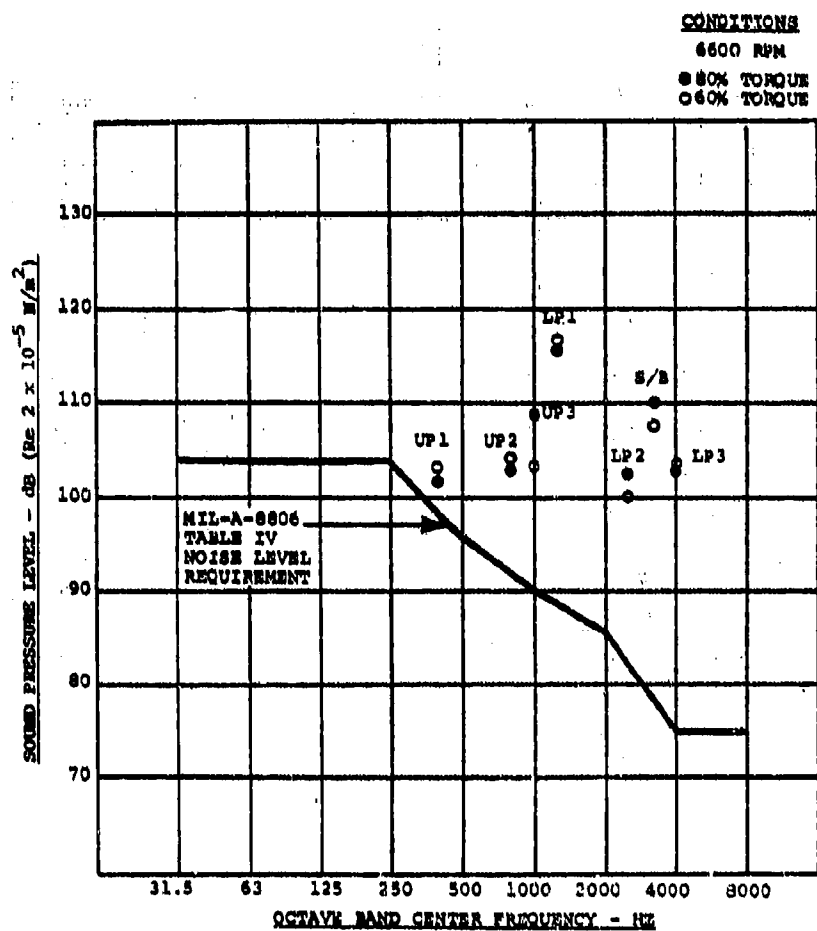


Figure 119. Relationship of CH-7C Forward Transmission Noise to MIL-A-8806 Requirements at Ground Operation Speed.

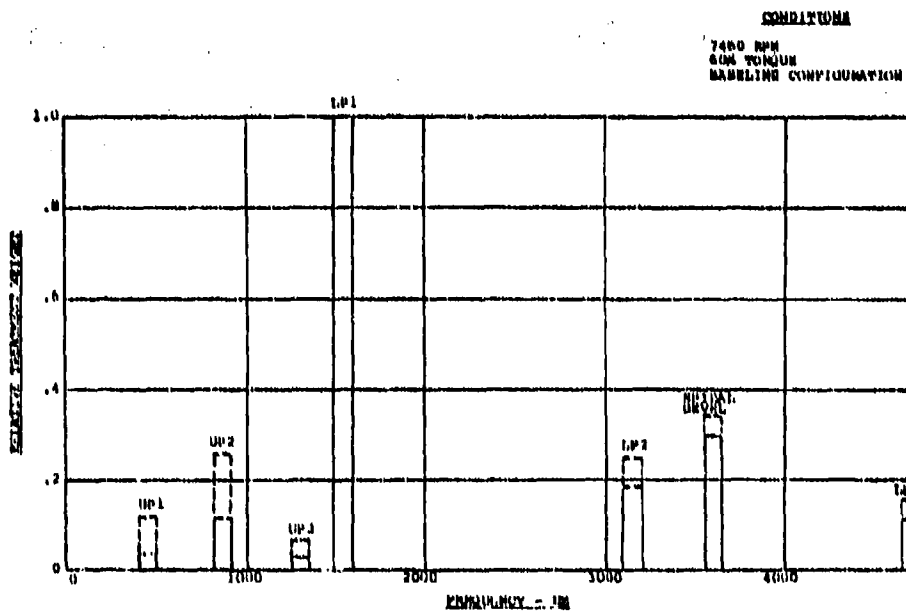
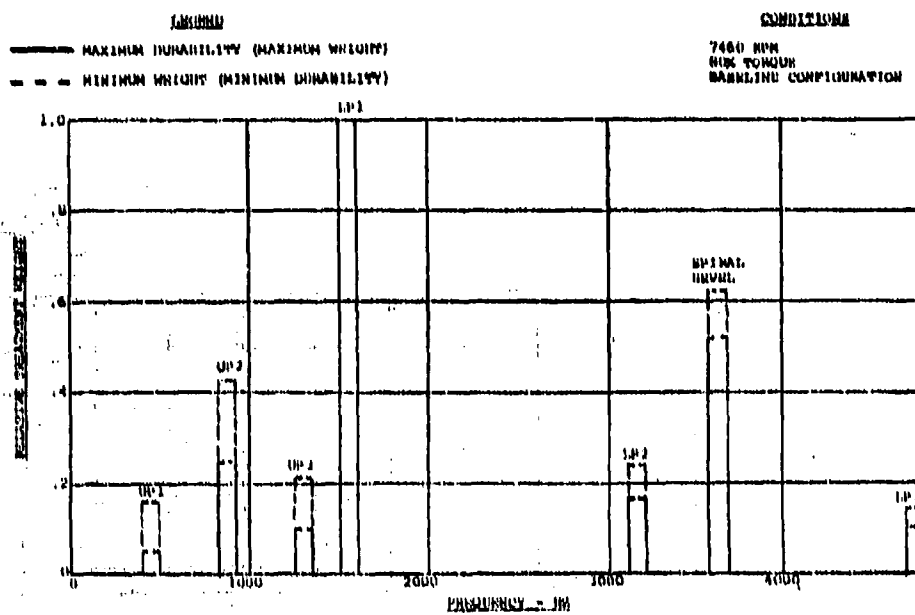


Figure 120. Relative Weight of Acoustical Treatment Required to Reduce CH-47C Forward Transmission Noise Levels to MIL-A-8806 Requirements.

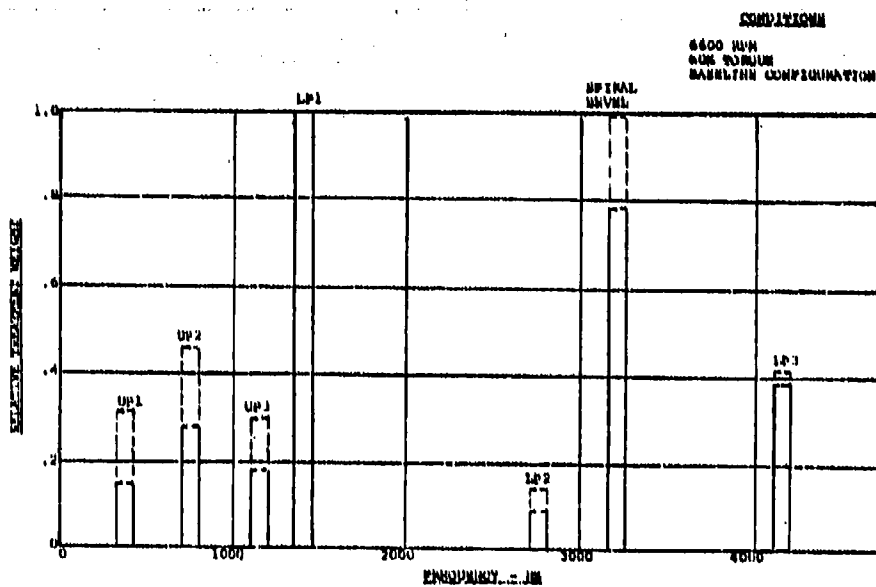
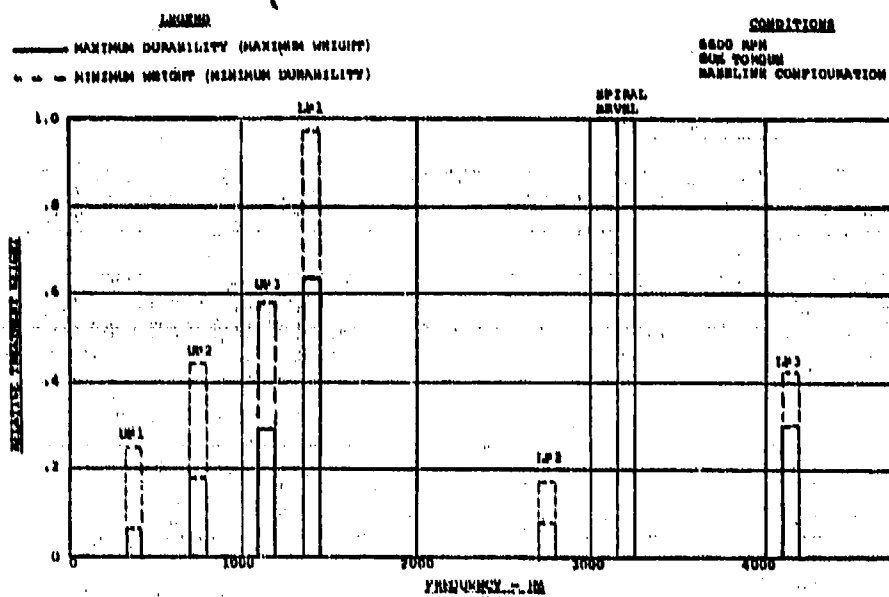


Figure 120. Continued.

LIMP BLANKETS

DURABLE TRIM

- | | |
|---------------------------------|--------------------------------|
| •Glass Fiber Batting 1.0" Thick | ○.040 Stratoglas/1.5" Batting/ |
| +Porous Trim 0.5" Batting | .020 Stratoglas |
| ●Porous Trim 1.0" Batting | ⊕.040 Stratoglas/1.0" Foam/ |
| ▲Porous Trim 1.5" Batting | .020 Stratoglas |
| ■Scrim Cloth 1.0" Batting/ | △.040 Stratoglas |
| Scrim Cloth | □.040 Aluminum Alloy Panel |
| ◆Impervious Trim 1.5" Batting/ | ◇.040 Aluminum Alloy Panel/ |
| Scrim Cloth | Aluminum Alloy Damping Tape |
| | ○.040 Stratoglas/2.0" Foam/ |
| | .020 Stratoglas |

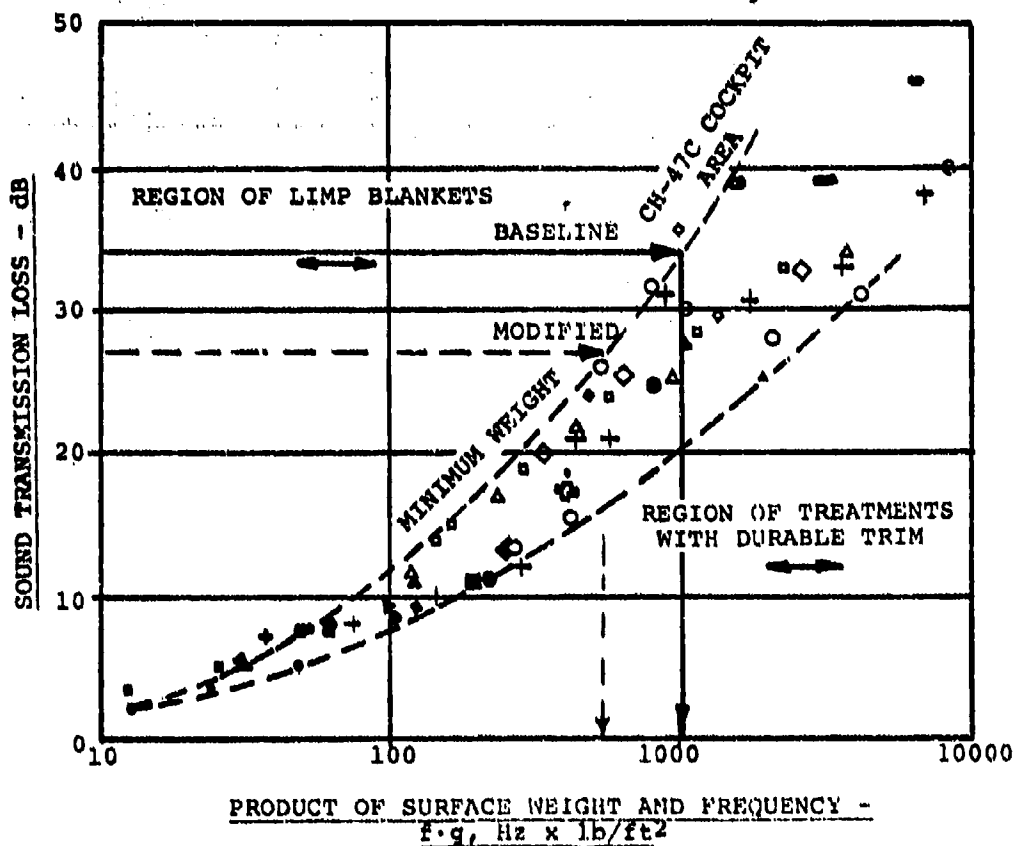


Figure 121. Effect of Sound Transmission Enclosures on Source Attenuation of CH-47C Forward Transmission Noise.

LIMP BLANKETS

- Glass Fiber Batting 1.0" Thick
- + Porous Trim 0.5" Batting
- Porous Trim 1.0" Batting
- ▲ Porous Trim 1.5" Batting
- Scrim Cloth 1.0" Batting/
Scrim Cloth
- ◆ Impervious Trim 1.5" Batting/
Scrim Cloth

DURABLE TRIM

- .040 Stratoglas/1.5" Batting/
.020 Stratoglas
- ⊕ .040 Stratoglas/1.0" Foam/
.020 Stratoglas
- △ .040 Stratoglas
- .040 Aluminum Alloy Panel
- ◇ .040 Aluminum Alloy Panel/
Aluminum Alloy Damping Tape
- .040 Stratoglas/2.0" Foam/
.020 Stratoglas

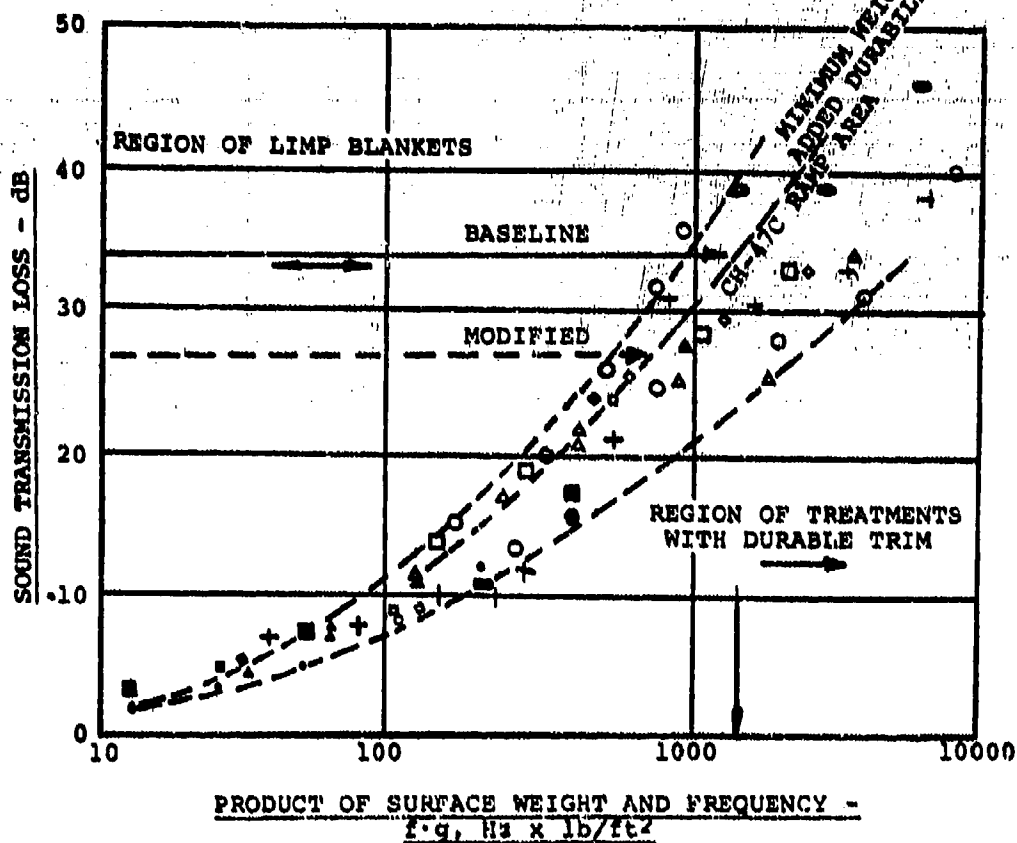


Figure 122. Effect of Sound Transmission Enclosures on Source Attenuation of CH-47C Aft Transmission Noise.

TABLE 10. ACOUSTICAL TREATMENT WEIGHT COMPARISON FOR
BASELINE AND MODIFIED TRANSMISSIONS

	FORWARD TRANSMISSION		APT TRANSMISSION	
	BASELINE	MODIFIED	BASELINE	MODIFIED
1. Average Noise Level, dB (Figure 118, LPL = 1556 Hz)	120	113	120	113
2. Noise Limit of MIL-A-8806A, Table IV, dB (Figure 118, 2000 Hz Octave)	86	86	86	86
3. Transmission Enclosure Attenuation Required, dB	34	27	34	27
4. Product of Surface Weight and Frequency, f_w , Hz x Lb/ft ² (Figures 121 and 122)	1000	560	1500	770
5. Surface Weight of Required Enclosure, Lb/ft ² ($f_w / f \phi$ $f = 1556$ Hz)	0.64	0.36	0.96	0.49
6. Area of Enclosure (Approx), ft ²	110	110	155	155
7. Required Treatment Weight, Lb	70	40	149	76
8. Enclosure Weight Reduction (Baseline WT - Modified WT = Reduction)	-	30	-	73
9. Total Weight of Transmission Modifications (Gear Shaft and Magnesium Plates), Lb	-	3.3	-	3.3
10. Net Weight Reduction per Transmission, Lb	-	26.7	-	69.7

TOTAL WEIGHT SAVINGS OF
96.4 LBS PER AIRCRAFT

NOTES:

1. Total acoustical insulation weight of CH-47C to comply with MIL-A-8806A, Table IV is approximately 500 lb.
2. Figures shown represent immediate transmission enclosure areas and do not reflect probable additional savings in main cabin area.

CONCLUSIONS

The basic analytical approach as a design tool for transmission vibration/noise reduction has been validated. This method unites the internal components and the housing, hence will aid in optimizing the transmission as a complete operating subsystem. Since the housing provides structural support to the internal components, its physical characteristics grossly affect the performance, wear and fatigue lives of the bearings, gears, splines and shafts due to misalignments and load concentrations. Therefore, housing optimization is essential if the full benefits of advancements in gear and bearing technology are to be realized.

The methods described herein have proved to be valuable analytical and design tools. The contractor has applied portions of the analysis to drive system projects such as the Boeing/Seattle Hydrofoil Boat, the modernized CH-47(D) helicopter, and the Boeing Vertol advanced concept transmission program. Using the existing finite element housing model, further investigations utilizing NASTRAN to evaluate static and dynamic stresses, thermal distortions, deflections and load paths due to any type loading, fail-safety, vulnerability, and composite materials (Figures 123 and 124) have been efficiently conducted (Reference 14).

The fabrication technology for complex structures such as the subject doubler plates has been demonstrated successfully in this program, and this progress offers considerable encouragement for additional fabrication development and evaluation of complex composite structural components.

Specifically, the following conclusions have been reached as a direct result of this program.

- An analytical approach to the source reduction of the noise and vibration associated with high power, high speed, lightweight aircraft transmissions has been developed and applied. This effort included the following major areas of investigation:
 1. The dynamic response of a CH-47C forward transmission shaft/case system was defined by finite element techniques. This analysis, which included the damped forced response of the case and determination of those areas of the case with the highest strain energy density, correlated well with existing baseline data.
 2. The utility of the basic computer analysis system, by which the dynamic response was calculated, was improved by providing a graphical representation of the damped

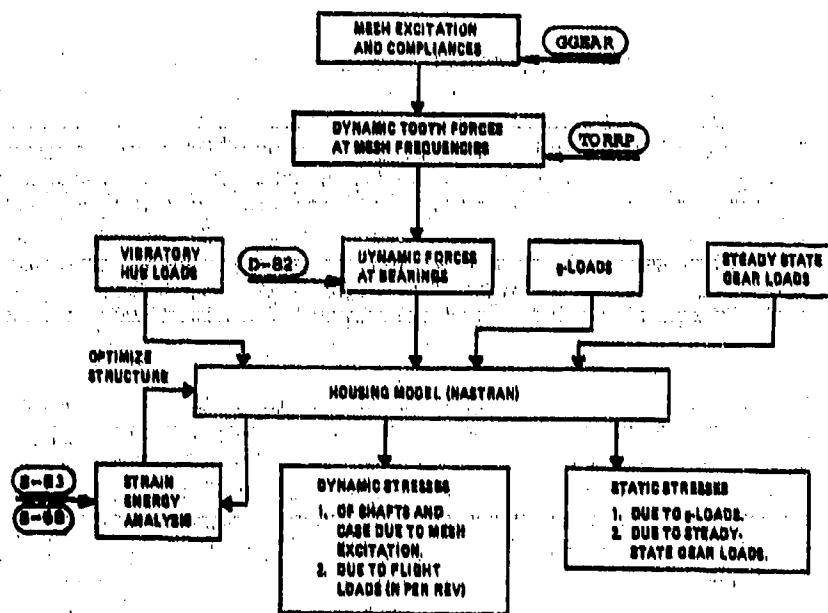


Figure 123. Flow Diagram of NASTRAN Stress Analysis.

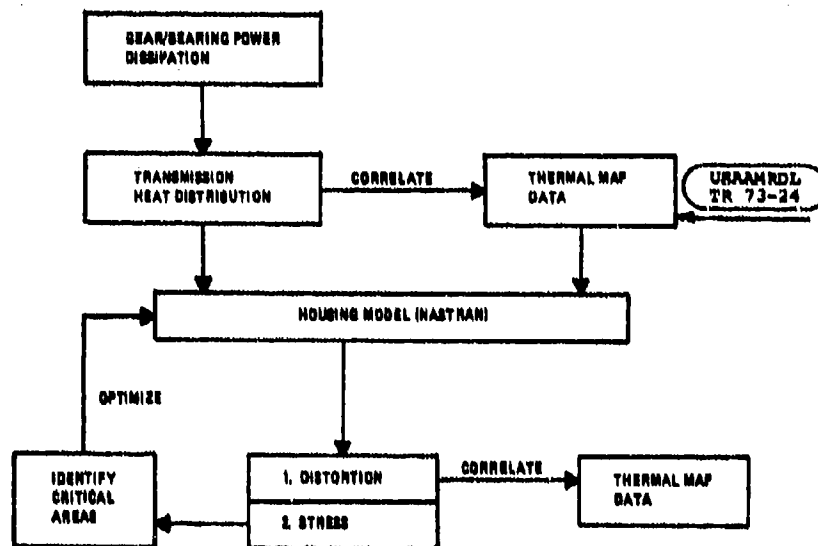


Figure 124. Flow Diagram of NASTRAN Thermal Analysis.

forced response and by expanding the computer program GGEAR to incorporate high contact ratio (HCR) gearing.

- The test data available from a previously conducted HLH/ATC noise reduction program, which also utilized the CH-47C forward transmission, was further reduced and analyzed in order to provide an extensive file of baseline data. This data was then used to validate and improve the baseline computer model. The correlation obtained with the initial model indicated a need for revision to include the coupling effect observed between the shafts, and the spring effect of the planets in holding the sun gear in position. After these improvements were made, agreement between experiment and analysis was excellent.
- Using the improved model, the standard production components were analyzed to define the design modifications which would be required to provide a significant reduction in source noise and vibration levels.
- A test program, conducted to verify the noise/vibration reductions predicted by the improved analysis through the use of the modified components, clearly demonstrated the utility of this method in minimizing source noise/vibration at the design stage.

The most general, overall conclusion which may be reached as a result of this program is that the analysis and modification of a helicopter gearbox system in the design phase, prior to the manufacture of any hardware, is not only possible but, through the use of the computer-aided system herein defined, will result in a final gearbox configuration with a lower source noise and vibration level than would otherwise be attainable. Moreover, this minimum noise and vibration configuration, while slightly increasing the weight of the transmission subsystem, yields a substantial savings in the overall aircraft system weight by reducing the amount (weight) of add-on materials required to provide the desired cabin noise and vibration levels.

Although the overall results of this program were favorable and quite encouraging, the need for further effort is quite clear. The basic analytical method has demonstrated reasonable accuracy; however, several areas were determined to be deficient for universal application. Additionally, the system as currently presented, while sufficient for the needs of this endeavor, is somewhat cumbersome and difficult to apply, particularly for the uninitiated.

RECOMMENDATIONS

In order to increase the accuracy and utility of the analysis described in this report and bring it from the status of a research tool to that of a practical design and analysis system, it is recommended that the following specific items be considered to further advance the state of the art:

- The gear tooth mesh compliance analysis (GGEAR/HCR) should be extended to include rigorous calculations for helical gears and an improved method for spiral bevel gears. The results of this analysis would include a foundation for the eventual incorporation of a rigorous treatment of spiral bevel gears and a much-improved helical gear load sharing calculation.
- Present methods of transmission noise prediction are based upon the cycled energy at the gear meshes, while methods of noise reduction are based upon reducing displacements at the shaft support bearings. This inconsistency of approach has presented considerable difficulty in performing comparative studies; thus, an analytical technique for calculating the overall sound spectrum directly from the dynamic shaft displacements must be developed.
- The computer-aided transmission design techniques, as well as the already established computer programs, although complete in themselves, are in a "bits and pieces" state. Considerable manual manipulation of data and various input/output sequences with these numerous independent programs are required. This introduces potential inaccuracies and is quite time consuming. A way to circumvent this problem is to develop an efficient closed-loop total system optimization master computer-aided design program incorporating the many individual analyses now existing. Interactive computer graphics and automatic plotting interwoven throughout the design cycle would be key features contributing to efficiency and versatility. Such a system is now achievable for the future design of new transmissions. It is recommended that a program be undertaken to develop a total, efficient design tool as stated above.
- An experimental program should be conducted using small mechanical shakers to excite a transmission case in an anechoic room to determine its response to various stimuli. In this way, it will be possible to accurately record the case response on an acoustic sphere so that a determination may be made of those modes, or general classes of modes, which are of greatest significance to the noise and vibration problem.

REFERENCES

1. Sternfeld, H., Spencer, R. H., and Schaeffer, E. G., STUDY TO ESTABLISH REALISTIC ACOUSTIC DESIGN CRITERIA FOR FUTURE ARMY AIRCRAFT, Vertol Division, The Boeing Company, TREC TR 61-72, U.S. Army Transportation Research Command, Fort Eustis, Virginia, June 1961.
2. Sternfeld, H., Schairer, J., and Spencer, R., AN INVESTIGATION OF HELICOPTER TRANSMISSION NOISE REDUCTION BY VIBRATION ABSORBERS AND DAMPING, Vertol Division, The Boeing Company, USAAMRDL TR 72-34, U.S. Army Air Mobility Research and Development Laboratory, Fort Eustis, Virginia, August 1972, AD752579.
3. Hartman, R. M., A DYNAMICS APPROACH TO HELICOPTER TRANSMISSION NOISE REDUCTION AND IMPROVED RELIABILITY, Paper Presented at the 29th Annual National Forum of the American Helicopter Society, Washington, D. C., May 1973, Preprint No. 772.
4. Hartman, R. M., and Badgley, R., MODEL 301 HLH/ATC TRANSMISSION NOISE REDUCTION PROGRAM, Vertol Division, The Boeing Company, USAAMRDL TR 74-58, Eustis Directorate, U.S. Army Air Mobility Research and Development Laboratory, Fort Eustis, Virginia, May 1974, AD784132.
5. Lawrence, H. C., NOISE AND OSHA, Design News, March 17, 1975, Pages 61-64.
6. George, C., GEAR NOISE SOURCES AND CONTROLS, Detroit Diesel Allison Division of General Motors Corporation, Presentation Notes.
7. Munch, C., A STUDY OF NOISE GUIDELINES FOR COMMUNITY ACCEPTANCE OF CIVIL HELICOPTER OPERATIONS, Journal of the American Helicopter Society, January 1975, Pages 11-19.
8. Sciarra, J. J., USE OF THE FINITE ELEMENT DAMPED FORCED RESPONSE STRAIN ENERGY DISTRIBUTION FOR VIBRATION REDUCTION, U.S. Army Research Office-Durham, Contract DAHC04-71-C-0048, Boeing Vertol Document D210-10819-1, July 1974.
9. Everstine, G., BANDIT - A COMPUTER PROGRAM TO RENUMBER NASTRAN GRID POINTS FOR REDUCED BANDWIDTH, Naval Ship Research and Development Center Technical Note AML-6-70, February 1970.

10. Soedel, Werner, SHELL VIBRATIONS WITHOUT MATHEMATICS - PART II, Sound and Vibration, April 1976, p. 12-15.
11. Sciarra, J. J., VIBRATION REDUCTION BY USING BOTH THE FINITE ELEMENT STRAIN ENERGY DISTRIBUTION AND MOBILITY TECHNIQUES, 45th Shock and Vibration Symposium, Dayton, Ohio, August 1974.
12. Beranek, L. L., NOISE REDUCTION, McGraw Hill Book Co, 1960.
13. Sternfeld, H., Schairer, J., and Spencer, R., AN INVESTIGATION OF HELICOPTER TRANSMISSION NOISE REDUCTION BY VIBRATION ABSORBERS AND DAMPING, Vertol Division, The Boeing Company, USAAMRDL Technical Report 72-34, Eustis Directorate, U.S. Army Air Mobility Research and Development Laboratory, Fort Eustis, Virginia, August 1972, AD752579.
14. Howells, R. W., and Sciarra, J. J., FINITE ELEMENT ANALYSIS USING NASTRAN APPLIED TO HELICOPTER TRANSMISSION VIBRATION/ NOISE REDUCTION, NASA TMX-3278, September 1975.
15. Badgley, R., and Laskin, I., PROGRAM FOR HELICOPTER GEAR-BOX NOISE PREDICTION AND REDUCTION, Mechanical Technology, Incorporated; USAAMRDL TR70-12, Eustis Directorate, U.S. Army Air Mobility Research and Development Laboratory, Fort Eustis, Virginia, March 1970, AD869822.
16. Badgley, R. H., A PLAN TO DEVELOP TECHNOLOGY FOR THE REDUCTION OF INTERNAL NOISE AND HIGH-FREQUENCY VIBRATION IN HELICOPTER AIRCRAFT SYSTEMS, MTI Technical Report MTI-71TR61, Prepared for Eustis Directorate, U. S. Army Air Mobility Research and Development Laboratory, Fort Eustis, Virginia, October 1971.
17. Gu, A. L., and Badgley, R. H., PREDICTION OF GEAR-MESH-INDUCED HIGH-FREQUENCY VIBRATION SPECTRA IN GEARED POWER TRAINS, USAAMRDL TR74-5, Mechanical Technology Incorporated, U.S. Army Air Mobility Research and Development Laboratory, Fort Eustis, Virginia, January 1974, AD777496.
18. Gray, D. E., Coordinating Editor, AMERICAN INSTITUTE OF PHYSICS HANDBOOK, Second Edition, McGraw-Hill Book Company, Inc., New York, 1963.
19. Reed, D. L., POINT STRESS LAMINATE ANALYSIS, Document FZM-5494, Prepared for Advanced Composite Division, Air Force Materials Laboratory, WPAFB, Ohio, April 1970.

BIBLIOGRAPHY

AGMA Sound Manual, American Gear Manufacturers Association, Washington, D. C., Section I, 299.XX, November 1975.

Badgley, R., and Hartman, R., GEARBOX NOISE REDUCTION: PREDICTION AND MEASUREMENT OF MESH-FREQUENCY VIBRATIONS WITHIN AN OPERATING HELICOPTER ROTOR-DRIVE GEARBOX, Paper No. 73-DET-31, Design Engineering Technical Conference of the American Society of Mechanical Engineers, Cincinnati, Ohio, September 1973.

Badgley, R. H., and Chiang, T., INVESTIGATION OF GEARBOX DESIGN MODIFICATIONS FOR REDUCING HELICOPTER GEARBOX NOISE, Mechanical Technology, Incorporated, USAAMRDL TR 72-6, U. S. Army Air Mobility Research and Development Laboratory, Fort Eustis, Virginia, March 1972, AD742735.

Badgley, R., REDUCTION OF NOISE AND ACOUSTIC FREQUENCY VIBRATIONS IN AIRCRAFT TRANSMISSIONS, Preprint 661, 28th Annual Forum of the American Helicopter Society, Washington, D. C., May 1972.

Gu, A., and Badgley, R., PREDICTION OF VIBRATION SIDEBANDS IN GEAR MESHES, ASME Paper 74-DET-95, Presented at the Design Engineering Technical Conference, New York, October 5-9, 1974.

Gu, A., Badgley, R., and Chiang, T., PLANET-PASS-INDUCED VIBRATION IN PLANETARY REDUCTION GEARS, ASME Paper 74-DET-93, Presented at the Design Engineering Technical Conference, New York, October 5-9, 1974.

Hawkings, D., SOME THOUGHTS ON THE EXCITATION OF GEAR NOISE, Westland Helicopters Research Memorandum RM.330, January 1976.

Jones, A. B., A GENERAL THEORY FOR ELASTICALLY CONSTRAINED BALL AND RADIAL ROLLER BEARINGS UNDER ARBITRARY LOAD AND SPEED CONDITIONS, ASME Publication 59-LUB-10, American Society of Mechanical Engineers, New York, New York, October 1959.

Laskin, I., Orcutt, F. K., and Shipley, E. E., ANALYSIS OF NOISE GENERATED BY UH-1 HELICOPTER TRANSMISSION, USAAMRDL TR68-41, Eustis Directorate, U. S. Army Air Mobility Research and Development Laboratory, Fort Eustis, Virginia, June 1968, AD675457.

McCormick, C. W. (Editor), NASTRAN USER'S MANUAL LEVEL 15, June 1972.

C. P. Rubin, DYNAMIC OPTIMIZATION OF COMPLEX STRUCTURES, AIAA Dynamics and Aeroelasticity Specialists Conference, New Orleans, Louisiana, April 1969.

Schaeffer, E., and Shadburn, E., TEST RESULTS REPORT - HLH/ATC EVALUATION OF NOISE ATTENUATION MATERIALS, Boeing Document T301-10176-1, Boeing Vertol Company, Philadelphia, Pennsylvania, December 1972.

Schlegel and Mard, TRANSMISSION NOISE CONTROL - APPROACHES IN HELICOPTER DESIGN, ASME 67-DE-58.

Sciarra, J., A COMPUTER METHOD FOR DYNAMIC STRUCTURAL ANALYSIS USING STIFFNESS MATRIXES, Journal of Aircraft, Volume 6, No. 1, January - February 1969, Pages 3-8.

Sciarra, J., APPLICATION OF COMBINED DIRECT STIFFNESS AND MOBILITY METHOD TO VIBRATION ABSORBER STUDIES, ASME/MDD Vibrations Conference, Paper 67-VIBR-65, March 1967.

Sciarra, J., APPLICATION OF IMPEDANCE METHODS TO HELICOPTER VIBRATION REDUCTION, Presented at the Imperial College of Science and Technology, London, England, July 3, 1973.

Thomson, W. T., MECHANICAL VIBRATIONS, Prentice-Hall Inc., Englewood Cliffs, New Jersey, Second Edition, 1960.

Timoshenko, S., VIBRATION PROBLEMS IN ENGINEERING, D. Van Nostrand Company, New York, Second Edition, Pages 428-441.

APPENDIX A TEST DATA

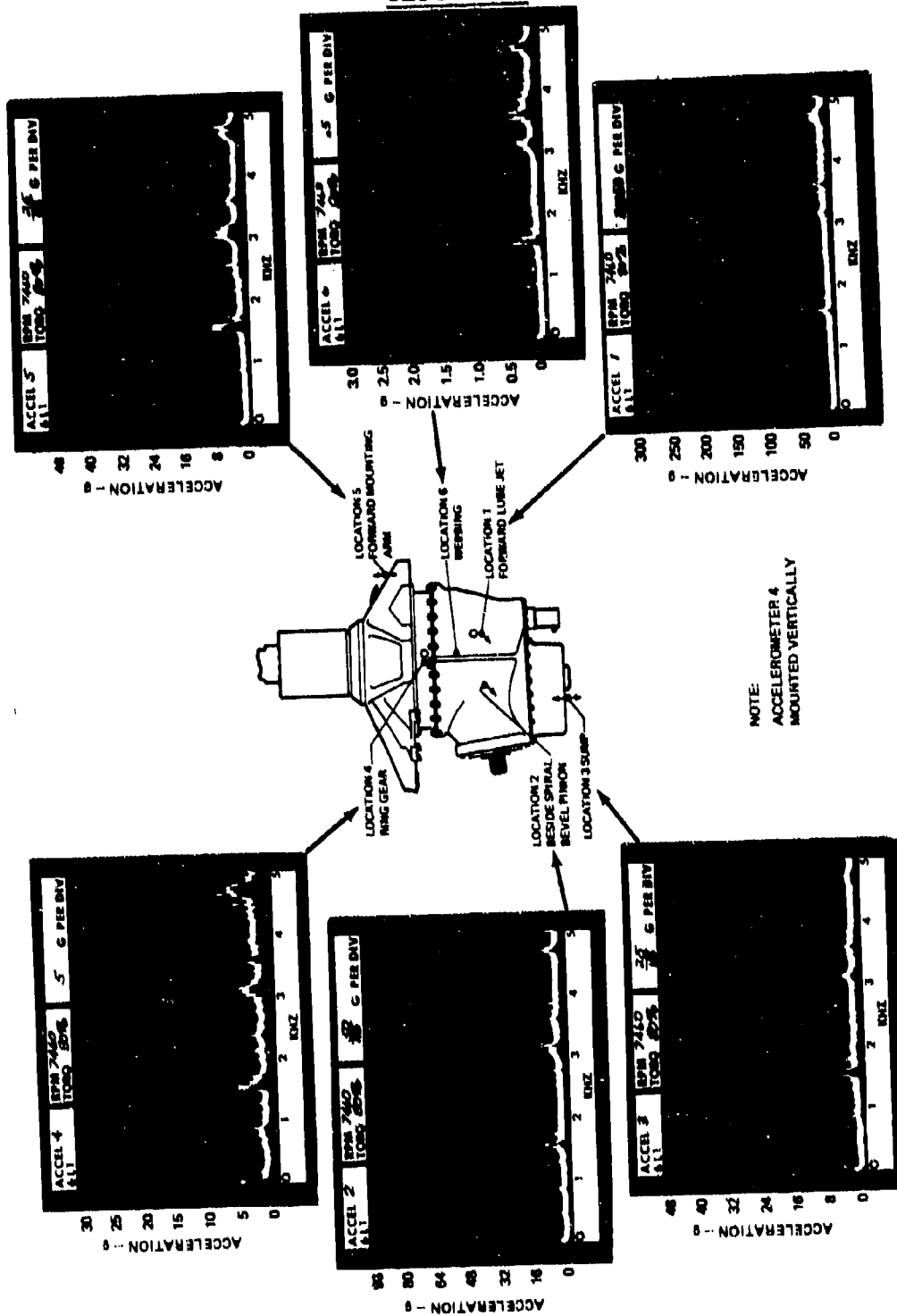


Figure A1. Accelerometer Data From Tape 6L1 With Baseline CH-47C Forward Transmission at 7,460 RPM and 80-Percent Torque.

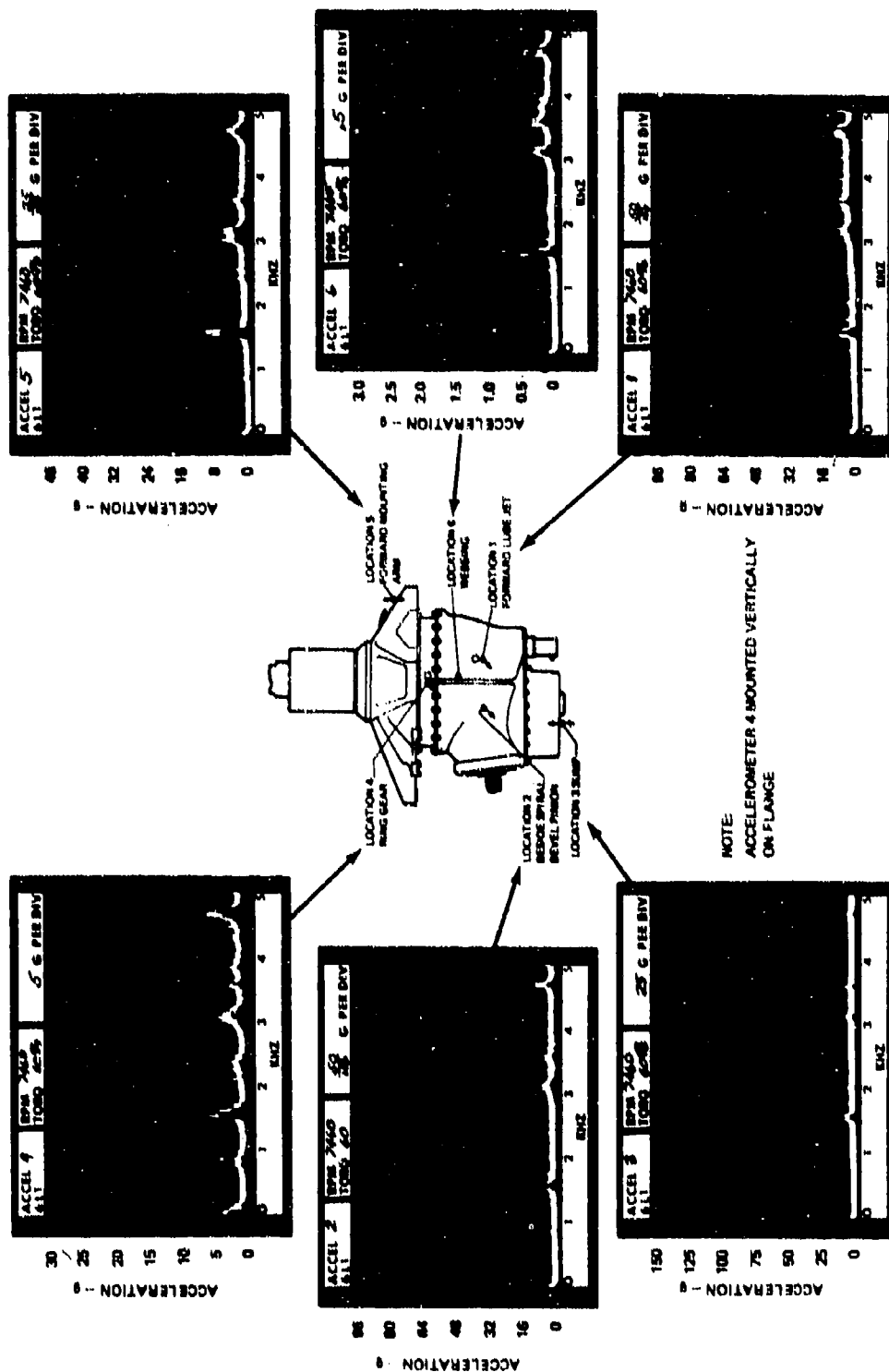


Figure A2. Accelerometer Data From Tape 6L1 With Baseline CH-47C Forward Transmission at 7,460 RPM and 60-Percent Torque.

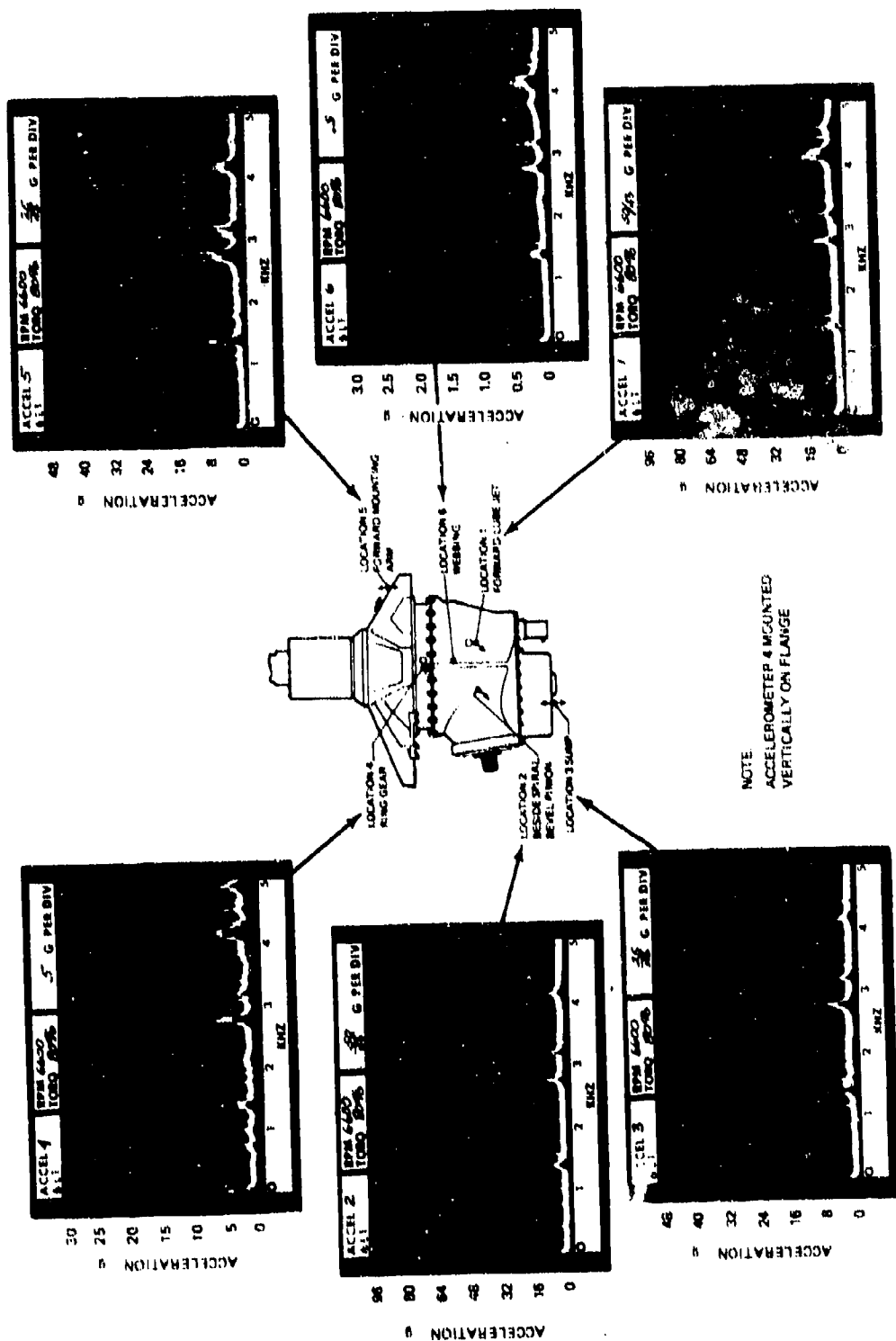


Figure A3. Accelerometer Data From Tape 6L1 With Baseline CH-47C Forward Transmission at 6,600 RPM and 80 Percent Torque.

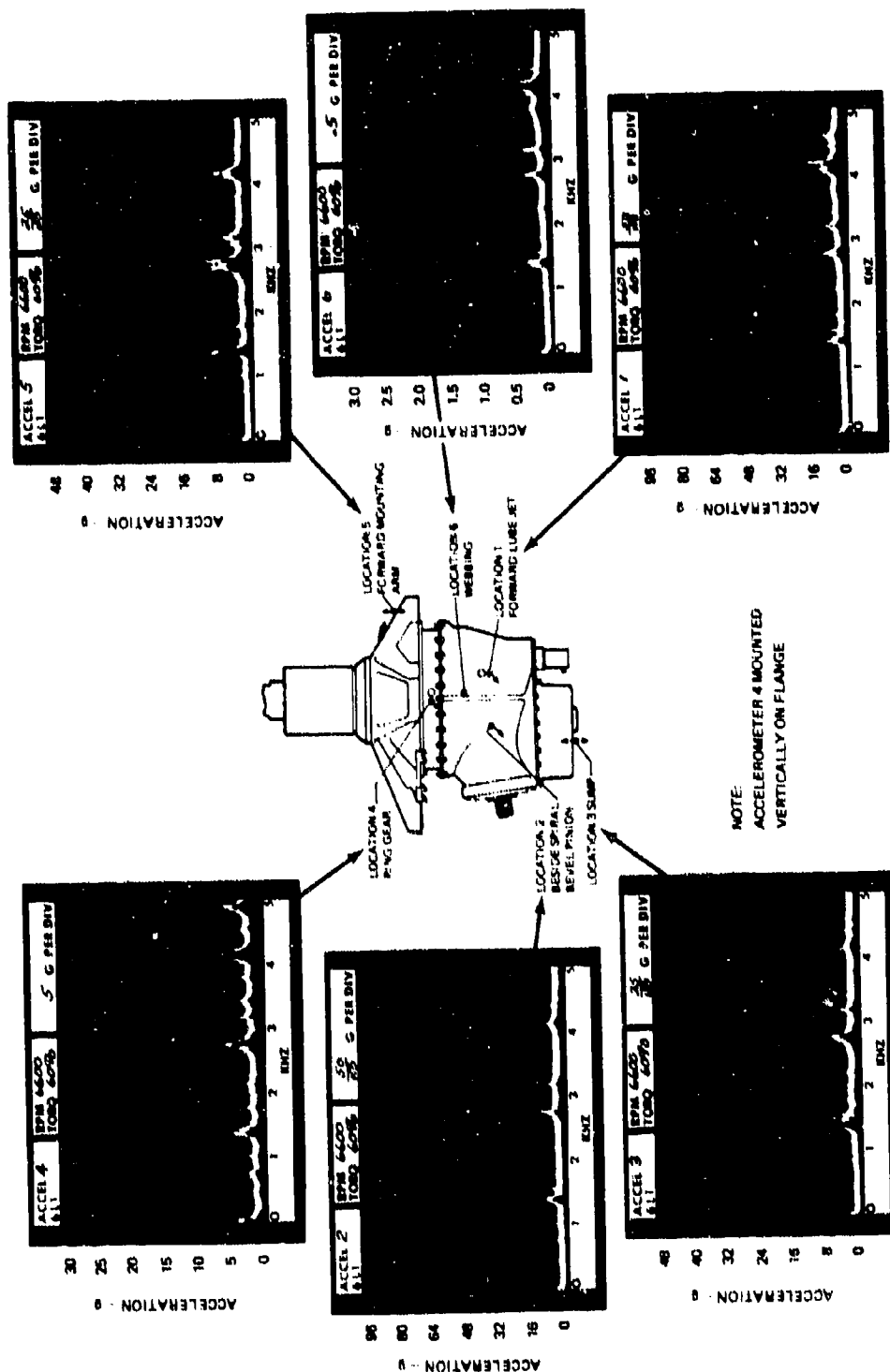


Figure A4. Accelerometer Data From Tape 6L1 With Baseline CH-47C Forward Transmission at 6,600 RPM and 60-Percent Torque.

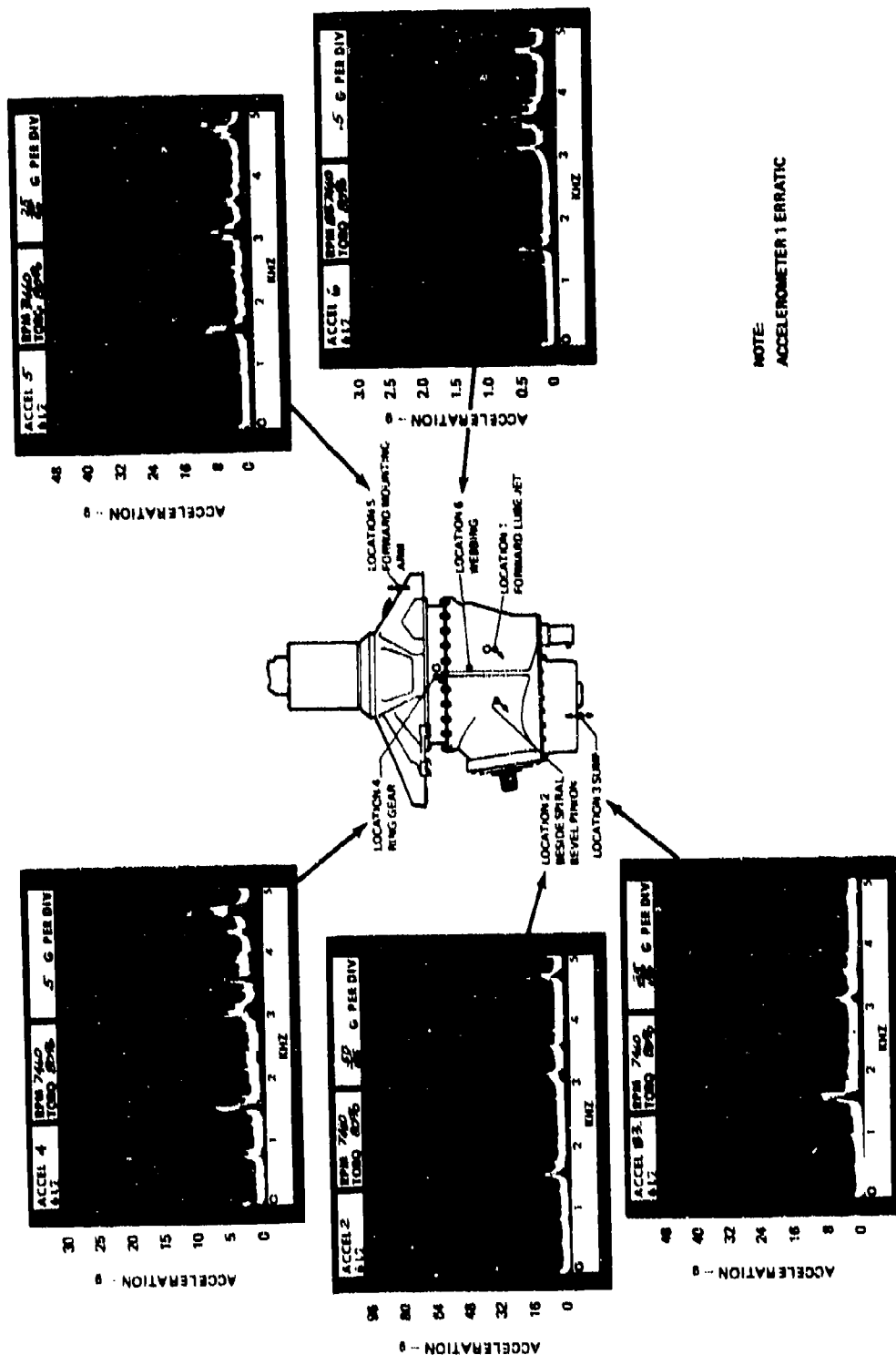


Figure A5. Accelerometer Data From Tape 6L2 With Baseline CH-47C Forward Transmission and Isolators at 7,460 RPM and 80-Percent Torque.

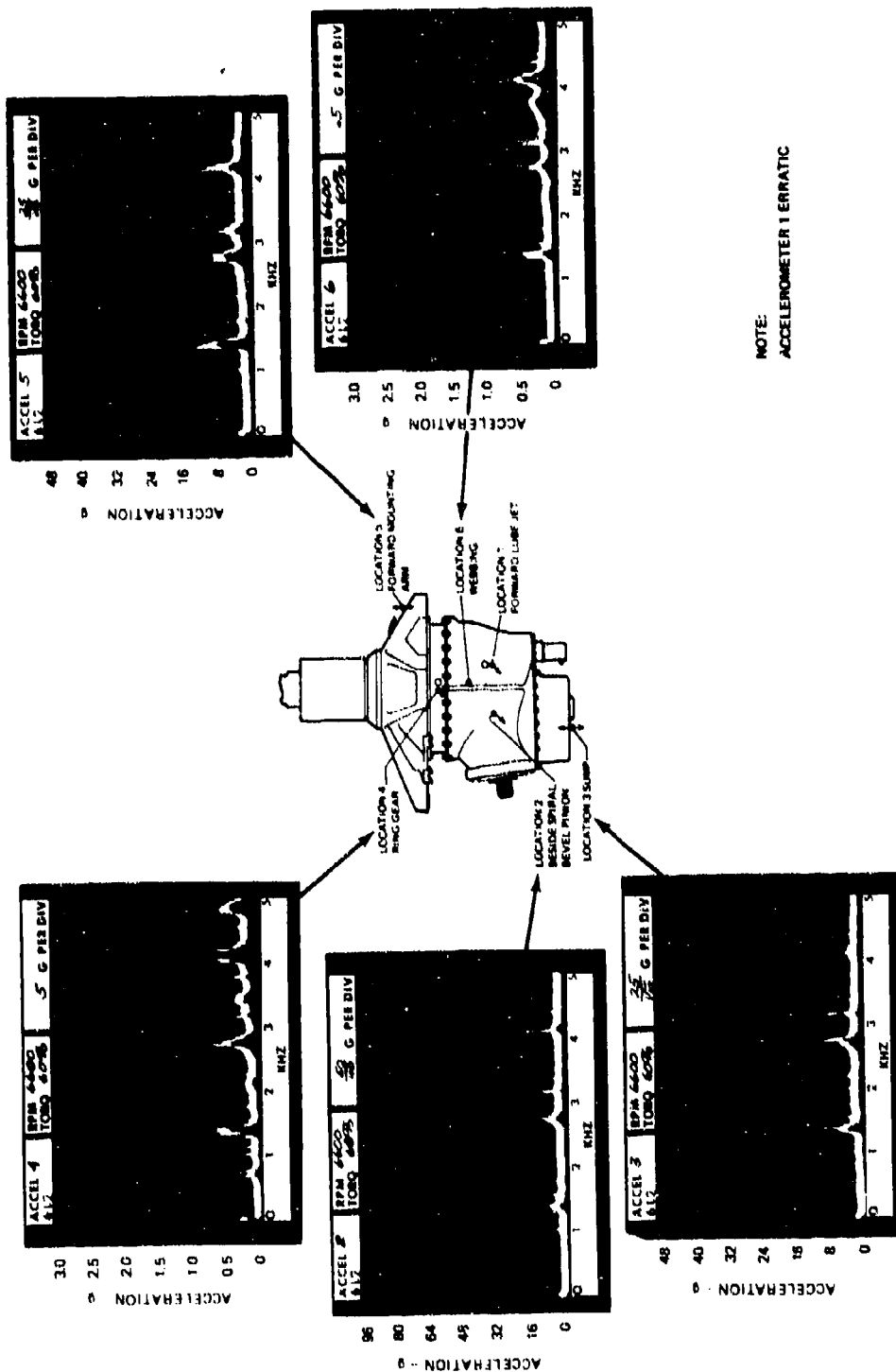


Figure A8. Accelerometer Data from Tape 6L2 With Baseline CH-47C Forward Transmission and Isolators at 6,600 RPM and 60-Percent Torque.

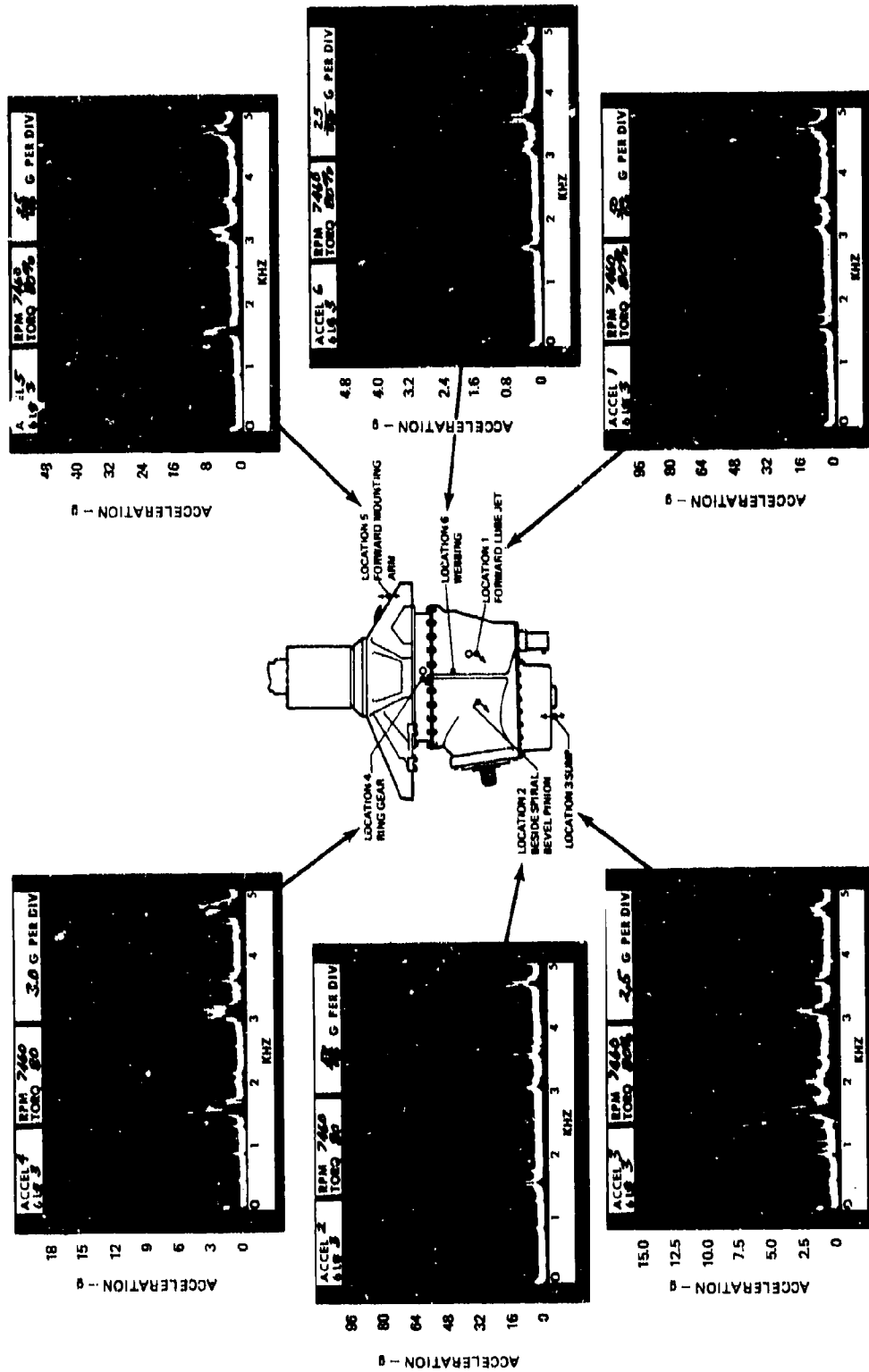


Figure A9. Accelerometer Data From Tape 6L3 With Detuned Sun Gear and No Isolators at 7,460 RPM and 80-Percent Torque.

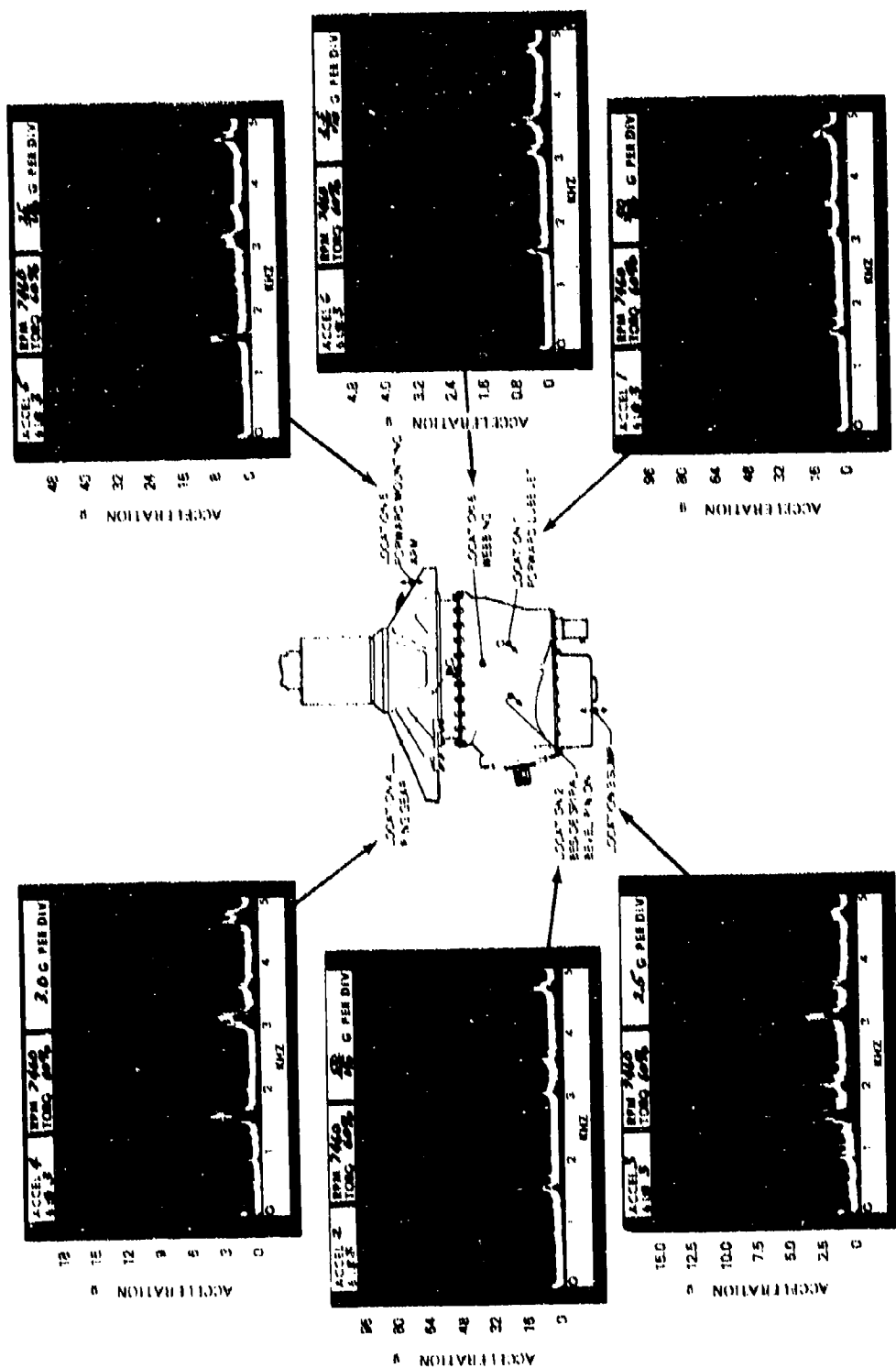


Figure A10. Accelerometer Data From Tape 6L3 With Detuned Sun Gear and No Isolators at 7,460 RPM and 60-Percent Torque.

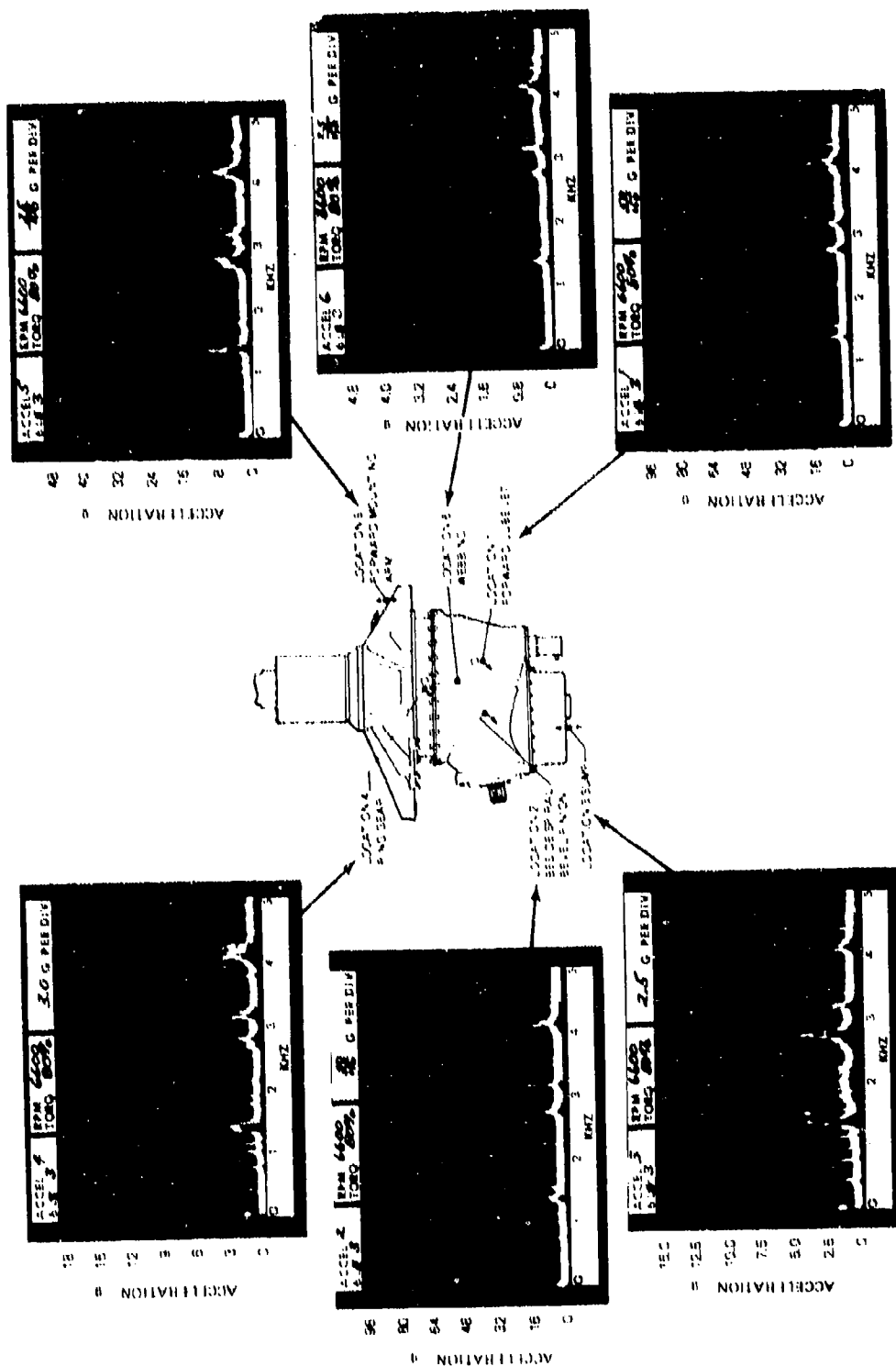


Figure A11. Accelerometer Data From Tape 6L3 With Detuned Sun Gear and No Isolators
at 6,600 RPM and 80-Percent Torque.

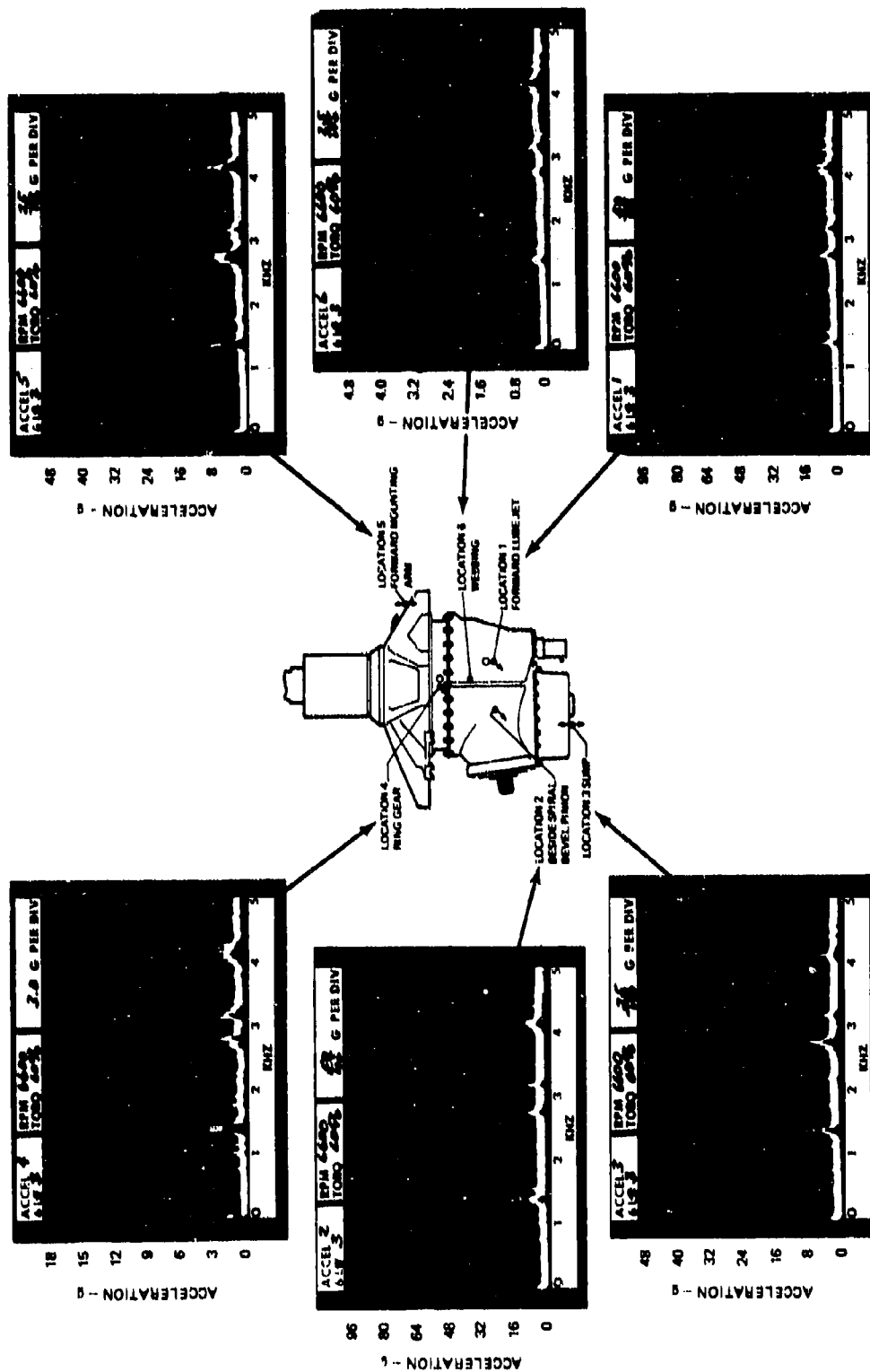


Figure A12. Accelerometer Data From Tape 6L3 With Detuned Sun Gear and No Isolators at 6,600 RPM and 60-Percent Torque.

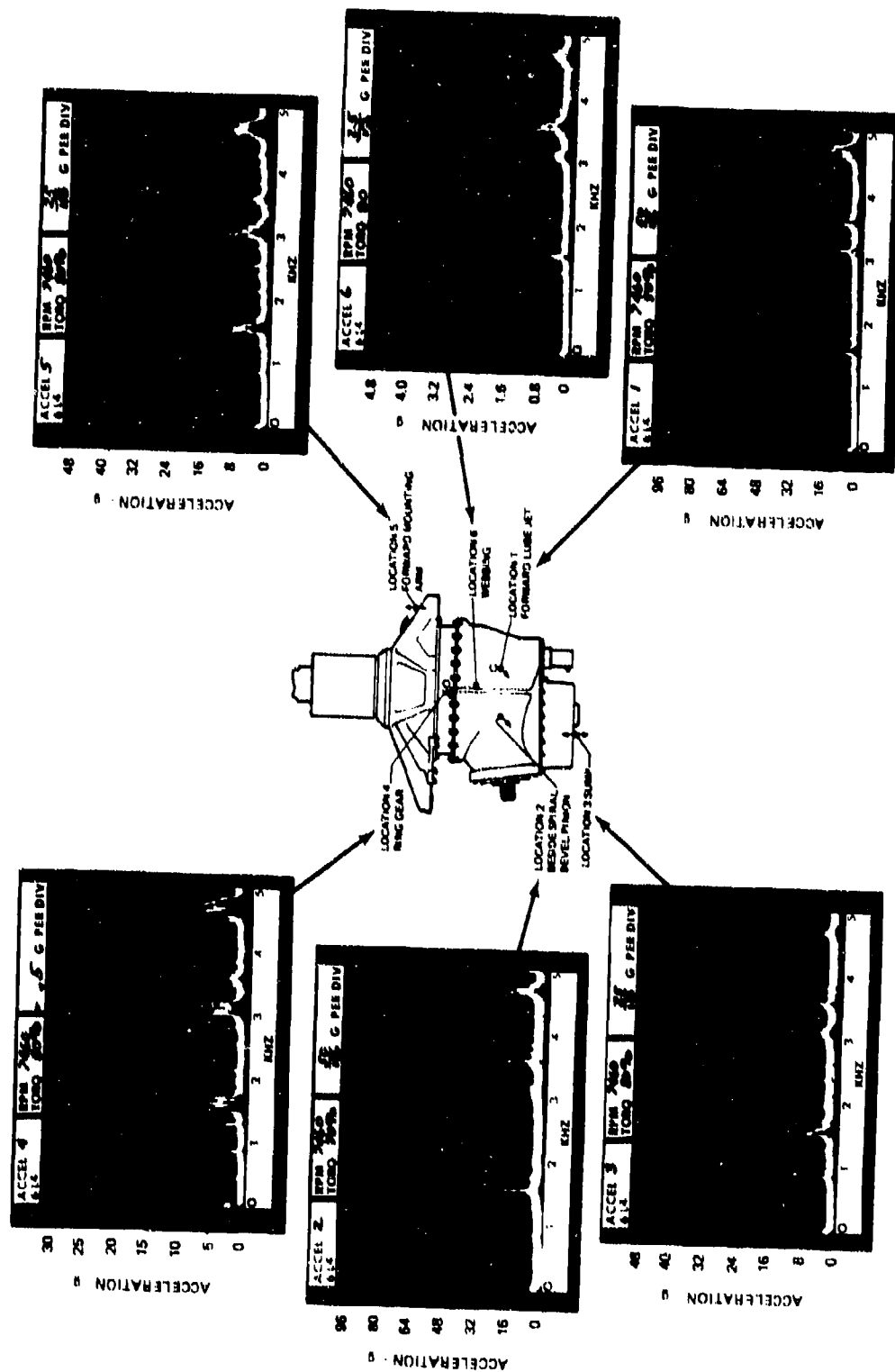


Figure A13. Accelerometer Data From Tape 6L4 With Detuned Sun Gear and Isolators at 7,460 RPM and 80-Percent Torque.

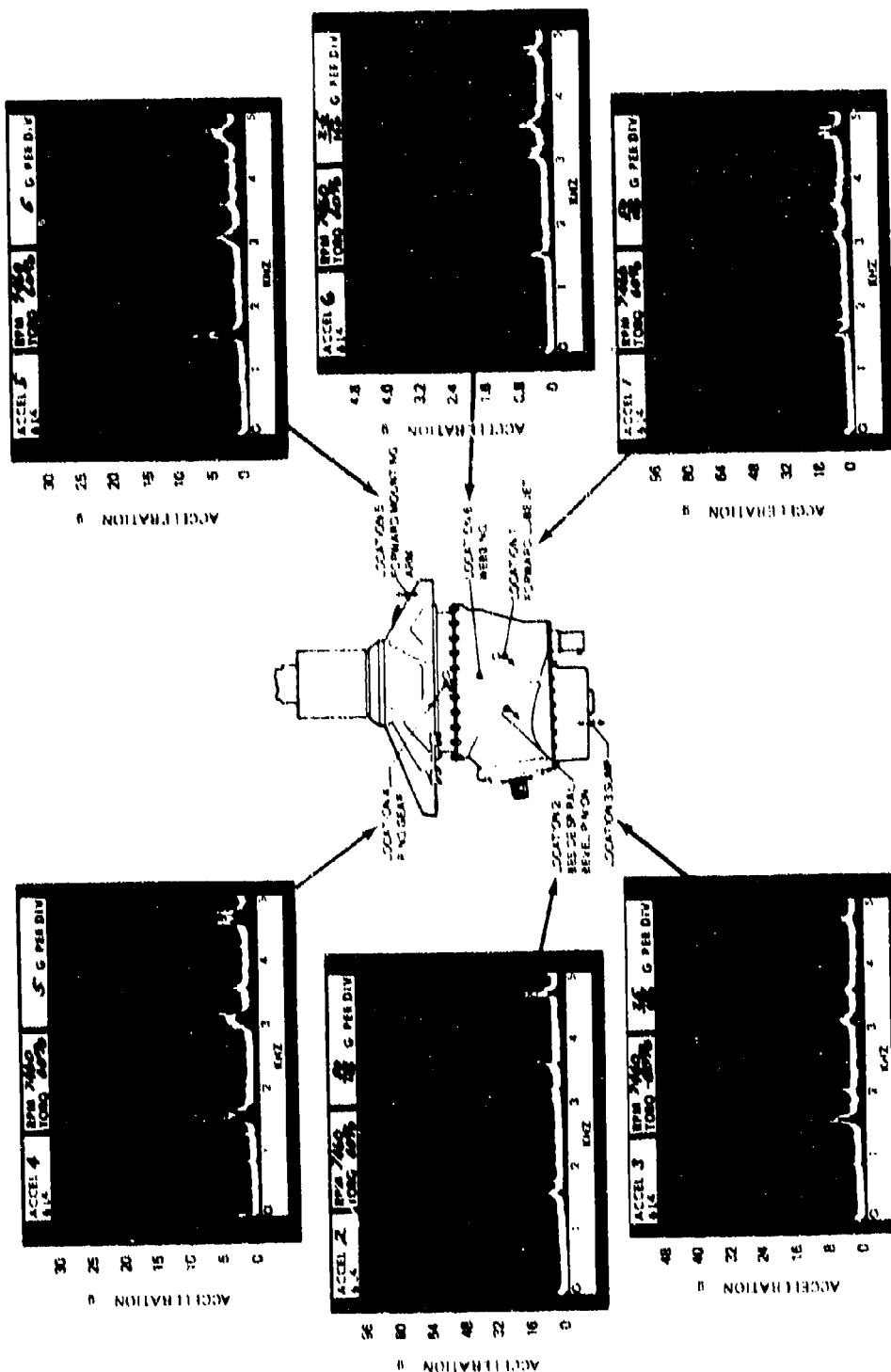


Figure A14. Accelerometer Data From Tape 6L4 With Detuned Sun Gear and Isolators at 7,460 RPM and 60-Percent Torque.

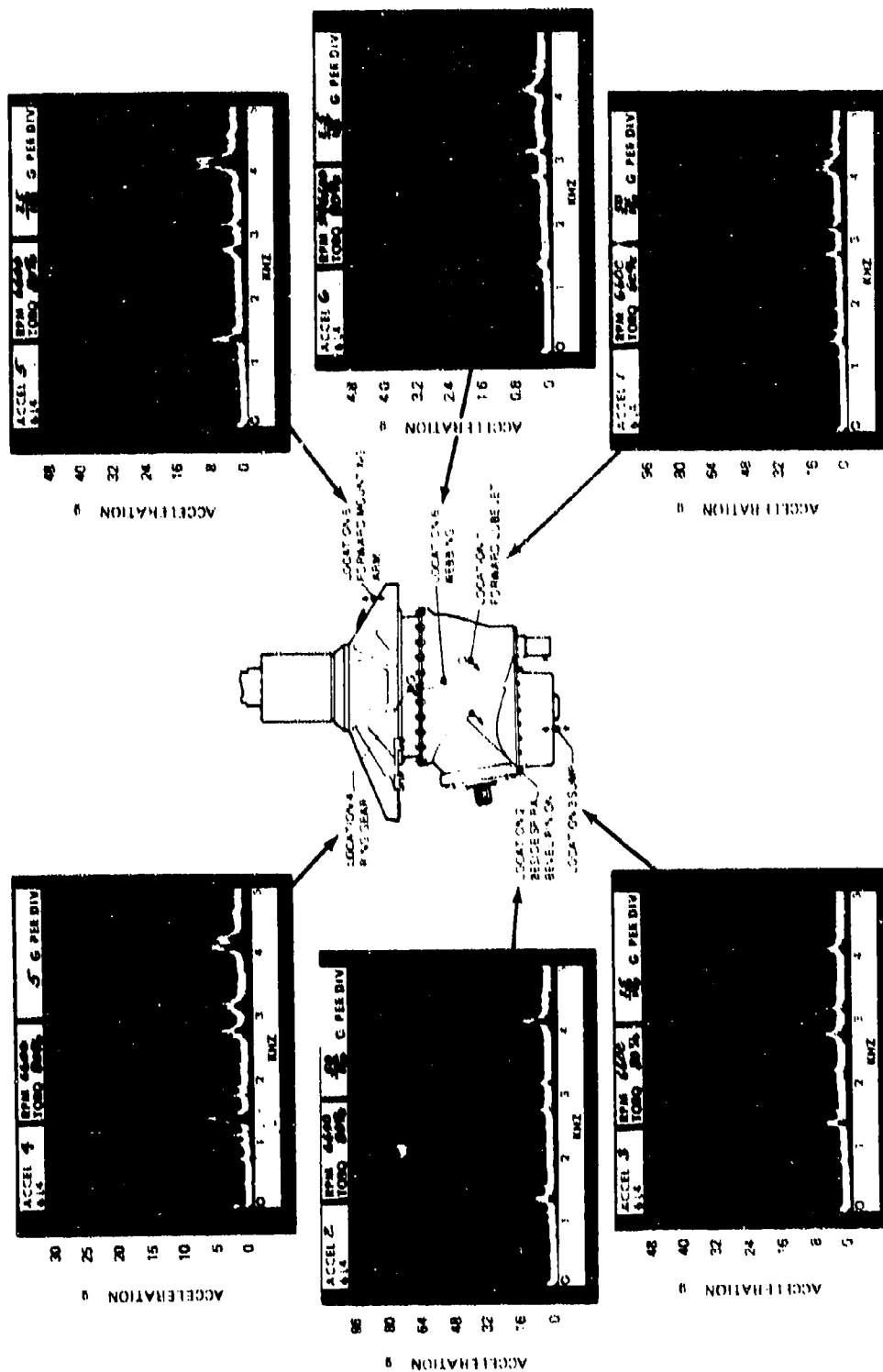


Figure A15. Accelerometer Data From Tape 6L4 With Detuned Sun Gear and Isolators at 6,600 RPM and 80-Percent Torque.

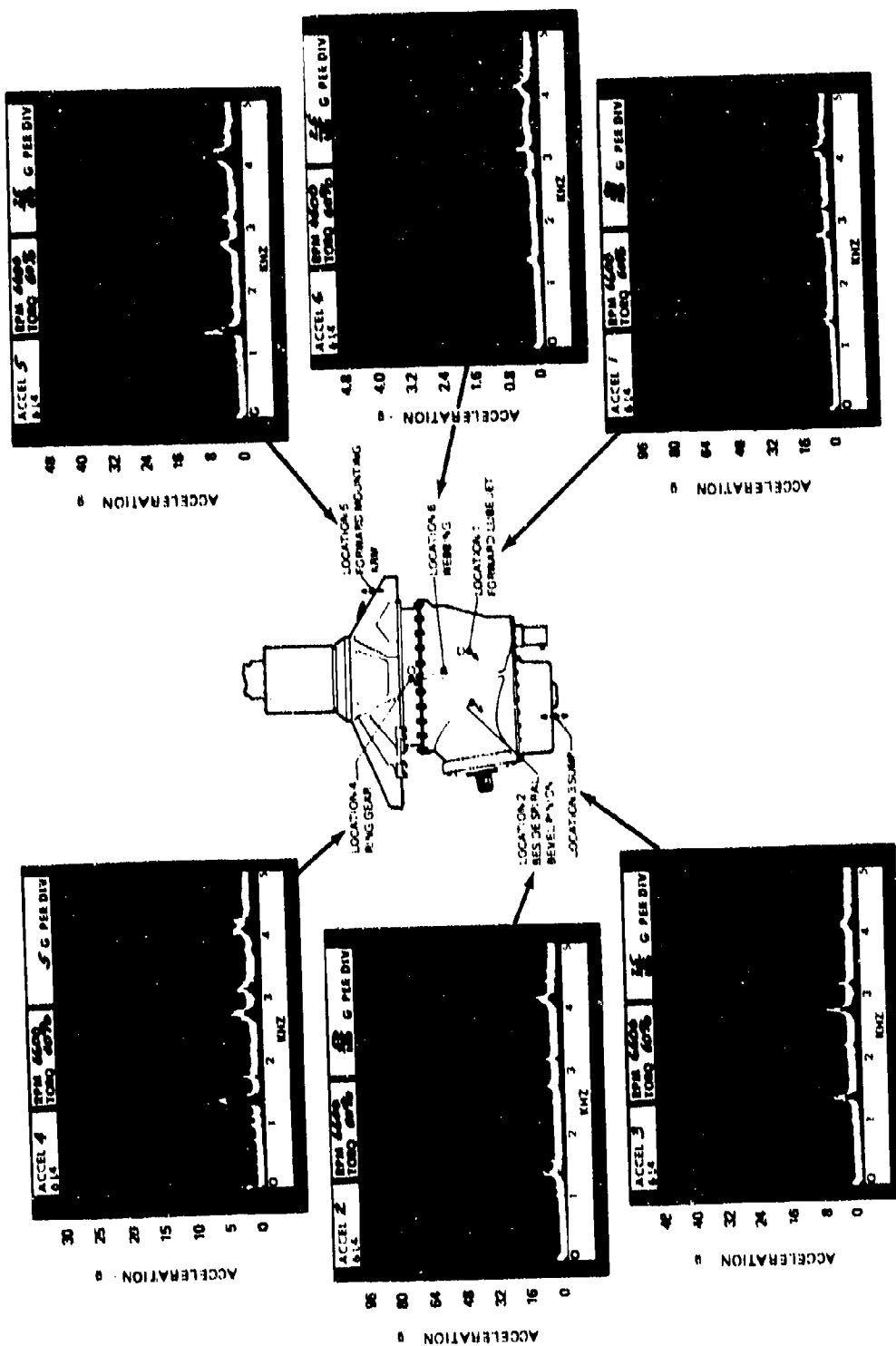


Figure A16. Accelerometer Data From Tape 6L4 With Detuned Sun Gear and Isolators at 6,600 RPM and 60-Percent Torque.

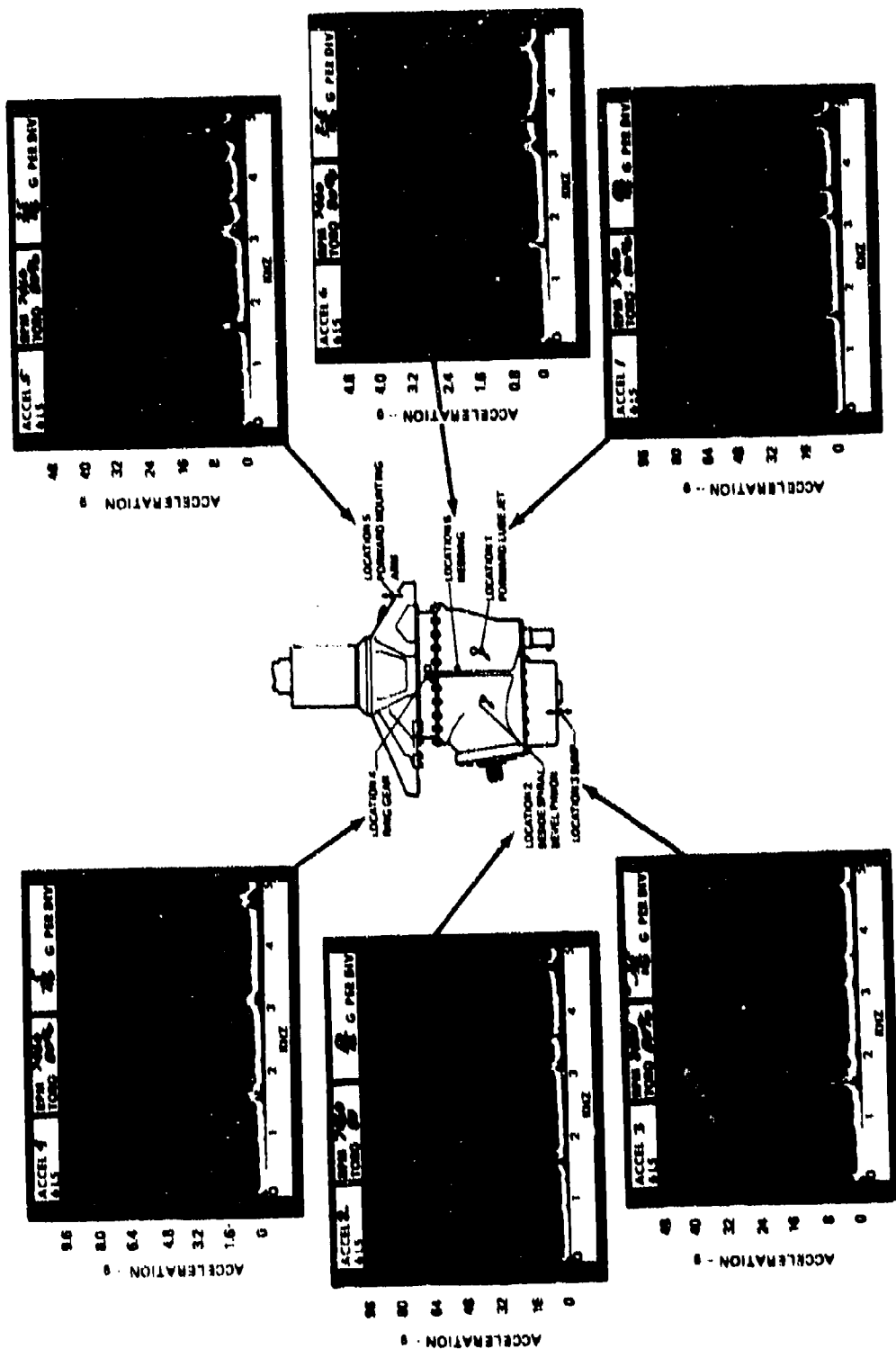


Figure A17. Accelerometer Data From Tape 6L5 With Detuning Magnesium Contour Plates, Detuned Sun Gear, and No Isolators at 7,460 RPM and 80-Percent Torque.

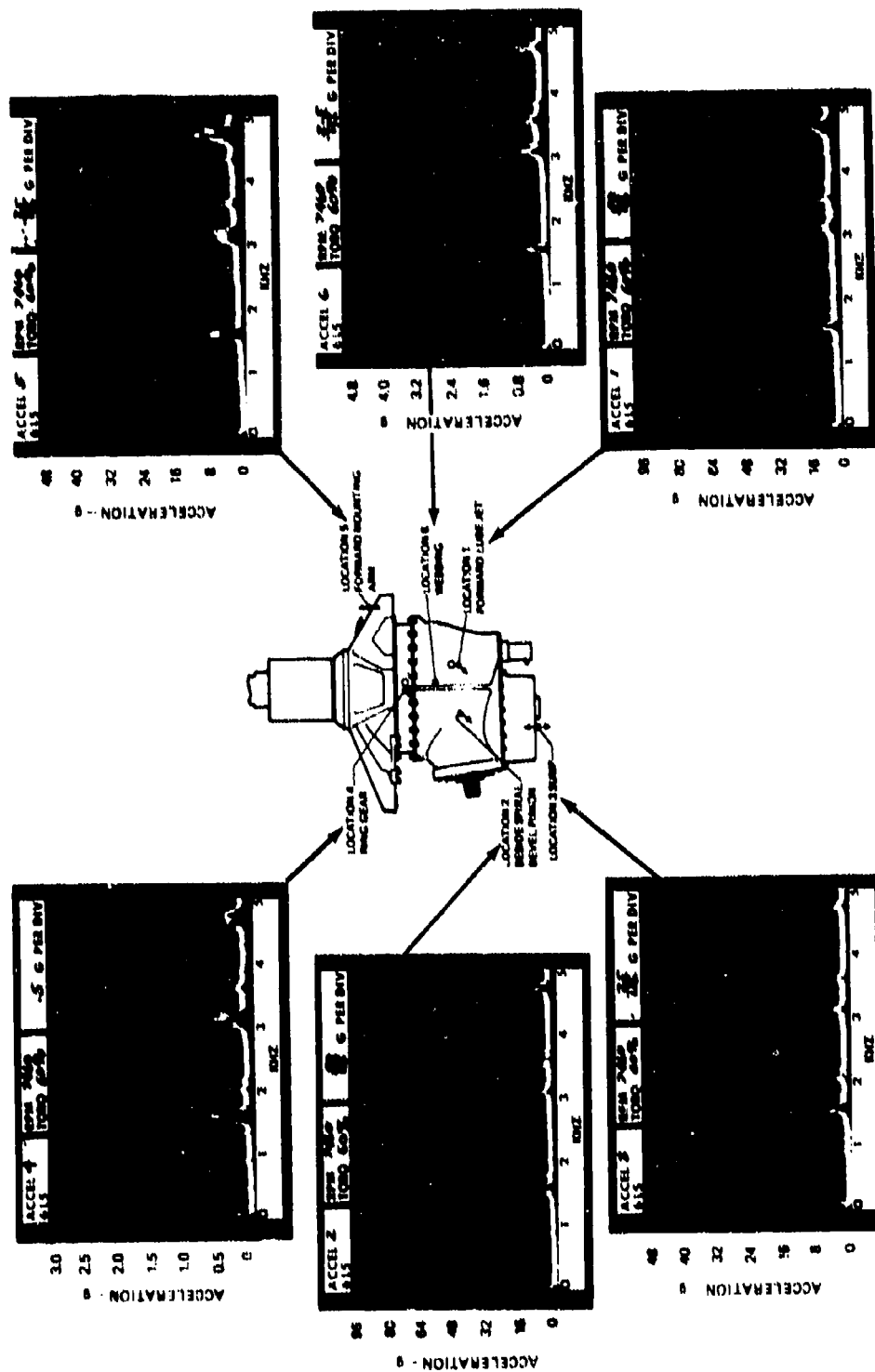


Figure A18. Accelerometer Data From Tape 6L5 With Detuning Magnesium Contour Plates, Detuned Sum Gear, and No Isolators at 7,460 RPM and 60-Percent Torque.

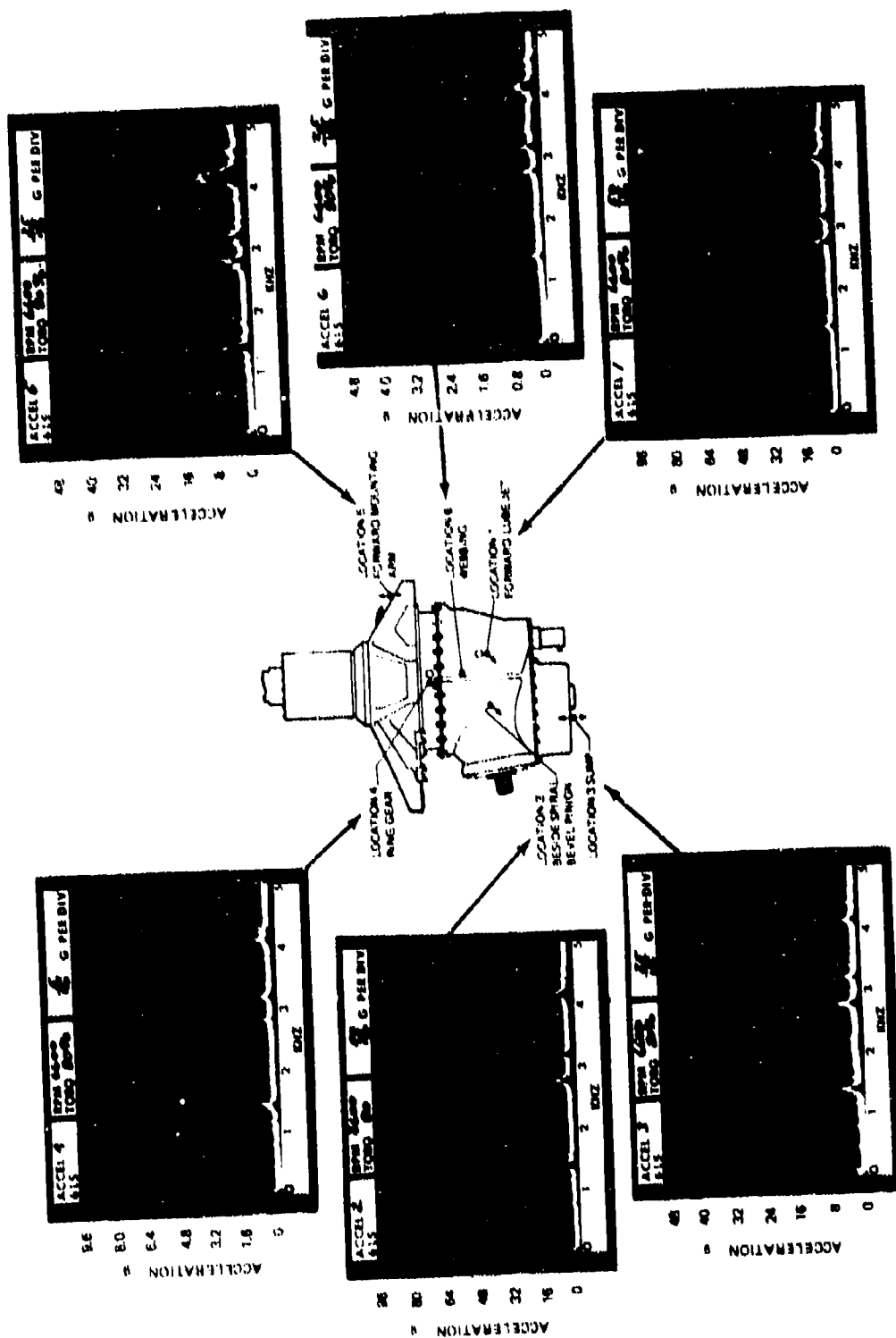


Figure A19. Accelerometer Data From Tape 6L5 With Detuning Magnesium Contour Plates, Detuned Sun Gear, and No Isolators at 6,600 RPM and 80-Percent Torque.

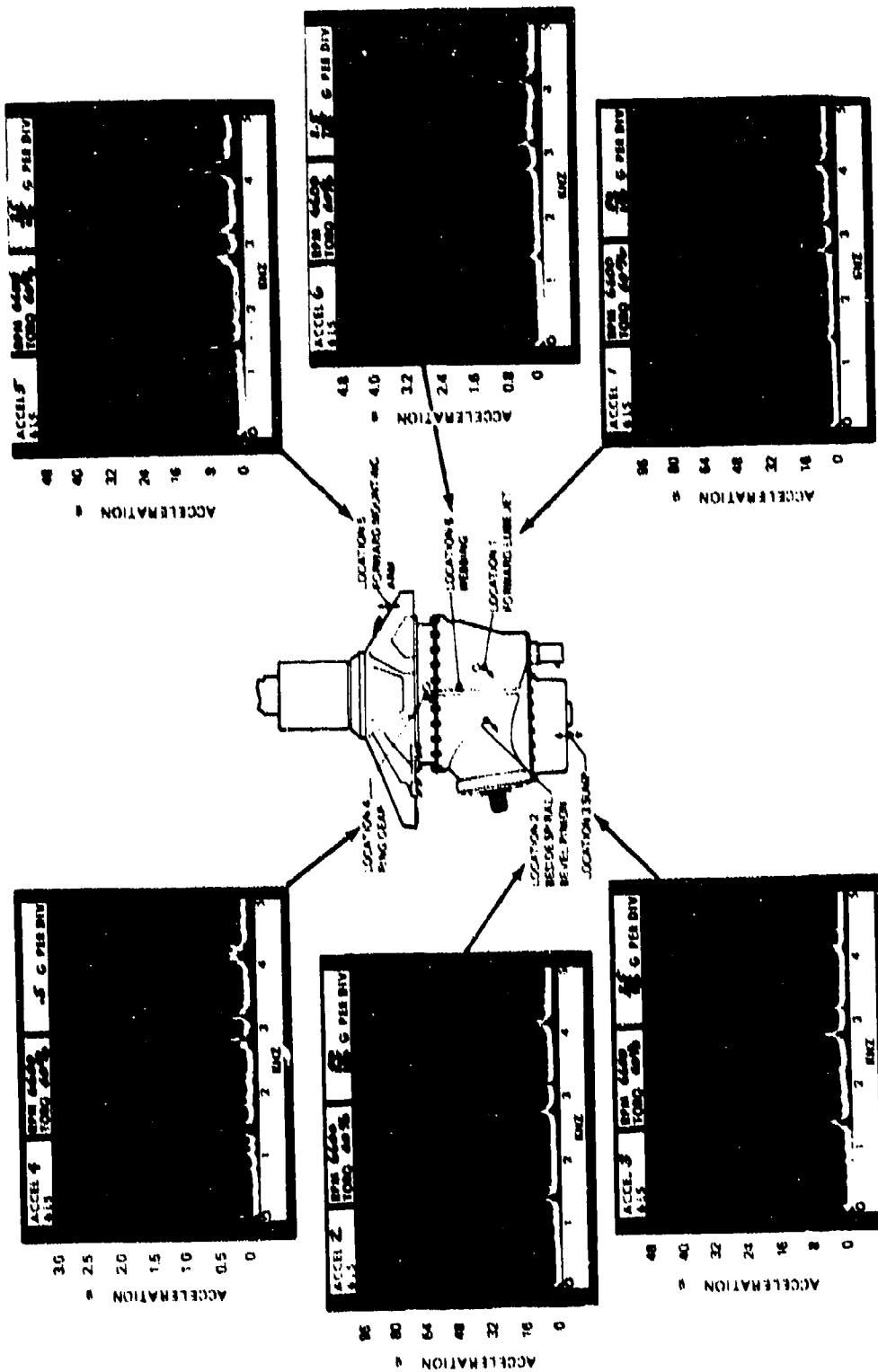


Figure A20. Accelerometer Data From Tape 6L5 With Detuning Magnesium Contour Plates, Detuned Sun Gear, and No Isolators at 6,600 RPM and 60-Percent Torque.

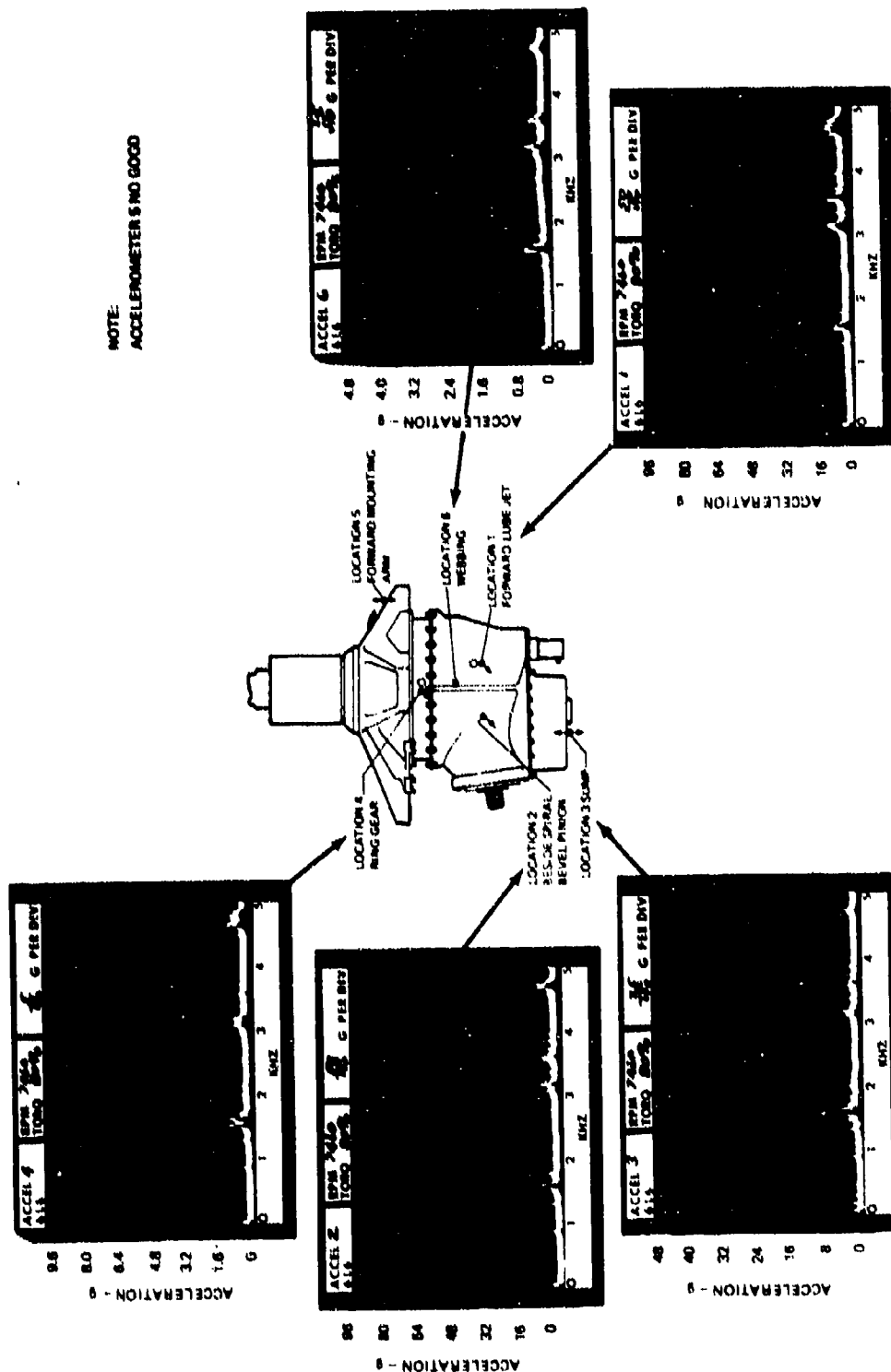


Figure A21. Accelerometer Data From Tape 6L6 With Detuning Magnesium Contour Plates, Original Sun Gear, and No Isolators at 7,460 RPM and 80 Percent Torque.

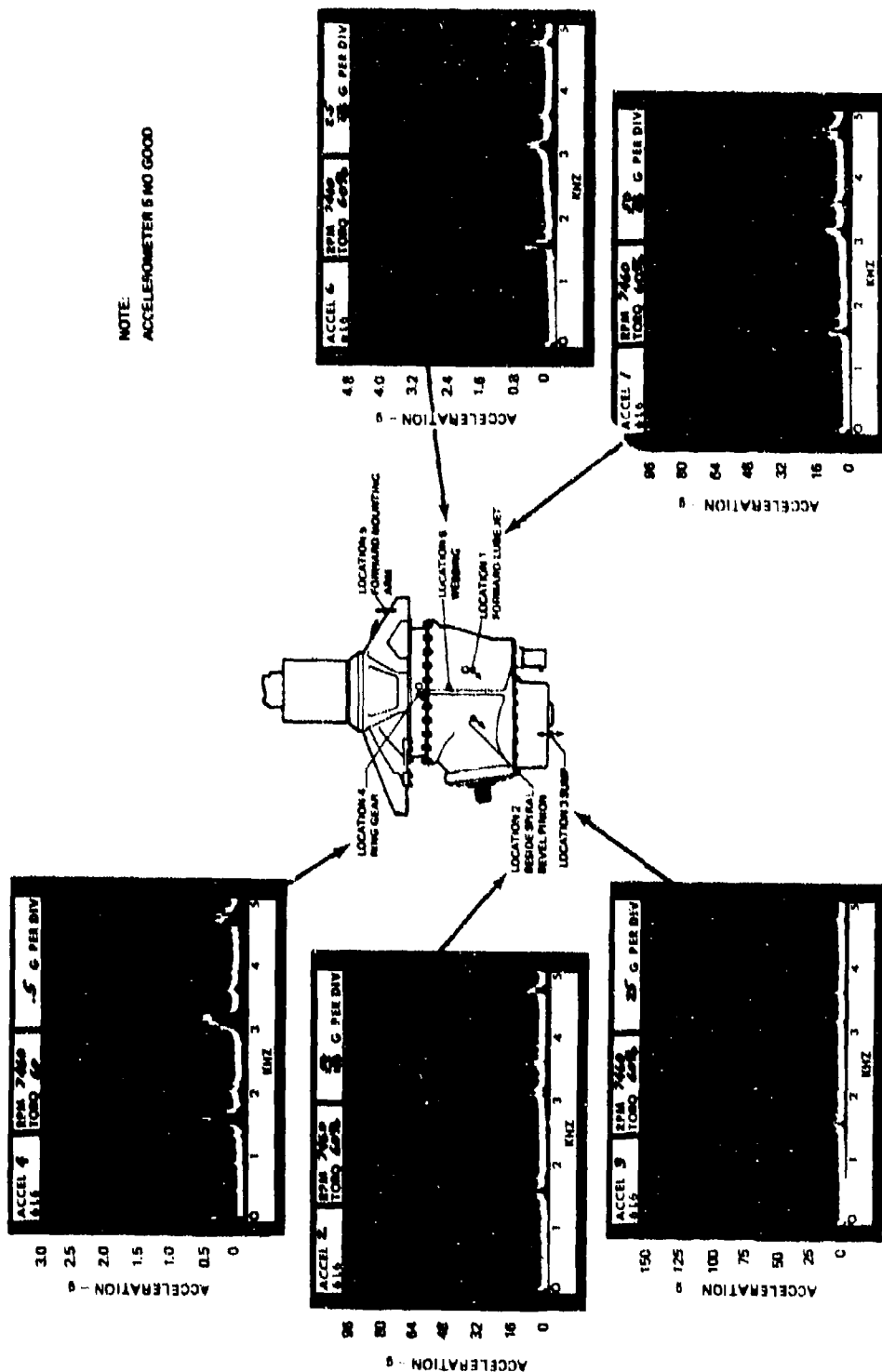


Figure A22. Accelerometer Data From Tape 6L6 With Detuning Magnesium Contour Plates, Original Sun Gear, and No Isolators at 7,450 RPM and 60-Percent Torque.

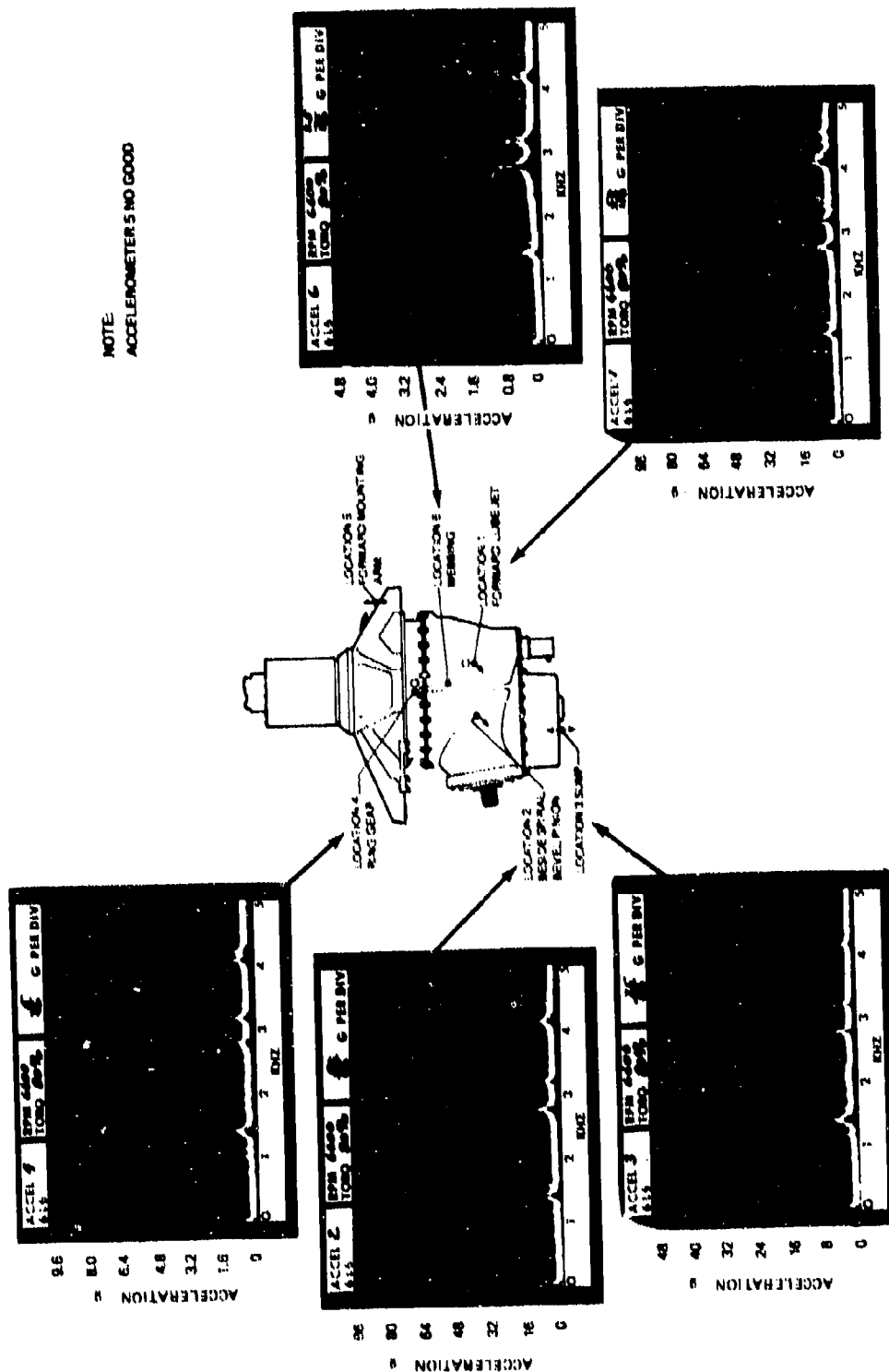


Figure A23. Accelerometer Data From Tape 6L6 With Detuning Magnesium Contour Plates,
Original Sun Gear, and No Isolators at 6,600 RPM and 80 Percent Torque.

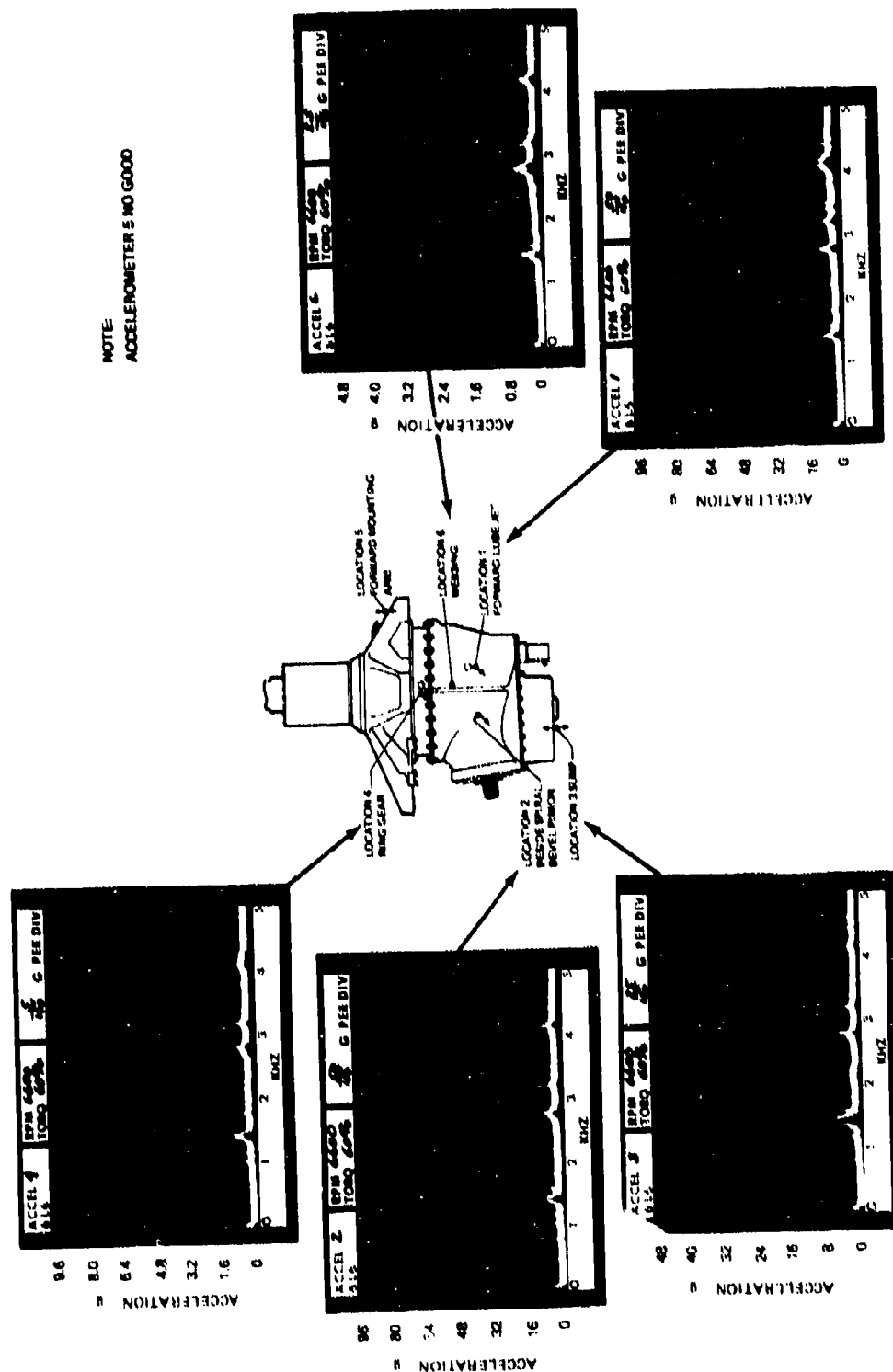


Figure A24. Accelerometer Data From Tape 616 With Detuning Magnesium Contour Plates, Original Sun Gear, and No Isolators at 6,600 RPM and 60-Percent Torque.

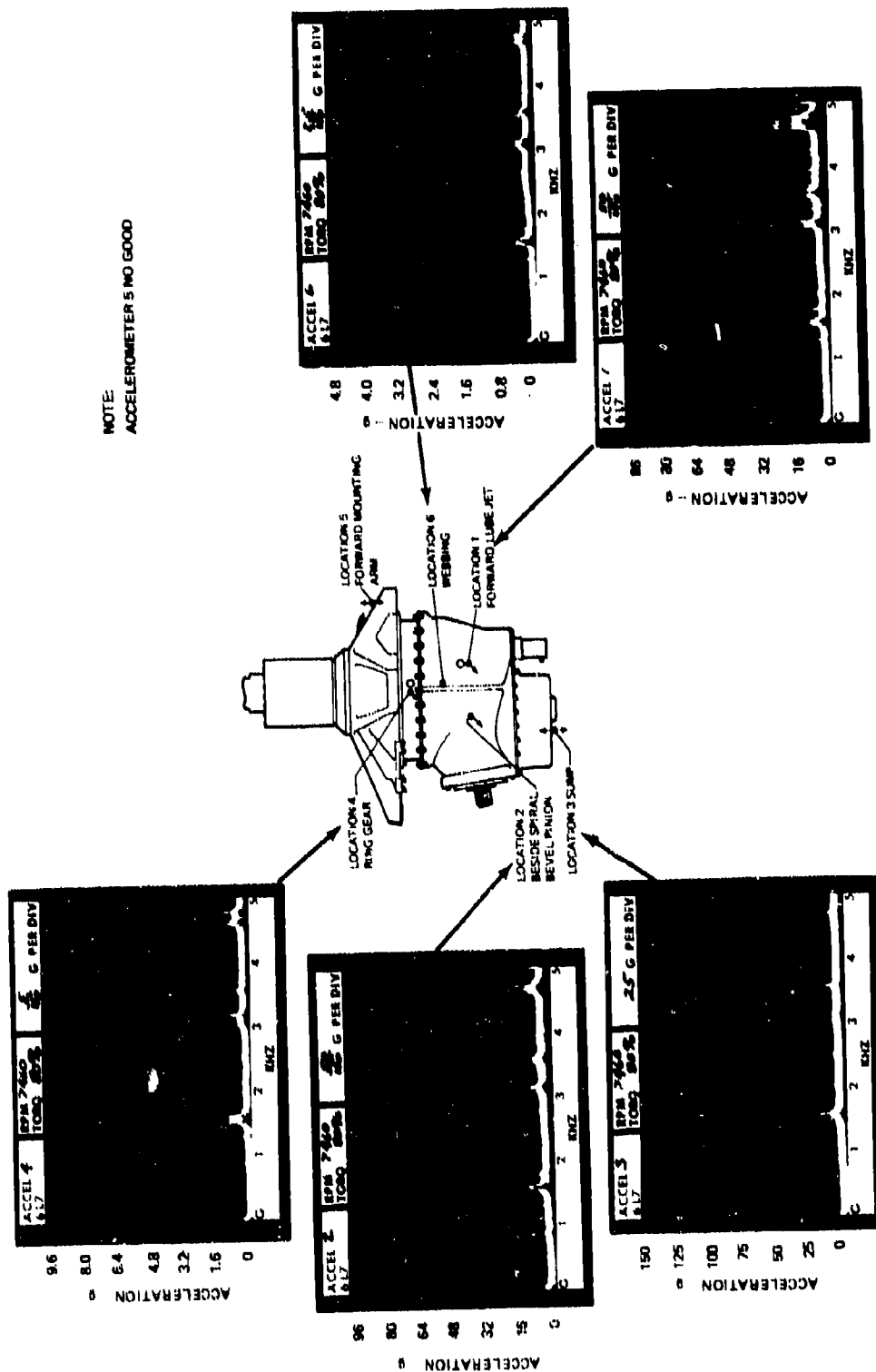


Figure A25. Accelerometer Data From Tape 6L7 With Detuning Magnesium Contour Plates, Original Sun Gear, Thickened Ring Gear, and No Isolators at 7,460 RPM and 80 Percent Torque.

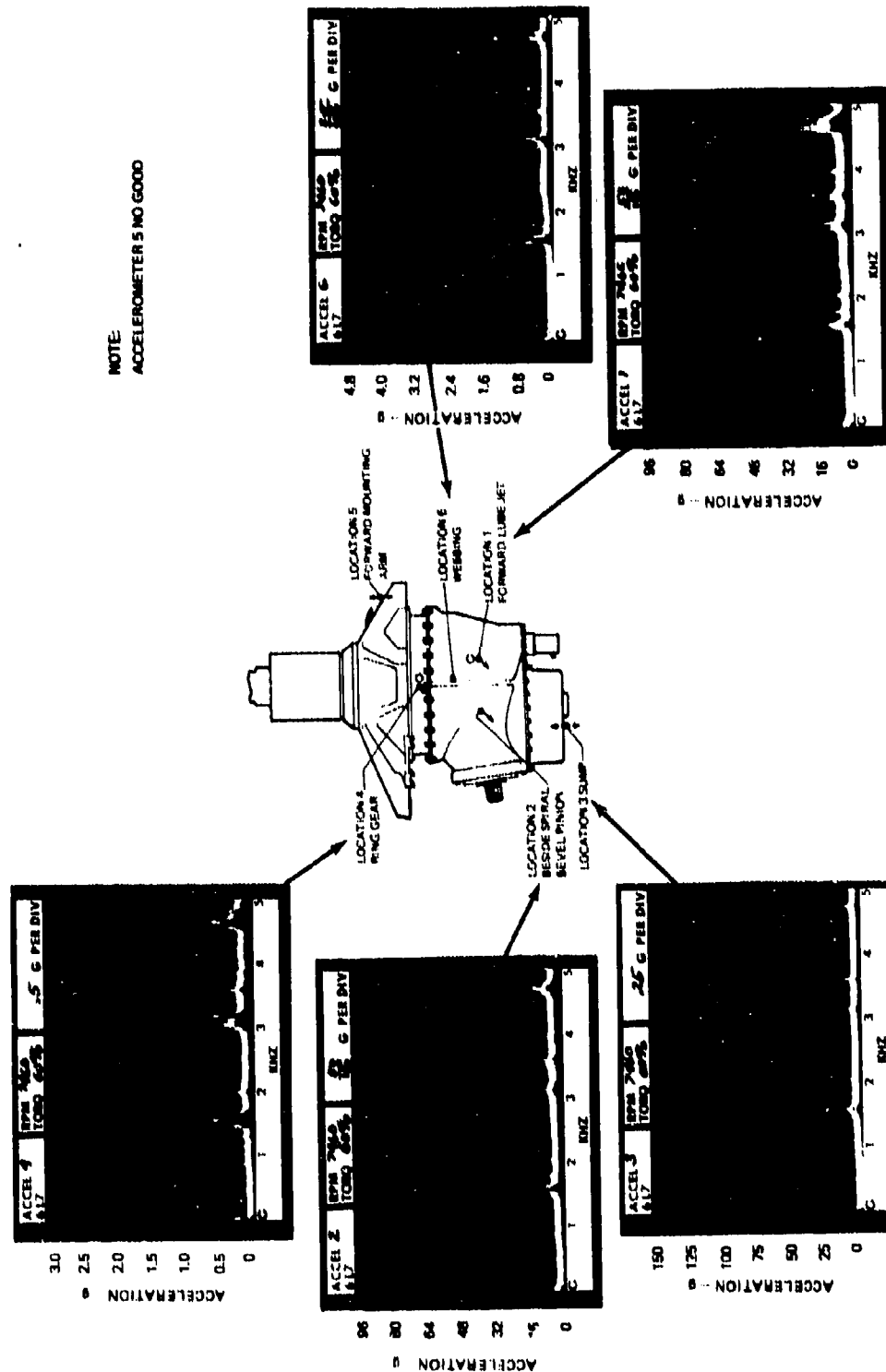


Figure A26. Accelerometer Data From Tape 6L7 With Detuning Magnesium Contour Plates, Original Sun Gear, Thickened Ring Gear, and No Isolators at 7,460 RPM and 60-Percent Torque.

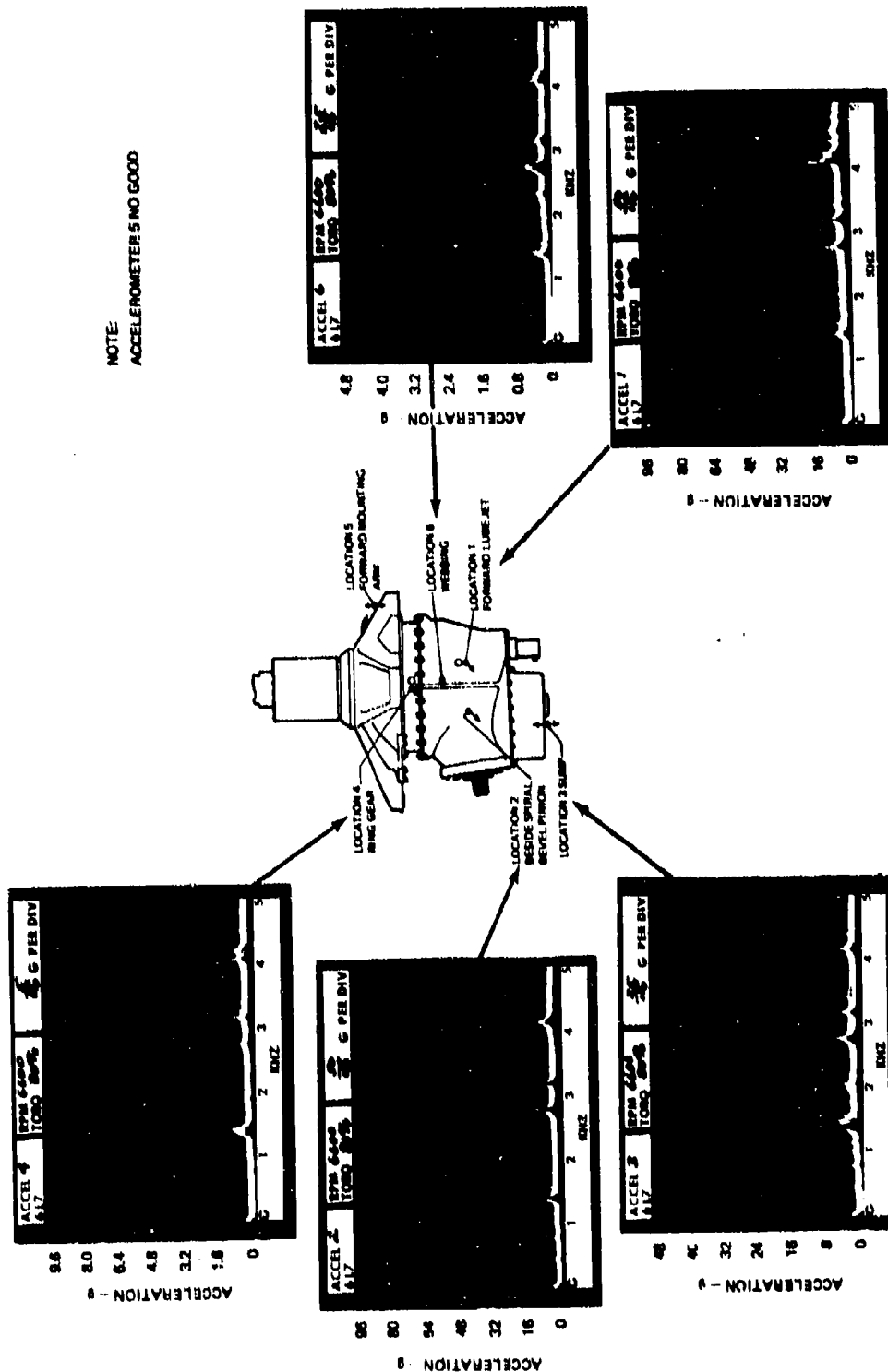


Figure A27. Accelerometer Data From Tape 6L7 With Detuning Magnesium Contour Plates, Original Sum Gear, Thickened Ring Gear, and No Isolators at 6,600 RPM and 80-Percent Torque.

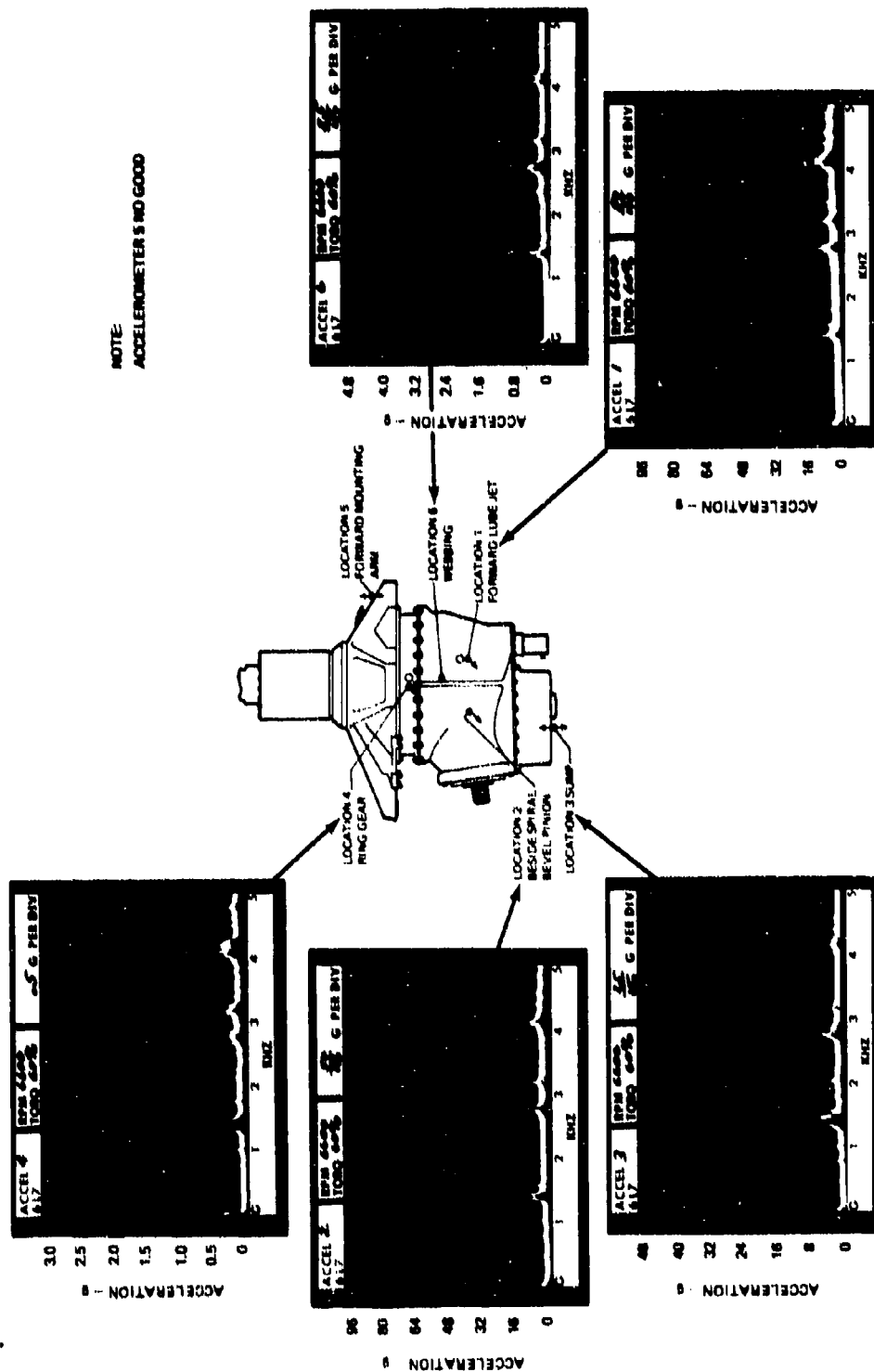


Figure A28. Accelerometer Data From Tape 6L7 With Detuning Magnesium Contour Plates, Original Sun Gear, Thickened Ring Gear, and No Isolators at 6,600 RPM and 60-Percent Torque.

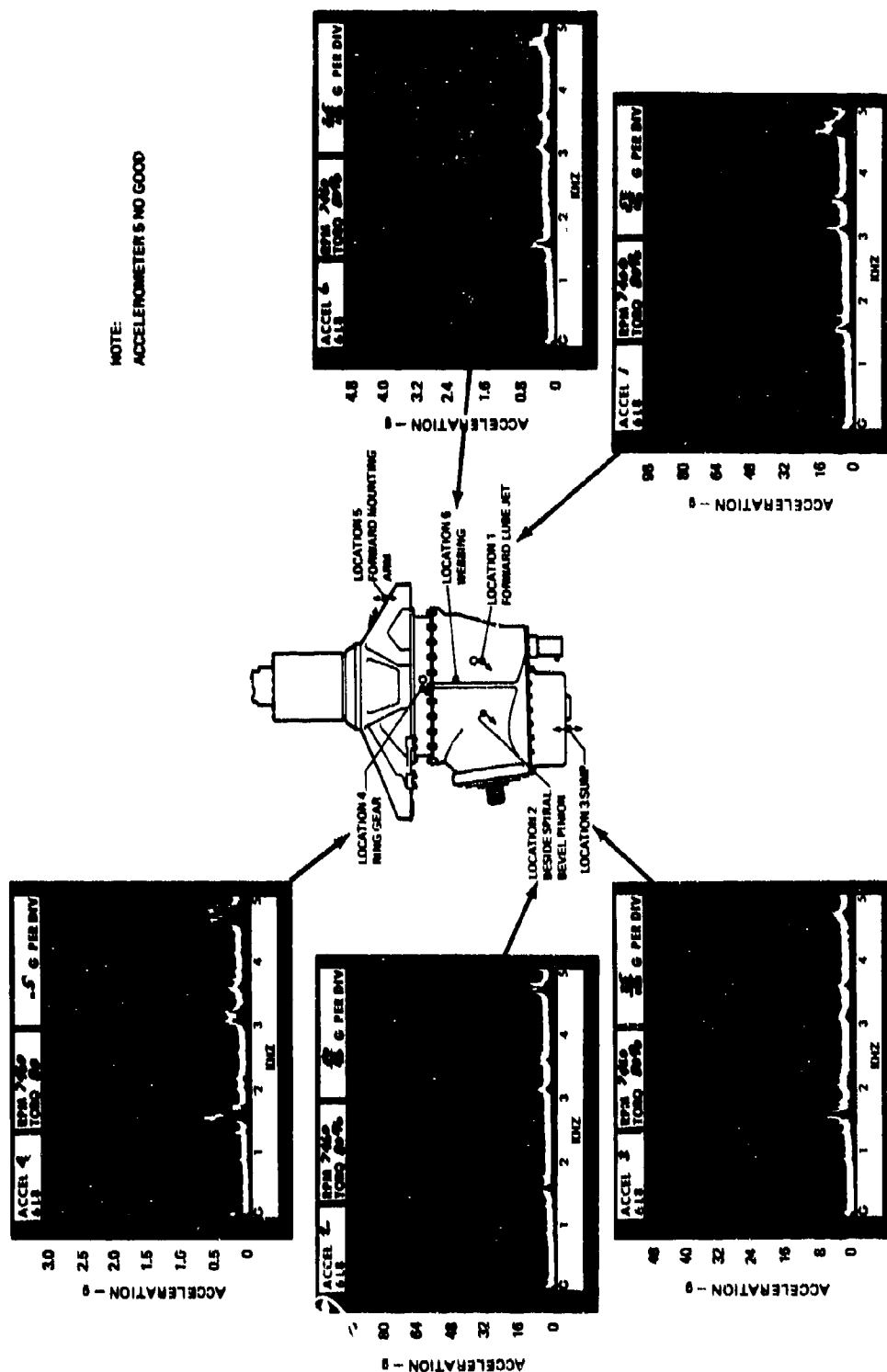


Figure A29. Accelerometer Data From Tape 6L8 With Detuning Magnesium Contour Plates,
Detuned Sun Gear, Thickened Ring Gear, and No Isolators at 7,460 RPM and
80-Percent Torque.

Figure A30. Accelerometer Data From Tape 6L8 With Detuning Magnesium Contour Plates, Detuned Sun Gear, Thickened Ring Gear, and No Isolators at 7,460 RPM and 60-Percent Torque.

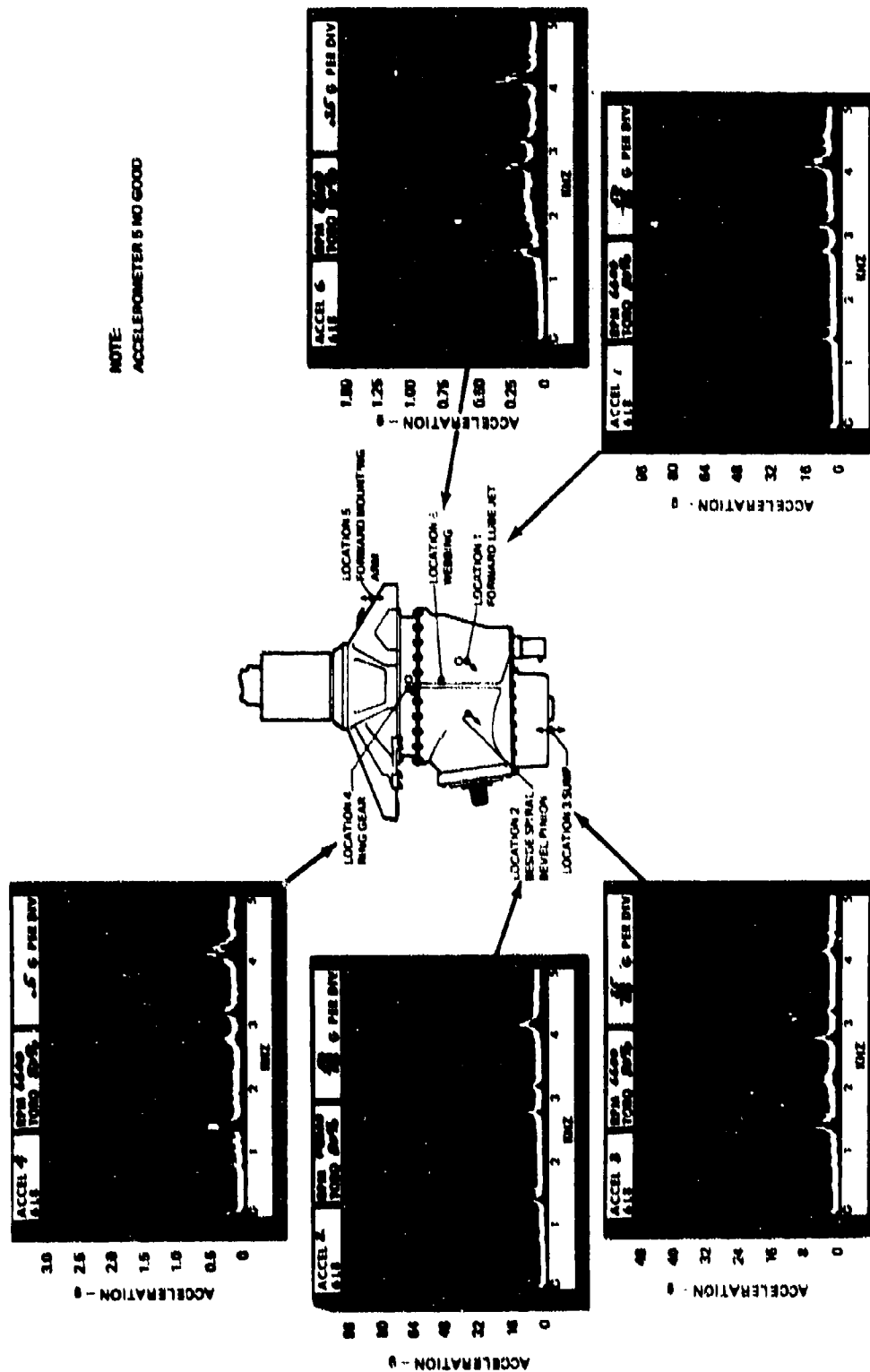


Figure A31. Accelerometer Data From Tape 6L8 With Detuning Magnesium Contour Plates, Detuned Sun Gear, Thickened Ring Gear, and No Isolators at 6,600 RPM and 80-Percent Torque.

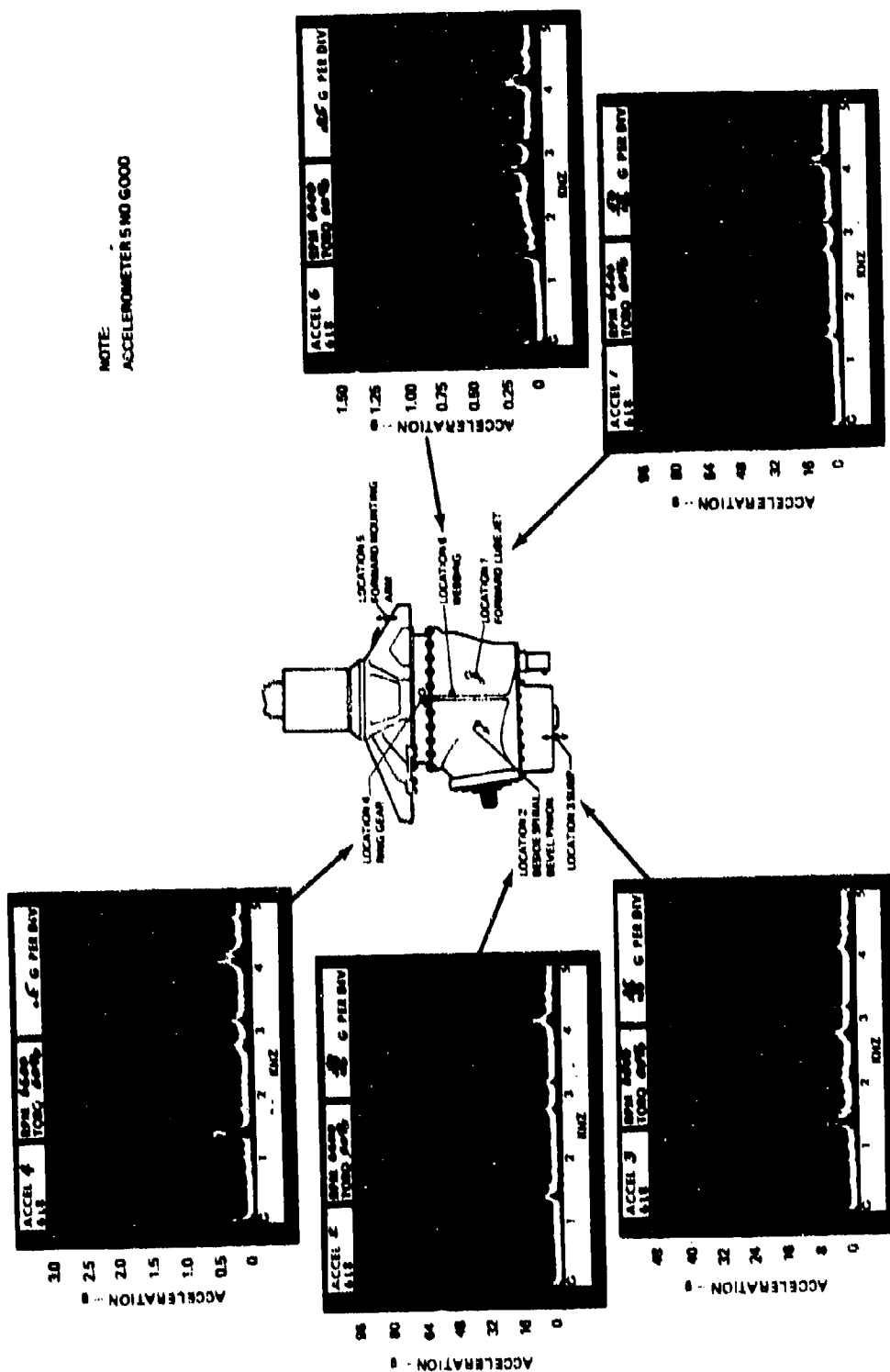


Figure A32. Accelerometer Data From Tape 6L8 With Detuning Magnesium Contour Plates, Detuned Sun Gear, Thickened Ring Gear, and No Isolators at 6,600 RPM and 60-Percent Torque.

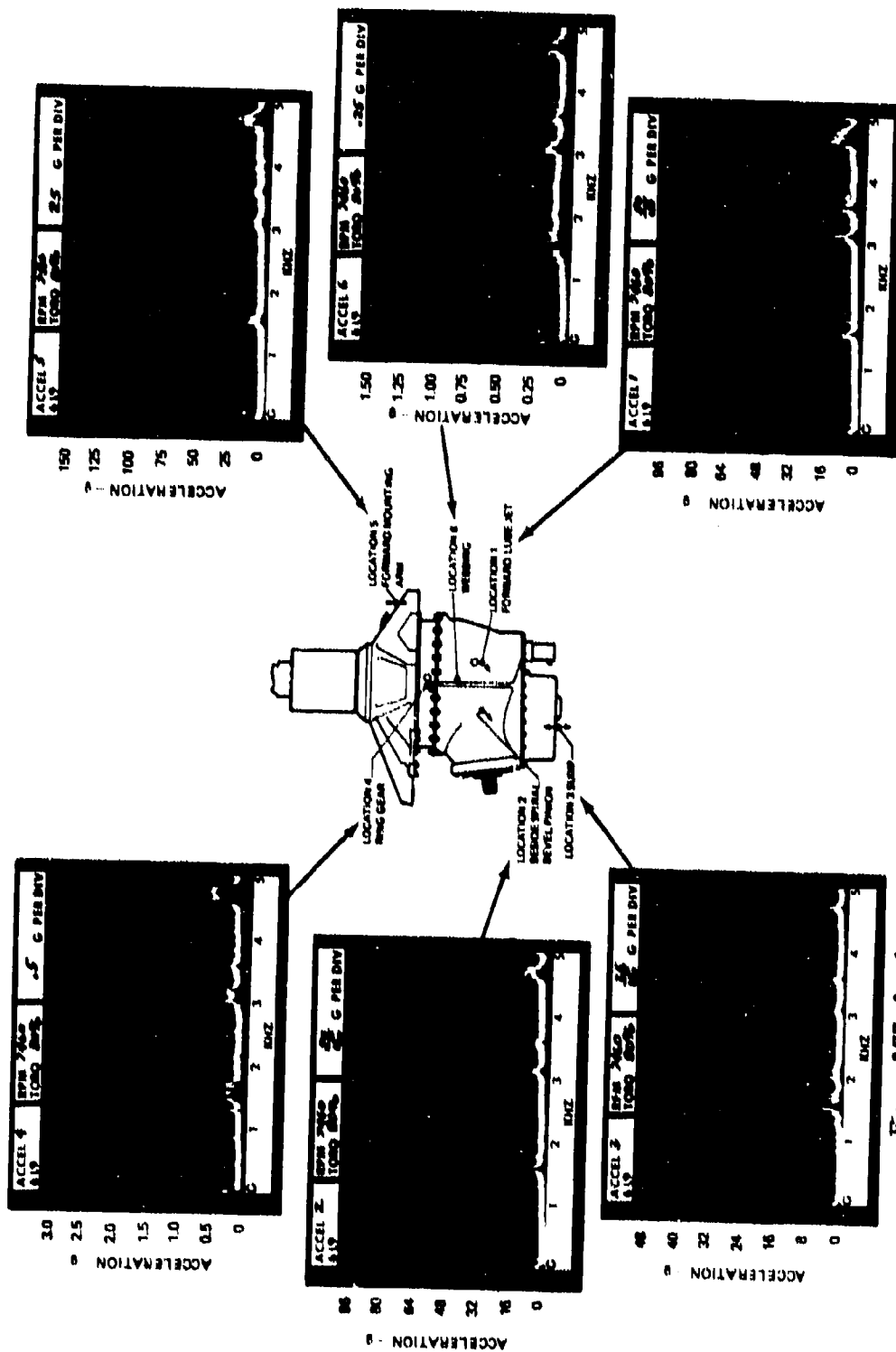


Figure A33. Accelerometer Data From Tape 6L9 With Detuning Magnesium Contour Plates, Detuned Sun Gear, Thickened Ring Gear, and Isolators at 7,460 RPM and 80-Percent Torque.

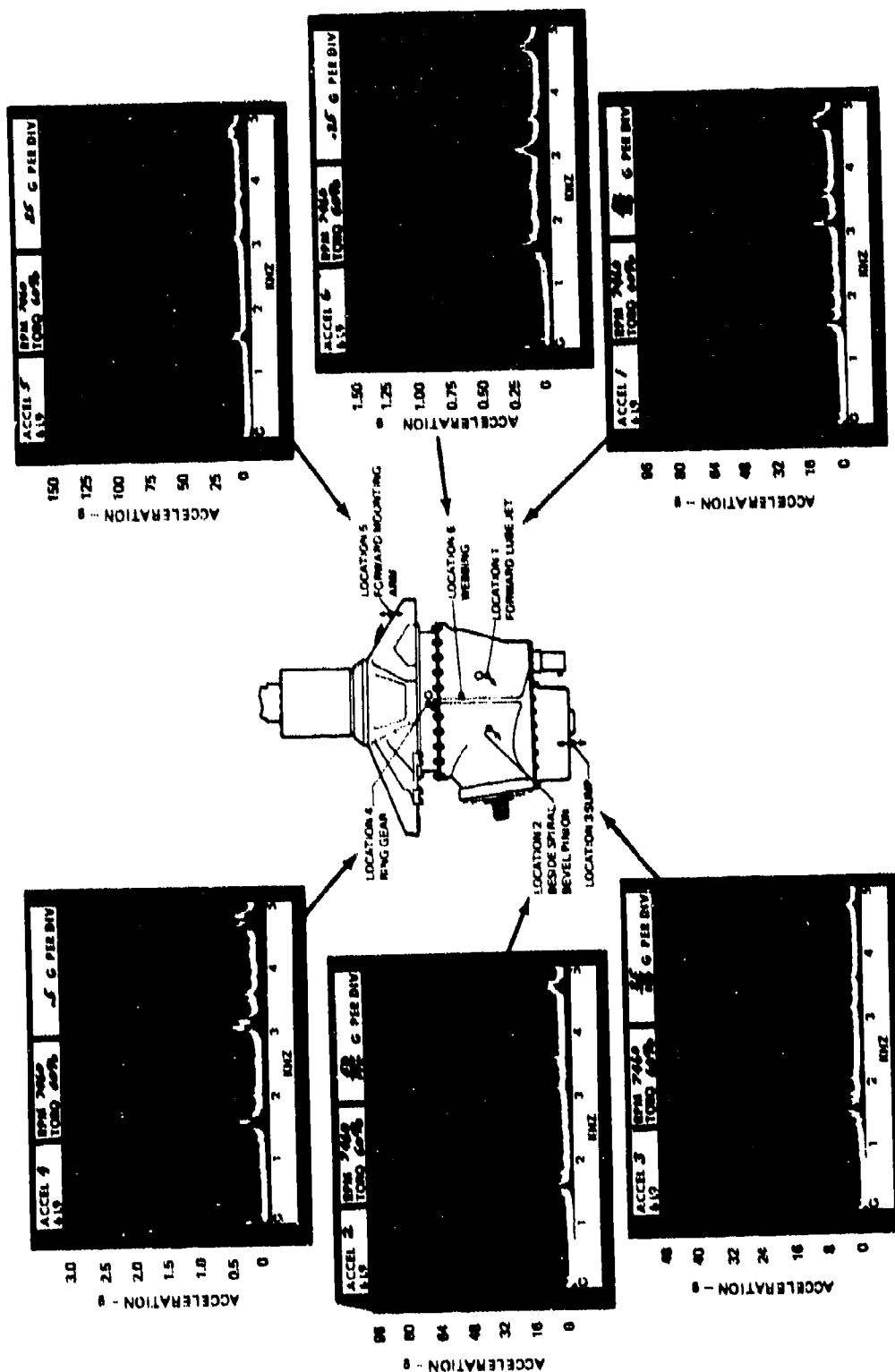


Figure A34. Accelerometer Data From Tape 6L9 With Detuning Magnesium Contour Plates, Detuned Sun Gear, Thickened Ring Gear, and Isolators at 7,460 RPM and 60-Percent Torque.

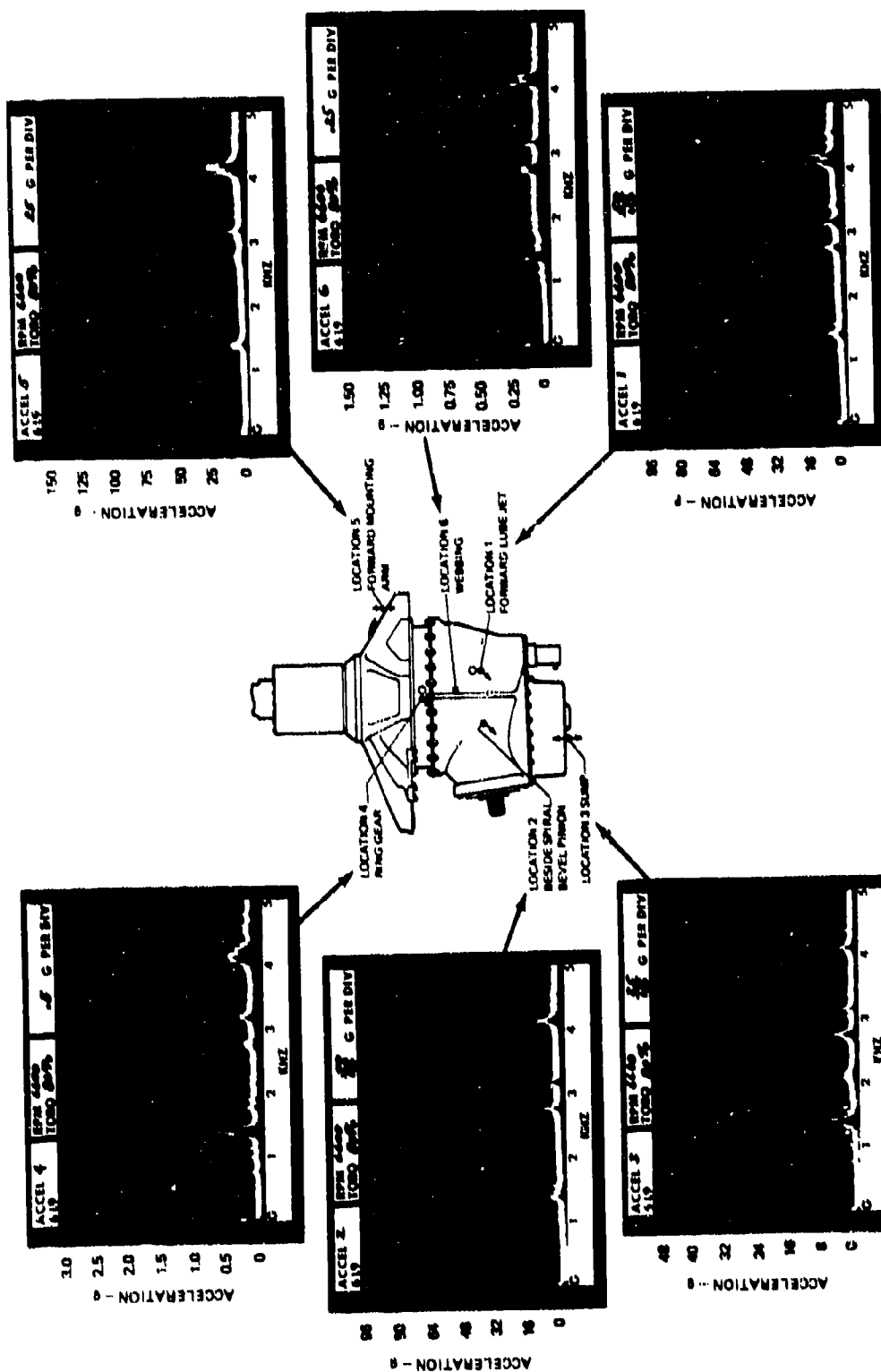


Figure A35. Accelerometer Data From Tape 6L9 With Detuning Magnesium Contour Plates, Detuned Sun Gear, Thickened Ring Gear, and Isolators at 6,600 RPM and 80-Percent Torque.

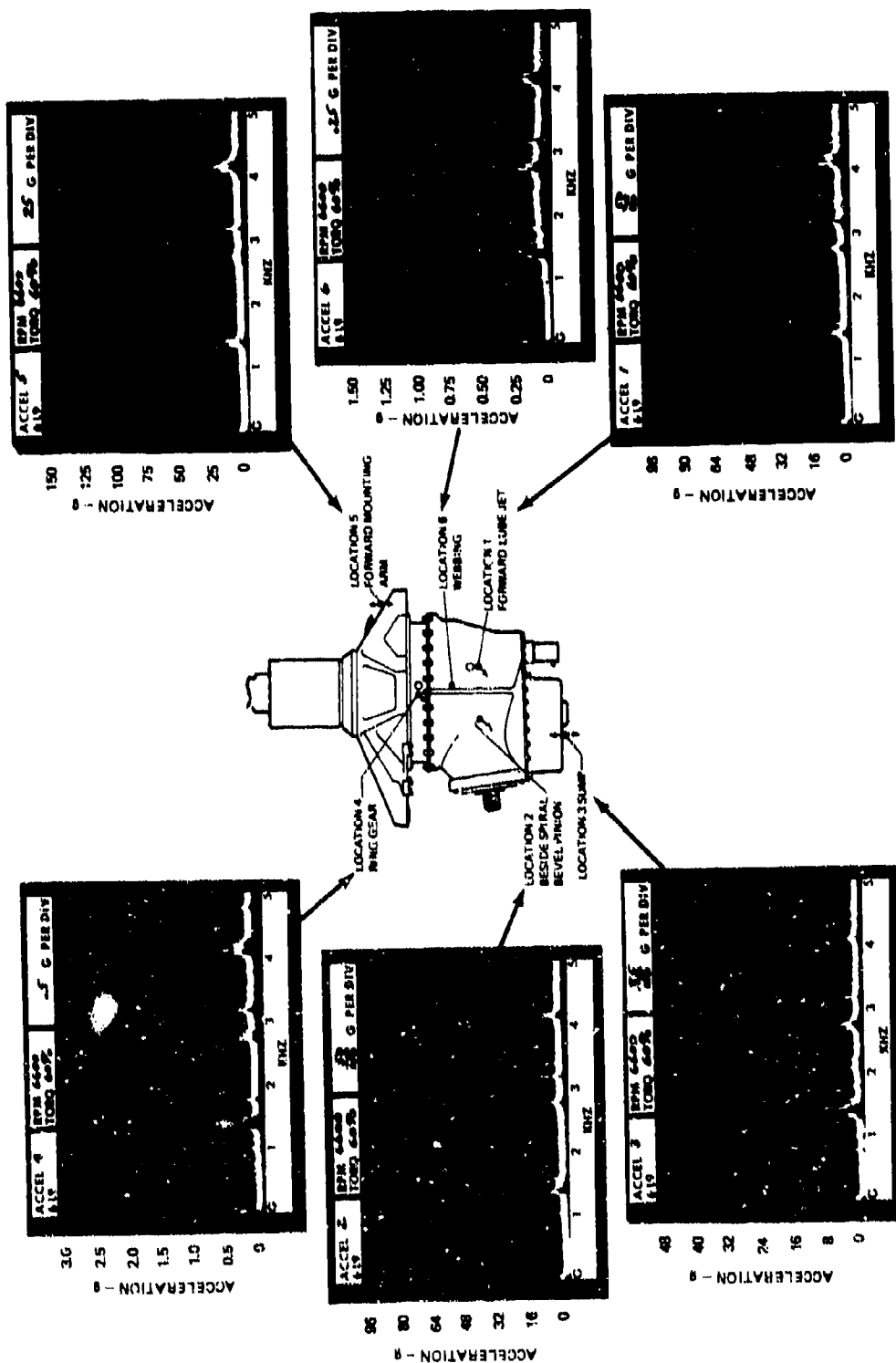


Figure A36. Accelerometer Data From Tape 6L9 With Detuning Magnesium Contour Plates, Detuned Sun Gear, Thickened Ring Gear, and Isolators at 6,600 RPM and 60-Percent Torque.

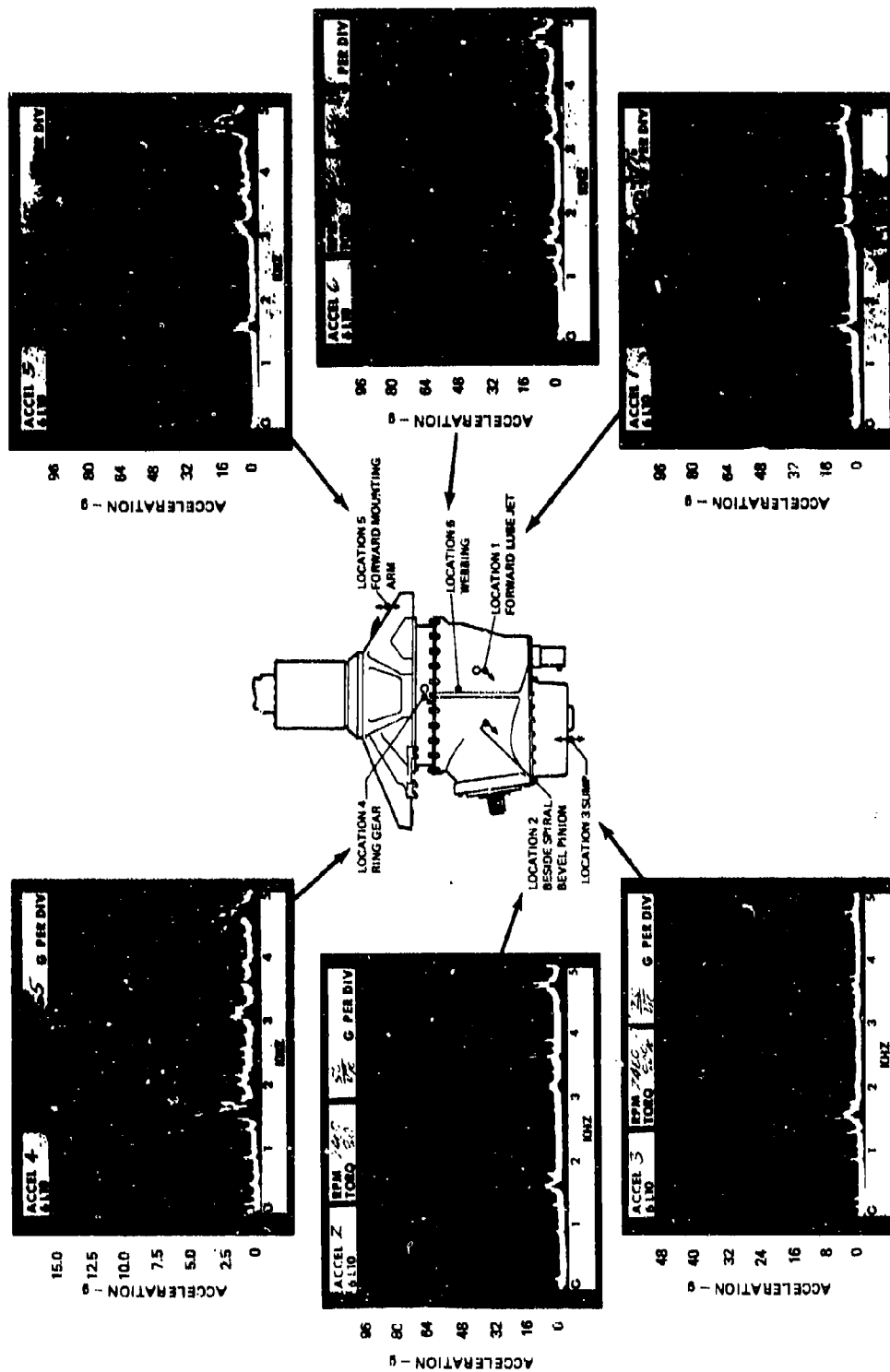


Figure A37. Accelerometer Data From Tape 6L10 With Detuning Graphite-Aluminum Composite Contour Plates and Detuned Sun Gear at 7,460 RPM and 80-Percent Torque.

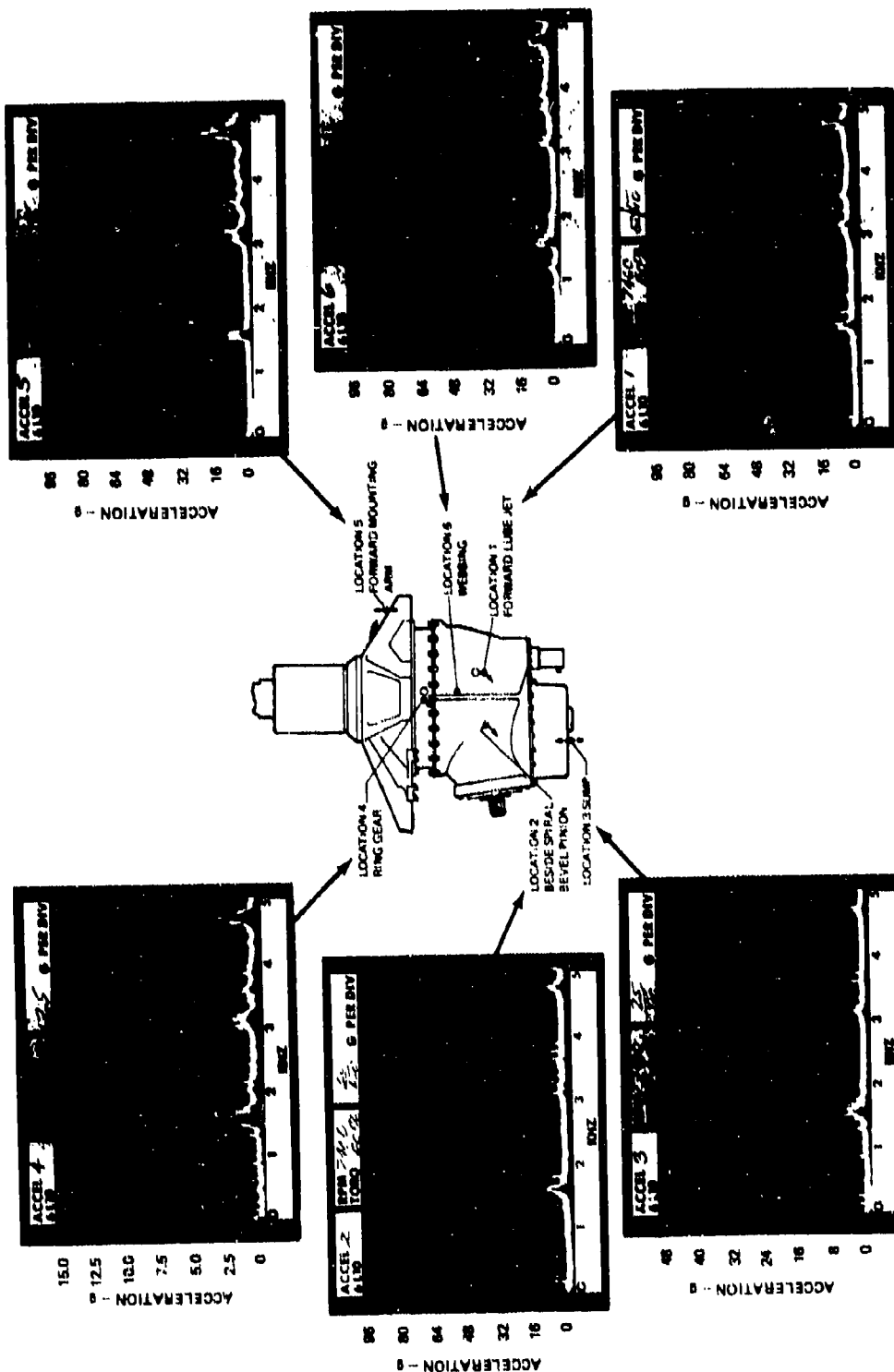


Figure A38. Accelerometer Data From Tape 6L10 With Detuning Graphite-Aluminum Composite Contour Plates and Detuned Sun Gear at 7,460 RPM and 60-Percent Torque.

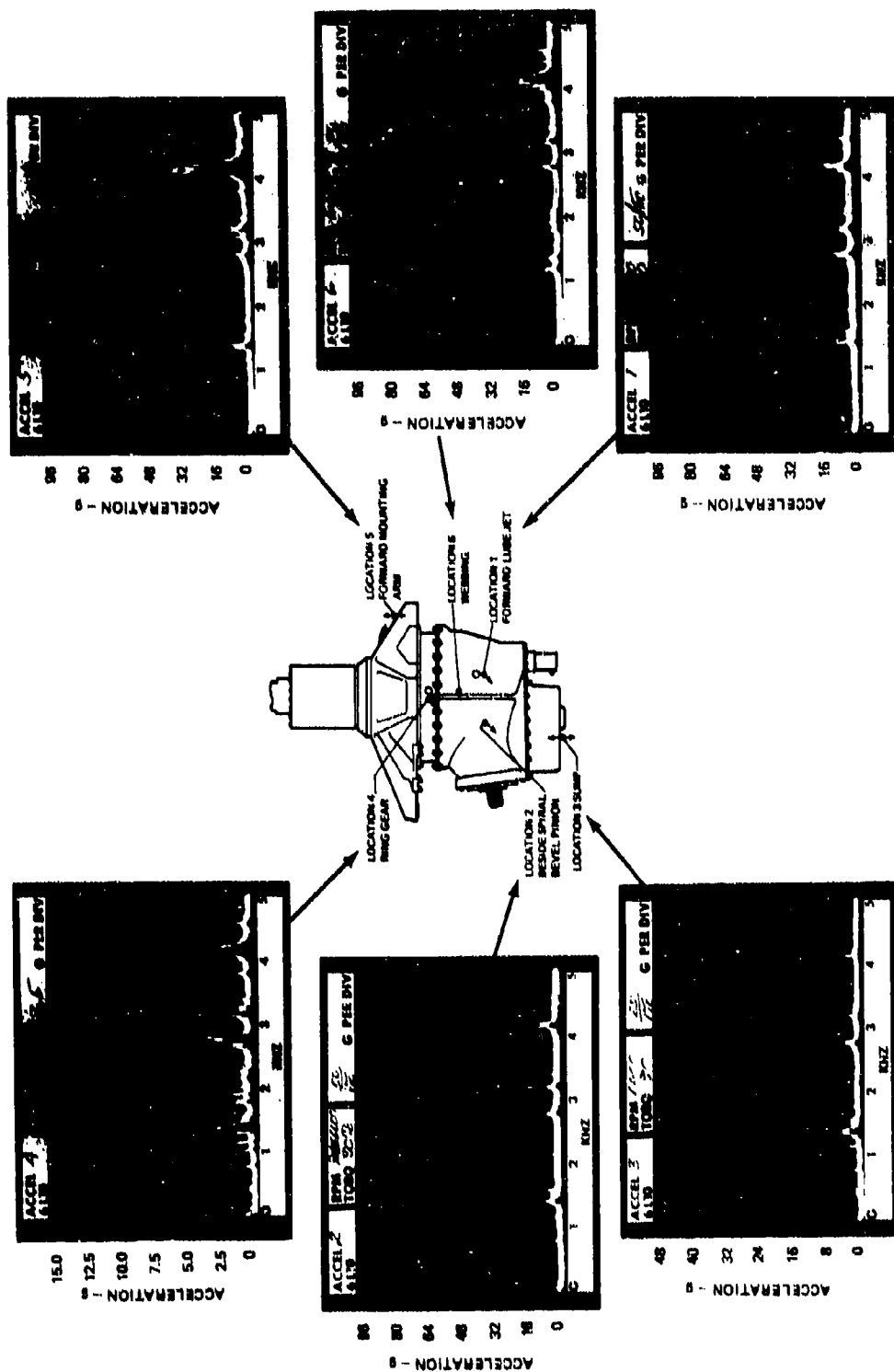


Figure A39. Accelerometer Data From Tape 6L10 With Detuning Graphite-Aluminum Composite Contour Plates and Detuned Sun Gear at 6,600 RPM and 80-Percent Torque.

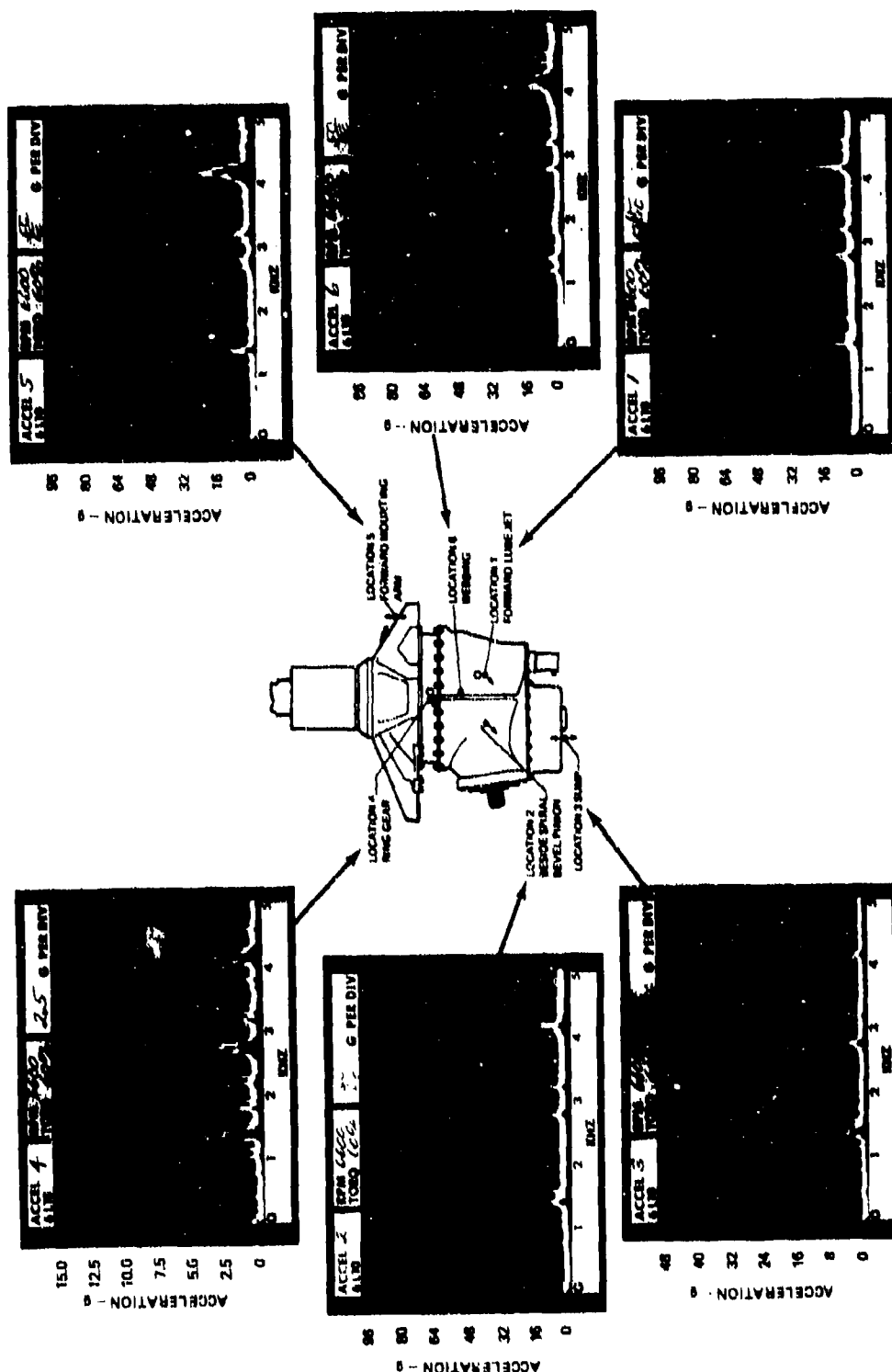


Figure A40. Accelerometer Data From Tape 6L10 With Detuning Graphite-Aluminum Composite Contour Plates and Detuned Sun Gear at 6,600 RPM and 60-Percent Torque.

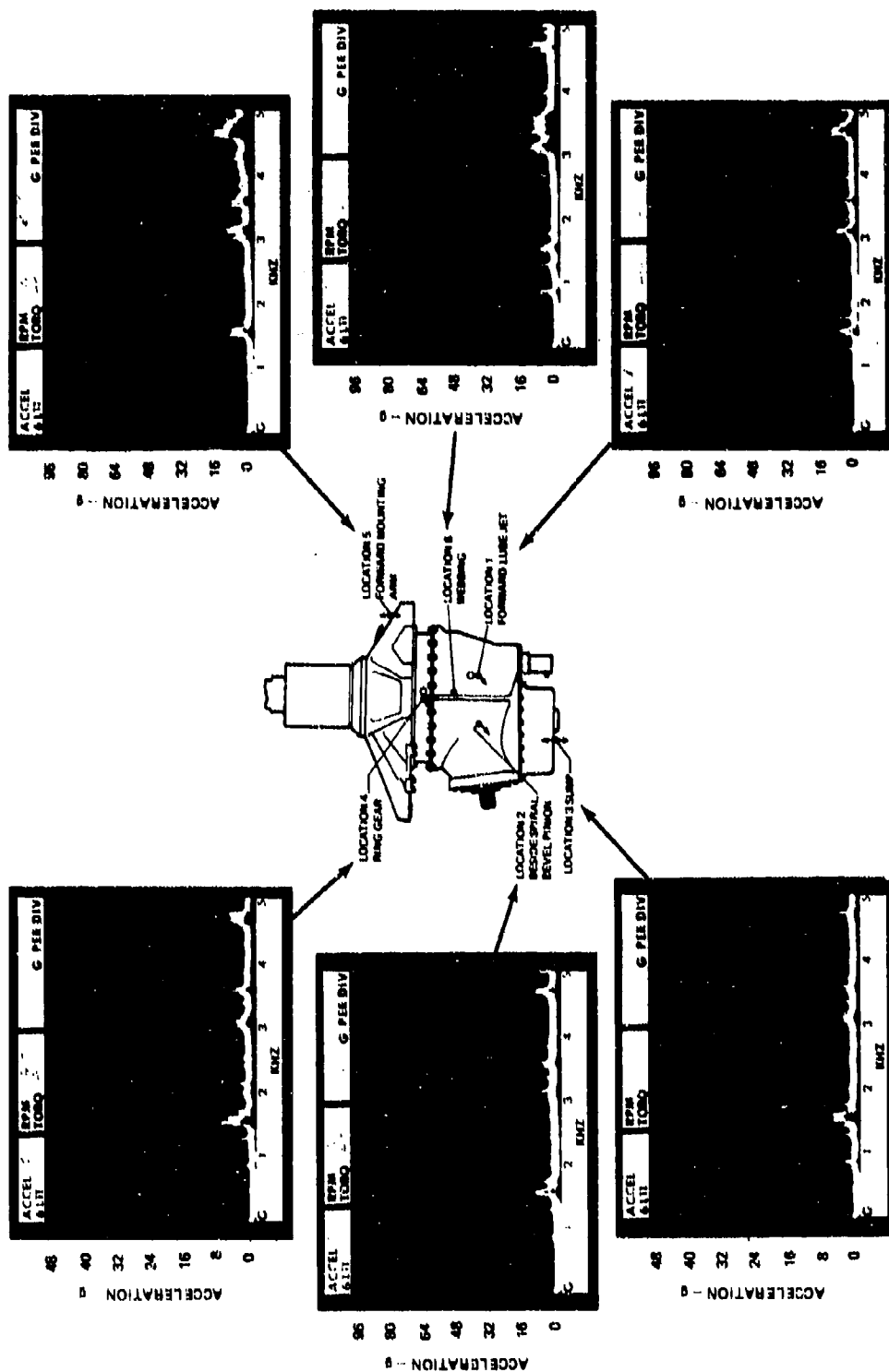


Figure A41. Accelerometer Data From Tape 6L11 With Detuning Graphite-Aluminum Composite Contour Plates at 7,460 RPM and 80-Percent Torque.

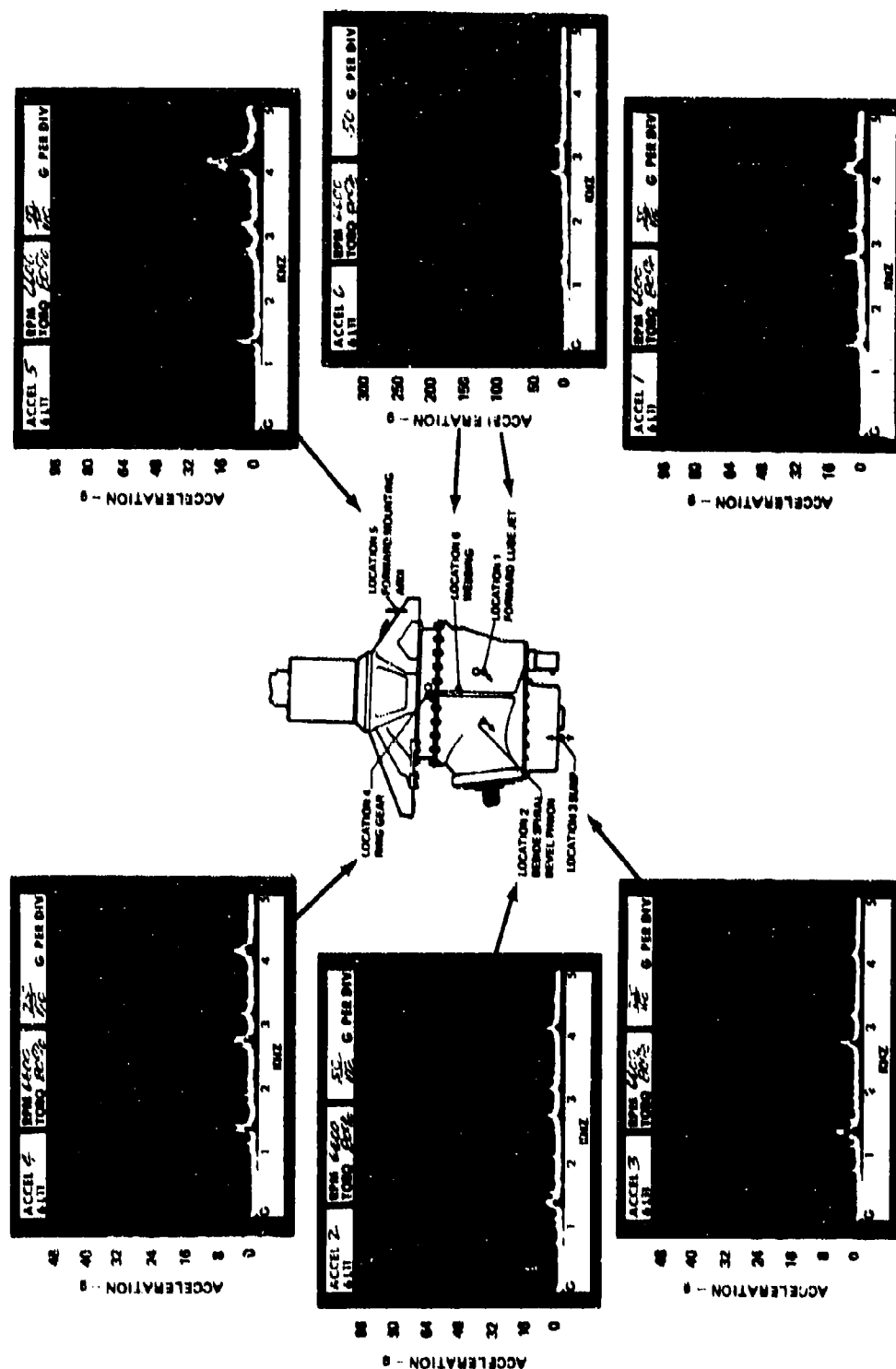


Figure A43. Accelerometer Data From Tape 6L11 With Detuning Graphite-Aluminum Composite Contour Plates at 6,600 RPM and 80-Percent Torque.

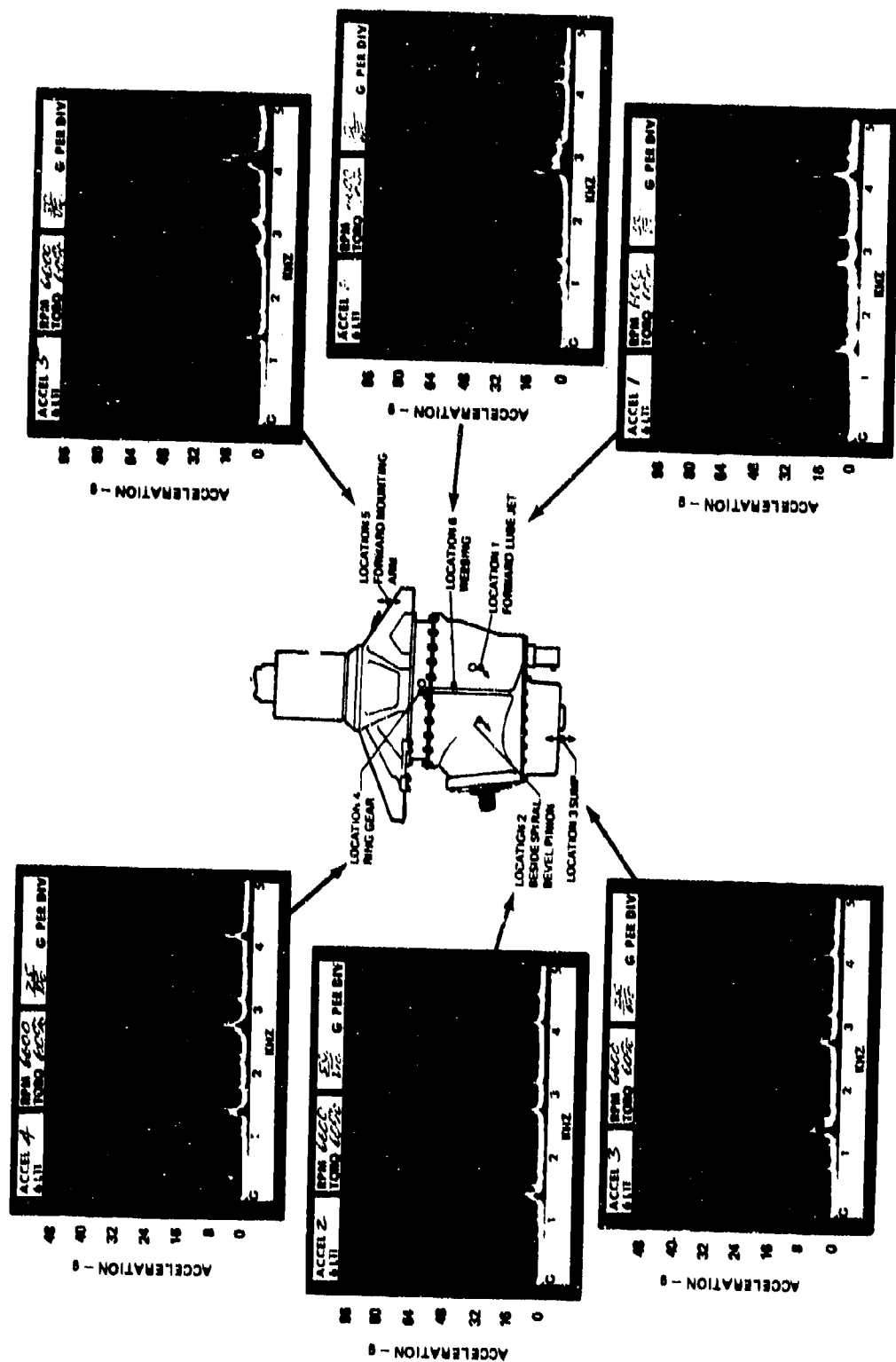


Figure A44. Accelerometer Data From Tape 6L1.1 With Detuning Graphite-Aluminum Contour Plates at 6,600 RPM and 60-Percent Torque.

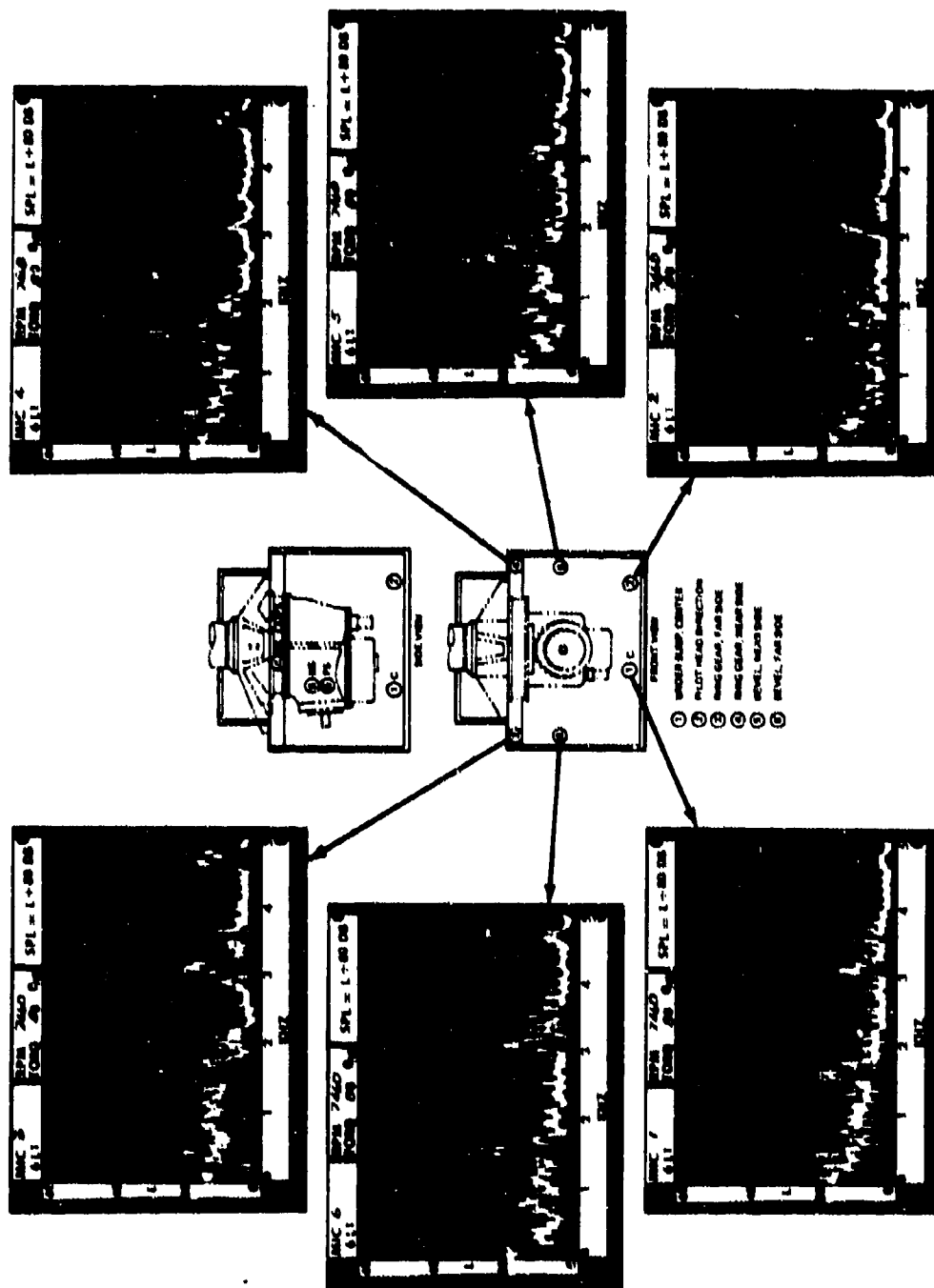


Figure A45. Microphone Data From Tape 6L1 With Baseline C51-47C Forward Transmission at 7,460 RPM and 80-Percent Torque.

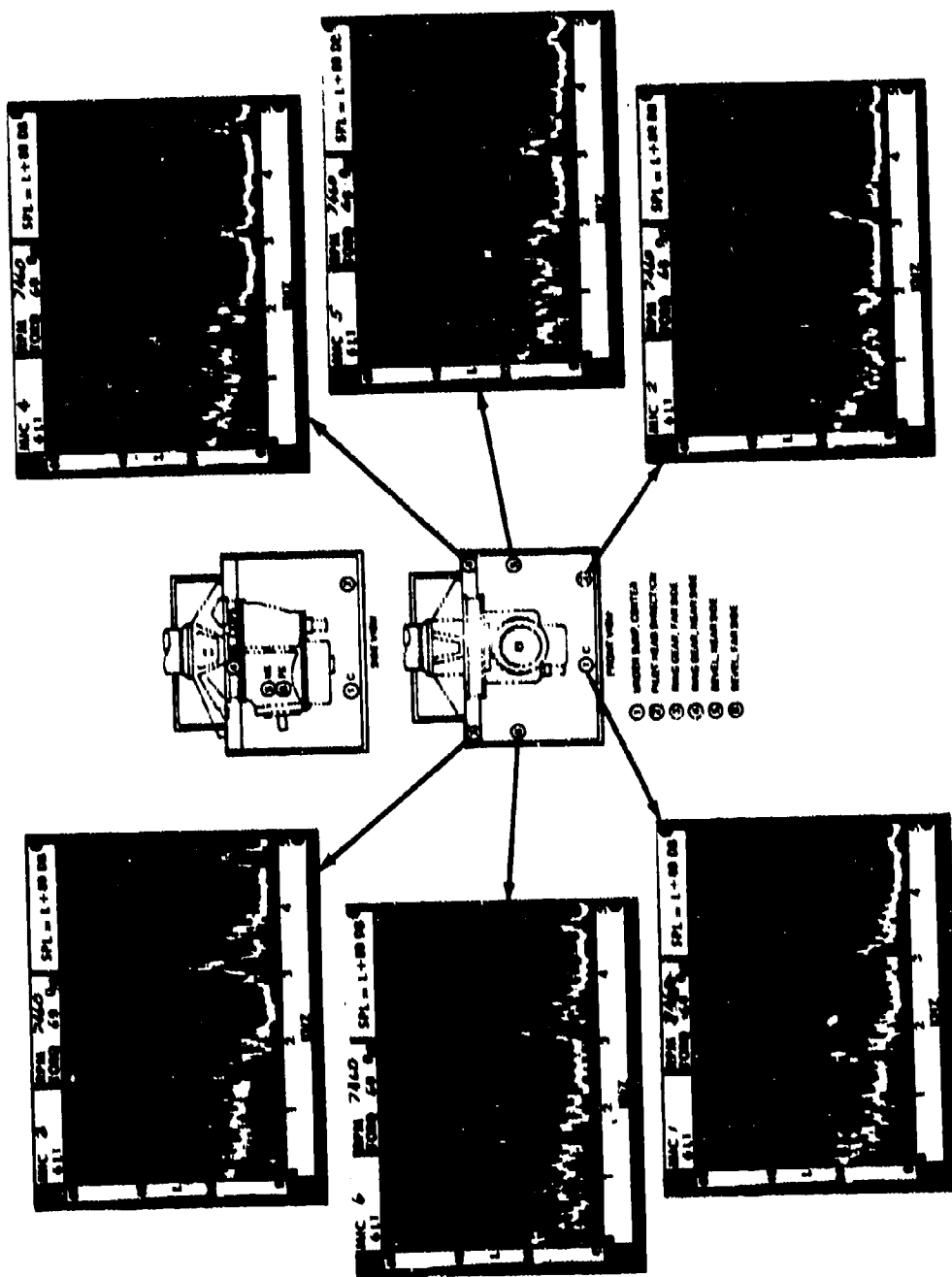


Figure A46. Microphone Data From Tape 6L1 With Baseline CH-47C Forward Transmission at 7,460 RPM and 60-Percent Torque.

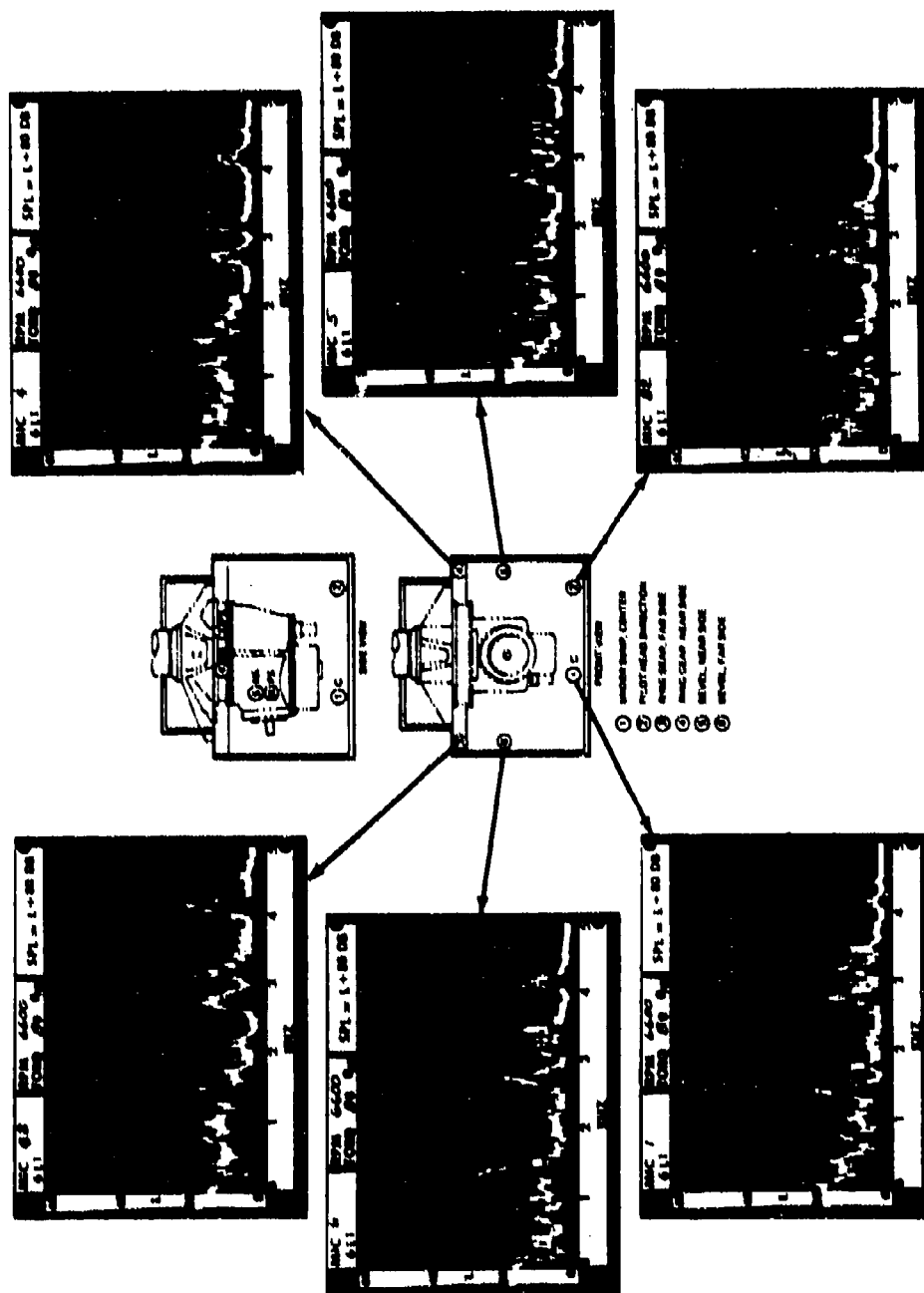


Figure A47. Microphone Data From Tape 6L1 With Baseline CH-47C Forward Transmission at 6,600 RPM and 80-Percent Torque.

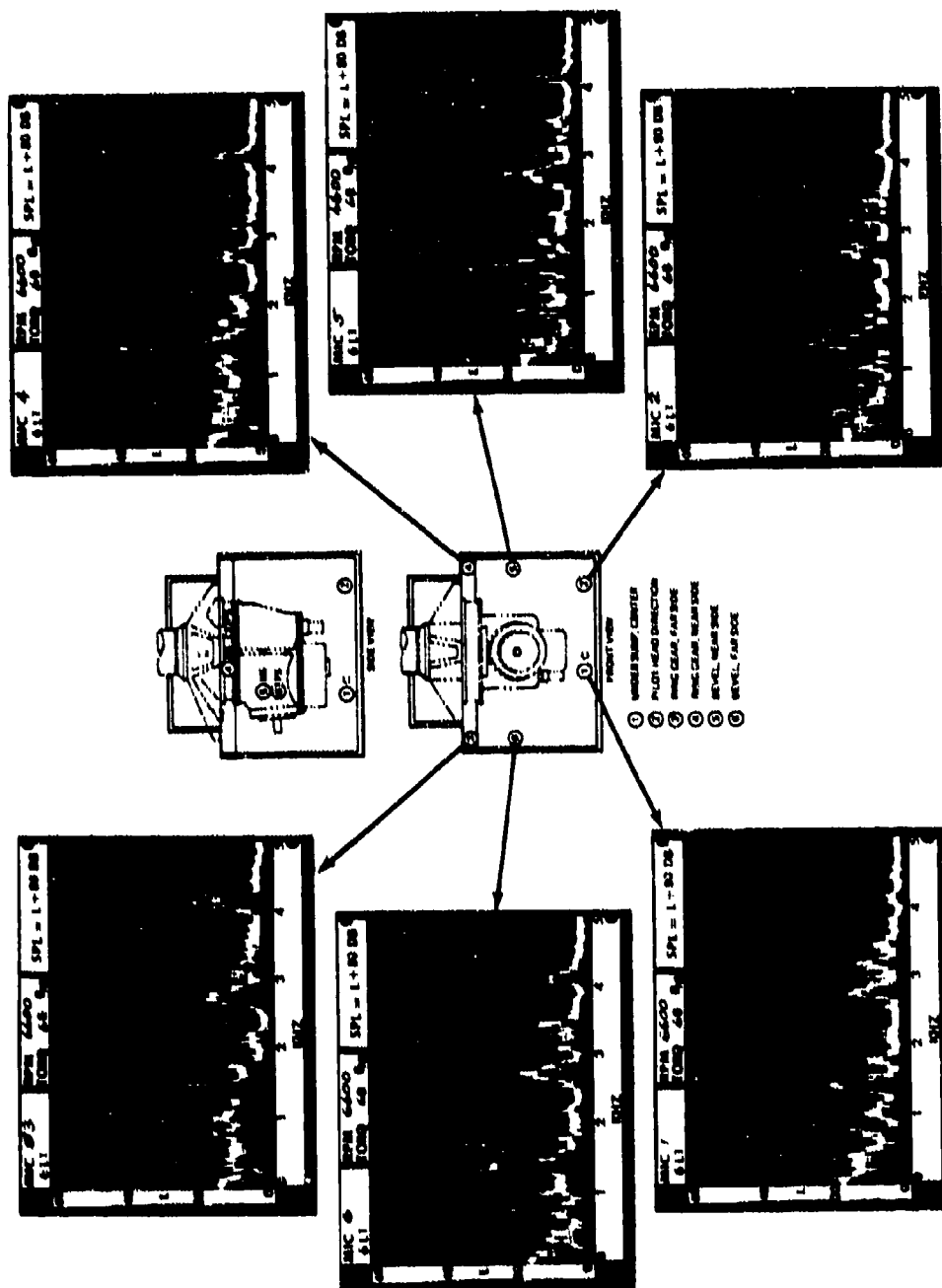


Figure A48. Microphone Data From Tape 6Li With Baseline CH-47C Forward Transmission at 6,600 RPM and 60-Percent Torque.

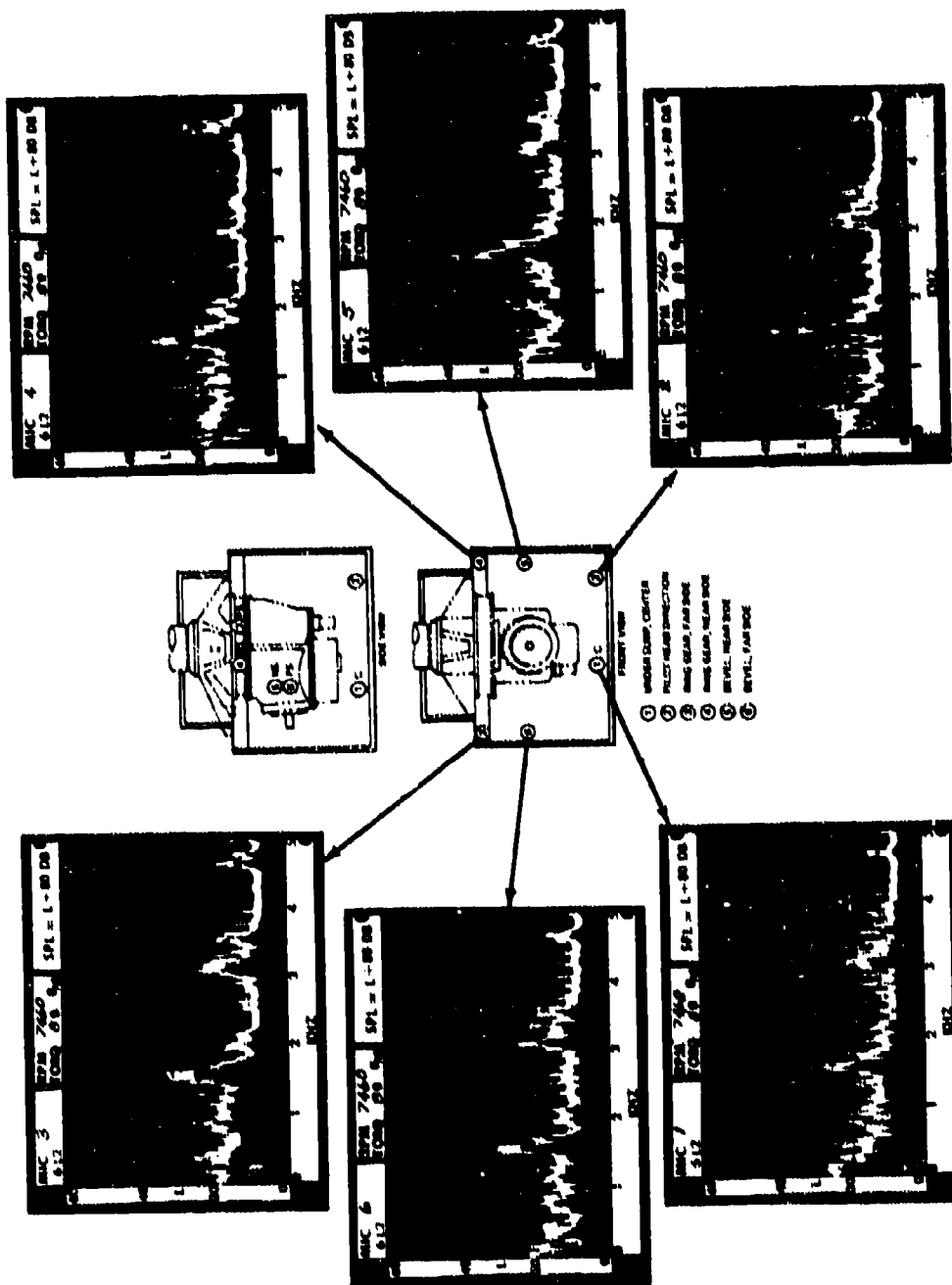


Figure A49. Microphone Data From Tape 6L2 With Baseline CH-47C Forward Transmissiön and Isolators at 7,460 RPM and 80-Percent Torque.

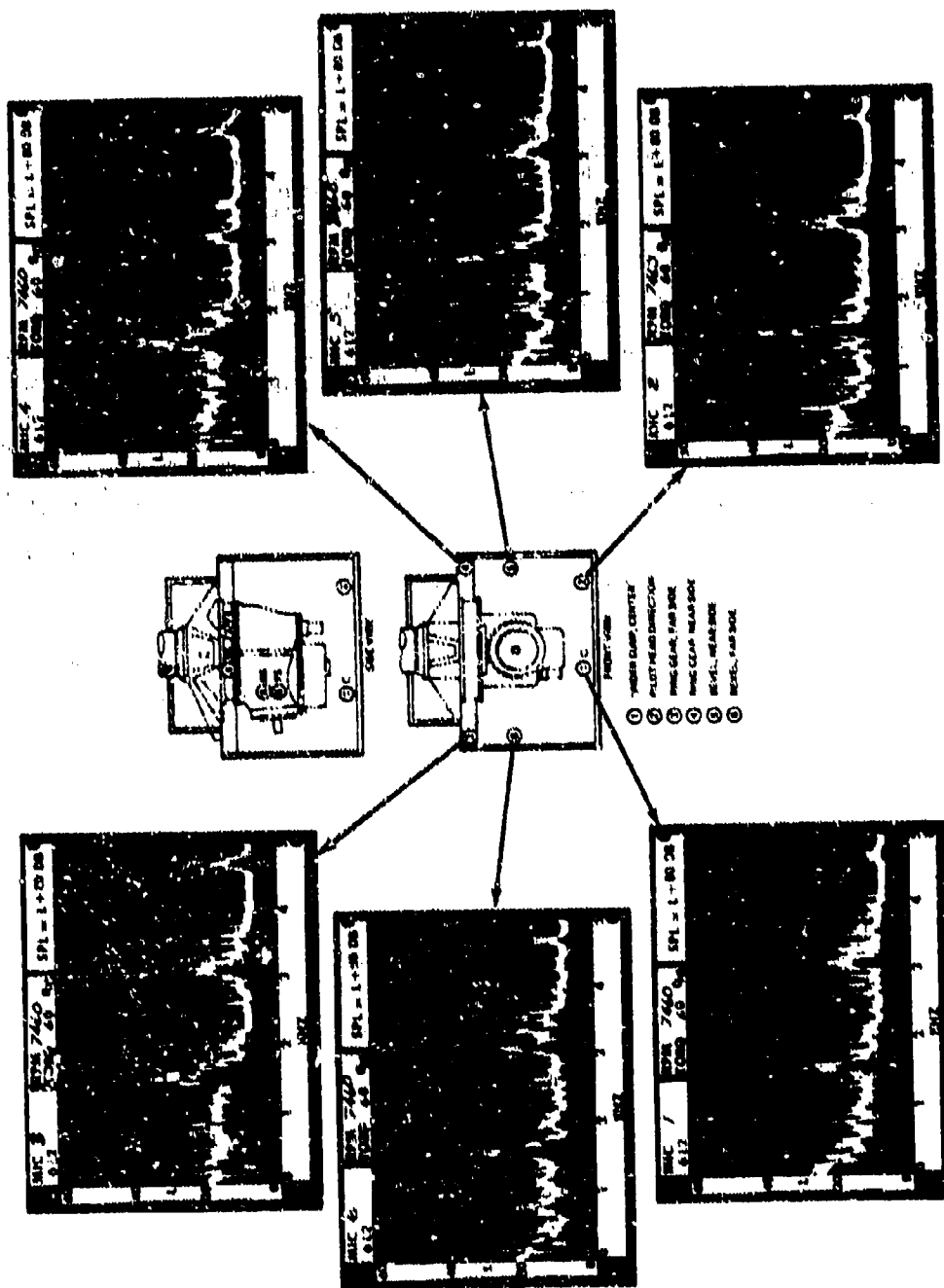


Figure A50. Microphone Data From Tape 6L2 With Baseline CH-47C Forward Transmission and Isolators at 7,460 RPM and 60-Percent Torque.

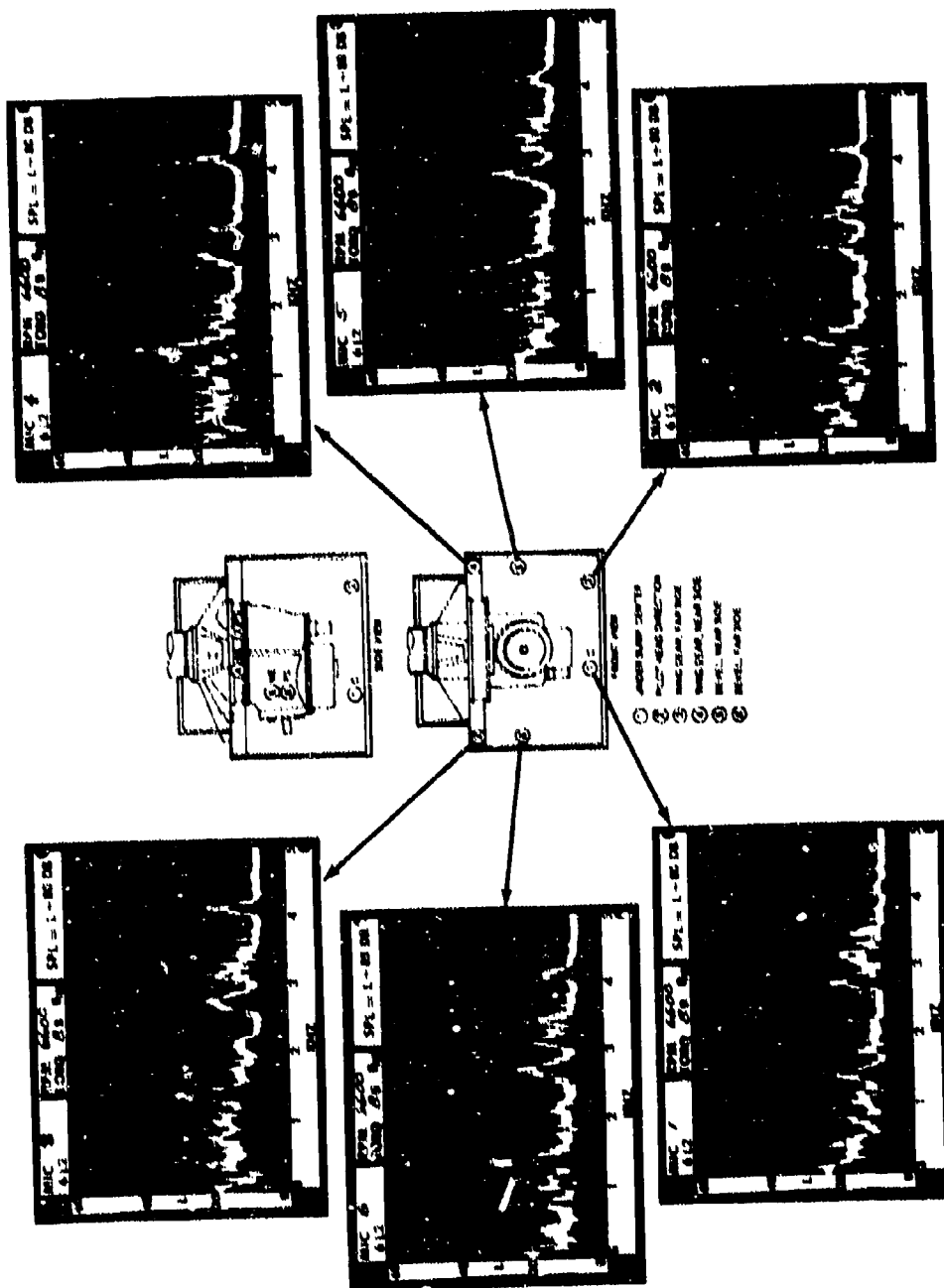


Figure A51. Microphone Data From Tape 61.2 With Baseline CH-47C Forward Transmission and Isolators at 6,600 RPM and 80-Percent Torque.

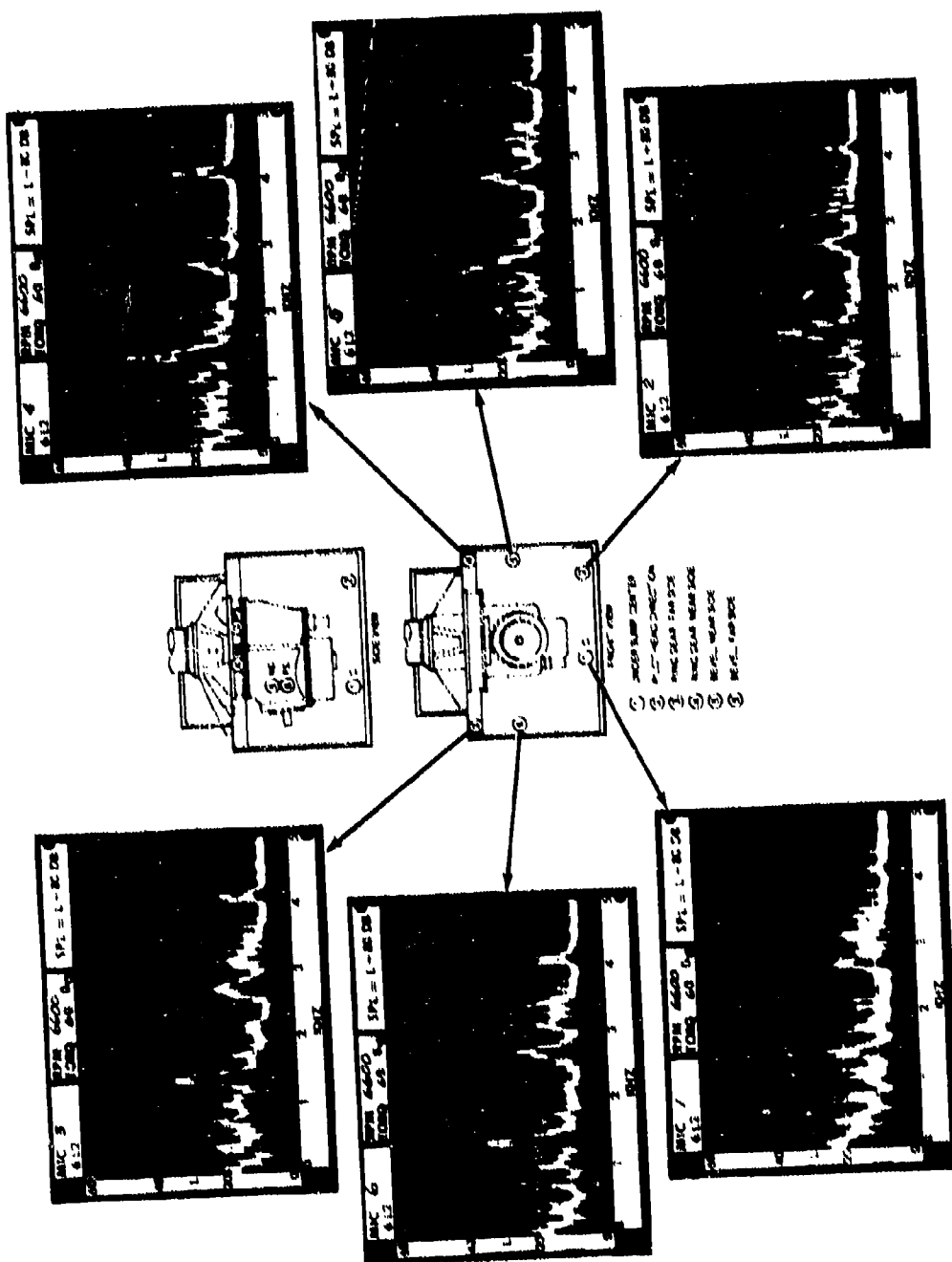


Figure A52. Microphone Data From Tape 61.2 With Baseline CH-47C Forward Transmission and Isolators at 6,600 RPM and 60-Percent Torque.

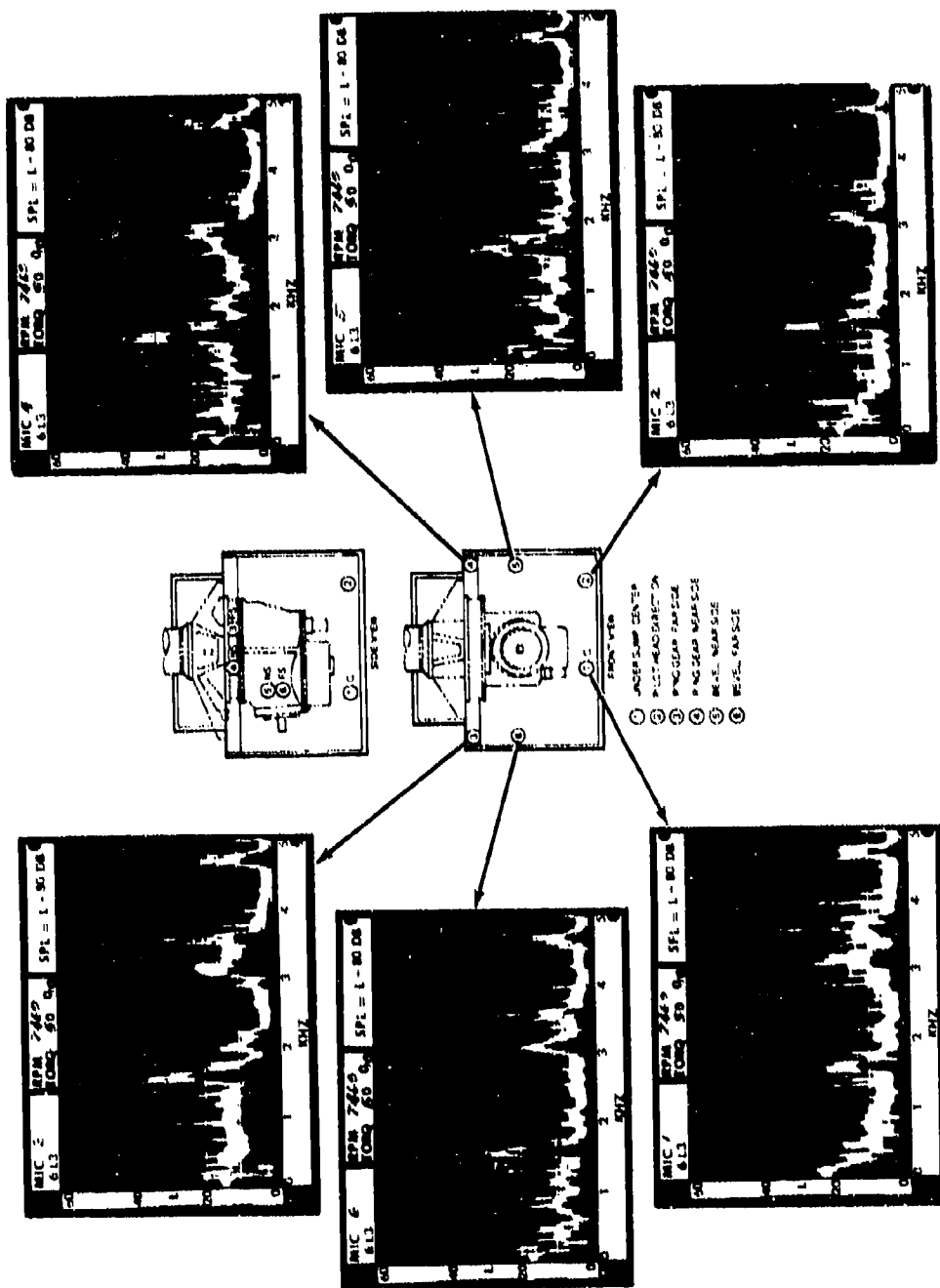


Figure A53. Microphone Data From Tape 6L3 With Detuned Sun Gear and No Isolators at 7,460 RPM and 80-Percent Torque.

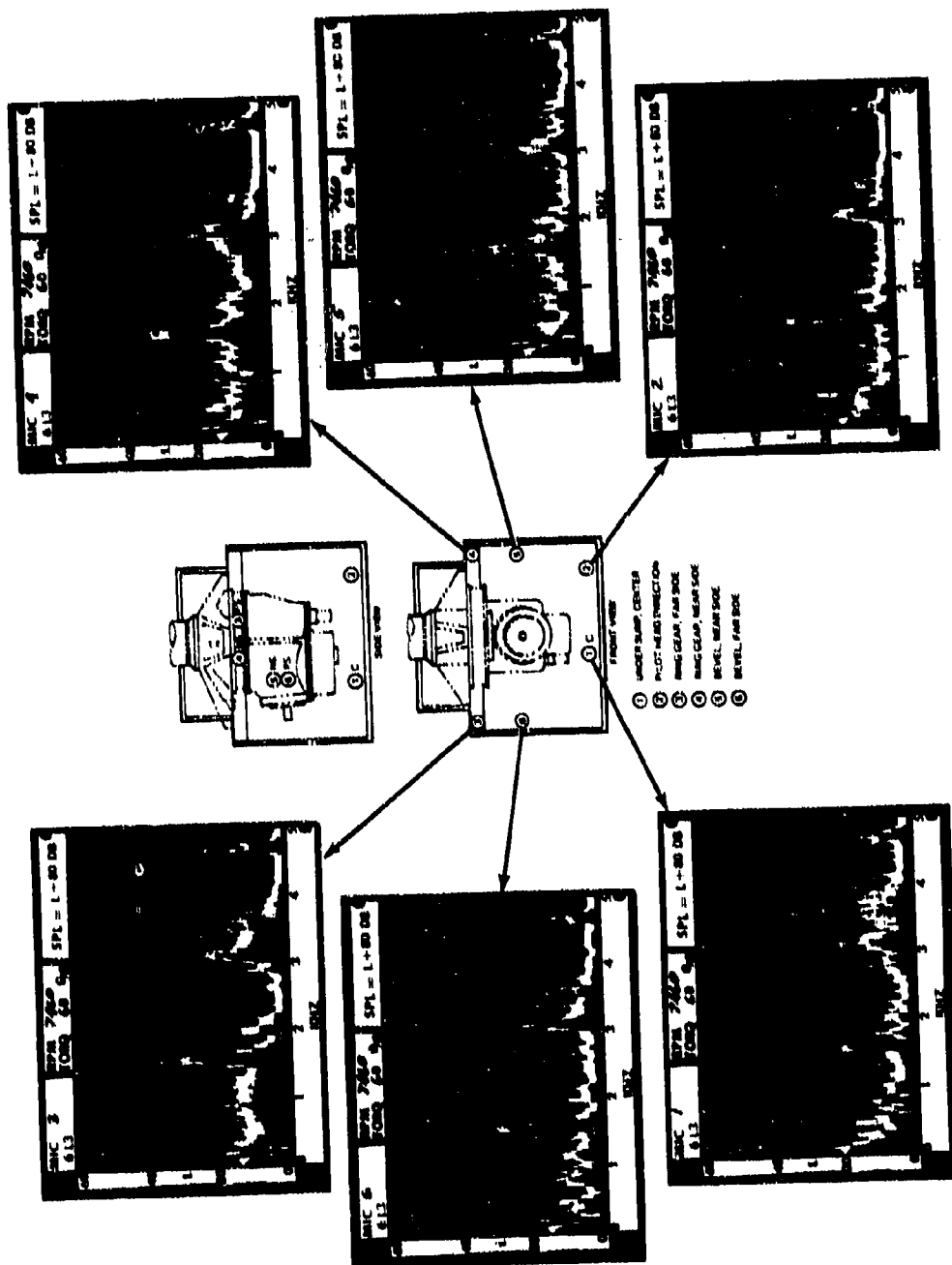


Figure A54. Microphone Data From Tape 6L3 With Detuned Sun Gear and No Isolators at 7,460 RPM and 60-Percent Torque.

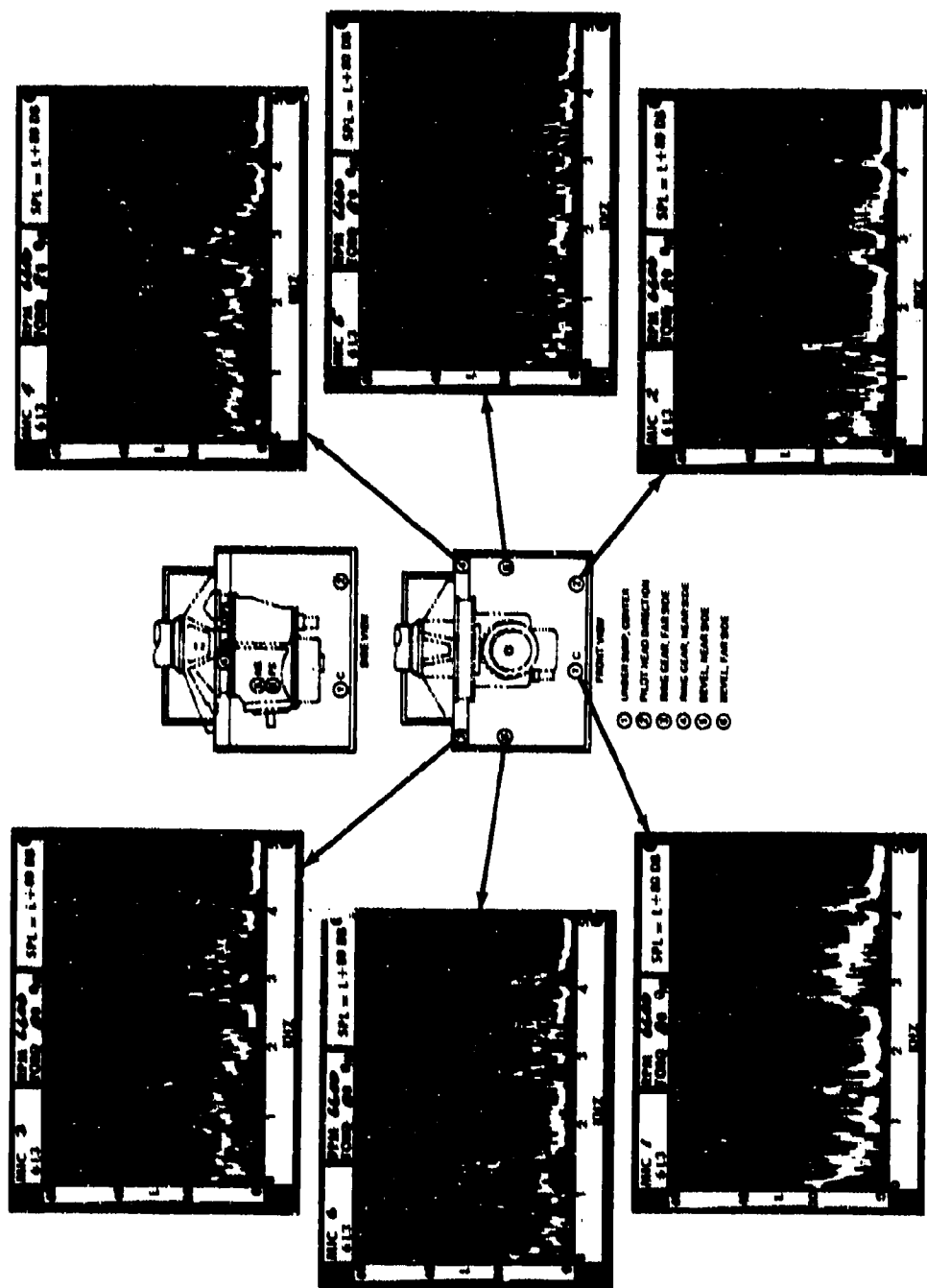


Figure A55. Microphone Data From Tape 6L3 With Detuned Sun Gear and No Isolators at 6,600 RPM and 80-Percent Torque.

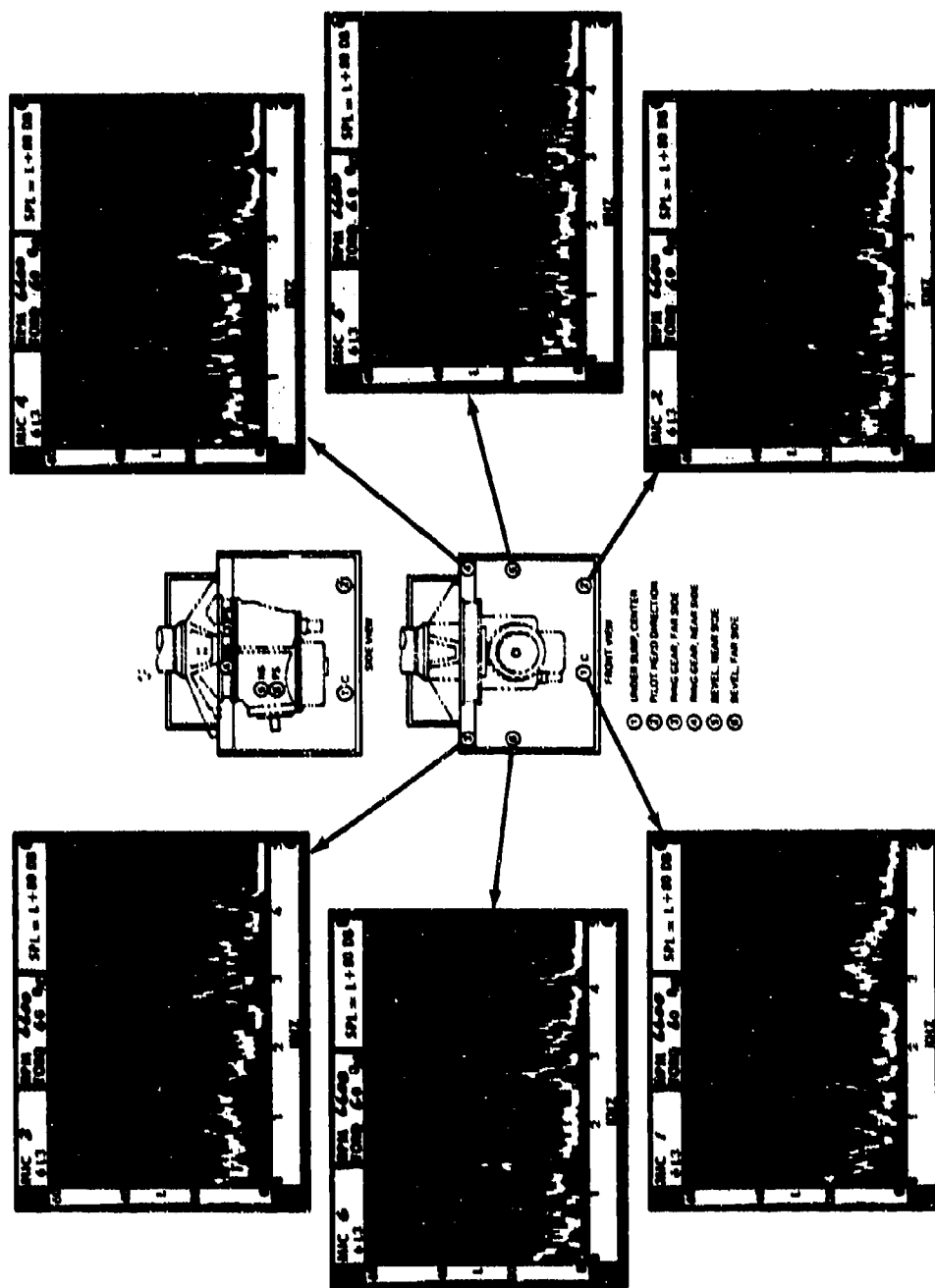


Figure A56. Microphone Data From Tape 6L3 With Detuned Sun Gear and No Isolators at 6,600 RPM and 60-Percent Torque.

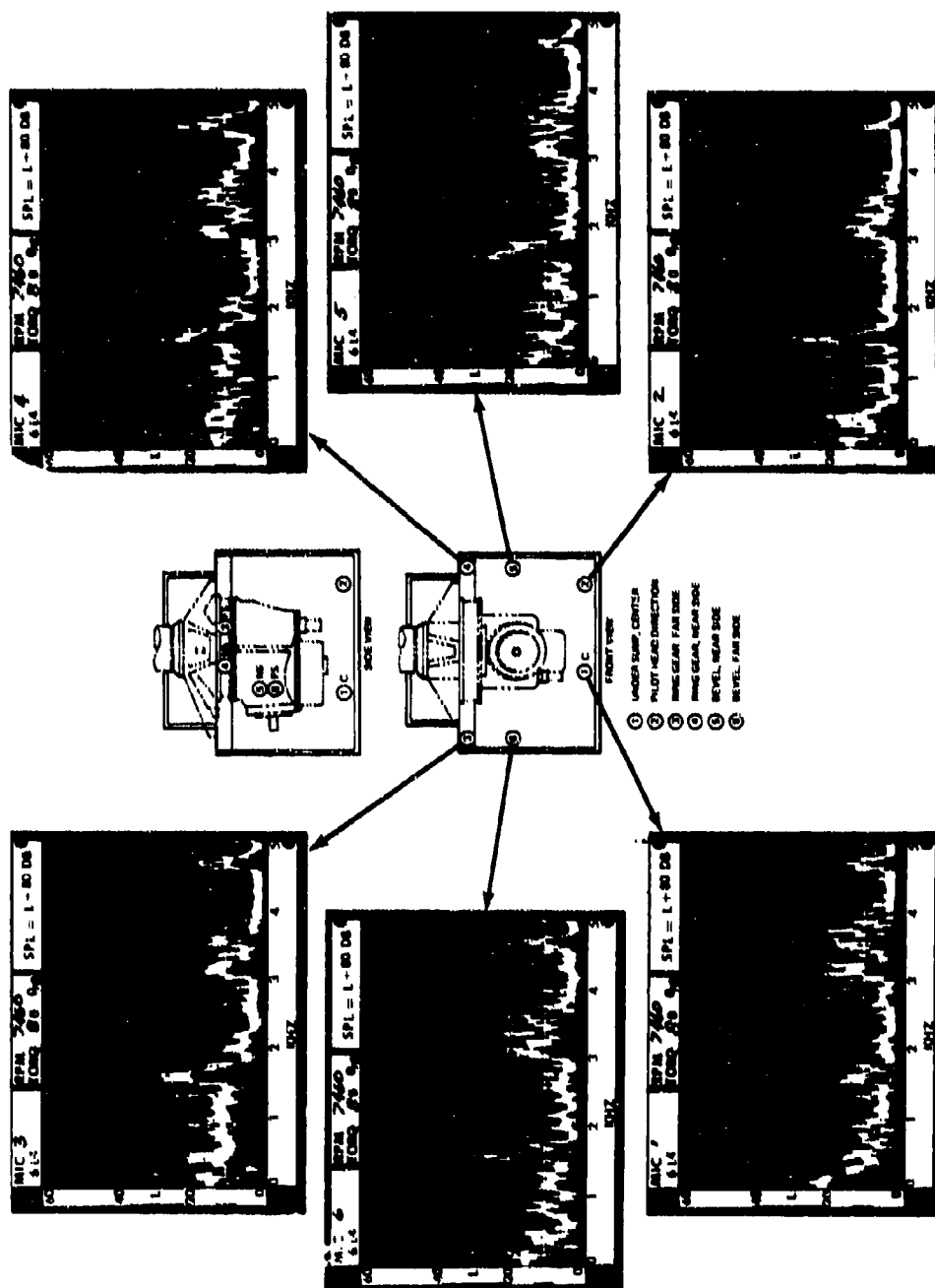


Figure A57. Microphone Data From Tape 6L4 With Detuned Sun Gear and Isolators at 7,460 RPM and 80-Percent Torque.

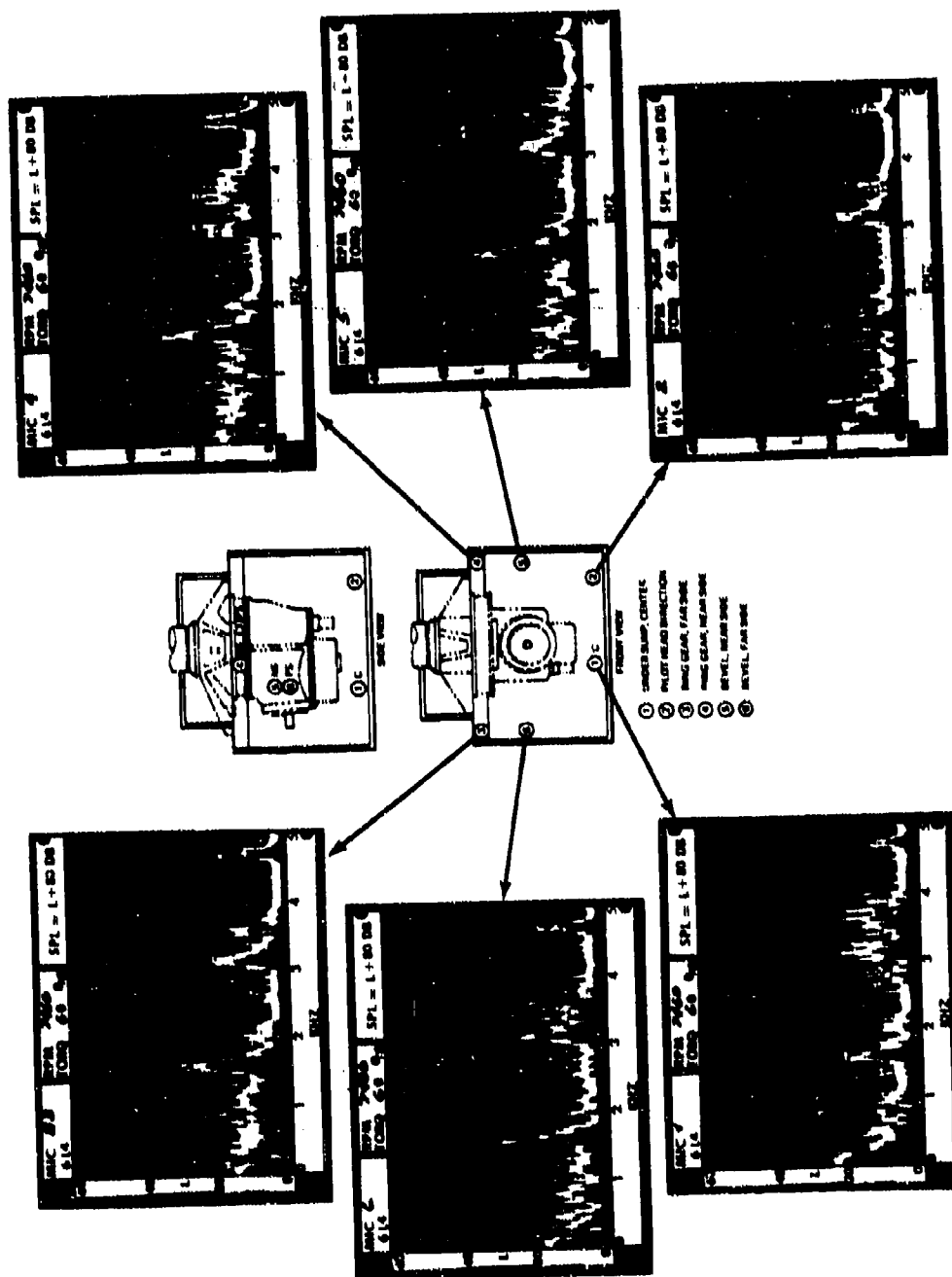


Figure A58. Microphone Data From Tape 6L4 With Detuned Sun Gear and Isolators at 7,460 RPM and 60-Percent Torque.

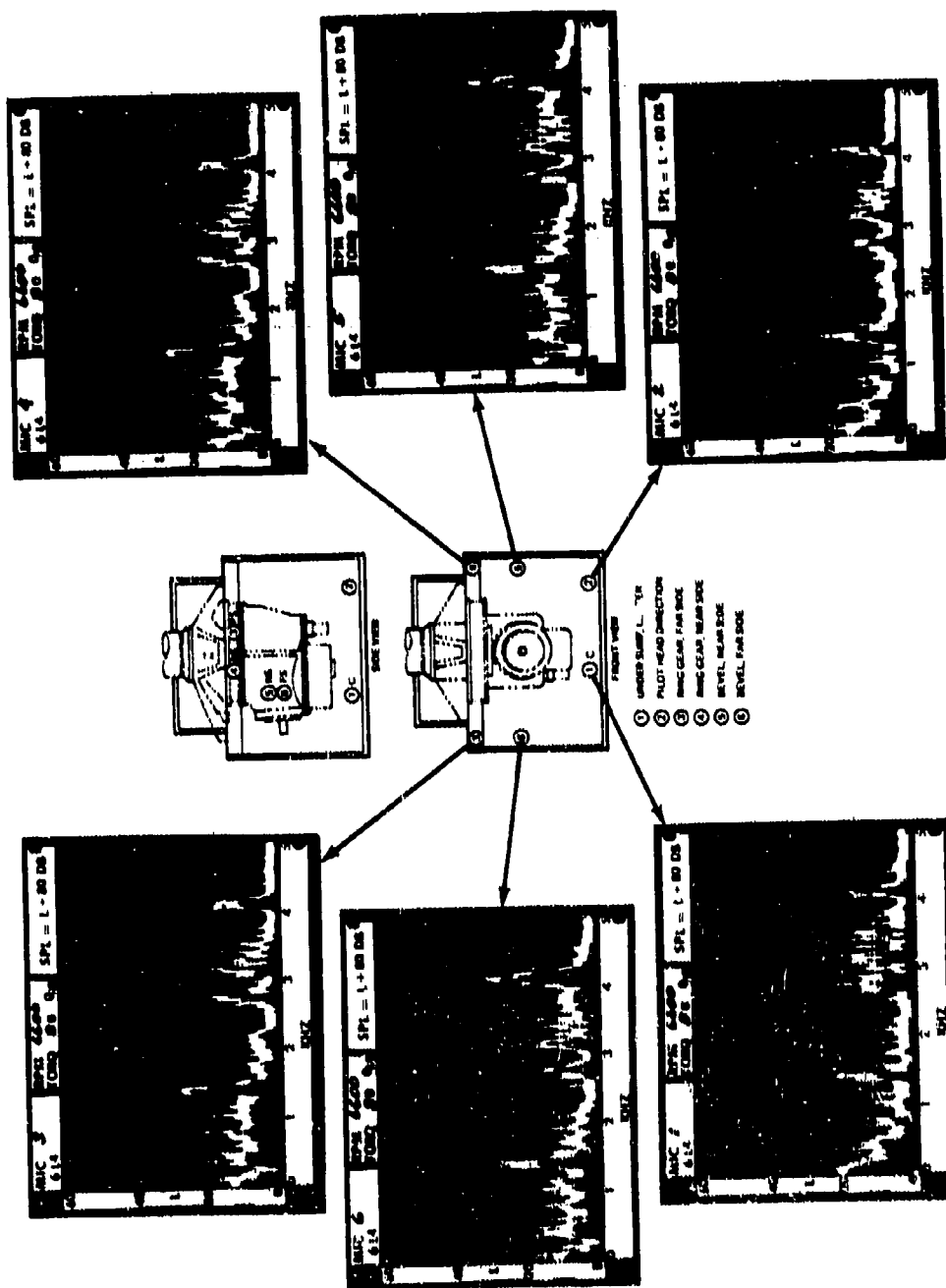


Figure A59. Microphone Data From Tape 6L4 With Detuned Sun Gear and Isolators at 6,600 RPM and 80-Percent Torque.

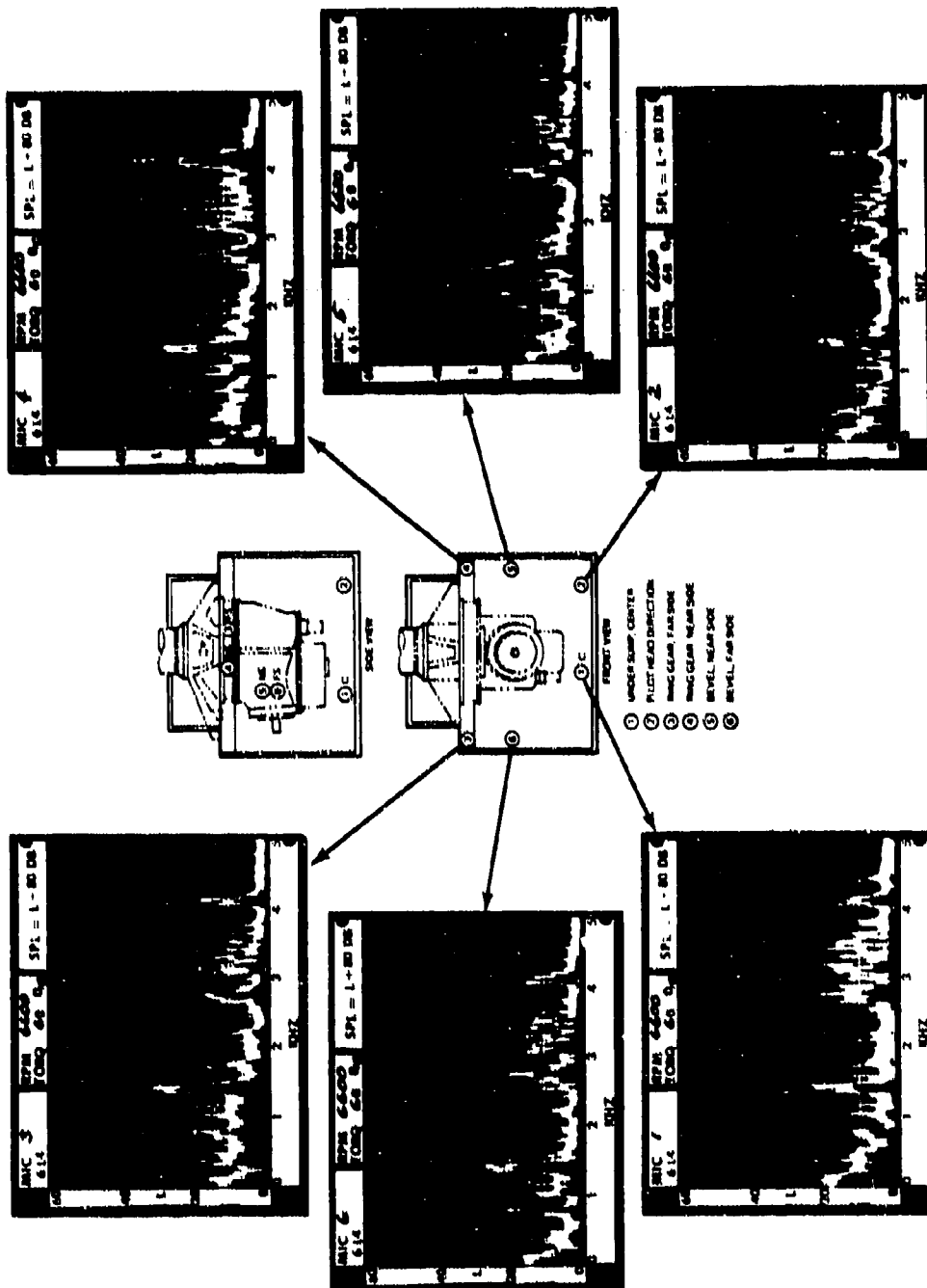


Figure A60. Microphone Data From Tape 6L4 With Detuned Sun Gear and Isolators at 6,600 RPM and 60-Percent Torque.

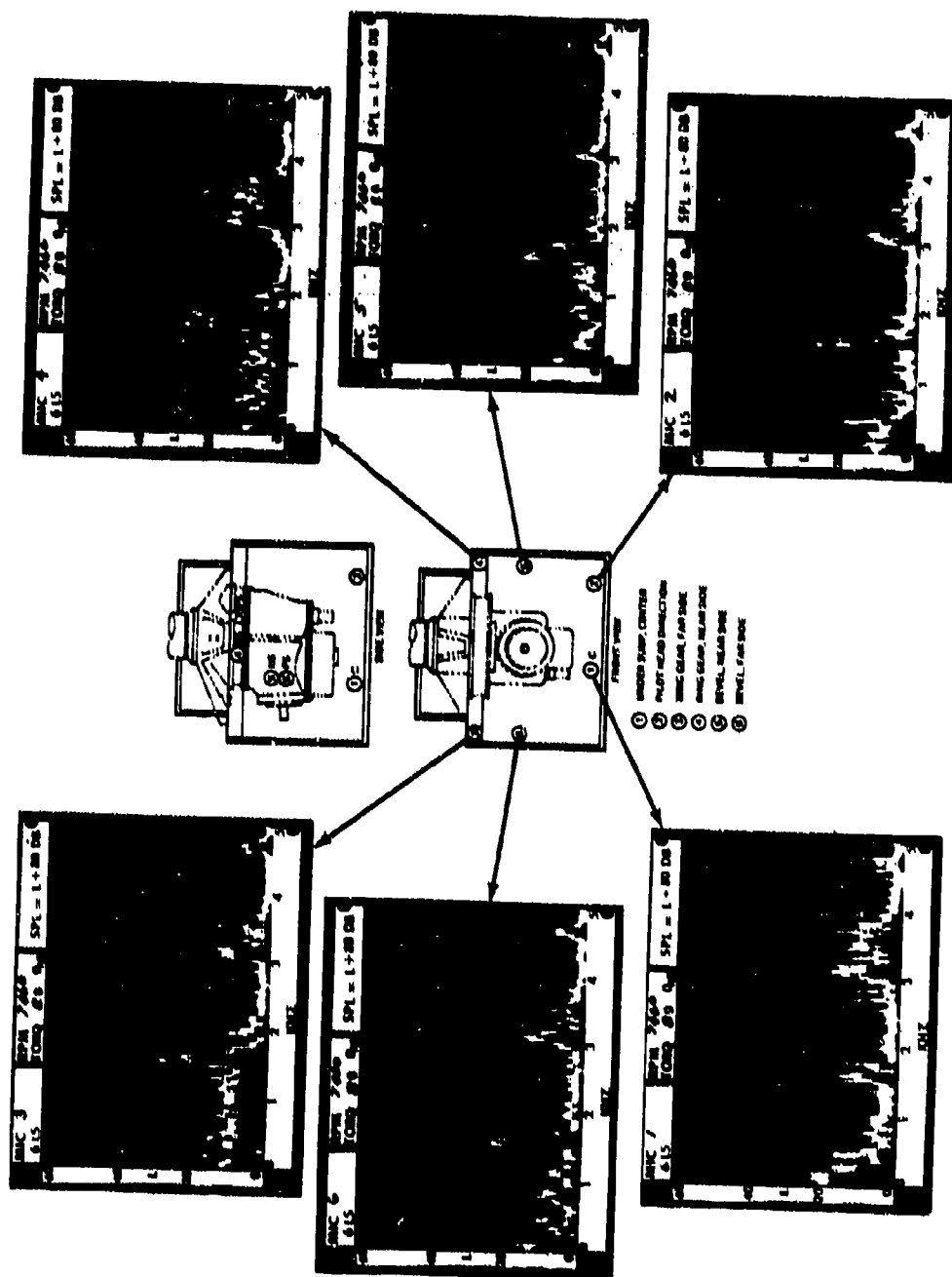


Figure A61. Microphone Data From Tape 615 With Detuning Magnesium Contour Plates, Detuned Sum Gear, and No Isolators at 7,460 RPM and 80-Percent Torque.

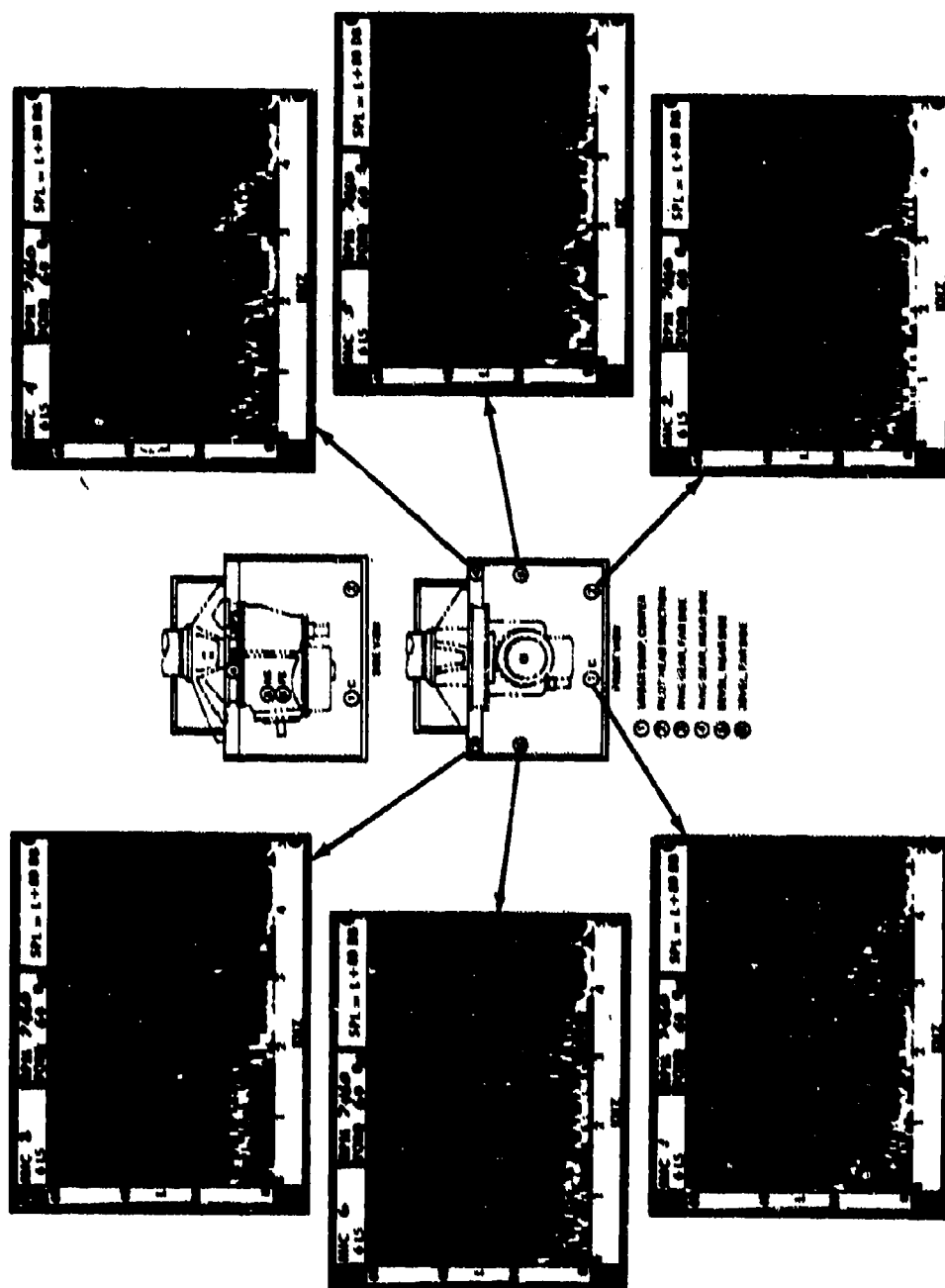
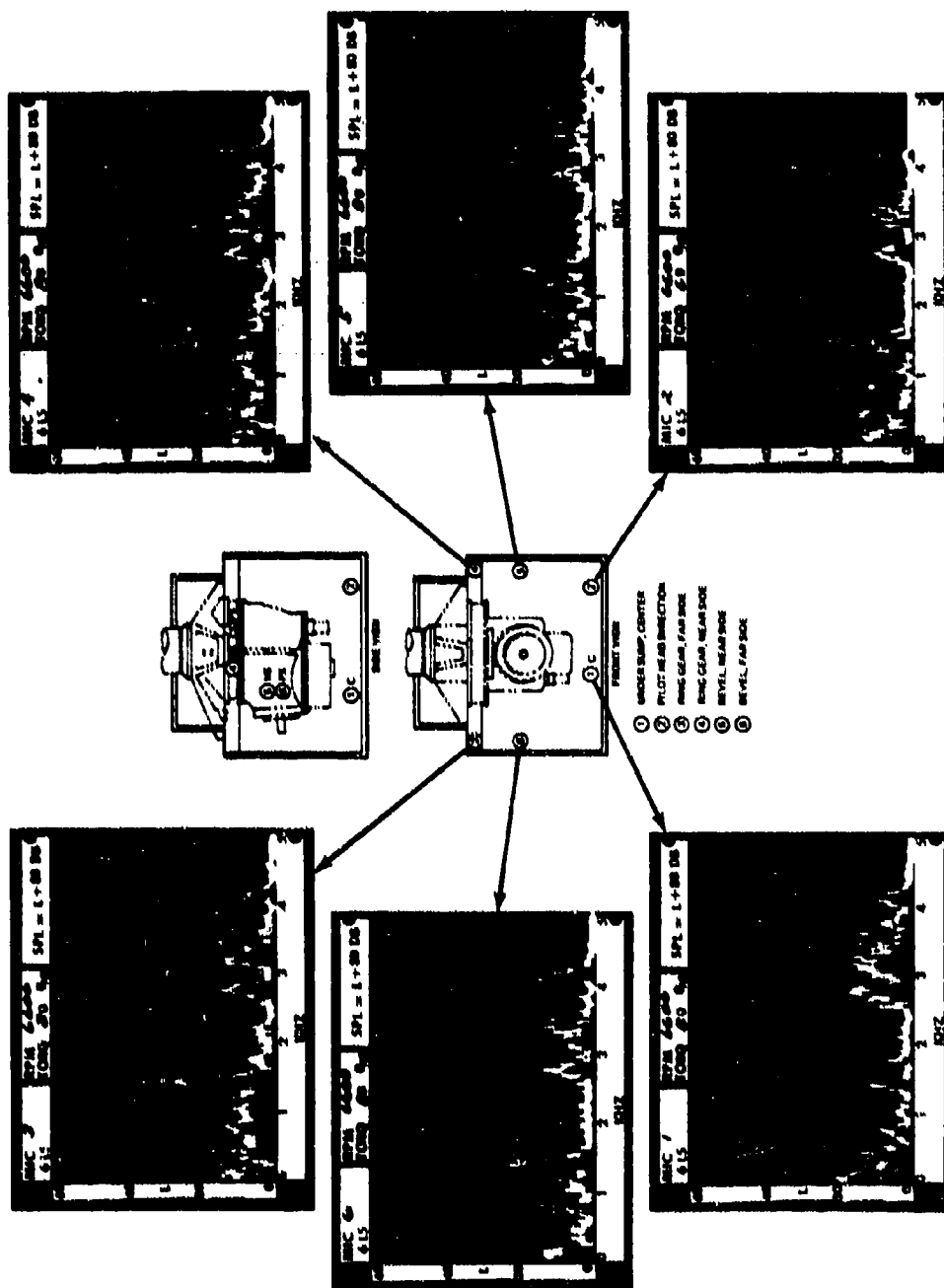


Figure A62. Microphone Data From Tape 6L5 With Detuning Magnesium Contour Plates, Detuned Sun Gear, and No Isolators at 7,460 RPM and 60-Percent Torque.



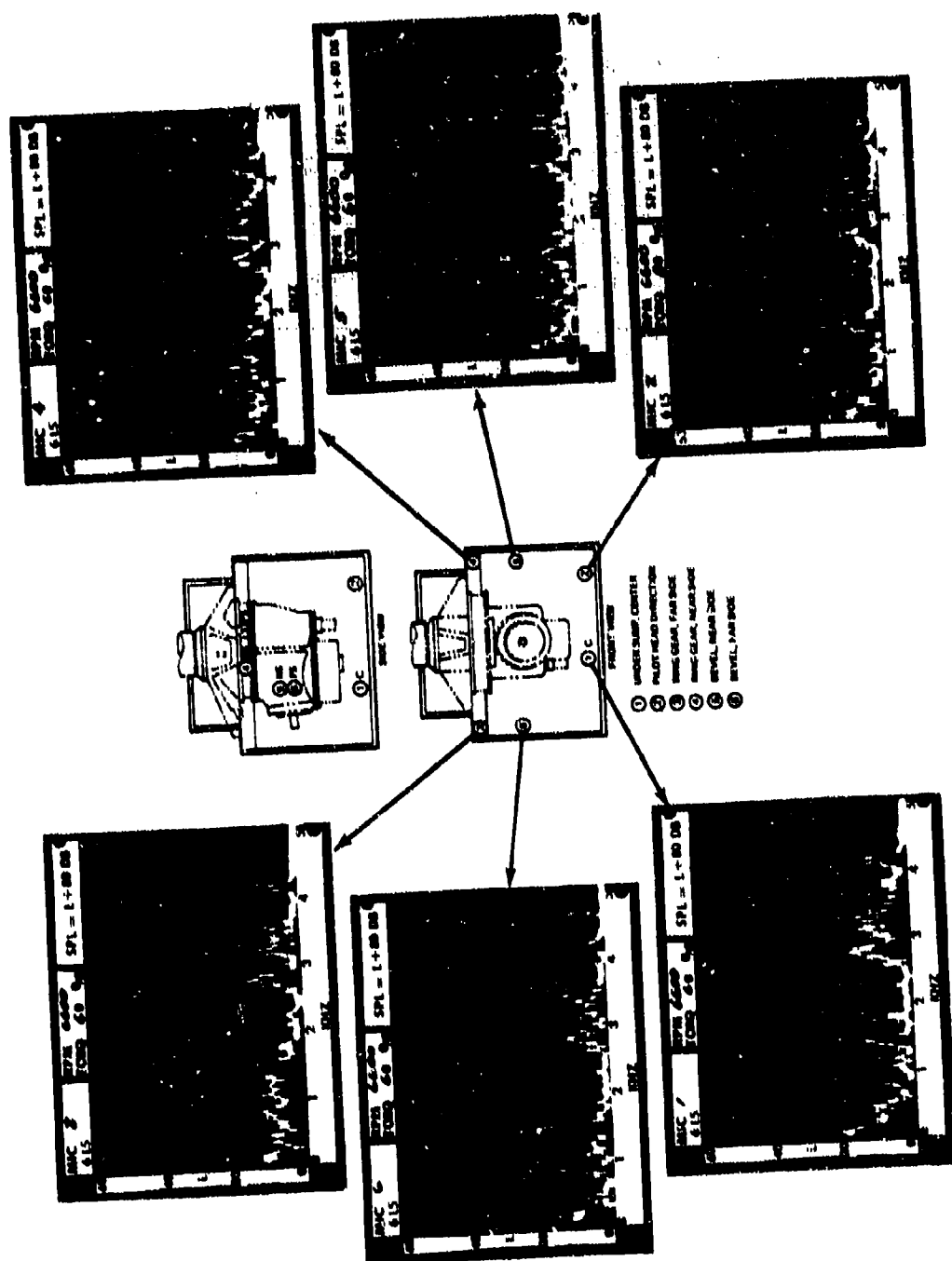


Figure A6-4. Microphone Data From Tape 6L5 With Detuning Magnesium Contour Plates, Detuned Sun Gear, and No Isolators at 6,600-RPM and 60-Percent Torque.

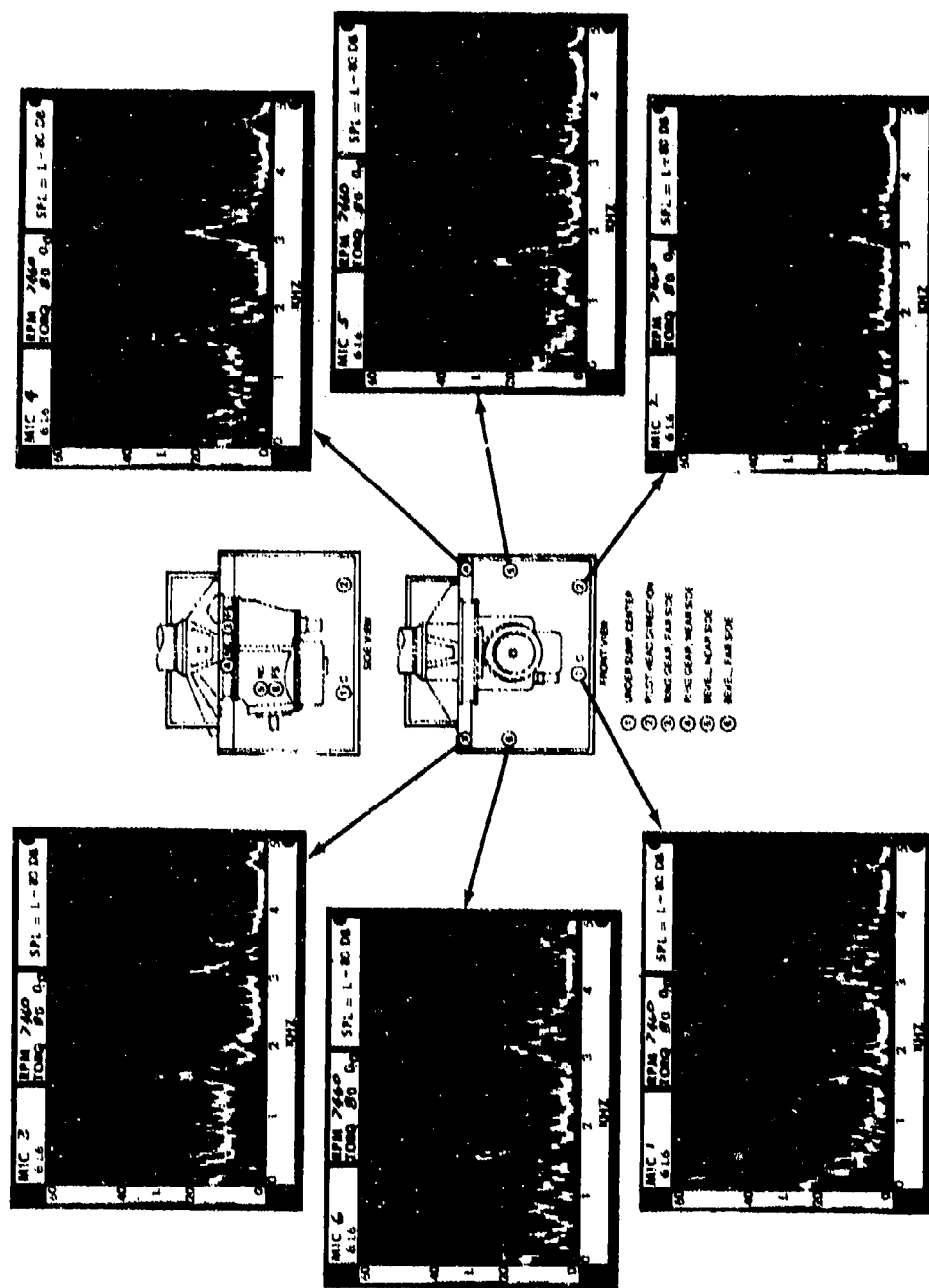


Figure A65. Microphone Data From Tape 6L6 With Detuning Magnesium Contour Plates, Original Sun Gear, and No Isolators at 7,460 RPM and 80-Percent Torque.

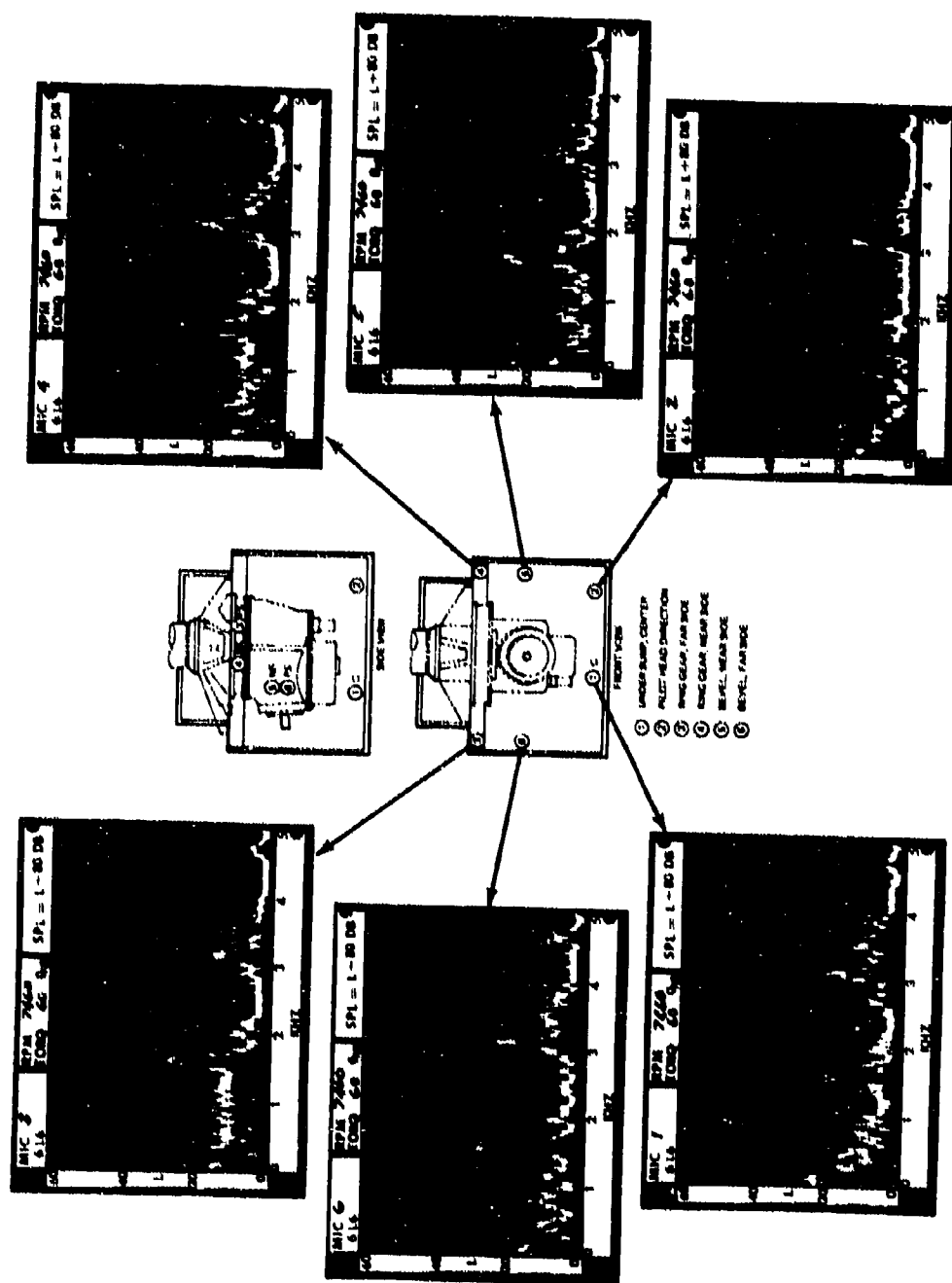


Figure A66. Microphone Data From Tape 6L6 With Detuning Magnesium Contour Plates, Original Sun Gear, and No Isolators at 7,460 RPM and 60-Percent Torque.

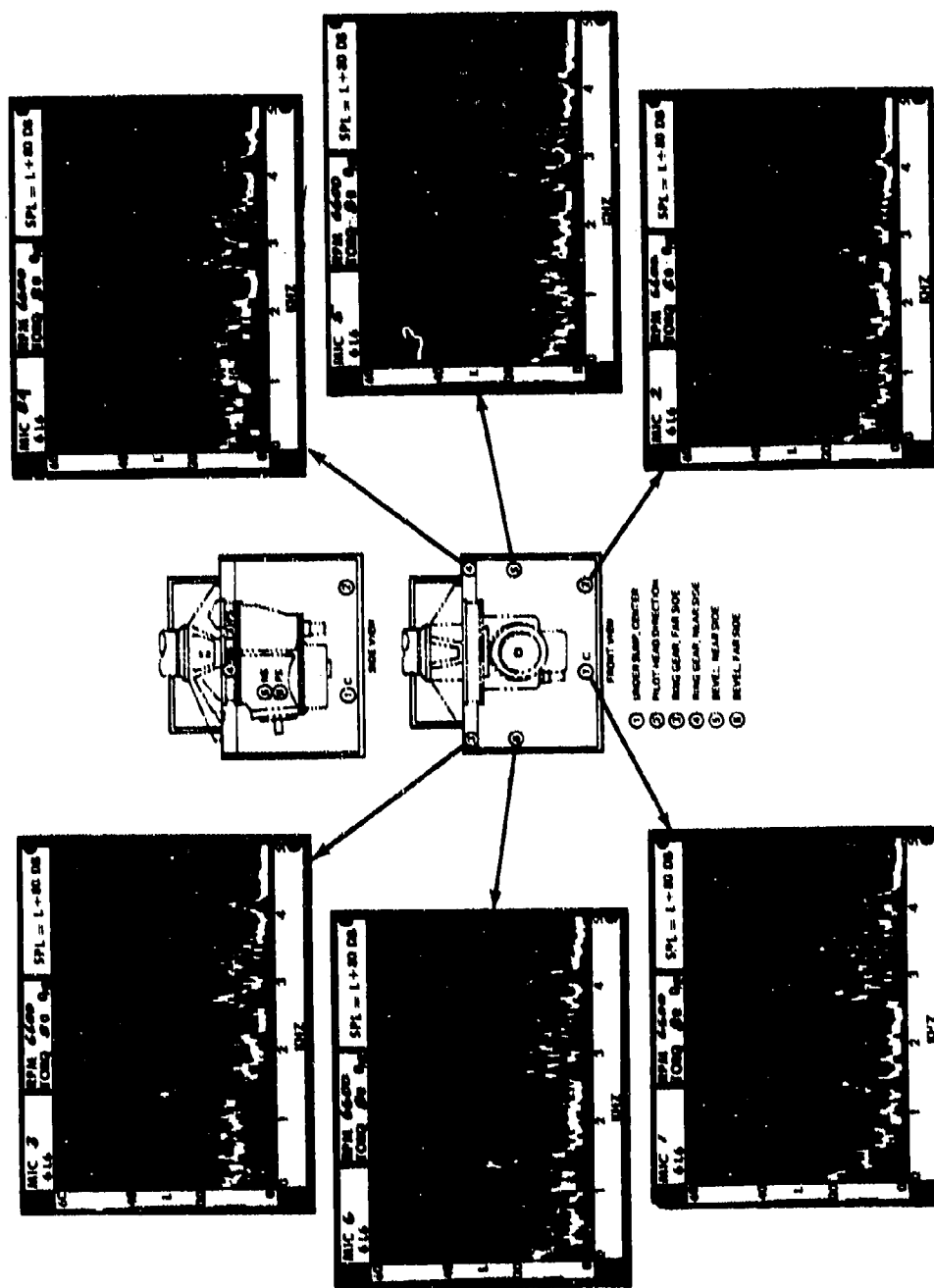


Figure A67. Microphone Data From Tape 6L6 With Detuning Magnesium Contour Plates, Original Sun Gear, and No Isolators at 6,600 RPM and 80-Percent Torque.

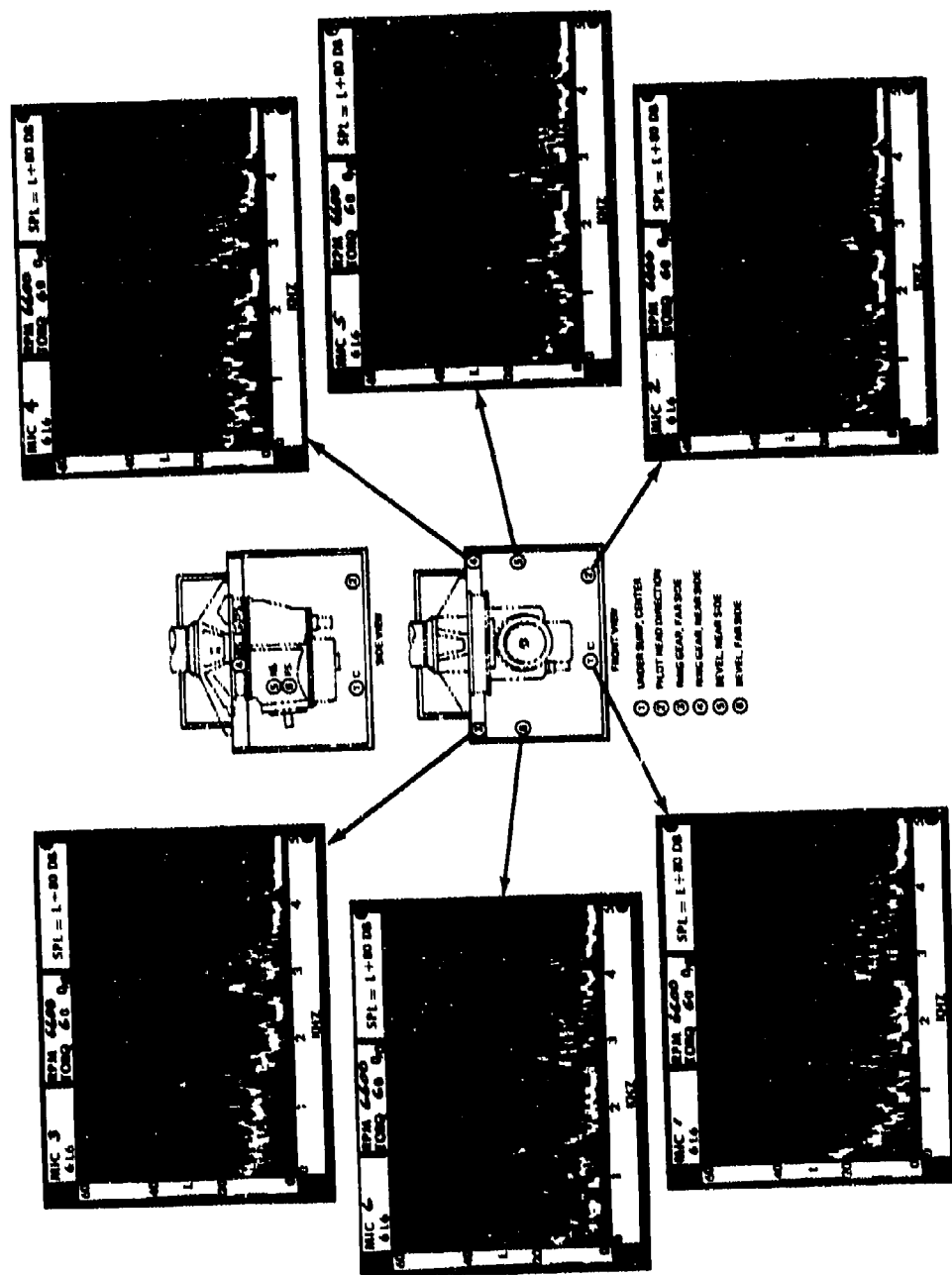


Figure A68. Microphone Data From Tape 6L6 With Detuning Magnesium Contour Plates, Original Sum Gear, and No Isolators at 6,600 RPM and 60-Percent Torque.

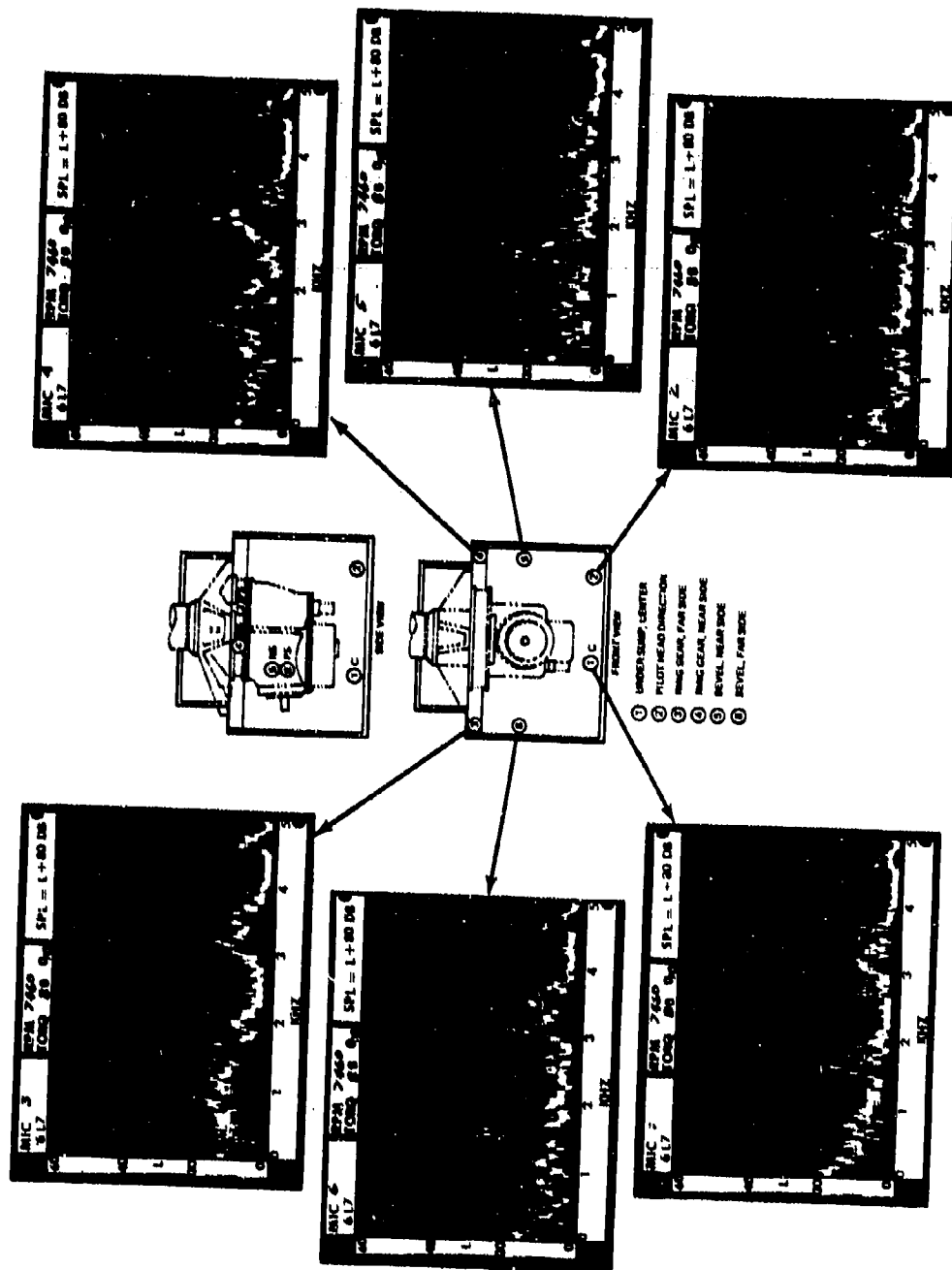


Figure A69. Microphone Data From Tape 6L7 With Detuning Magnesium Contour Plates, Original Sun Gear, Thickened Ring Gear, and No Isolators at 7,460 RPM and 80-Percent Torque.

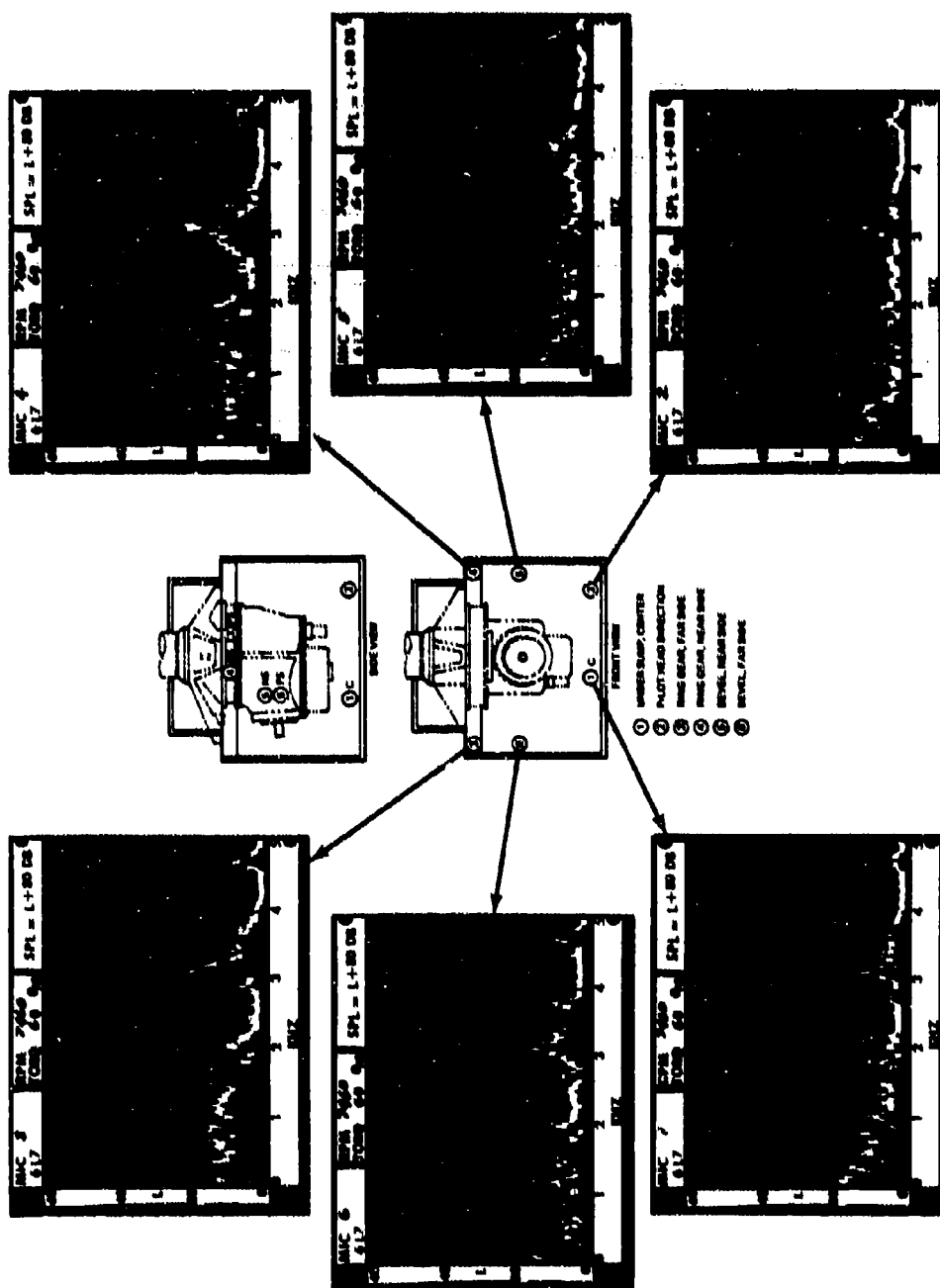


Figure A70. Microphone Data From Tape 6L7 With Detuning Magnesium Contour Plates, Original Sun Gear, Thickened Ring Gear, and No Isolators at 7,460 RPM and 60-Percent Torque.

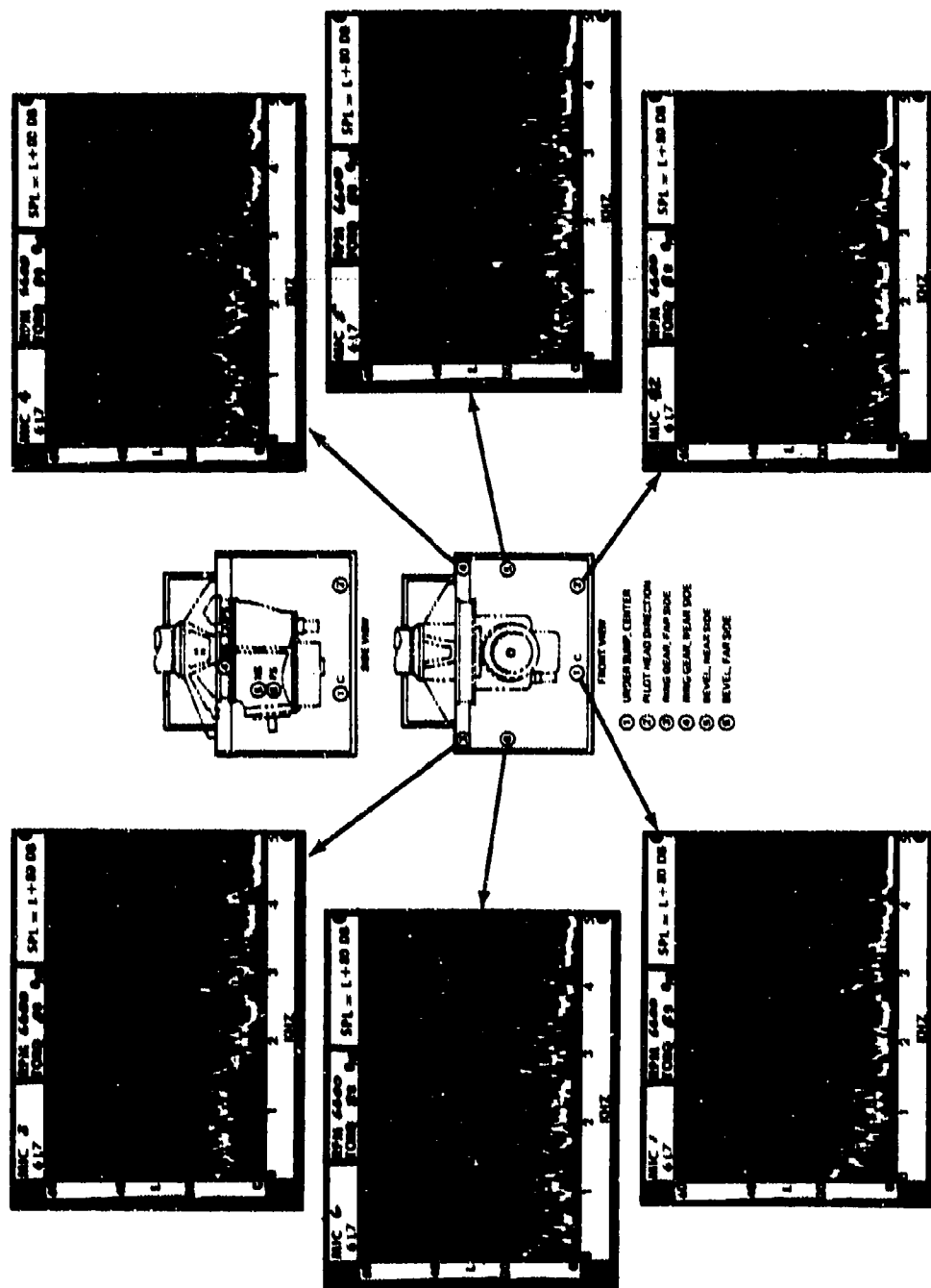


Figure A71. Microphone Data From Tape 6L7 With Detuning Magnesium Contour Plates, Original Sun Gear, Thickened Ring Gear, and No Isolators at 6,600 RPM and 80-Percent Torque.

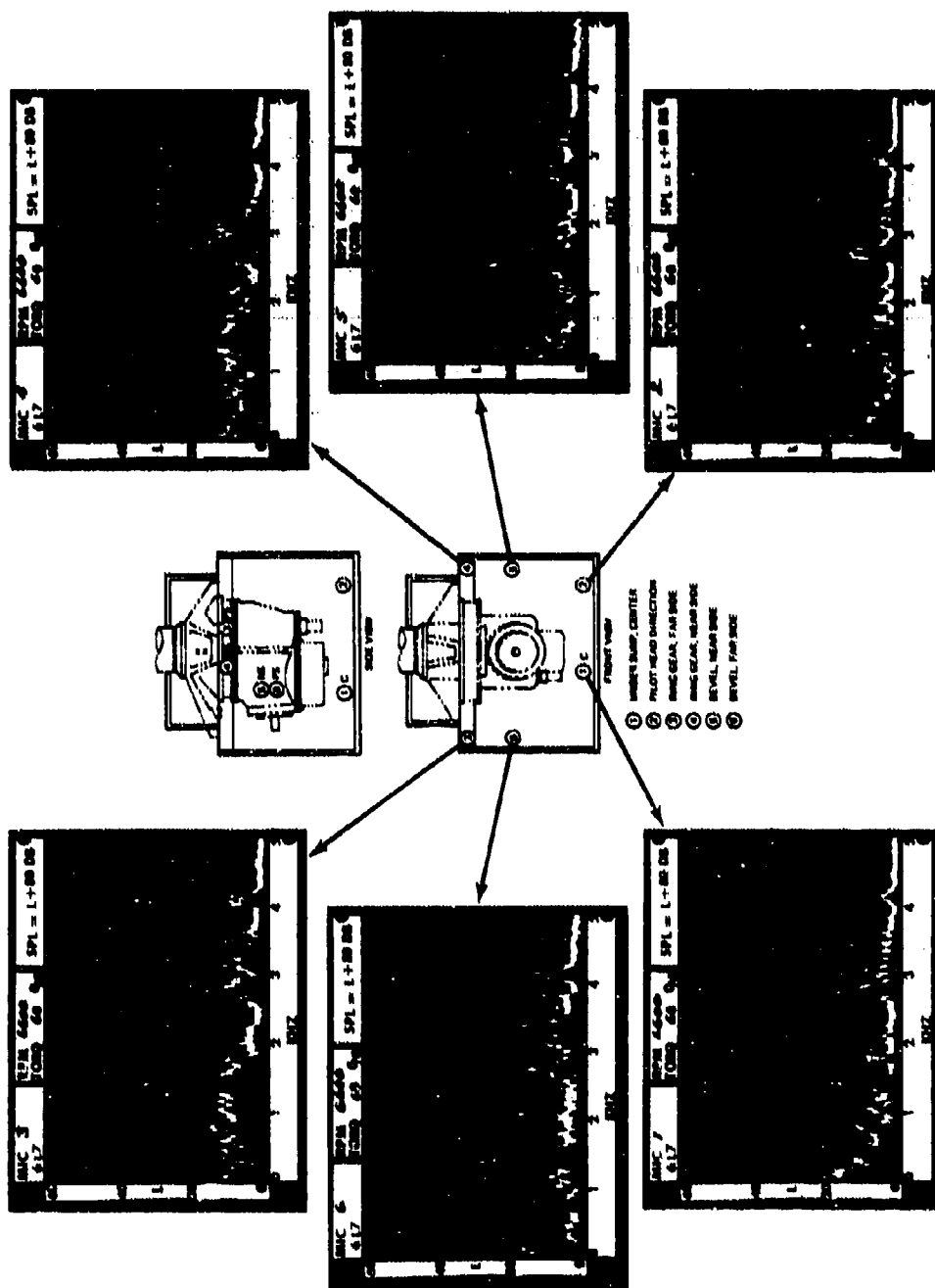


Figure A72 Microphone Data From Tape 6L7 With Detuning Magnesium Contour Plates, Original Sun Gear, Thickened Ring Gear, and No Isolators at 6,600 RPM and 60-Percent Torque.

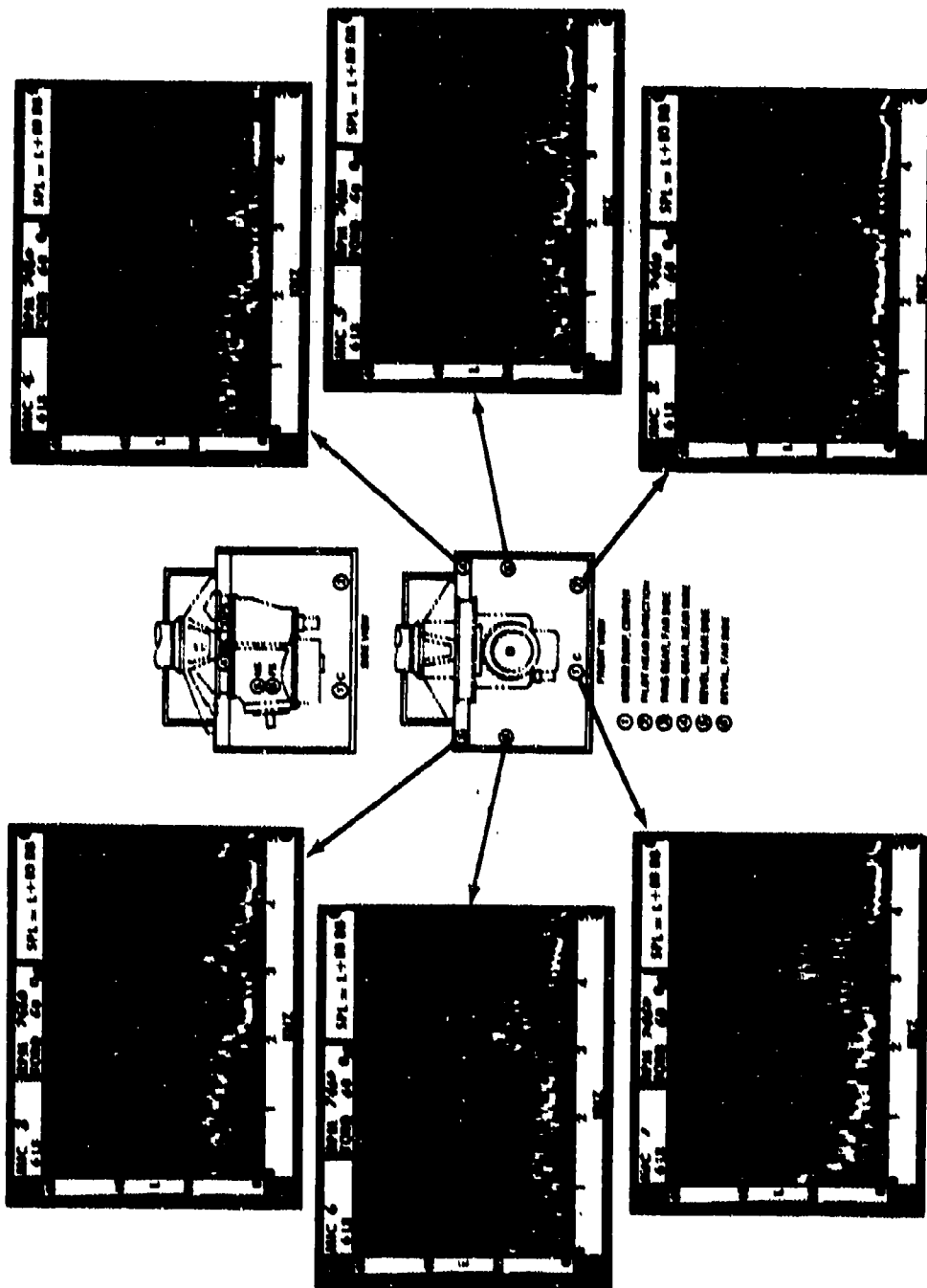


Figure A74. Microphone Data From Tape 6L8 With Detuning Magnesium Contour Plates, Detuned Sum Gear, Thickened Ring Gear, and No Isolators at 7,460 RPM and 60-Percent Torque.

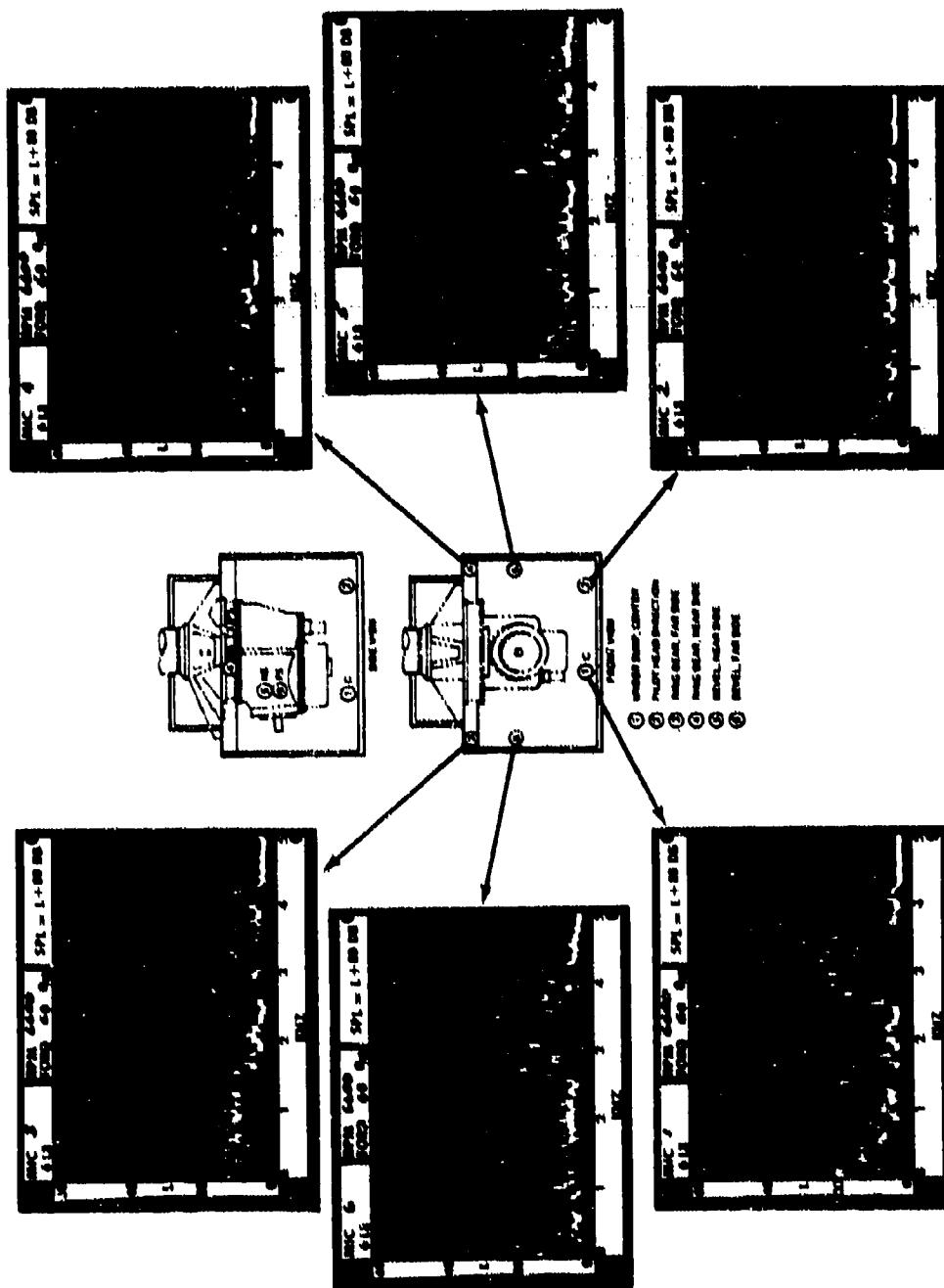


Figure A76. Microphone Data From Tape 6L8 With Detuning Magnesium Contour Plates, Detuned Sun Gear, Thickened Ring Gear, and No Isolators at 6,600 RPM and 60-Percent Torque.

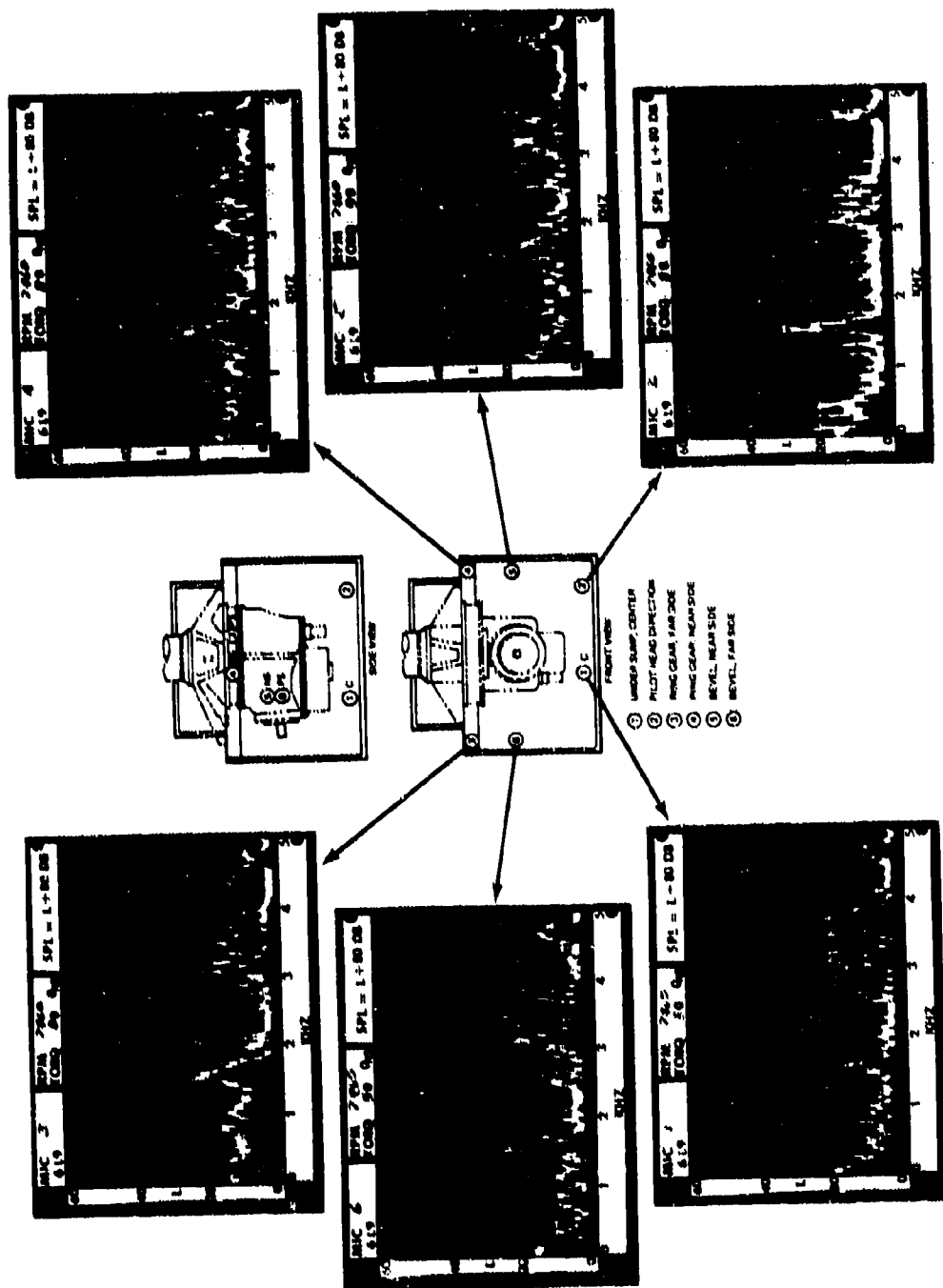


Figure A77. Microphone Data From Tape 6L9 With Detuning Magnesium Contour Plates, Detuned Sun Gear, Thickened Ring Gear, and Isolators at 7,460 RPM and 80-Percent Torque.

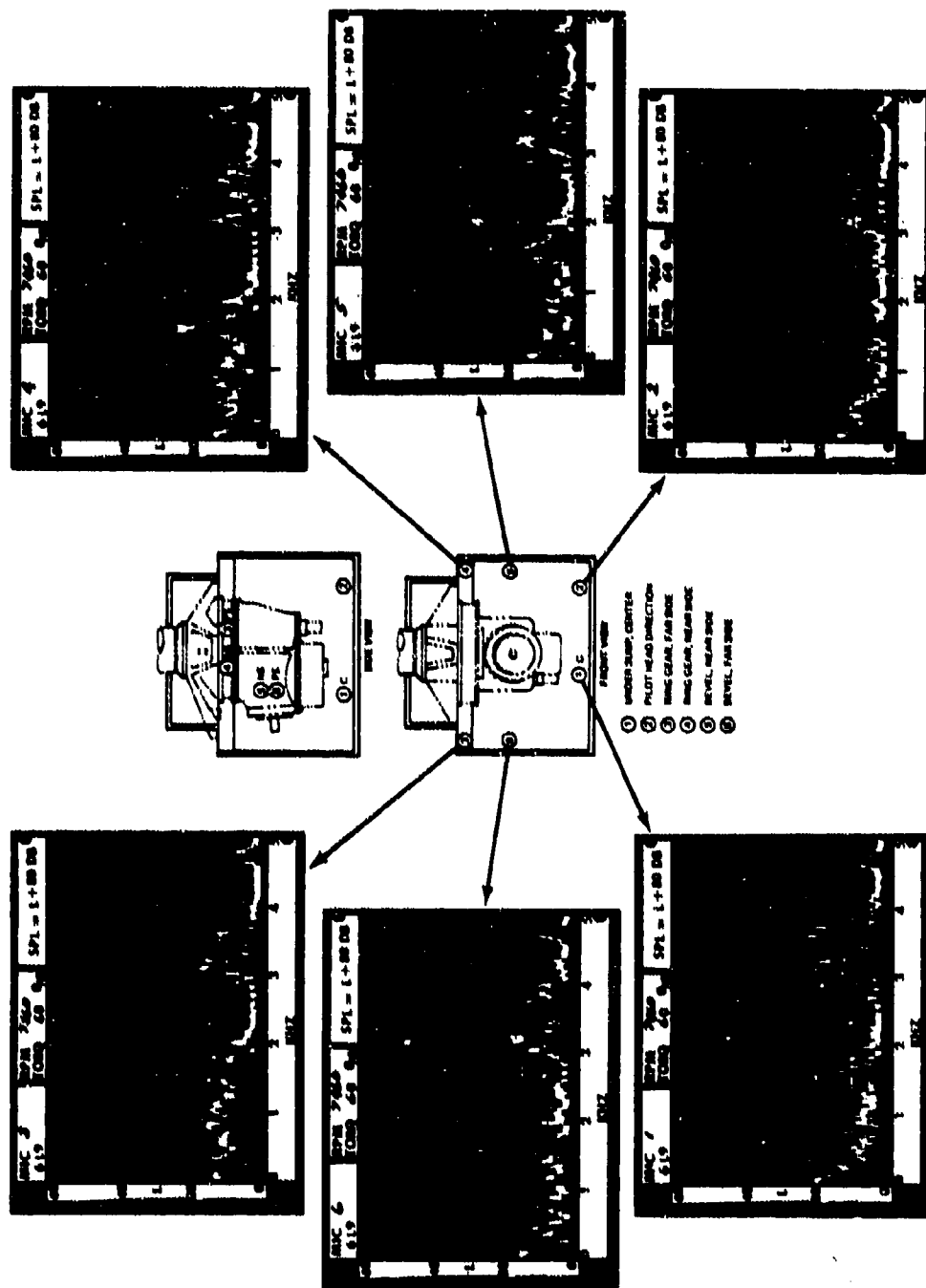


Figure A78. Microphone Data From Tape 6L9 With Detuning Magnesium Contour Plates, Detuned Sun Gear, Thickened Ring Gear, and Isolators at 7,460 RPM and 60-Percent Torque.

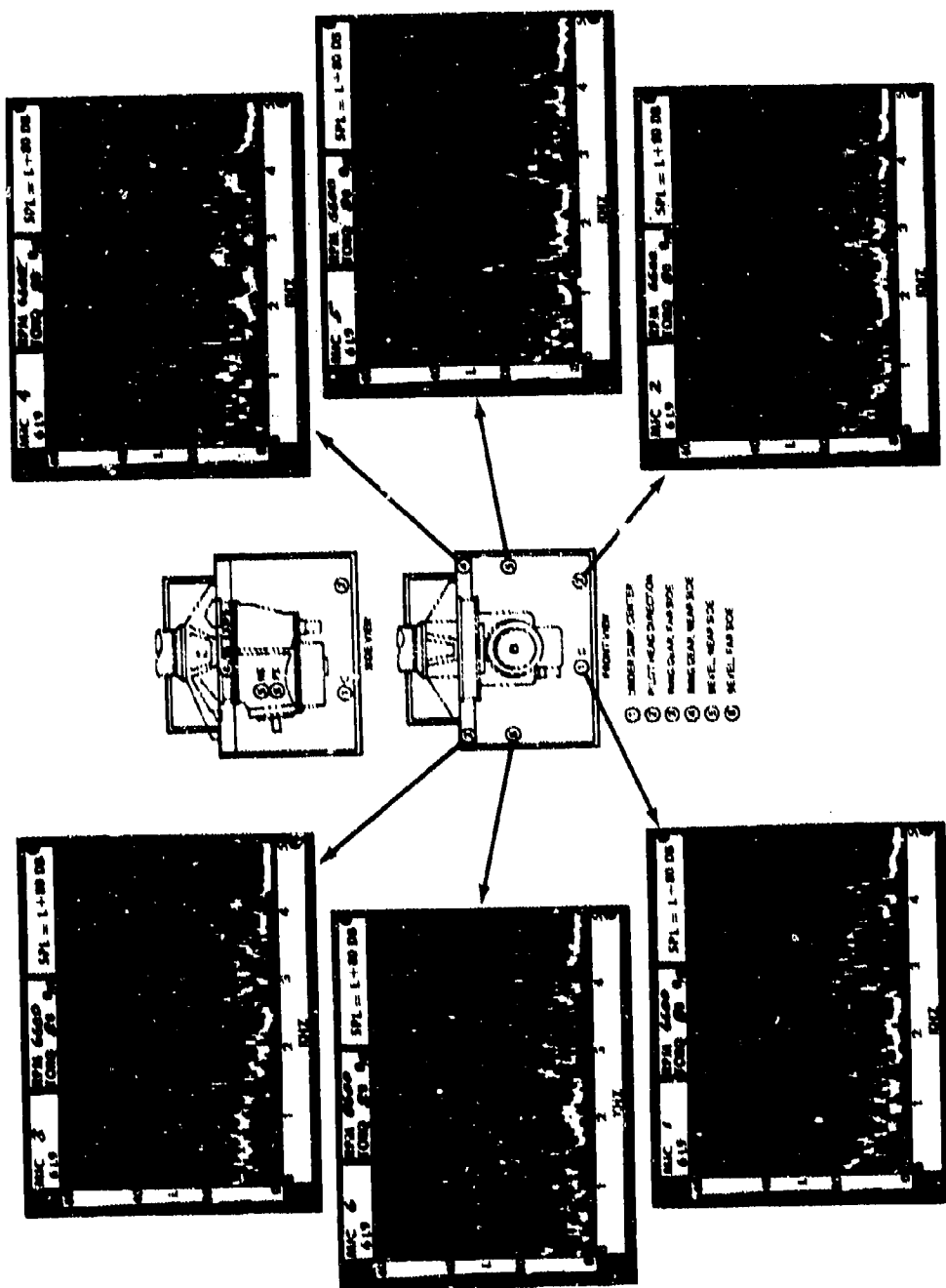


Figure A79. Microphone Data From Tape 6L9 With Detuning Magnesium Contour Plates, Detuned Sun Gear, Thickened Ring Gear, and Isolators at 6,600 RPM and 80-Percent Torque.

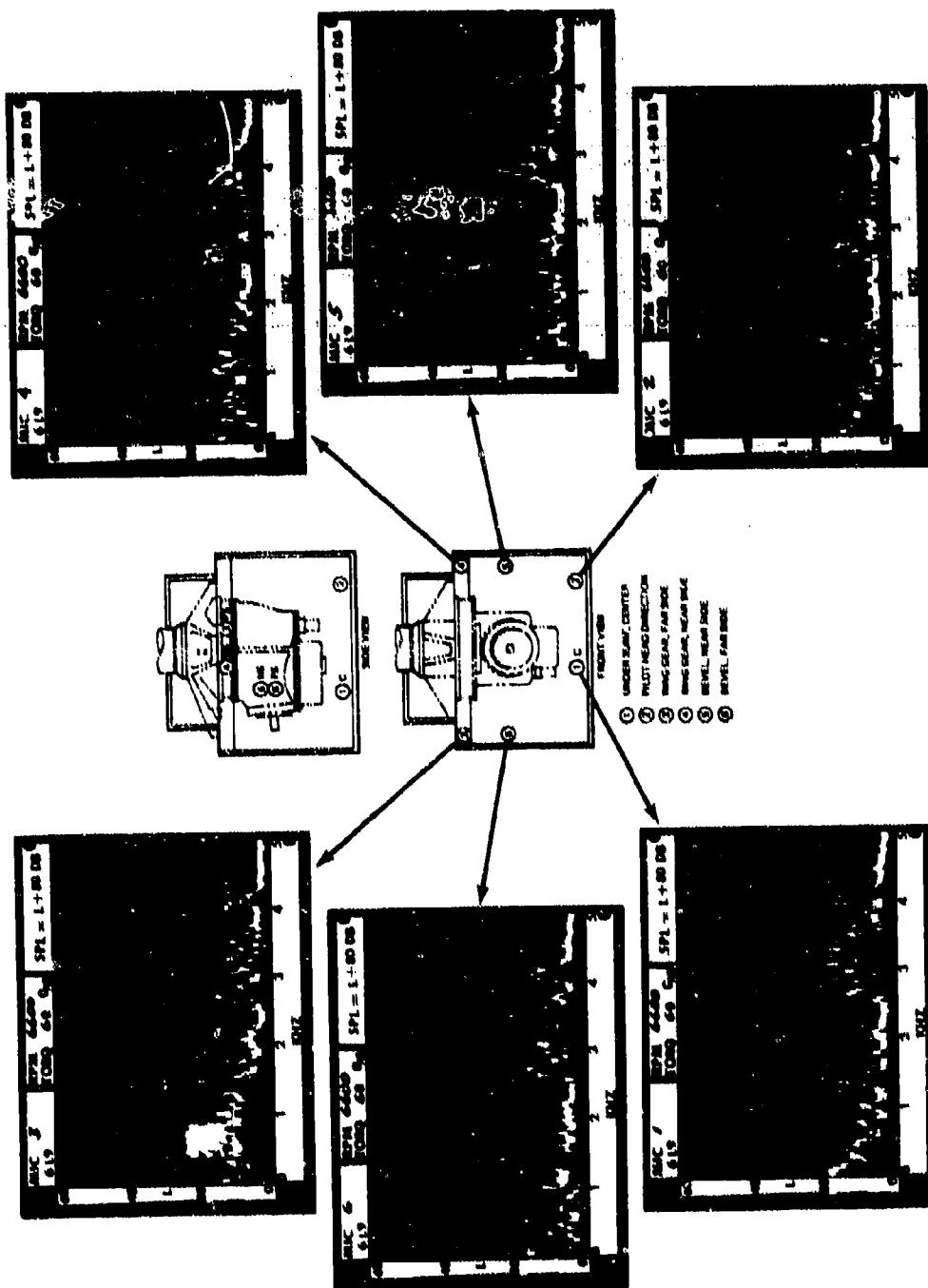
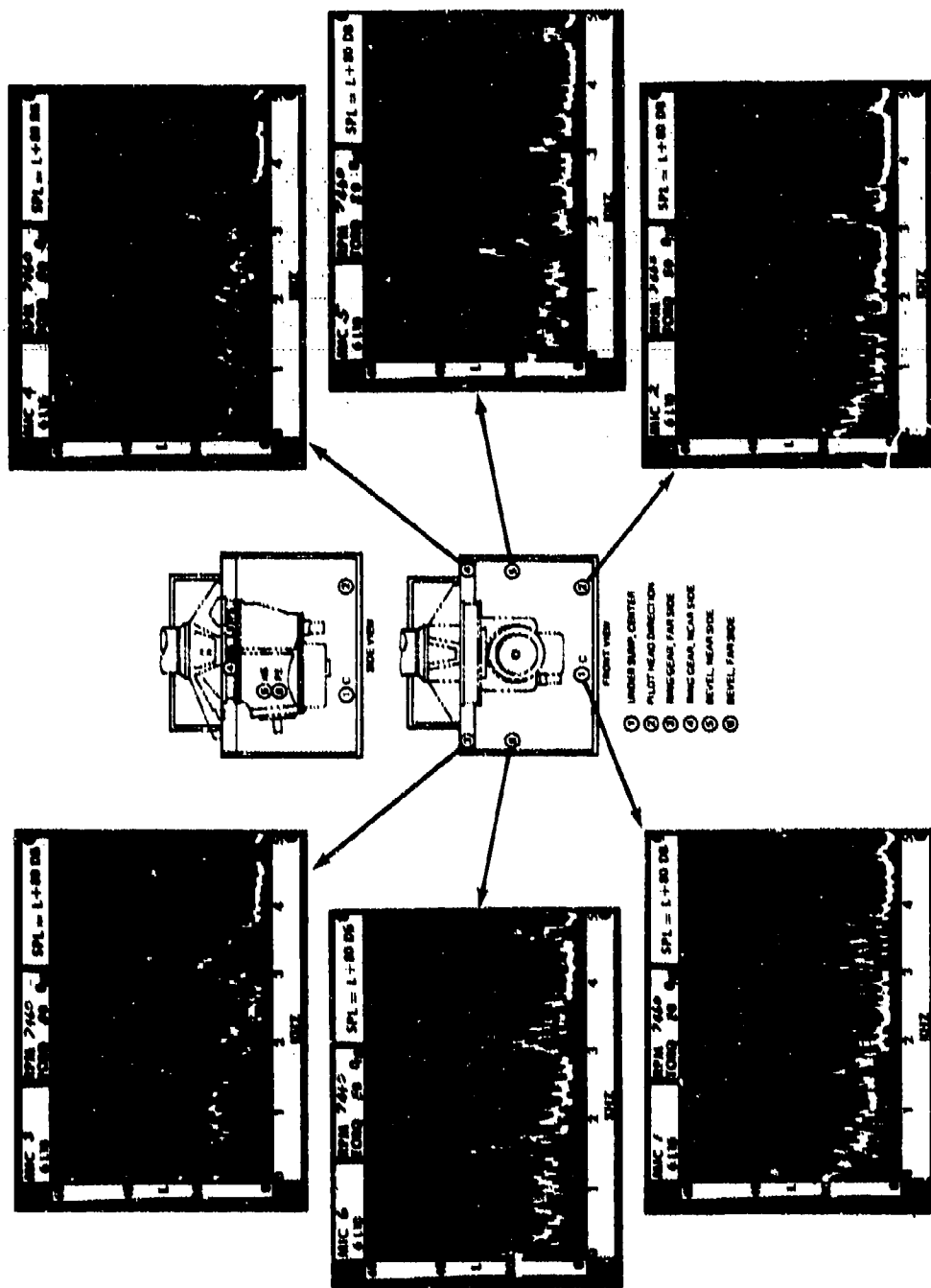


Figure A80. Microphone Data From Tape 6L9 With Detuning Magnesium Contour Plates, Detuned Sun Gear, Thickened Ring Gear, and Isolators at 6,600 RPM and 60-Percent Torque.



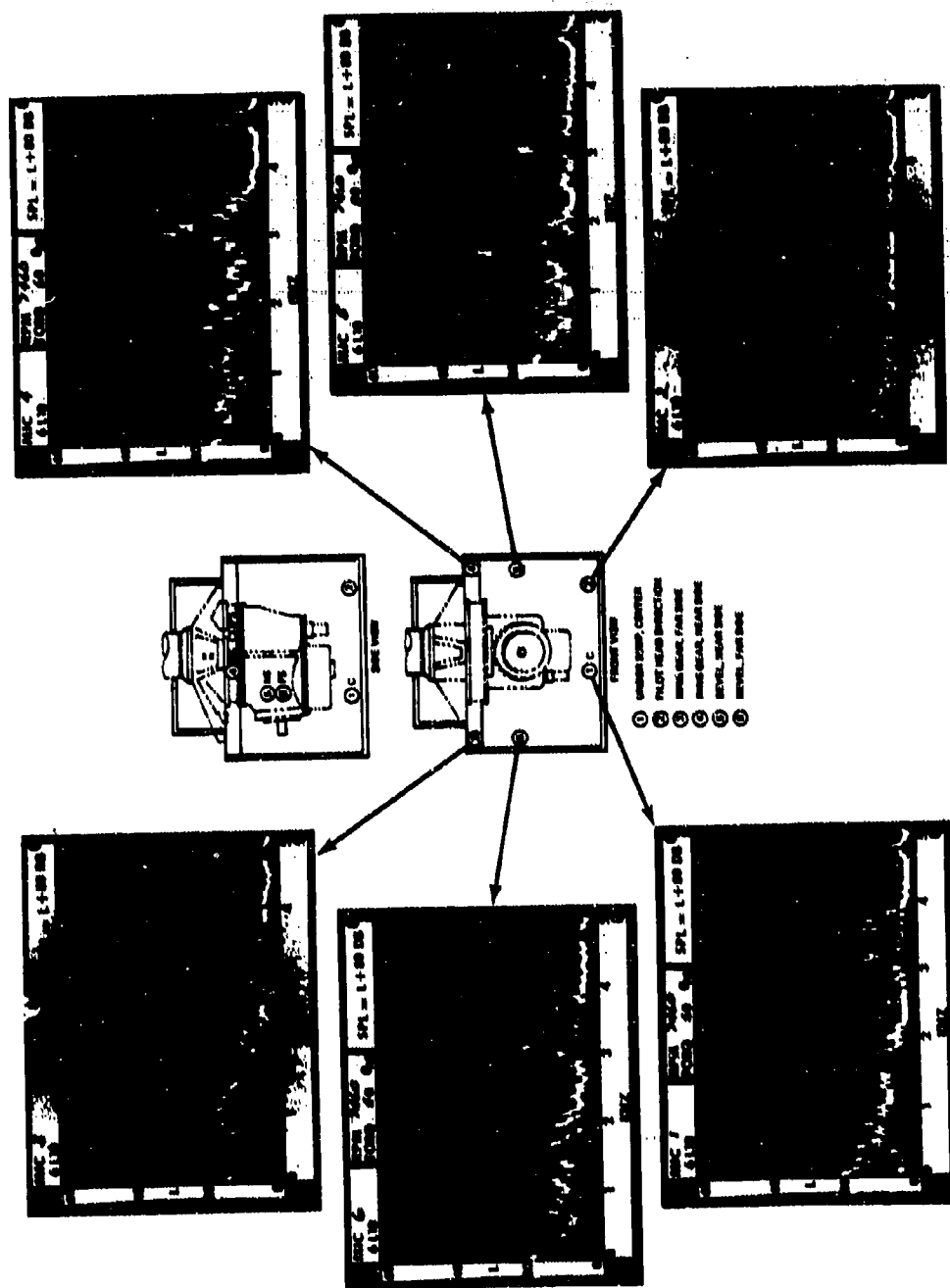


Figure A82. Microphone Data From Tape 6L1G With Detuning Graphite-Aluminum Composite Contour Plates and Detuned Sun Gear at 7,460 RPM and 60-Percent Torque.

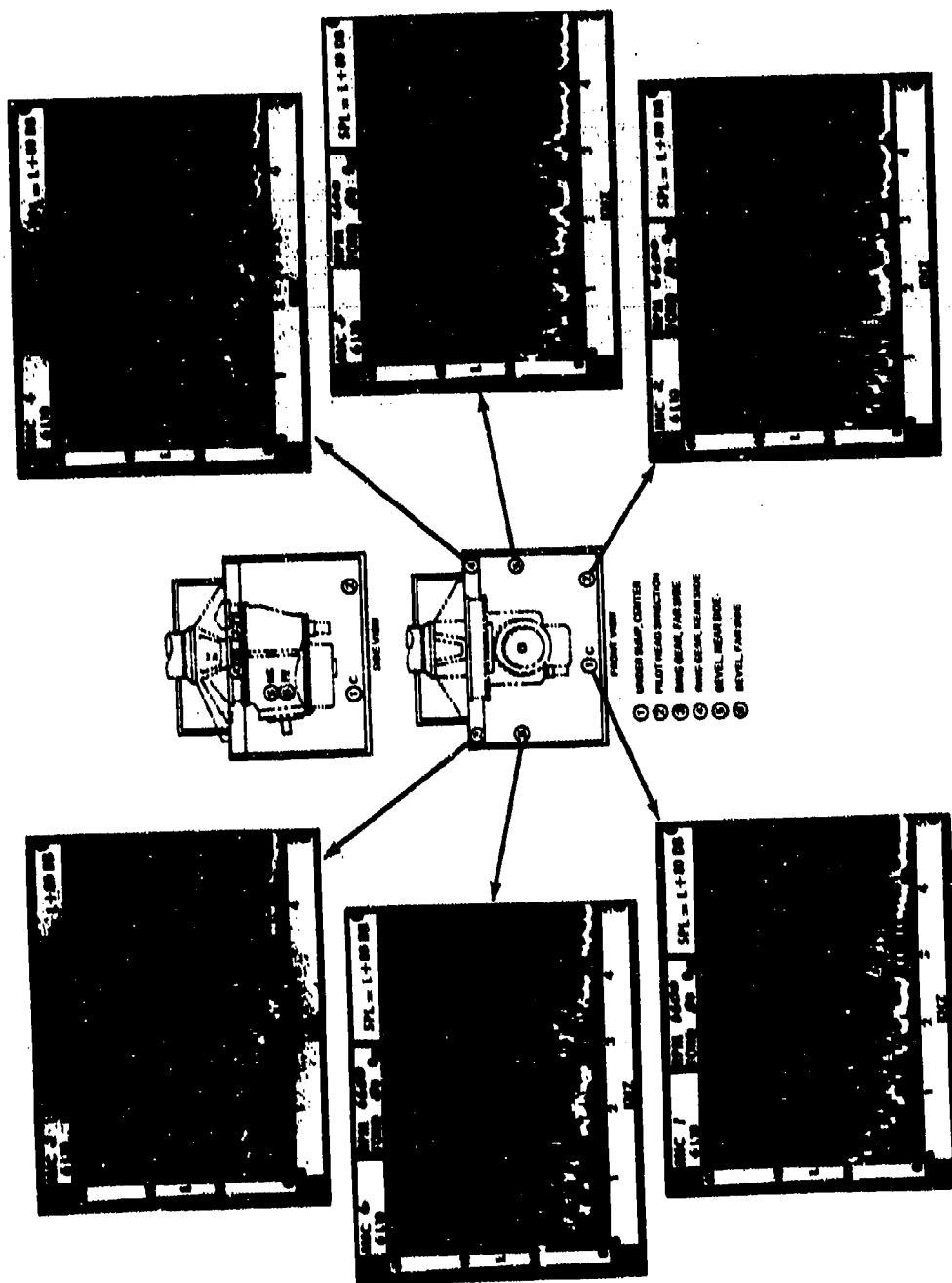


Figure A83. Microphone Data From Tape 6L10 With Detuning Graphite-Aluminum Composite Contour Plates and Detuned Sun Gear at 6,600 RPM and 80-Percent Torque.

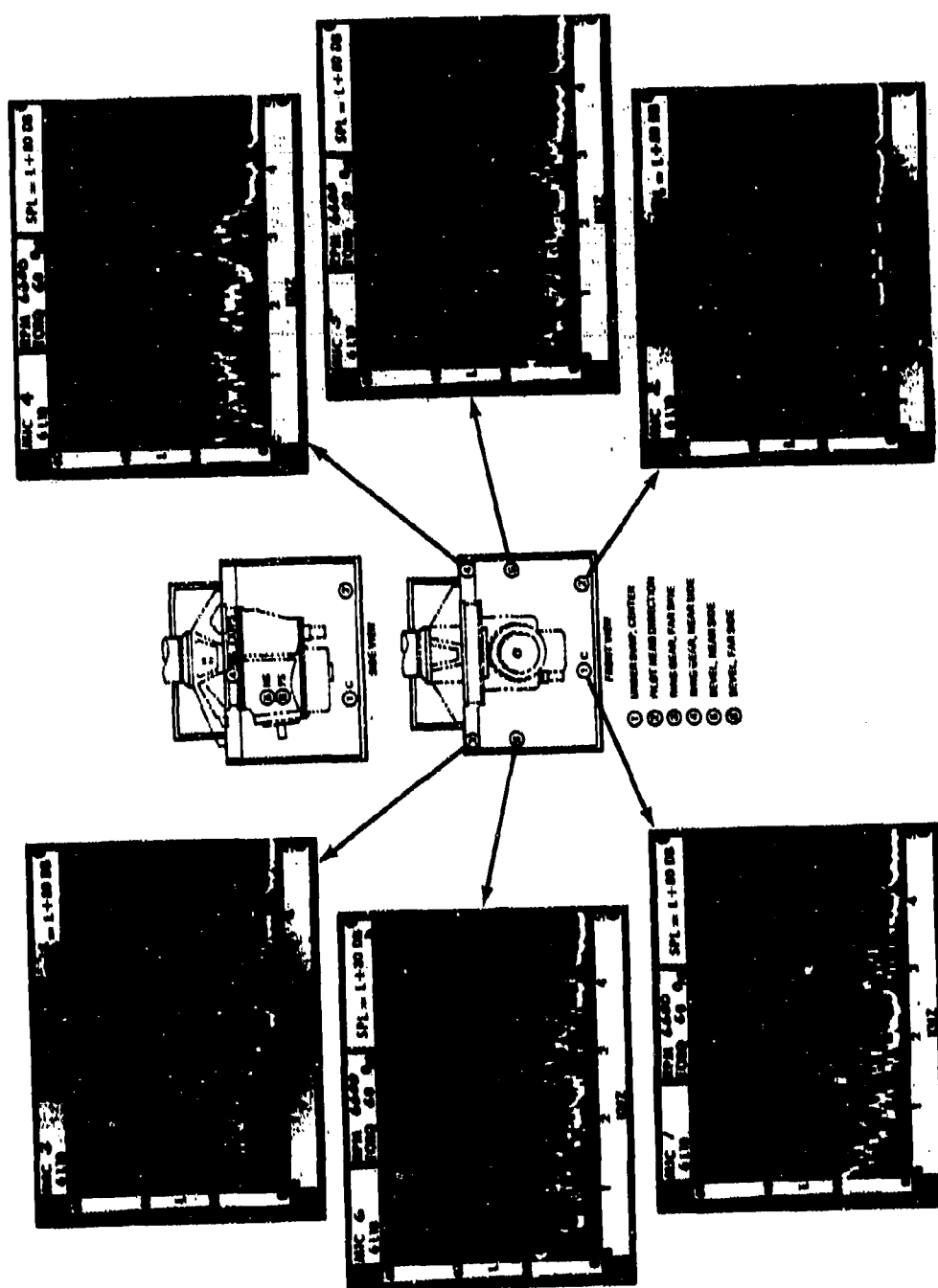


Figure A84. Microphone Data From Tape 6L10 With Detuning Graphite-Aluminum Composite Contour Plates and Detuned Sun Gear at 6,600 RPM and 60-Percent Torque.

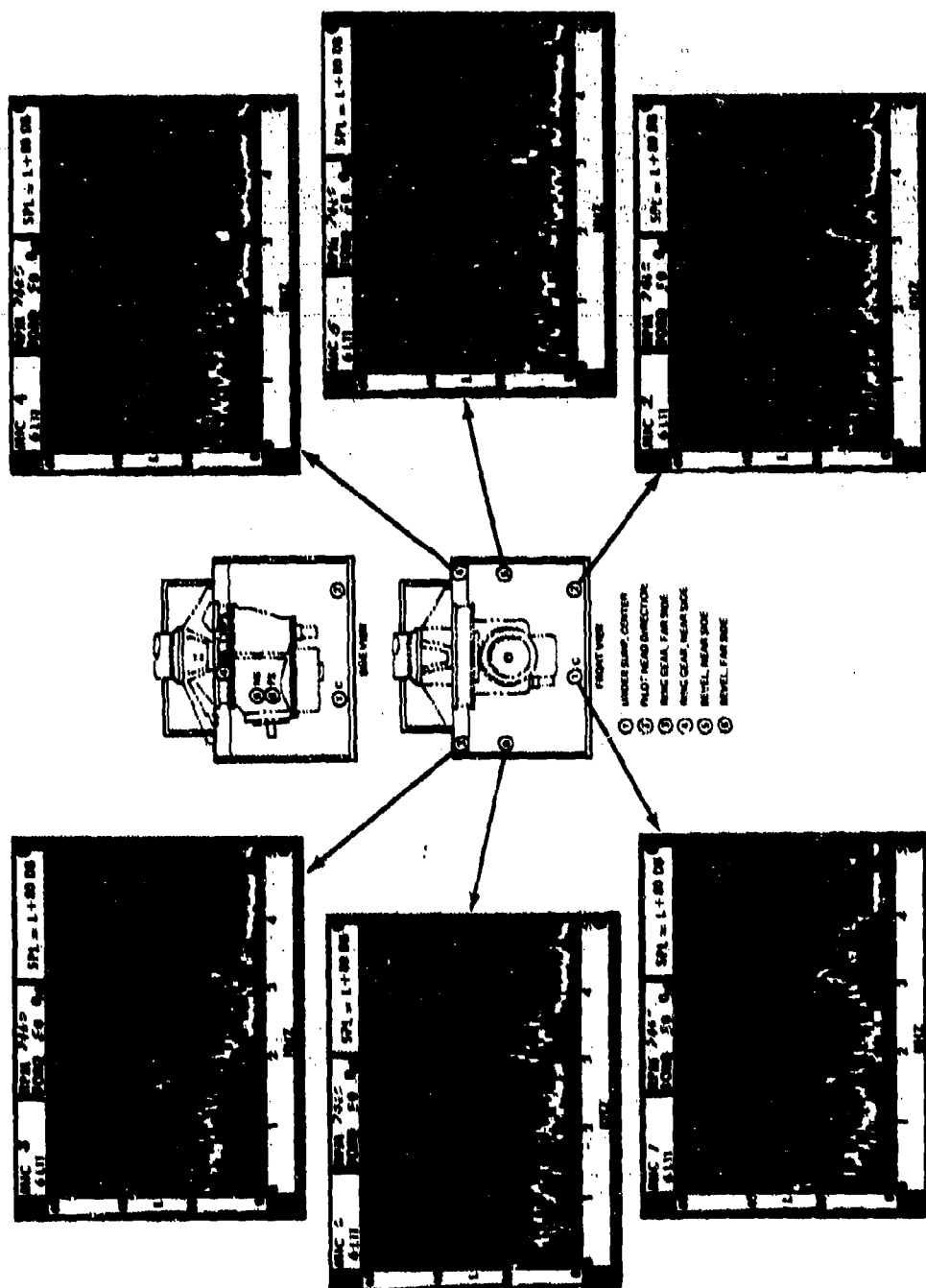


Figure A85. Microphone Data From Tape 6L1.1 With Detuning Graphite-Aluminum Composite Contour Plates at 7,460 RPM and 80-Percent Torque.

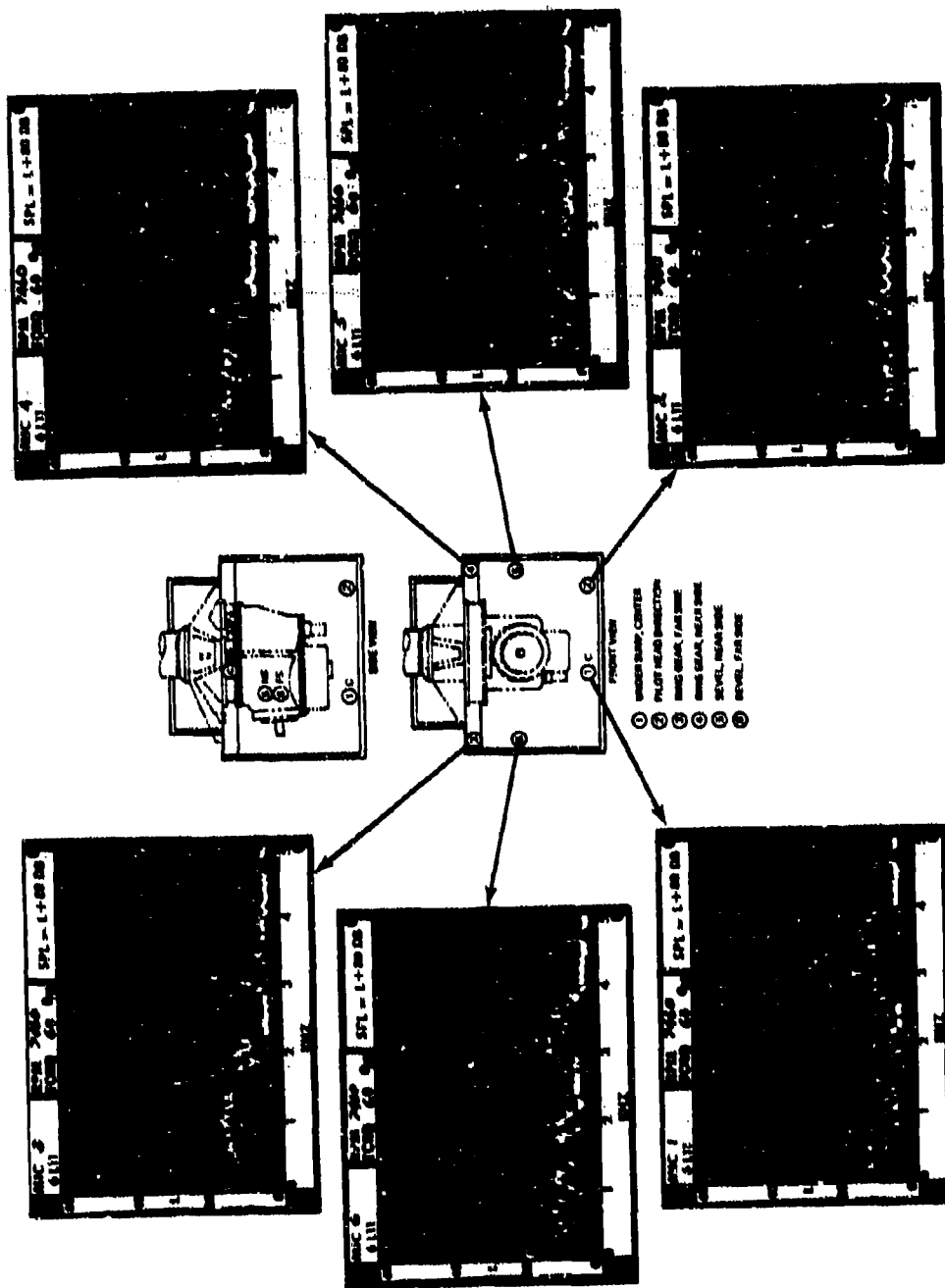


Figure A86. Microphone Data From Tape 6L11 With Detuning Graphite-Aluminum Composite Contour Plates at 7,460 RPM and 60-Percent Torque.

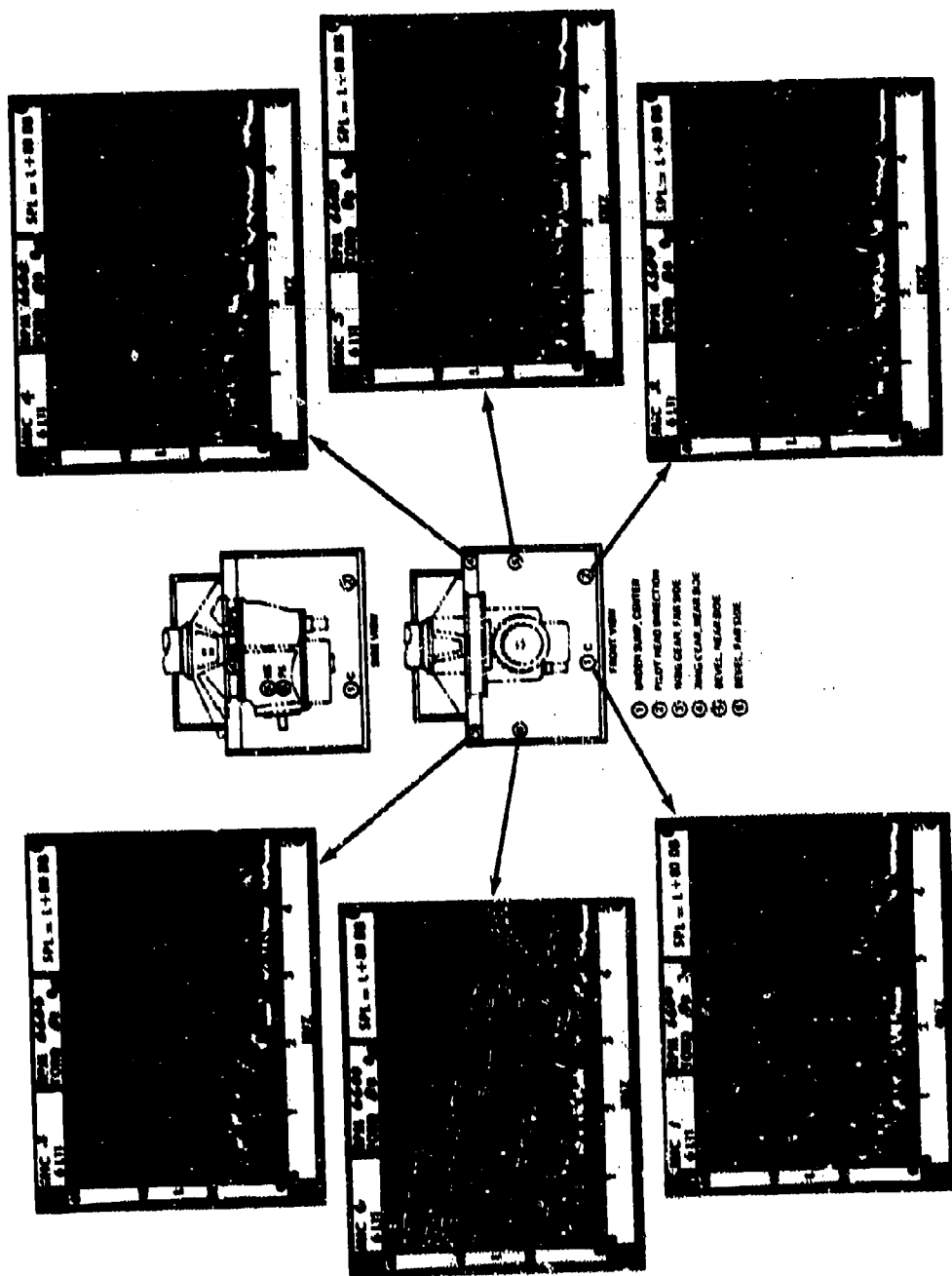


Figure A87. Microphone Data From Tape 6L11 With Detuning Graphite-Aluminum Composite Contour Plates at 6,600 RPM and 80-Percent Torque.

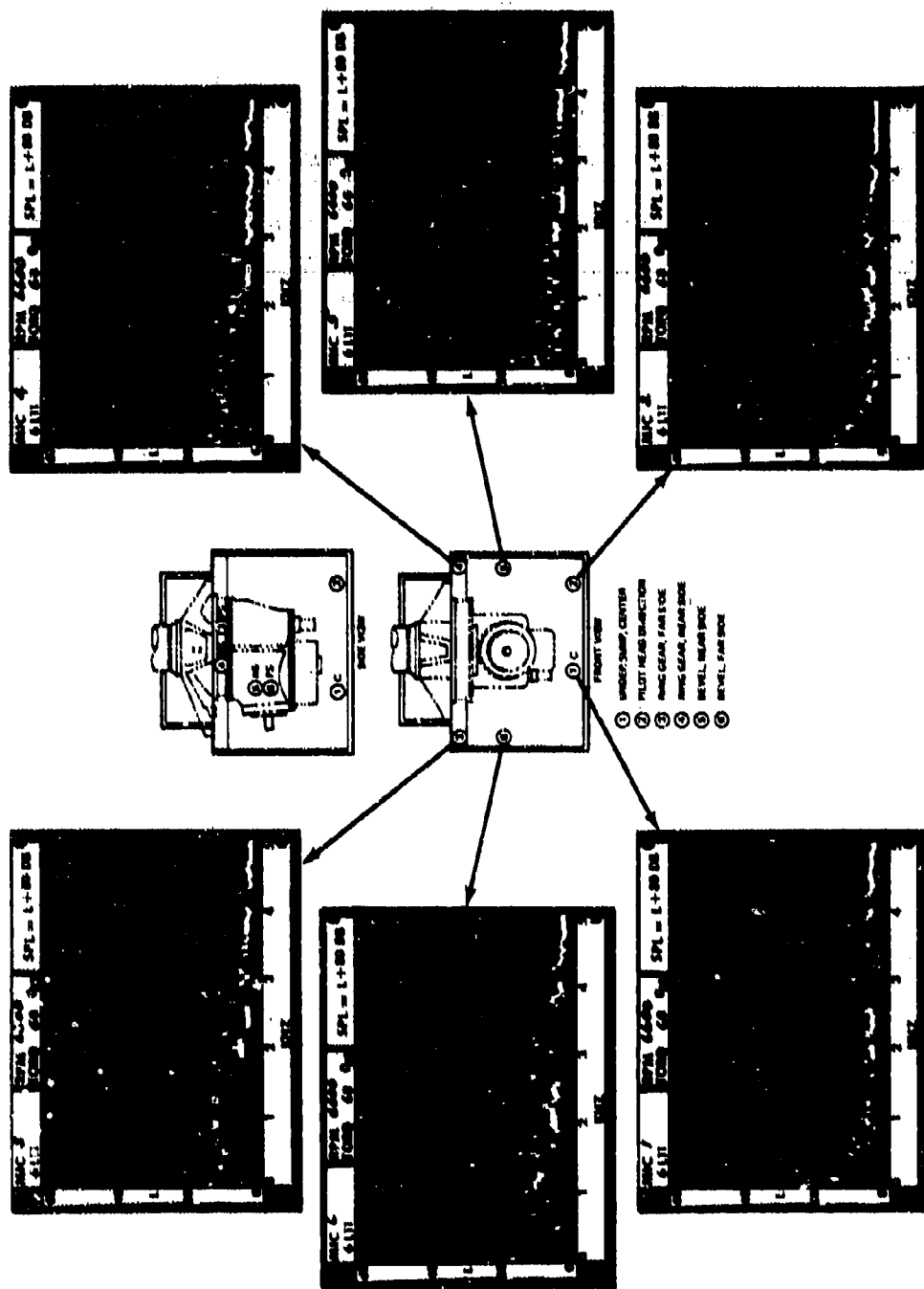


Figure A88. Microphone Data From Tape 61.11 With Detuning Graphite-Aluminum Composite Contour Plates at 6,600 RPM and 60-Percent Torque.

APPENDIX B

VIBRATION/NOISE ASPECTS OF METAL MATRIX COMPOSITE
REINFORCED TRANSMISSION HOUSINGS

NOTE: The fabrication of graphite/aluminum doubler plates was sponsored by the U.S. Army Materials and Mechanics Research Center, Watertown, Massachusetts, under the technical cognizance of Mr. Albert P. Levitt.

INTRODUCTION

Current cast light alloy transmission housing technology does not provide an optimum support structure for power train dynamic components under operating loads. These structures, limited by current materials and processing techniques which do not permit structural design optimization, exhibit excessive deflections and displacements under load which result in gear misalignment and vibration and noise generation. The increases in helicopter size, performance, and payload have intensified the need for high-strength, lightweight materials. The metal industry has been endeavoring to develop alloys with higher strength-to-weight and modulus-to-weight values. New alloys and new methods of working and heat treating have brought about small improvements, but the gains are no longer proportional to the effort that must be expended. Since all of the widely used structural metals reach limits of specific strength at about 1 million inches and of specific modulus at about 100 million inches, a search has been going on for some way to get around these specific strength and specific modulus barriers. Several metal matrix candidate systems exhibit specific strength in the range of 2 to 3 million inches and specific moduli of 400 to 500 million inches. Thus, there are many areas where metal matrix composites offer unique combinations of improved performance for helicopter applications.

The development of composite materials and the refinement of manufacturing technology for these materials have provided extended capabilities for the reinforcement of structures. Application of finite element analyses to transmission housing design has permitted the utilization of optimization methods such as strain energy. Previous optimization work, although quite extensive, had been limited to varying the wall thickness of a conventional cast magnesium housing. The analytical techniques have indicated the potential for more efficient application of the optimization methods by taking advantage of the improved properties and capability for selective reinforcement offered by composite materials. The ability to build up composite material elements with specified property orientations allows selective reinforcement of predetermined housing regions and provides improved flexibility for optimization of the structure.

The objective here was to assess the potential applicability of composite materials for housing optimization through selective stiffening by analyzing and testing a CH-47C forward transmission housing which was selectively stiffened by the addition of graphite/aluminum composite material. The most effective portions of the housing to be reinforced were defined by using the strain energy method in conjunction with the finite element model. Incorporating an analysis for determining average properties of arbitrary laminate materials extended the finite element method to consider the orientation of the composite material properties. Contoured graphite/aluminum doubler plates which were designed, fabricated, and bonded to the transmission housing wall to modify the local mass and stiffness properties changed the frequencies at which the housing responded when excited by the rotating internal components. By shifting these natural frequencies away from the exciting frequencies, the housing response (vibration/noise) was reduced. Measured vibration/noise data was compared with similar data from baseline (unreinforced) housing tests.

BACKGROUND

The use of metal matrix composite materials for helicopter transmission housings has many potential benefits, including reduced vibration/noise levels and improved stiffness. These improved vibration/noise characteristics are due to the increased overall stiffness and the ability to further selectively stiffen identified areas. By increasing the housing wall stiffness, the resulting static and dynamic displacements will be reduced for a specified load condition. This is evident, for example, from

$$F = Kx$$

where F = applied static or dynamic load

K = stiffness

x = displacement

The plots of displacement versus load for various materials shown in Figure B1 indicate that the magnitude of the housing displacements can be reduced substantially by the use of stiffer metal matrix materials. Steel is also shown in the figure as a point of reference. Since the amplitude of the vibration and resulting soundwaves are proportional to the magnitude of the displacement of the structure, the overall effect of increased stiffness would be to reduce the vibration/noise level.

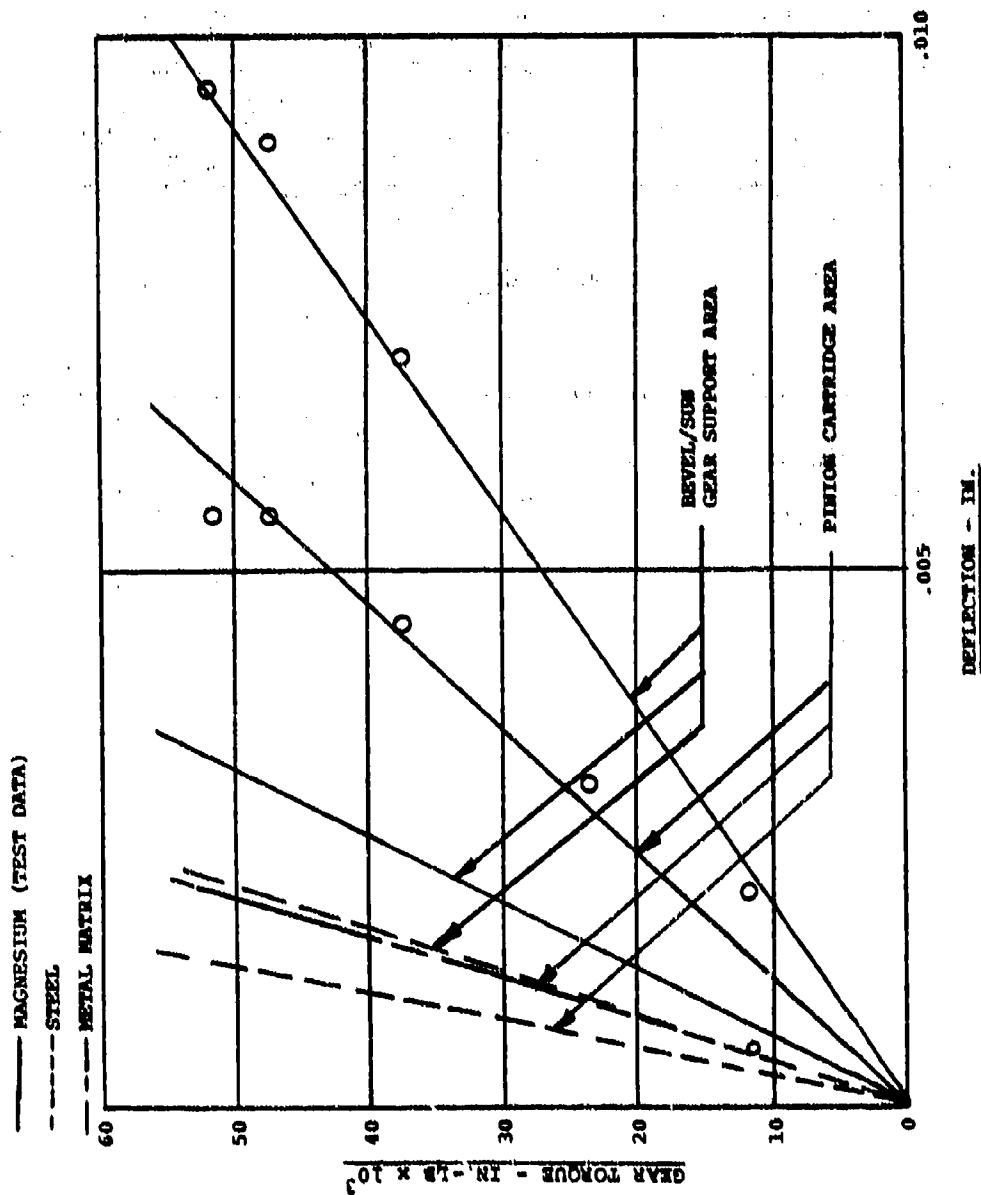


Figure B1. CH-47C Forward Transmission Dynamic Housing
 Deflection at Operating Temperature.

A further benefit of the metal matrix configuration is that it is much better suited for detuning of the housing than the conventional monolithic cast structure. A typical transmission frequency spectrum is presented in Figure B2a. Because of the multiple forcing frequencies and the many natural frequencies of the structure which occur, detuning of this housing is extremely difficult. Although the natural frequencies can be shifted by modifying the wall thickness, the multitude of closely packed frequencies generally will cause the tuning process to be only minimally effective. The new frequency spectrum which results after substituting a typical metal matrix material for monolithic magnesium is presented in Figure B2b. It is significant that the natural frequencies have been shifted toward the high end of the spectrum and that only about 40% of the frequencies remain in the range of interest (below approximately 5000 Hz) as compared to the solid magnesium configuration. Those natural frequencies remaining in the range of interest also have been dispersed and are thus much more amenable to the detuning process. Using the selective stiffening capability provided by the metal matrix design, the housing can be tuned to reduce the vibration/noise levels. Further areas of potential vibration/noise improvement for the metal matrix structure include structural damping and acoustic transmission loss (TL). Little data is available on these aspects, and therefore they must be investigated fully.

COMPOSITE DOUBLER PLATES: ANALYSIS AND TEST

In order to determine the applicability of composite materials for the selective stiffening of transmission housings, graphite/aluminum doubler plates were fabricated, affixed to the CH-47C transmission housing, and tested in a manner similar to the magnesium doubler plates described within the basic program. The finite element NASTRAN model was used to analyze the transmission housing loads and to determine the areas for attachment of the doubler plates. Computer-generated plots of the doubler plates are shown in Figures B3 and B4. A preprocessor (Point Stress Laminate Analysis - Reference 19) was used in conjunction with NASTRAN to define the orientation of the graphite fibers for the optimum stiffening in the composite plates. This preprocessor accounts for the anisotropic characteristics of the composite by using the basic single-ply (lamina) material properties to calculate the equivalent orthotropic material properties of the laminate. These are used in the NASTRAN analysis. Figure B5 illustrates the lamina or layer coordinate system (1-2) which is transformed to the laminate (X-Y) axis system. The resultant stresses and moments, representing a system which is statically equivalent to the stress system acting on the laminate, are also shown.

19. Reed, D. L., POINT STRESS LAMINATE ANALYSIS, Document FZM-5494, Prepared for Advanced Composite Division, Air Force Materials Laboratory, WPAFB, Ohio, April 1970.

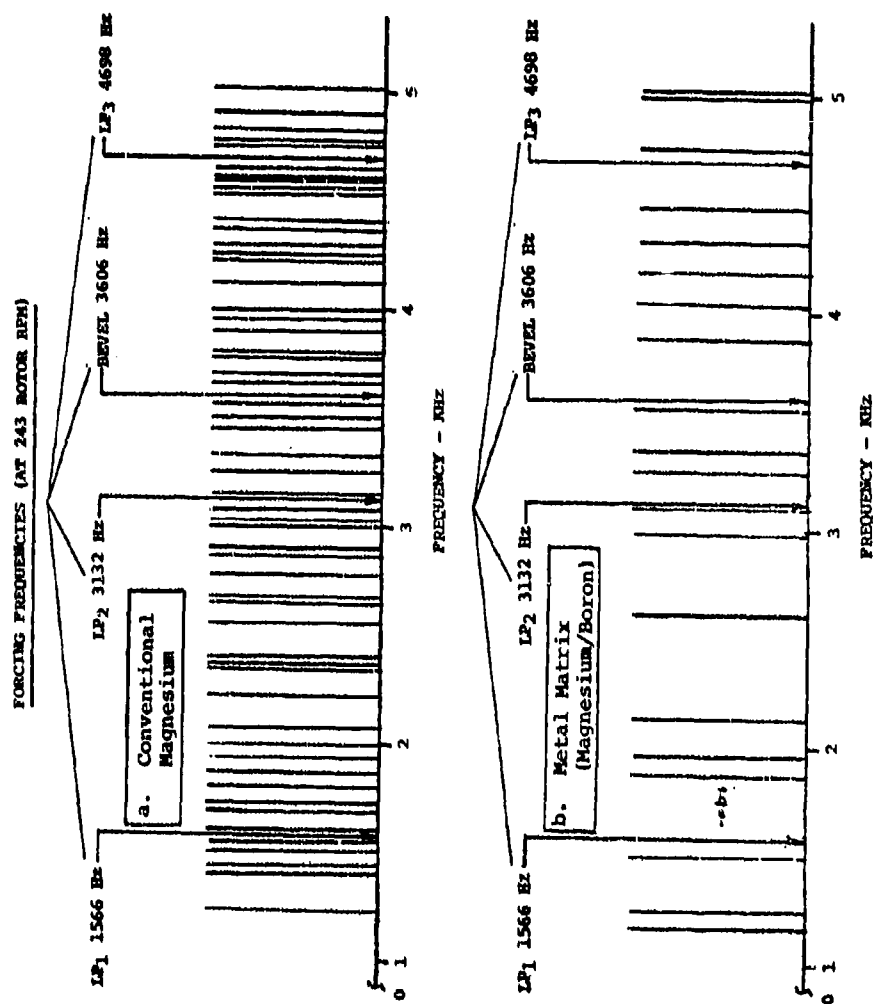


Figure B2. Typical Spectrum of Forcing Frequencies Versus Natural Frequencies.

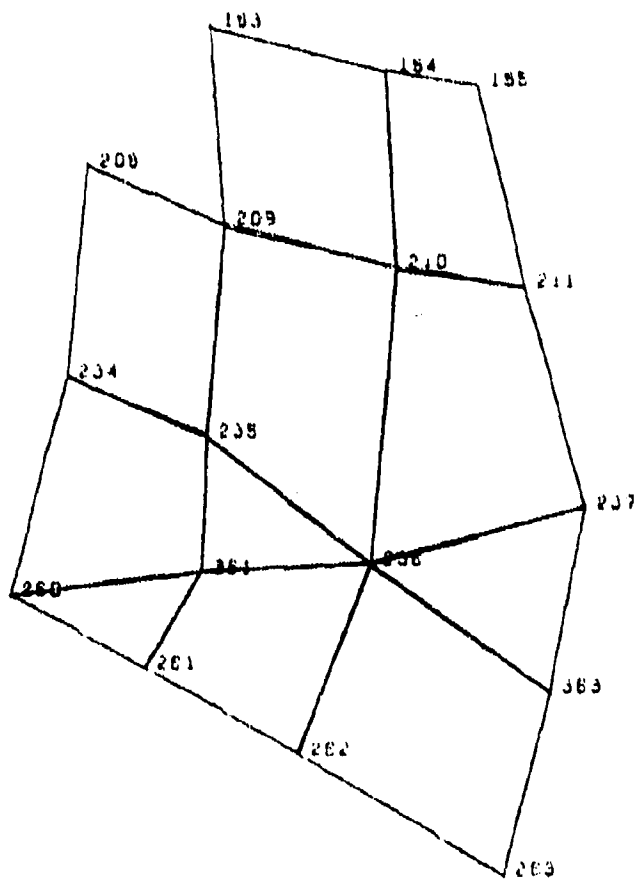


Figure B3. Computer-Generated Plot of -1 Graphite/
Aluminum Doubler Plate.

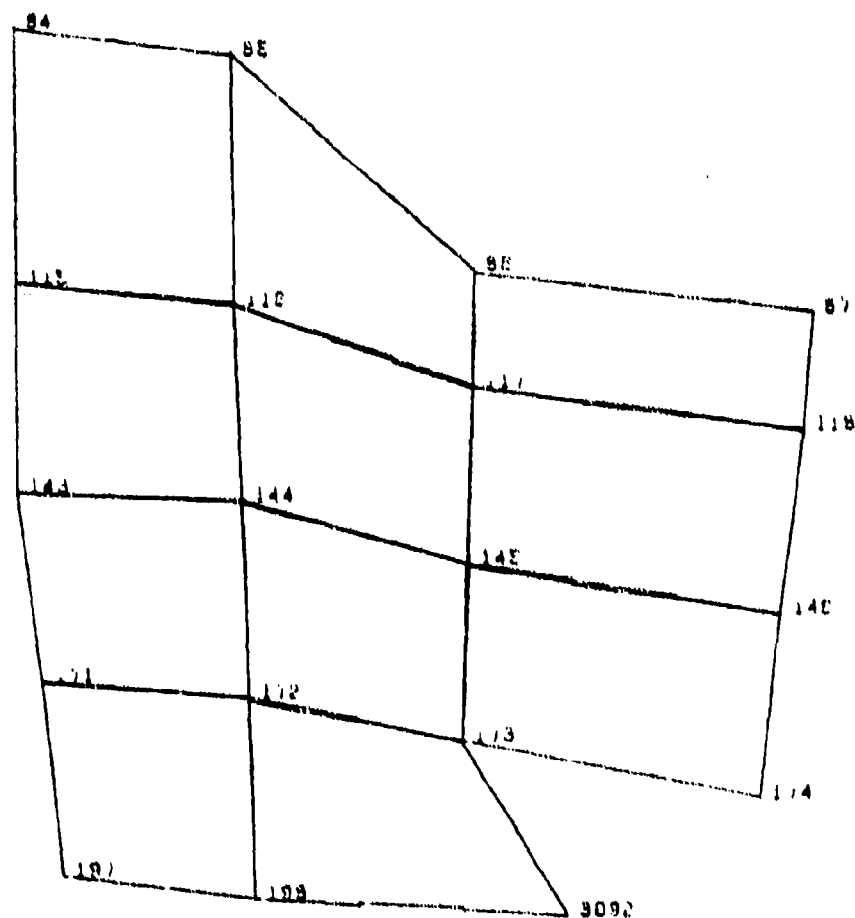


Figure B4. Computer-Generated Plot of -2 Graphite/
Aluminum Doubler Plate.

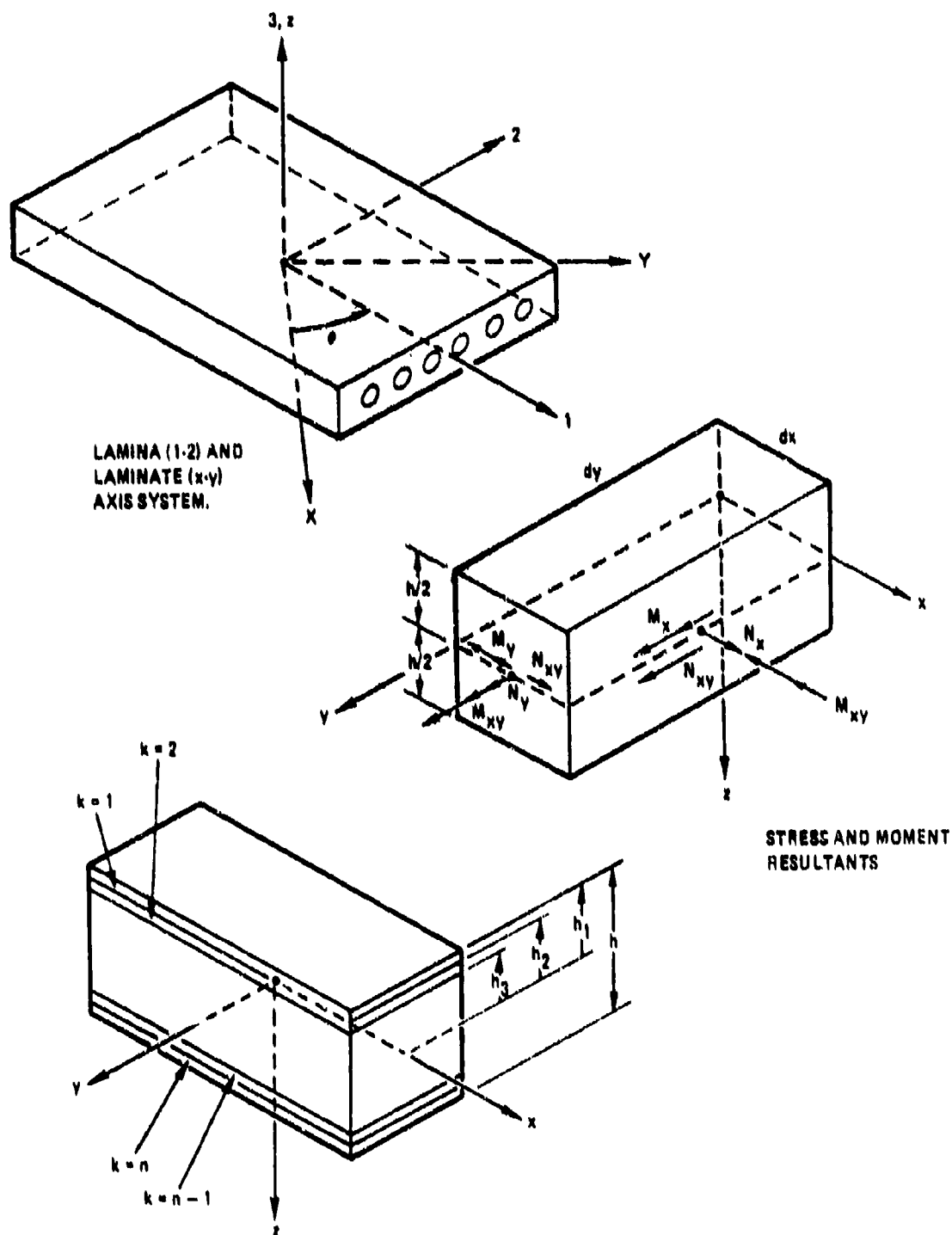


Figure B5. Lamina Notation.

computer program may be used after the NASTRAN analysis as a post-processor to obtain interlaminar and laminar stresses.

Based on an evaluation of the loads, the constraints imposed by ply thickness and symmetry, and the need for comparability with the baseline magnesium plates, the following specifications were established:

- Material system = T50 graphite filaments/201 aluminum matrix (see Table B1)
- Total number of plies = 6
- Total finished thickness of plate = approximately 0.204 inch
- Ply orientation [$\pm 60^\circ/0^\circ$]

The reference axis for the lamina orientations is the vertically upward direction of the 114D1089 transmission housing.

A significant problem experienced in the application of finite element methods to the analysis of composite structures is the difficulty of compiling a complete data base to define the anisotropic material property matrix typical of composite materials. Much of the test data available is derived from specific application and hence is concerned with specific fiber orientations and fiber volume percentage, of which there are essentially an infinite variety of combinations for a given material system, rather than basic unidirectional single ply data. Single ply data is most useful since it can be used to generate properties for any orientation and stack-up combination. Conversely, specimen data has limited value unless it happens to be for the same material configuration as that being analyzed, which is not likely since composites are typically tailored to meet the specific application. The material properties used for the analyses are shown in Table B1, which is based upon a compilation of basic material properties and test data from several sources.

After establishing the material properties for the composite structural elements, the transmission model was adapted to represent the addition of the composite doubler plates and a NASTRAN analysis was run. The stiffness and deflection characteristics of the baseline housing, the housing modified with the magnesium doubler plates, and the housing modified with the graphite/aluminum doubler plates were compared. The NASTRAN weight generator was used to evaluate the weight of each configuration. The three configurations evaluated are summarized in Table B2. The design of the graphite/aluminum plates is based upon conservative values of the basic single ply material properties. Since the purposes of this developmental work were to verify the analytical procedures and to

TABLE B1. MATERIAL PROPERTIES: T50 GRAPHITE FIBER/
201 ALUMINUM MATRIX

	T50 GRAPHITE FIBER	201 ALUMINUM MATRIX	SINGLE PLY T50/201	SIX PLY $\pm 60^\circ/0^\circ$ T50/201 COMPOSITE
Modulus of Elasticity (Longitudinal) (PSI)	57.0×10^6	10.6×10^6	24.5×10^6	9.6×10^6
Modulus of Elasticity (Transverse) (PSI)	-	10.6×10^6	10.6×10^6	9.6×10^6
Poisson's Ratio	-	.3	.3	.303
Shear Modulus (PSI)	-	-	4.0×10^6	3.6×10^7
Density (LB/IN ³)	.060	.101	.0887	.0887
Fiber Volume Fraction	-	-	30%	30%
Thermal Expansion Coefficient (Longitudinal) (IN/IN/°F)	-	10.7×10^{-6}	1.8×10^{-6}	-
Thermal Expansion Coefficient (Transverse) (IN/IN/°F)	-	10.7×10^{-6}	1.3×10^{-5}	-
Ultimate Strength, Tension (Longitudinal) (KSI)	315	60	90	-
Ultimate Strength, Tension (Transverse) (KSI)	-	60	4.5	-

TABLE B2. STIFFENER COMPARISON

	WEIGHT	(At Load) R DISPLACEMENT	ρ	$\frac{1}{(wt) (Disp)}$	THICKNESS (Nominal)
-1					
BASELINE	0.71	.024	.0650	59	.330
.300 MAG*	1.36*	.005	.0650	147	.630
PLATE					
.204 Gr/A1	1.31*	.004	(.0887 Plate)	191	.504
PLATE*			** .0741 Total Section		
-2					
BASELINE	1.25	.032	.0650	25	.359
.300 MAG*	2.30*	.007	.0650	62	.659
PLATE					
.204 Gr/A1	2.22*	.007	(.0887 Plate)	64	.563
PLATE*			** .0740 Total Section		

*Includes basic wall also

**At 30% fiber

compare with the baseline magnesium plates, rather than to actually design an optimum housing by a rigorous application of the analysis, trade-offs and compromises were made. Also, the design does not use the directivity of the fiber properties to the best possible advantage since the intent herein was to simulate the stiffness of the magnesium plates. The overall results would be even more favorable for a graphite/aluminum version of a housing that was designed to take maximum advantage of the directional properties of the composite. With the above constraints considered, the areas reinforced were the same as those for the magnesium plates (see Figure 50). Figure 49 illustrates the more multitudinous areas that should have been stiffened for a rigorous application of the analysis. The technology is now emerging in the form of metal matrix composites to manufacture a housing which is selectively stiffened in the areas such as indicated in Figure 49. The modeling procedure and the strain energy technique have been described in further detail in the basic report.

The graphite/aluminum composite doubler plates were fabricated by DWA Composite Specialties, Inc., Chatsworth, California. The subcontractor procured the necessary graphite/aluminum tape material and fabricated one SK27064-3 contoured doubler plate (L) and one SK27064-4 contoured doubler plate (R) (Figure B6). This material system was selected because of the availability of the graphite/aluminum material and the production-ready status of the manufacturing procedure. These plates were contoured to fit the exterior surface of the existing CH-47C helicopter forward rotor transmission housing (114D1089). Using molds of the areas of the outer surface of the transmission housing to be reinforced by the doubler plates as patterns, tooling in the form of matching dies necessary to fabricate the doubler plates was manufactured. The plates were formed by a layup of the graphite/aluminum lamina (tape) at the orientations and to the thickness specified, and then hot-pressure bonded using the matched die set. The outer edges of the finished doubler plates were then trimmed and rounded off, and the plates were nondestructively inspected to insure integrity of their structure. Inspection of the doubler plates was made by tapping to indicate completeness of consolidation and bonding, visual inspection, and thickness measurements. The plates appeared to be generally well bonded and consolidated with thicknesses within the normal range and uniformity. Visual inspection indicated sound material at the trimmed edges and also indicated an excellent fit of the contoured plate on the housing exterior wall. One corner of the SK27064-3 doubler plate was partially delaminated and the 6 individual lamina could be observed (Figure B7).

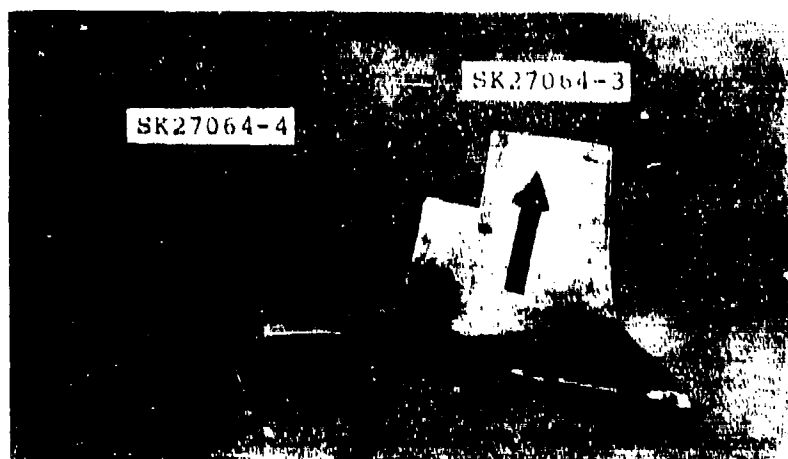


Figure B6. Graphite/Aluminum Doubler Plates.

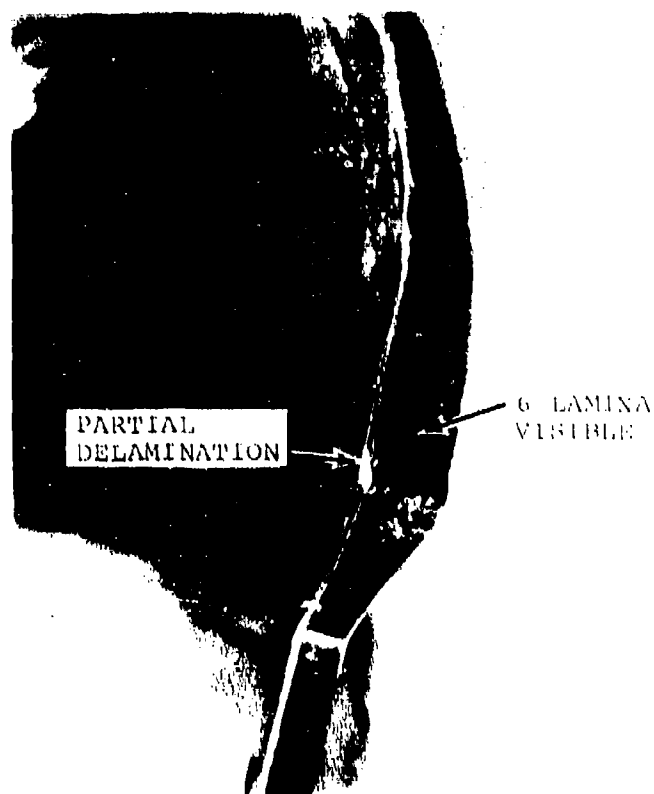


Figure B7. Partially Delaminated Corner of SK27064-3 Graphite/Aluminum Contoured Doubler Plate (1).

Using an adhesive resistant of temperatures up to 250°F, the two graphite/aluminum composite plates were bonded to the surfaces of the CH-47 lower housing. The bonding was conducted under conditions which minimized the thermal stresses in the adhesive and the composite plates due to differences in thermal expansion coefficient between the housing and the composite plates. After the adhesive had been cured and it was determined that the plates were fully bonded at all points to the housing, a complete CH-47C forward transmission including the reinforced housing was built up, installed in the instrumented test stand, and run for sustained operating times to determine the noise and vibration generated.

The test procedures and instrumentation used were identical to those described previously for the basic test program, except that only Dynamic Test 3 (Dynamic Tests 6A and 6B, Table 7) was repeated to evaluate the effect of the case modification. The objective of this testing was to assess the effectiveness of the graphite/aluminum doubler plates for reducing vibration and noise caused by the gear mesh excitation of a CH-47C forward transmission. Noise levels were measured utilizing six microphones located within an acoustically insulated enclosure which houses an operating CH-47C forward transmission. In addition, by measuring accelerations using accelerometers attached at six locations on the transmission, the effectiveness of the above structural changes for reducing transmission vibrations was evaluated. The transmission was tested at a baseline (7460 rpm) and an off-design (6600 rpm) condition for two torque levels (80%, $.85 \times 10^6$ inch-lbs output shaft and 60%, $.64 \times 10^6$ inch-lbs). Each of the above variations was harmonically analyzed as to mesh content, resulting in 48 items of noise information and 48 items of accelerometer information. These results were compared with noise and vibration data from the baseline unreinforced housing and the magnesium reinforced housing to determine the extent to which noise and vibration caused by gear mesh excitation were reduced by the composite plates.

APPENDIX C
KAMAN UH-2 TRANSMISSION NASTRAN MODEL

To provide additional verification of the analytical method, a second transmission, the Kaman UH-2 main rotor transmission (Figure C1), was originally to be analyzed by Boeing Vertol using the computer-aided system defined in the body of this report. Testing of this second transmission was to have been conducted by Kaman under a separately contracted, parallel program, in a manner such that the predictions obtained through the Boeing Vertol analysis could be verified. Unfortunately, the Kaman effort was terminated prior to any testing. As a result, the only information presented to Boeing Vertol was that contained on the engineering drawings of the Kaman housing.

At the direction of the contracting officer's technical representative, the Boeing Vertol effort on the Kaman housing analysis was also terminated after the preliminary NASTRAN model of the basic housing was completed.

The Kaman UH-2 transmission NASTRAN model plots are shown in Figures C2 through C5, while Table C1 shows the basic model parameters. Since this effort was terminated, no further results are available.

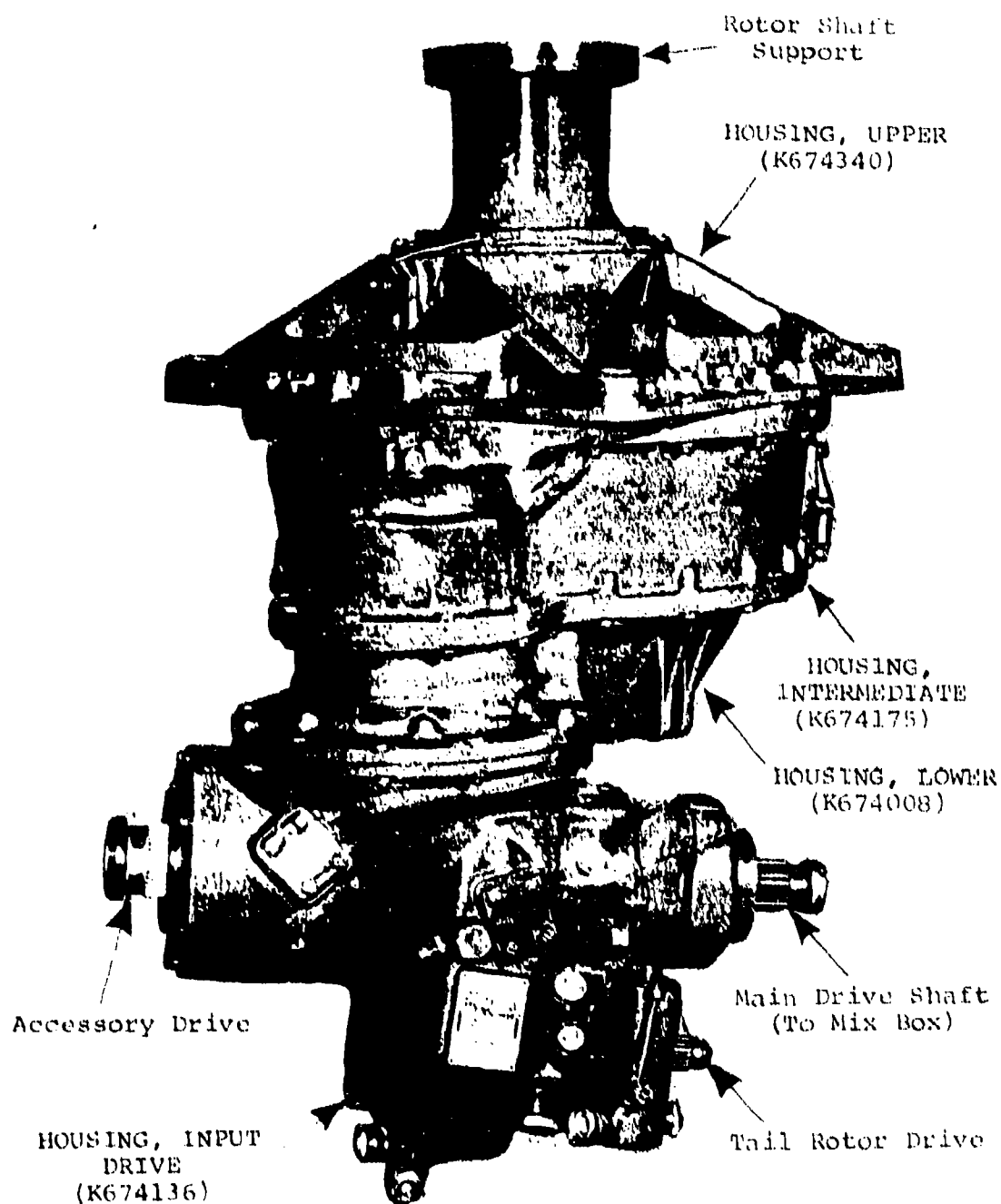


Figure C1. Kaman UH-2 Helicopter Main Transmission.

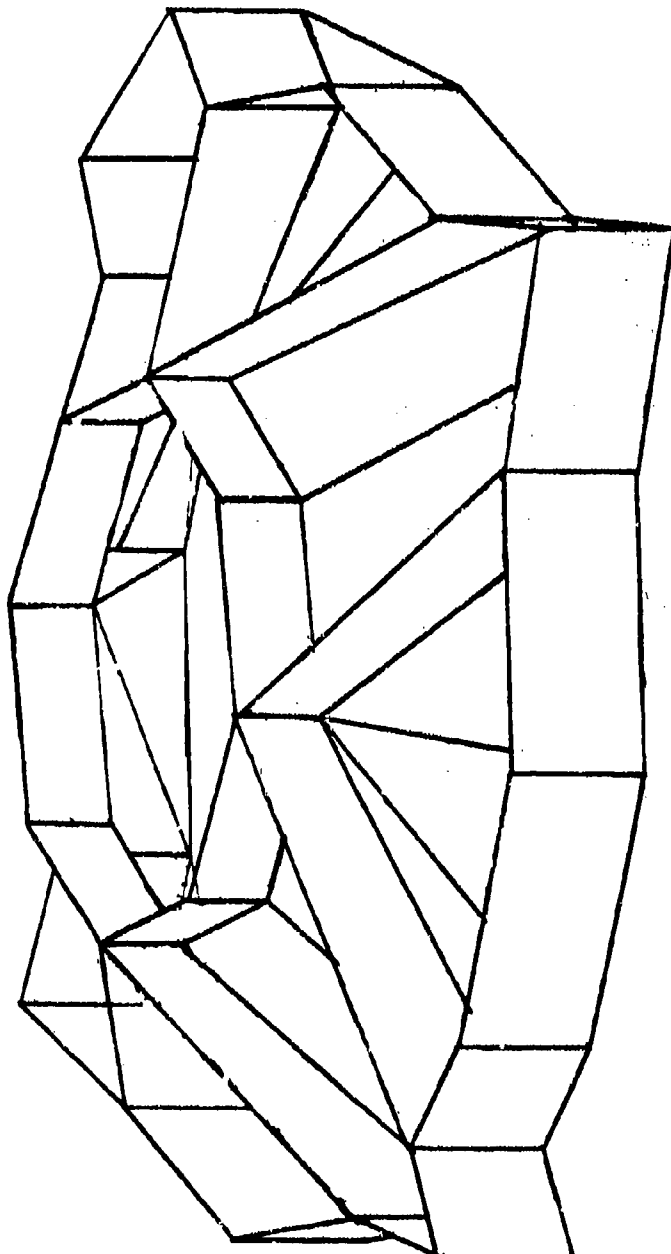


Figure C2. Noise/Vibration Reduction Program, Kaman UH-2 Main Transmission, Upper Housing (Undeformed Shape).

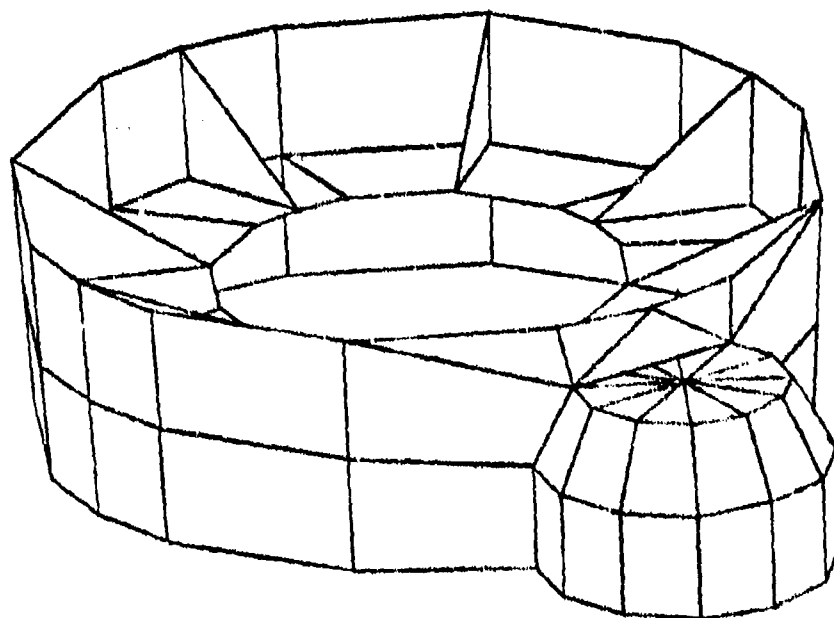
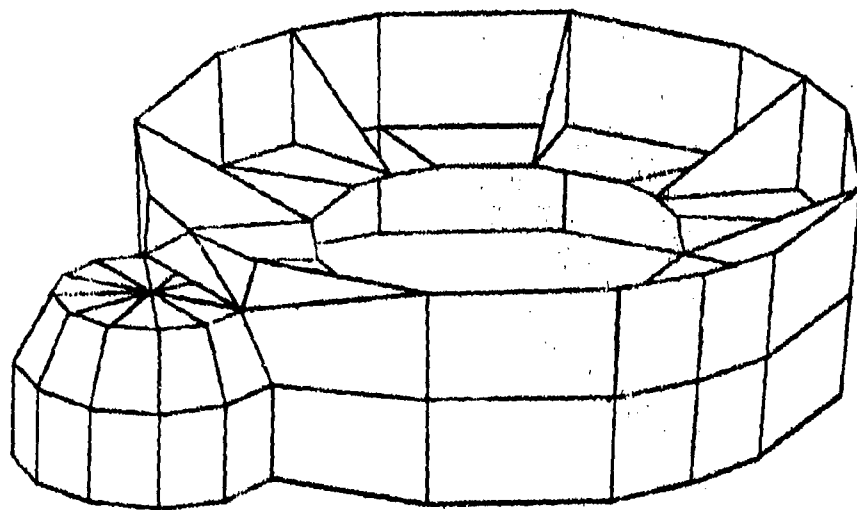


Figure C3. Noise/Vibration Reduction Program,
Kaman UH-2 Main Transmission,
Intermediate Housing (Undeformed Shape).

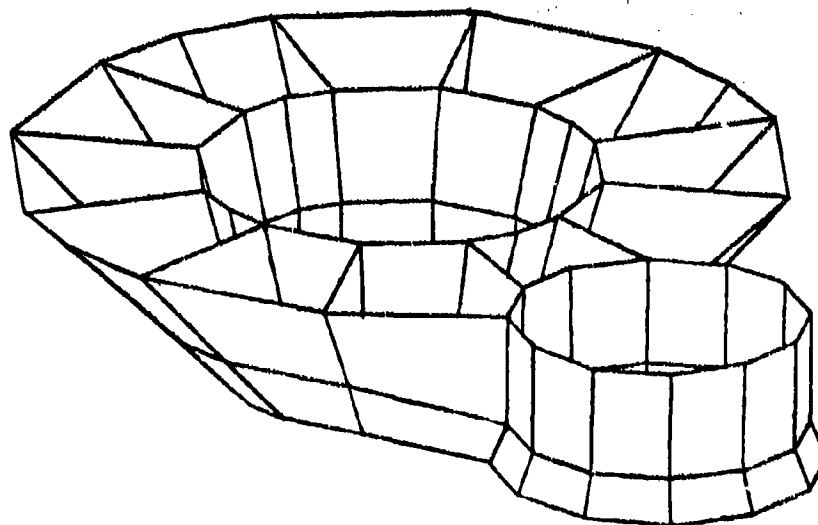
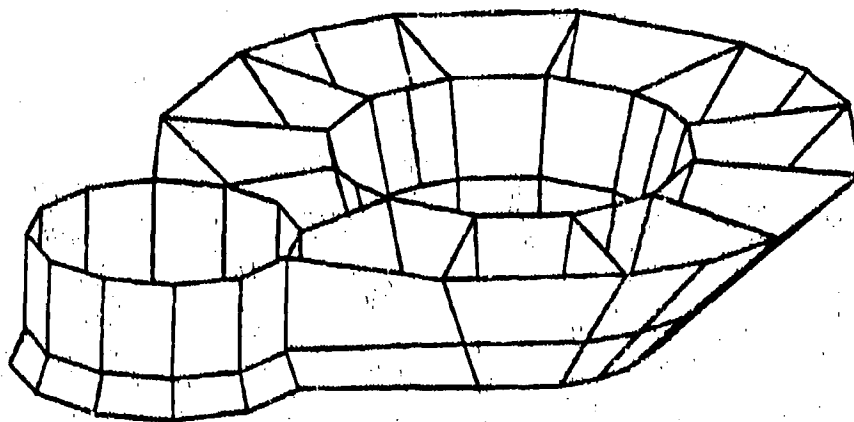


Figure C4. Noise/Vibration Reduction Program,
Kaman UH-2 Main Transmission,
Lower Housing (Undeformed Shape).

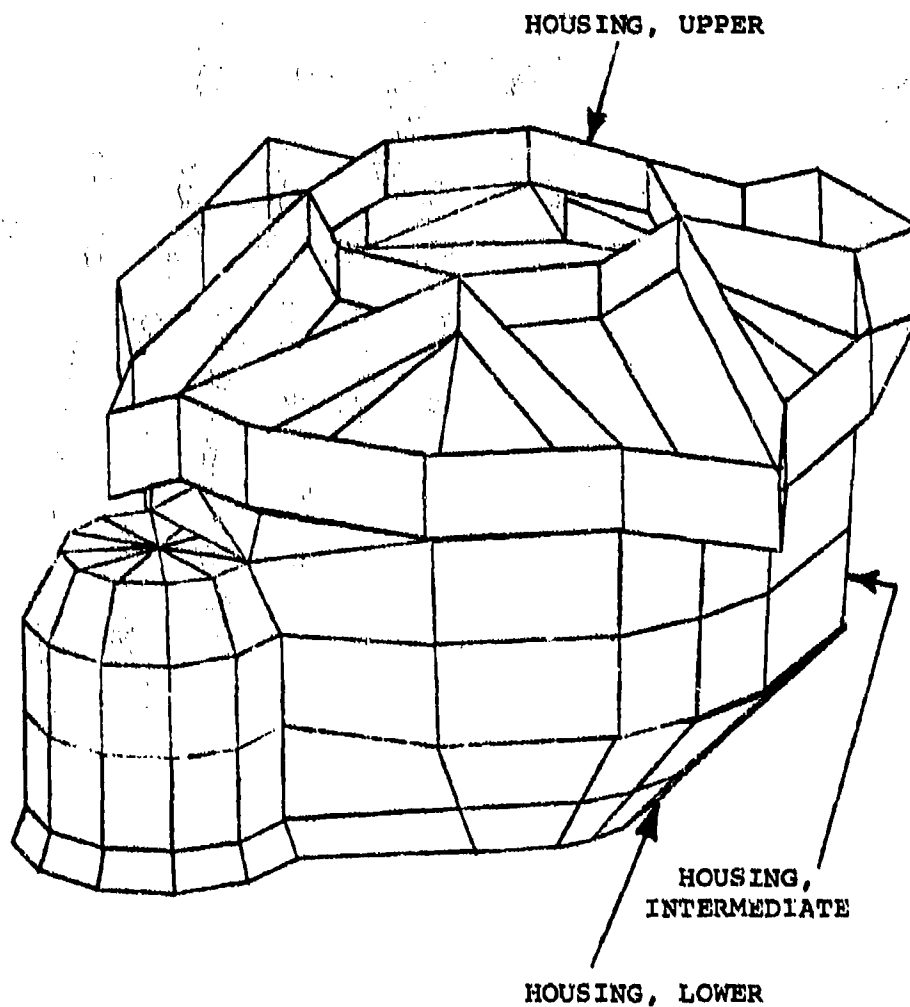


Figure C5. Noise/Vibration Reduction Program,
Kaman UH-2 Main Transmission,
Computer Generated Model (Incomplete -
Input Drive Housing Not Included).

TABLE C1. KAMAN UH-2 HELICOPTER MAIN TRANSMISSION
NASTRAN MODEL PARAMETERS

	MODEL PARAMETERS			NUMBER DEGREES OF FREEDOM
	NUMBER GRID POINTS	NUMBER ELEMENTS		
Housing, Upper	55	59		270
Housing, Intermediate	100	95		487
Housing, Lower	115	77		554
Housing, Input Drive	≈175	≈150		843
TOTAL	<u>445</u>	<u>381</u>		

LIST OF SYMBOLS

(C)	damping matrix
DFR	damped forced response
D-82	unified structural analysis or damped forced response computer program
E_A	acoustical energy per cycle
E_M	mechanical energy per cycle
e	excitation, μ -in.
F	force, lb
F_s, F_c	sine or cosine components of the exciting load, lb, in.-lb
f	gear mesh frequency, Hz
GGEAR	gear mesh excitation computer program
H	heat energy
(K)	stiffness matrix
k	bearing stiffness, lb/in.
L	sound pressure level, dB
M	mobility or mass
(M)	mass matrix
n	number of bearings
P_A	sound power, watt
P_0	reference pressure, μ -bar
P_s	sound pressure, μ -bar
PWL	sound power
r	distance to radiating surface, ft
SPL	sound pressure level referred to 0.0002 μ -bar
T	period, sec

t	time, sec
TL	sound transmission loss
TORRP	torsional response computer program
W	heat rate
X	displacement (in.) or rotation (rad)
X_s, X_c	sine or cosine components of the displacement (or rotation), in. (or rad)
α	energy conversion factor
β	geometry correction factor, damping ratio, frequency ratio
δ_{ik}	$\delta_{ik} = 1$, if $i=k$ and 0 if $i \neq k$
ϵ	environment constant
λ	test condition constant = $10 \log (\alpha \beta f / 2 P_0^2 \epsilon r^2)$ or bearing heat conversion factor
ζ	mesh heat conversion factor or critical damping ratio
θ, ϕ	phase angles, deg
ω, Ω	natural frequency, excitation frequency, rad/sec
dB	a logarithmic measure used for sound pressure levels (SPL) and sound power (PWL)
dBA	a weighted unit used to bias sound measurements with a correction approximating the sensitivity characteristics of the human ear